National Roadmap for Adaptation 2100
Portuguese Territorial Climate Change Vulnerability Assessment for XXI Century

REPORT

WP4 – SECTORAL IMPACTS AND MODELLING

WP4.5/6 – The impact of climate change on the Portuguese coastal areas: from sea level rise to coastal erosion

Mainland Portugal

Final Version

National Roadmap for Adaptation 2100
Portuguese Territorial Climate Change Vulnerability Assessment for XXI Century

---

Title: RNA2100 – Sectoral Impacts and Modelling – The impact of climate change on the Portuguese coastal areas: from sea level rise to coastal erosion

Authors: Carlos Antunes and Gil Lemos (coord.), Ivana Bosnic, Pedro Matos Soares, Álvaro Semedo (IHE-Delft), Pedro Costa, Daniela Lima, Carolina Rocha, Cristina Catita, Vanessa Ferreira, Miguel Espírito Santo e Sílvia Mourão.

February 2024

This report is a product of the National Roadmap for Adaptation 2100 project.

Through the Agreement on the European Economic Area (EEA), Iceland, Liechtenstein and Norway are partners in the internal market with the Member States of the European Union.

In order to promote a continuous and balanced strengthening of economic and trade relations, the parties to the EEA Agreement have established a and trade relations, the parties to the EEA Agreement established a multi-annual Financial Mechanism, known as the EEA. known as EEA Grants.

The EEA Grants aim to reduce social and economic disparities in Europe and to strengthen bilateral relations between these three countries and the beneficiary countries.

For the 2014-2021 period, a total contribution of 2.8 billion euros has been agreed for 15 beneficiary countries. for 15 beneficiary countries. Portugal will receive 102.7 million euros.

Funded by:

Promoter:

Partners:

Contents

List of Figures

List of Tables

Executive Summary

Some of the most disruptive effects of climate change are projected to be felt along the coastlines. From flooding to extreme coastal erosion, future changes in coastal dynamics are particularly feared, especially if combined with sea level rise, tides, storm surges and changes in wave climate. Coastal areas are amongst the most vulnerable regions to climate change, comprising important populational centres and economically relevant hubs. The portion of total population living in coastal areas has rapidly increased in the last decades, being estimated that at least 10% of the current world's population lives near the coast, less than 10 m above sea-level. In Portugal, data from the CENSOS2011 shows that 14% of the national population lives within 2 km of the sea, with the most recent update (CENSOS2021) pointing to increases in the Lisbon and Algarve regions, of 1.7% and 3.7%, respectively, in comparison with 2011.

Rising sea levels, together with the effects of tides, storm surges and extreme waves are considered key-drivers of coastal hazards, threatening coastal infrastructures, ecosystems, and communities. The increase in human pressure along the Portuguese coastlines calls for a reliable, long-term coastal vulnerability assessment, paramount for effective coastal management, sustainable development, adaptation, and impact mitigation strategies.

In the context of an increasing need for accurate physical and socioeconomic coastal vulnerability assessments, and incorporated in the National Roadmap for Adaptation XXI, we present a thorough and comprehensive assessment of future projected hydro-morpho-dynamical changes along the Portuguese coastlines. Future shoreline evolution and extreme coastal flooding projections are obtained, through high-resolution hydro- and morpho-dynamic modelling, for five coastal key-locations, selected due to their higher currently perceived vulnerability to climate change (based on historical records). Ensemble-based projections forced by Coupled Model Intercomparison Project phase 5 (CMIP5) Global Climate Models (GCMs), are used to drive an innovative methodology, focused on dealing with the multivariate challenges of an accurate coastal vulnerability assessment for Portugal, aiming to accurately assess the extension of future projected extreme coastal flooding. Two Representative Concentration Pathway scenarios are considered, namely the RCP4.5 and the RCP8.5. These baseline results are used to train a parametric approach designed for the complete, national-scale coastal vulnerability assessment, supported by a composed coastal vulnerability index.

At a local scale, our results indicate that future nearshore wave action, projected to become more northerly and less energetic, is expected to lead to northward beach rotations especially along the northern and central Portuguese coastal stretches. Nevertheless, the impact of SLR is shown to lead to consistent shoreline retreats throughout all analyzed key-locations. Such results are in agreement with several studies indicating that while wave action is projected to dominate morphological response until the mid-21st century, SLR should become the main driver of shoreline evolution beyond that time-frame. Final projected shoreline retreats are shown to locally reach 100 m (120 m) by 2100 under RCP4.5 (RCP8.5) at Ofir, 200 m (210 m) at Costa Nova, 140 m (150 m) at Cova Gala, 290 m (300 m) along Costa da Caparica, and 65 m (80 m) in Praia de Faro. The projected lost areas between the reference (2018) and future mean shorelines range between 0.088 km^2 and 0.184 km^2 (0.118 km^2 and 0.197 km^2) by 2100, under RCP4.5 (RCP8.5), the smallest (greatest) losses expected to take place at Faro and Cova Gala (Costa Nova). Throughout all key-locations (approximately 14 km of coastline), the cumulative amount of projected lost area from 2018 to 2100 ascends to 0.786 km^2 (2100 under RCP8.5), relevant when compared to the historical nationwide area lost to the sea between 1958 and 2021, which amounted to 13.5 km^2 for over 980 km of coastline.

The synchronized action of extreme total water levels, resulting essentially from SLR, but also from the joint occurrence of high spring tides or storm surge conditions, in the context of weaker natural protection structures due to erosion, is shown to lead to unprecedented coastal flooding in the future. Throughout the five key-locations, the future projected threatened area, expected to become flooded under extreme conditions, is projected to ascend to 0.657 km^2 (0.738 km^2) by 2070 under RCP4.5 (RCP8.5), and 0.841 km^2 (1.47 km^2) by 2100 under RCP4.5 (RCP8.5).

Based on the dynamical modelling at the five key-locations, a parametric approach is calibrated to characterize coastal retreat, flooding and the overall vulnerability along the entire Portuguese coastline. The coastal vulnerability index, divided into three levels (low, moderate and high), is inversely related to the projected flooding extent, so that areas under high CVI are the ones showing increased vulnerability to less extreme (more frequent) events, and vice-versa.

Finally, the ocean-facing areas under CVI along Mainland Portugal are projected to ascend to 41.7 km^2 (2070 under RCP4.5), 49.7 km^2 (2070 under RCP8.5), 54.7 km^2 (2100 under RCP4.5) and 55.9 km^2 (2100 under RCP8.5). These areas, related to episodically flooded territory, are projected to amount to 3.09, 3.68, 4.05 and 4.14 times the area observed to have been lost between 1958 and 2021 (13.5 km^2). However, when considering inland waters, an additional value between 514 km^2 and 548 km^2 (2070 under RCP4.5 and 2100 under RCP8.5, respectively) must be considered. Therefore, for all types of coastlines along Mainland Portugal, the future area under CVI is projected to ascend to 604 km^2 by 2100, under the RCP8.5 scenario.

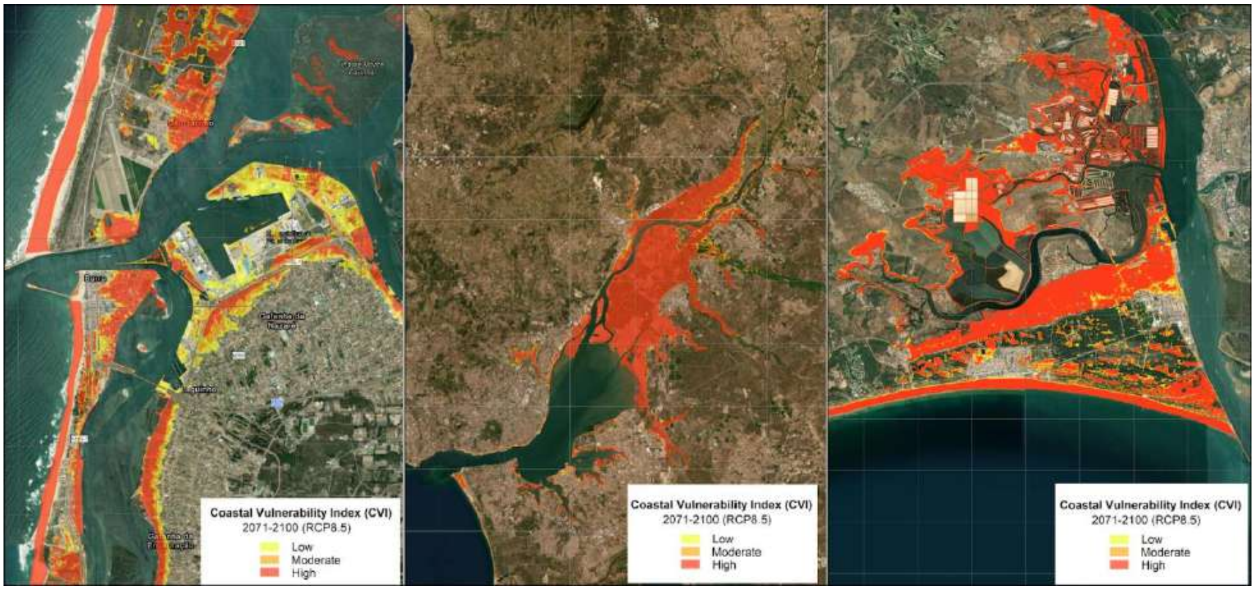

Projected areas under CVI for Aveiro, Lisbon and Vila Real de Santo António regions, by the end of the 2071-2100 future period (2100), under the RCP8.5 scenario.

The combination of coastal retreat with high-frequency flooding could result in loss of coastal ecosystems and fertile soil for agriculture given the potential landward intrusion of saltwater, besides the imminent risks for human life. Our results call for the implementation of adequate coastal management and adaptation plans, strategically defined to withstand changes until 2100 and beyond.

1. Introduction

Potential increases of coastal hazards, like flooding or extreme coastal erosion, are amongst the most disruptive effects of climate change. The physical processes driving coastal erosion, shoreline changes and coastal floods are mainly related with local hydrodynamic forcing (waves and currents), sea level rise (SLR), extreme storm events and sediment budget imbalances in the coastal system. Changes in wave climate at the coast are particularly important (Serafin *et al.*, 2019), especially when combined with other phenomena such as SLR (Storlazzi *et al.*, 2018), storm surges (*e.g.*, Camelo *et al.*, 2020) and wave run-up (Senechal *et al.*, 2011), considered key-drivers of coastal hazards. Increased wave energy is also responsible for aggravated loads in coastal structures, decreasing their life span with direct socioeconomic impacts (IPCC, 2014).

Coastal areas have always been relevant to human development, providing numerous economic and social benefits. Therefore, a large portion of human settlements are located along the coastlines. The portion of the total population occupying coastal areas has been increasing rapidly (Neumann *et al.*, 2015). In fact, it is estimated that at least 10% of the current world's population lives in coastal areas less than 10 m above sea-level (McGranahan *et al.*, 2007). Additionally, around one third of the European Union population lives within 50 km from the coast. Morim *et al.* (2019) suggested that 48% of the global coastlines are at risk from wave climate change alone, owing to robust projected changes in at least two wave parameters (such as height, period or direction), until 2100. This value might be higher if other sources of risk are considered, exposing a large portion of the world's vulnerable coastal areas to hazards, projected to become more intense and frequent in the future, leading to property damage, loss of life and environmental degradation (Gornitz, 2005). The lack of sediment sources, SLR, sand mining and destruction of natural defence lines due to increasing human occupation are projected to create additional pressure on these areas and accelerate erosion mechanisms (Mangor *et al.*, 2017). It is estimated that the global mean sea level has already increased by 13-20 cm since pre-industrial times (Kopp *et al.*, 2016), accelerating since the 1990s (Watson *et al.*, 2015), which has already contributed to coastal recession in some areas of Europe (EUROSION, 2003; Leatherman *et al.*, 2000; Mentaschi *et al.*, 2018), and increased the susceptibility to coastal hazards. The continued global-warming-driven SLR along Portuguese coastlines, associated with the present scenario of coastal sedimentary imbalance, could result in unprecedented coastal flooding, in case no additional coastal protection and risk-reduction or adaptation measures are implemented (Duarte Santos *et al.*, 2017). Therefore, accurate physical and socioeconomic vulnerability assessments of the coastal areas must integrate the most important physical processes able to describe and quantify SLR, tides, storm surges, wave run-up and erosion, in the context of climate change.

The coastline of Mainland Portugal spans 987 km and is divided into different geomorphological stretches represented by sandy beaches, dunes, sandy rocky and soft cliffs, interspersed by river mouths, estuaries, lagoon systems, barrier islands and urbanized areas with maritime ports, sea walls, breakwaters, marginal roads and housing lots. Such a complex coastal setting poses enormous challenges for any approach trying to achieve a wide and complete coastal vulnerability and risk assessment. Therefore, a methodology that enables the assessment of physical and socioeconomic impacts of all coastal processes, forced by climate change, must rely on a composed coastal vulnerability index (CVI), which integrates coastal erosion and coastal flooding simulations from hydro- and morphodynamic models, adapted to each type of coastal stretch, either natural or urbanized.

General Circulation Models (GCMs) are presently the primary source of knowledge about climate dynamics and climate change impacts. Understanding and quantifying future climate projected changes is of high relevance, being, at the same time, the greatest challenge in climate modelling. GCM outputs are used in many climate change impact assessments, as well as forcing for wave models to generate wave climate simulations. Parameters such as the SLR, wind and air-pressure can be provided either from GCMs or from Regional Climate Models (RCMs), used to dynamically downscale the results from GCMs to be used in regional studies, with increased horizontal resolution. These physical-mathematical-based models (GCMs and RCMs) provide the base information for all wave, erosion, and coastal flooding modelling efforts. Therefore, wave climate simulations, together with hydrodynamic and morphodynamic models, as well as sedimentological and geomorphological characterization and a digital terrain model (DTM) with a high spatial resolution covering topography and bathymetry, constituted the research baseline for the Mainland Portugal's coastal vulnerability and risk assessments.

Coastal flooding is a relatively-well understood and widely modelled consequence of increasing total water levels (TWLs), which combine SLR, astronomical tides, storm surges and waves (wave set-up and run-up). Some of the most pressing challenges to coastal flood modelling include coherent approaches to obtain and assess TWL components in order to produce adequate (and accurate) results. While the probabilistic combination of the TWL components should be considered the methodology of choice, the deterministic approach of combining all TWL components is still common. Furthermore, when dealing with wave climate simulations and projections, the additional efforts required to account for the waves' interaction with bathymetry near the coast are usually neglected. In fact, coherent and comprehensive methodologies combining SLR with tides, storm surges and waves are scarce (Toimil et al., 2020; Vousdoukas et al., 2018). Despite some exceptions (Lin et al., 2016; Arns et al., 2017; Garner et al., 2017; Sayol and Marcos, 2018; Tebaldi et al., 2021), most studies focus uniquely on SLR, neglecting or considering the remaining variables stationary. Nevertheless, the combined impact of storm surges and extreme wave conditions, especially when synchronized with high tides, may produce variations in the TWLs greater than SLR, of up to a couple meters (Vousdoukas et al., 2018; Kirezci et al., 2020).

Due to the large amount of input data and complex computations needed for each GCM-forced hydrodynamic and morphodynamic model to simulate shoreline changes and coastal flooding for the entire coastal extension of Mainland Portugal at high resolution, five specific and representative coastal locations were firstly selected and analysed based on their geomorphological, sedimentological, economic and vulnerability characteristics. These served as reference locations, for the complete application of the described methodology, with the greatest detail possible, generating baseline results. The ability of the hydro- and morphodynamic models to generate local realistic results of coastal erosion and retreat was also evaluated at these reference locations. Upon validation, a set of empirical (and more manageable) methods were employed for the remainder of the coastline, evaluated through comparison with the reference modelling results. These were then used to replicate, with a sufficient approximation degree (validated at the reference locations), the time-consuming modelling efforts, to the entire coast of Mainland Portugal, as efficiently and accurately as possible.

Finally, based on the projections of coastal flooding, coastal erosion and response to extreme events (storm surge and wave run-up), the CVI was computed for each coastal section, enabling the identification of the potential risk zones. Physical and socioeconomic impacts along each risk zone were assessed and evaluated considering each climate change scenario, following the Representative Concentration Pathways (RCPs) 4.5 and 8.5.

This document is organized as follows: in section 2, the study area is defined, along with the five key-locations where the hydro- and morphodynamic models were applied. The datasets used are also defined. In section 3, the detailed methodology of each sub-task is presented. A thorough description of the results is offered in section 4, and conclusions are stated in section 5.

2. Study Area and Datasets

2.1. Study Area

The Portuguese west coast extends approximately in the N-S direction, between the mouth of the Minho river (41°52'N, 8°52'W) on the northern border, and Cape São Vicente (37°01'N, 9°00'W), while the southern coast extends from there to the mouth of the Guadiana river (37°14'N, 7°22'W) on the eastern border (Figure 1), for a total length of about 980 km.

Most Portuguese cities are located along the coastline, and therefore, most of the population. Data from the CENSOS2011 shows that 14% of the national population currently lives within 2 km of the sea (Rocha *et al.*, 2020). In a recent update (CENSOS2021), it was shown that the population living in the Lisboa and Algarve regions increased in comparison with the data from 2011, in 1.7% and 3.7%, respectively. The migratory flux that took place during the last century, from the interior to the littoral, contributed to an unprecedented increase in the population along the Portuguese coast. Presently, according to the National Statistics Institute (INE), the population contrast between the interior, rural areas and the coastal, urbanized ones is peaking, from average densities of approximately 40 hab./km^2 to more than 180 hab./km^2, respectively (2021). Note that the average population density throughout the European Union in 2019 was 109 hab./km^2 (Eurostat).

The Portuguese coastline contains extensive sandy beaches backed by dunes, high cliffs, bays, estuaries, lagoons, natural and artificialized inlets and barrier islands, and it hosts major political decision-making centres, commercial and industrial hubs and employment opportunities. The main economic activities in these areas are related to ports and maritime transport, tourism, leisure, boating, fishing, aquaculture, saliculture, mineral and energy activities. All of these are considered highly strategic activities for the country from the socioeconomic perspective.

Five specific key-locations were selected, after careful consideration of the coastal sectors. The current erosive trend and the imminent risky scenarios, such as overtopping and coastal flooding, together with increasing coastal population at those location justifiy the focused local modelling efforts. Additionally, the five locations benefit from a large field data set (mainly composed of topographic and bathymetric measurements) produced under the scope of the *Programa de Monitorização da Faixa Costeira de Portugal Continental* (COSMO) project (APA). This coastal monitoring information was used as a benchmark to the morphodynamic characterization of the key-locations.

Figure 1 – Study area, Mainland Portugal and its coastlines. The green dots mark que selected key-locations: 1 – Ofir – Praia de Pedrinhas (section 2.1.1), 2 – Costa Nova (section 2.1.2), 3 – Praia de Cova Gala – Praia da Leirosa (section 2.1.3), 4 – São João da Caparica – Fonte da Telha (section 2.1.4), 5 – Praia de Faro (section 2.1.5).

2.1.1. Ofir – Praia de Pedrinhas

This is the northernmost coastal location to be analysed in detail. Located in the northwestern coast of Portugal, it belongs to a wider geographic unit that extends from river Neiva's mouth, in the North, to Apúlia, in the South, following a general N-S orientation and having a linear extension of approximately 13.5 km (Figure 2). This area is particularly vulnerable due to the human occupation along the coastal fringe. This coastal stretch has been subjected to severe erosion and there are areas at high risk due to storm impacts, particularly during the winter. The potential breaching of Cávado sand spit is one of the main threats in this area, making Esposende extremely vulnerable to flooding. This coastal stretch is also experiencing shoreline regression and the decreasing of beach widths, which motivated the construction of structures for coastal defence between the 1970s and the 1990s (Veloso-Gomes *et al.*, 2004). During the winter season, waves are dominant from the NW-W and frequently exceed significant wave heights (H_S) of 6 m (Semedo *et al.*, 2011; Lemos *et al.*, 2019; 2020; 2020b; 2021; Figure 3).

Figure 2 – Aerial view of (before the groin) Praia de Ofir and (after the groin) Praia da Bonança, highlighting human intervention near the coast.

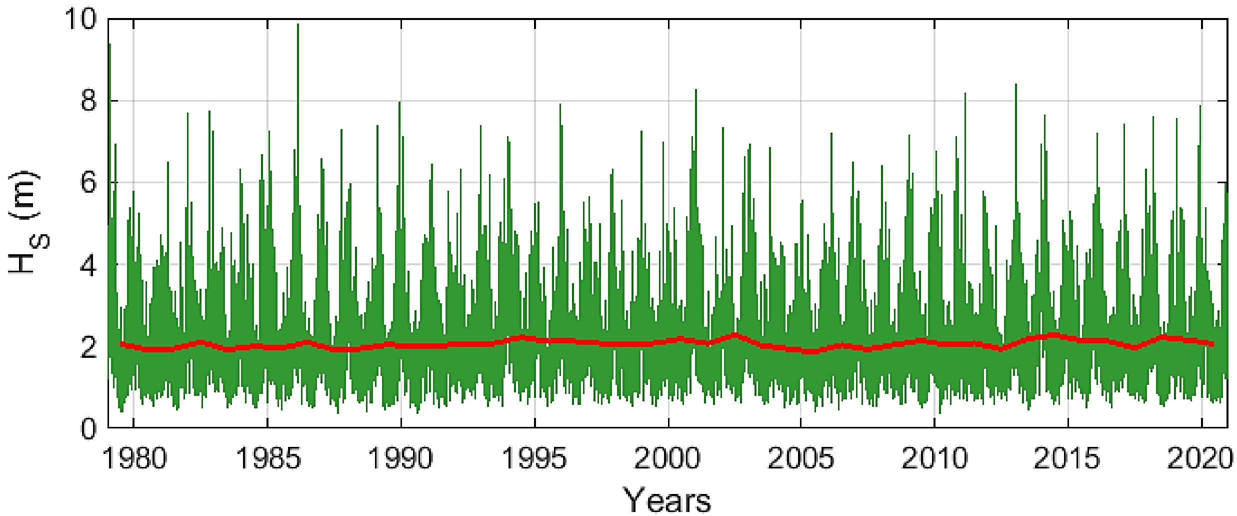

Figure 3 – H_S time-series (green) and annual means (red) for the ERA5 grid-point closer to the Ofir – Praia de Pedrinhas key-location (41.40ºN, 9.00ºW).

2.1.2. Costa Nova

This coastal sector of the central Portuguese western coast is located South of Ria de Aveiro mouth and it is part of its southern barrier (Figure 4). This sandy barrier extends from Mira to Barra and protects the southern arm of the Ria de Aveiro, with extensive agricultural and urbanized occupation. The dune system of Costa Nova is becoming more exposed to wave action due to the increasing erosion of this coastal stretch (Fernández-Fernández *et al.*, 2019). According to Vicente and Clímaco (2015), from 1958 until 2015 the shoreline along the coastal stretch between Costa Nova and Vagueira has retreated approximately 400 m, significantly affecting the coastal communities. Recent assessments suggest, however, that the areas North of the Ria de Aveiro mouth may be experiencing sedimentary accretion due to the new configuration of the jetty (Coelho *et al.*, 2021). In the southern sectors (including Costa Nova), nevertheless, a dominant erosive trend is still detectable, only becoming less severe due to the successive beach nourishments performed by the Aveiro Port Authority (Fernández-Fernández *et al.*, 2019; Bernardo *et al.*, 2020; Pinto *et al.*, 2022), totalizing, since 2010 and until 2021, 7 x 10^6 m^3. Given the measures already taken to reduce the erosive trend, data from APA reports that 75% of the coastal stretch comprising the two sides of the Ria de Aveiro mouth has been stable or under accretion for the last 4 years. Climatologically, similarly to the Ofir – Praia de Pedrinhas location, waves are dominant from the NW-W, presenting recurrent annual H_S maxima above 6 m (Figure 5). Major consequences are related to the subsequent flooding of agricultural lands and urbanized areas.

Figure 4 – Aerial view of Costa Nova, highlighting human intervention near the coast (source: DR).

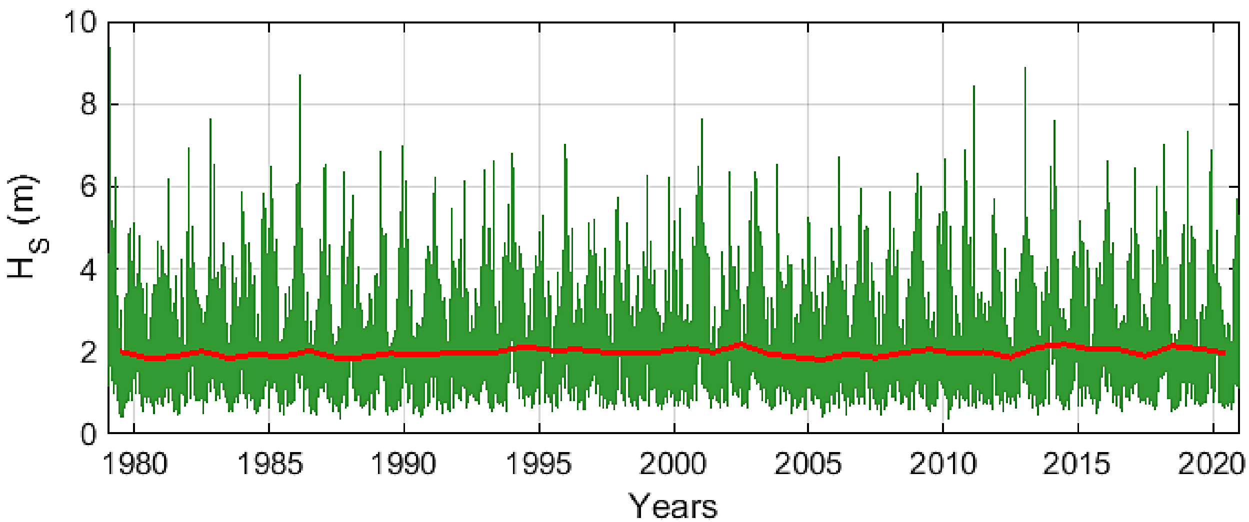

Figure 5 – H_S time-series (green) and annual means (red) for the ERA5 grid-point closer to the Costa Nova key-location (40.68ºN, 9.00ºW).

2.1.3. Praia da Cova Gala – Praia da Leirosa

This sector of the central Portuguese western coast is located South of the Figueira da Foz port and has an extension of approximately 3.5 km (Figure 6). The port was built inside the Mondego River estuary and has caused a great impact in the sediment dynamics along the coastal fringe. While the width of the beaches has increased in the northern sector (except for Praia de Buarcos), in the southern sector (where Cova Gala and Leirosa are located) the erosional potential has increased (Oliveira and Brito, 2015; Nunes and Cordeiro, 2013). Data from APA reports that 82% of the coastal stretch between Cova Gala and Lavos has experienced coastal retreat (from 2018 to 2021), with 66% of it classified as under severe or extreme erosion. The maximum retreat observed was of 42.5 m, with an average annual rate of -4 m/year. A series of cross-shore groynes delineate four sedimentary cells north of Cova Gala, three of which are equally backed by alongshore seawalls. South of the last breakwater, approximately 250 m of exposed geotextile sandbags protect the sand dunes. However, the effectiveness of such coastal structures remains questionable. Similarly to the previous locations, waves are dominant from the NW-W and frequently exceed H_S values of 6 m (Figure 7).

Figure 6 – Aerial view of Praia da Cova Gala, highlighting human intervention near the coast.

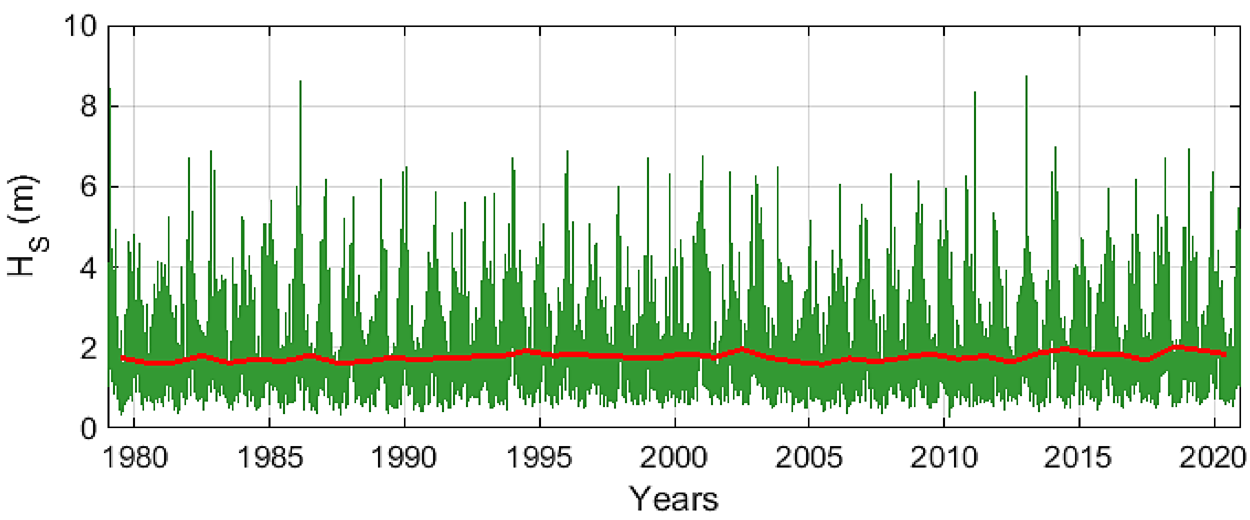

Figure 7 – H_S time-series (green) and annual means (red) for the ERA5 grid-point closer to the Praia de Cova Gala – Praia da Leirosa key-location (39.96ºN, 9.00ºW).

2.1.4. Costa da Caparica

This coastal sector is located South of the Tagus River mouth and is a well-known and densely occupied urban area and touristic resort, benefiting from its proximity to Lisbon. Major coastal planning efforts have been put in place over time to mitigate and to adapt to coastal erosion along the coastal sector, but more intensely on the northern part (S. João da Costa da Caparica; Figure 8). Between 1959 and 1963, three groynes and a longitudinal structure were placed to attenuate erosion on the northernmost part of this coastal stretch (Cova do Vapor). Between 1968 and 1971, seven more groynes were built, and the expansion of the northernmost structures was performed (IHRH, 2003). Also, APA has performed several beach nourishment interventions along this coastal stretch between 2007 and 2019, totalizing 4500000 m^3 and contributing to improve the coastal system robustness (Pinto *et al.*, 2007; 2015; Veloso Gomes *et al.*, 2009). More recently, the ReDuna project, promoted by the Almada Municipality, has been applying nature-based solutions to rehabilitate and dune systems between São João da Caparica and Cova do Vapor, in order to stimulate sediment accretion and increase protection against overtopping and coastal flooding. Nevertheless, in some areas of this coastal stretch, overtopping is still common during winter, especially under stormy weather or extreme swell events, affecting both the physical environment as well as urban areas and their population. Waves are dominant from the W, with H_S values frequently exceeding 4 m during winter, and 6 m about once every two years (Figure 9).

Figure 8 – Aerial view of Praia de São João da Caparica, highlighting human intervention near the coast (source: Cibersul).

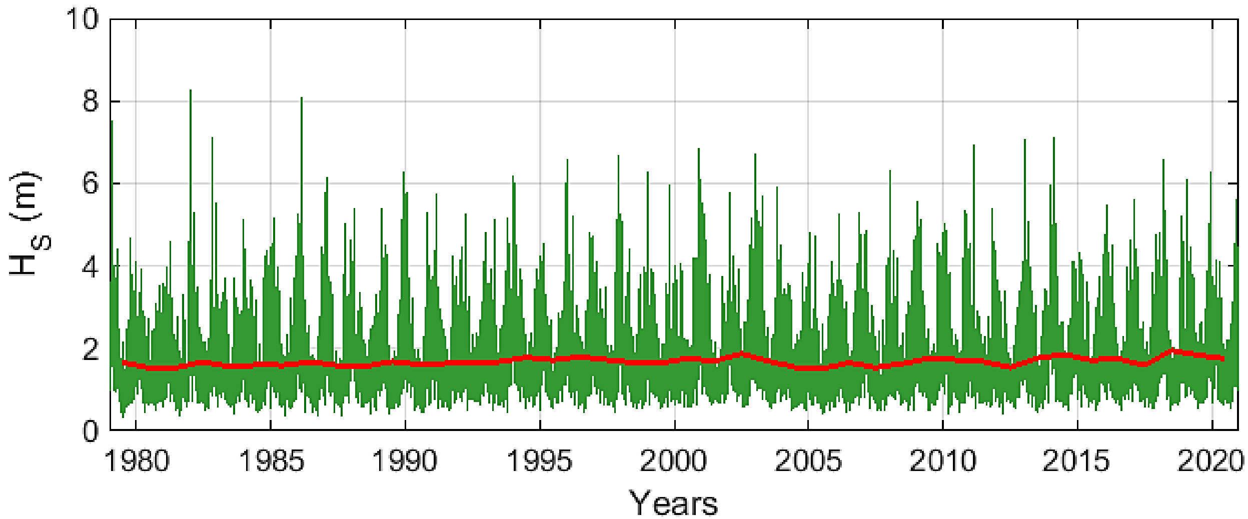

Figure 9 – H_S time-series (green) and annual means (red) for the ERA5 grid-point closer to the São João da Caparica – Fonte da Telha key-location (38.52ºN, 9.36ºW).

2.1.5. Praia de Faro

Praia de Faro is a coastal area in the South of Portugal, close to the city of Praia de Faro. This location is home to a small community of fishermen and used as a recreational area for tourists and locals. The area is a narrow dune strip between the Atlantic and Ria Formosa coastal lagoon, situated between the oceanic shore and the back barrier beach (Figure 10). Praia de Faro is affected by coastal erosion in the long-term, resulting from the impact of storms and human interventions that modify the natural configuration of the area, such as the use of summer houses and trampling paths, crossing the dune (Domingues *et al.*, 2021). In the medium and short-term, considering data from 2018 to 2021, no erosive trend has been detected, mainly due to the artificial beach nourishments conducted westward of Praia de Faro, in 1998, 2006 and 2010, totalizing 2.3 x 10^6 m^3 of sediments (Pinto and Teixeira, 2022). Ria Formosa is a shallow meso-tidal coastal lagoon protected by 2 peninsulas and 5 barrier islands. It is about 55 km long and has a maximum width of about 6 km. The barriers have an ocean beach, dunes and sandy back barrier (or salt marsh). Tidal range is 3.5–4 m on spring tides. Waves are dominant from the W-SW and although generally detaining low to moderate energy, relatively intense storms (with H_S values higher than 3 m) occur during winter (Figure 11), a significant portion of them with SE incoming wave direction (~ 20%; Figure 29).

Figure 10 – Aerial view of Praia de Faro, highlighting human intervention near the coast (source: Nit).

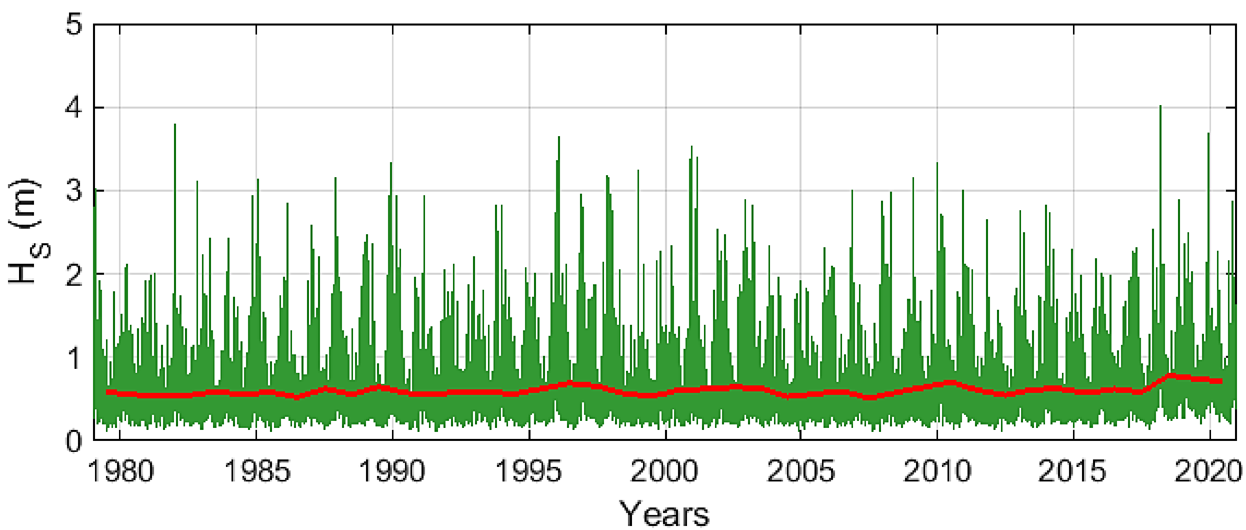

Figure 11 – H_S time-series (green) and annual means (red) for the ERA5 grid-point closer to the Praia de Faro key-location (37.08ºN, 7.92ºW).

2.2. Datasets

In order to fully analyse the impacts of climate change along the coast of Mainland Portugal and assess the vulnerability of the different areas, several datasets were used, comprising information from a number of sectors. The datasets described in the Table 3 were obtained from public domain, and official information sources provided by different national and international institutions (*e.g.*, the Portuguese Environment Agency — APA, the Directorate-General for Territorial Development — DGT, the Hydrographic Institute

— IH, the Military Geospatial Information Centre — CIGeoE, the Statistics Portugal — INE and the European Centre for Medium-Range Weather Forecasts — ECMWF). A geospatial database, built in a Geographic Information System (GIS), was created to store all spatial data (*e.g.*, digital terrain model, bathymetry, hydrographic network), as well as alphanumeric information (*e.g.*, census data), facilitating spatial data harmonization.

Data availability strongly determines the methods to be applied in the vulnerability assessment. The use of state-of-the-art datasets in all analysed fields and the coherence between such datasets is of paramount priority. All spatial data refer to PT-TM06, the national cartographic coordinate system referenced to the European Geodetic Reference System ETRS89. Administrative units were used to address the physical and socioeconomic impacts of climate change in different administrative areas. According to the overall accuracy, these impacts were investigated at national, regional (district or municipality) or local scales (coastal sector in specific municipality or parish, mainly focused in the five selected locations).

2.2.1. Land and ocean surface

The overall study area is described in detail using a digital terrain model obtained both from aero-photogrammetry and using Light Detection and Ranging (LiDAR) technology with enhanced spatial resolution. Additionally, field measurements from the COSMO project were also used (Table 3).

The Digital Terrain Model (DTM) used in this work was obtained from the photogrammetric model provided by the DGT, which resulted from a project ("Quadro do Plano de Ação para o Litoral 2007-2013") in a partnership with APA. The respective aerial photogrammetric survey for the basic cartographic data acquisition along Portugal's mainland coastal area, of approximately 513400 ha, was carried out in 2008 and updated in 2015 with a horizontal resolution of 2 m. In total, approximately 4140 files of elevation points (X, Y, Z) were processed for the coastal DTM generation. Additionally, the digital surface model obtained using LiDAR technology, provided by DGT and as a result of the same project with APA, was used. It covers a coastal strip of 1 km width, including 600 m of nearshore bathymetry with a 2 m horizontal resolution.

In order to improve the computational performance of the DTM processing, six separated geographical coastal sections were considered for the corresponding altimetric grid at 2 m spatial resolution. These sections (Caminha-Espinho, Espinho-Figueira da Foz, Figueira da Foz-Peniche, Peniche-Setúbal, Troia-Odeceixe e Odeceixe-Vila Real de Santo António) are intrinsically related to the territorial divisions proposed by the "Planos de Ordenamento da Orla Costeira" (POOCs) and the more recent "Planos de Programas da Orla Costeira" (POCs), as well as with the five key-locations. This territorial partition is advantageous for the assessment of the results at a local-to-regional scale, but also from the computation perspective, using regional coastal forcing for each of the sections from SLR, tide, storm surge, and wave set-up and run-up.

A positional quality-control procedure was required in the production of flooding cartography, to prevent the possibility of incorrect risk assessments. Photogrammetry, despite being a very efficient and accurate method, is not free of errors. The DTMs were generated from raw data through filtering, by the classification of points into “soil” and “non-soil” and by interpolation, to fill the gaps. More details on the quality control procedure can be found in Antunes *et al.* (2019).

2.2.2. GCMs and wave modelling

In this work, scenario-based GCMs outputs were considered as the primary source of information, needed to obtain the parameters used to assess the SLR and total water level (TWL: SLR plus tides plus storm surge levels) projections, as well as to force the wave and hydro-morphodynamic models. The selection of which GCMs and which GCM data to use is therefore critical, as it conveys the baseline for the remainder of the work. The GCM/RCM outputs considered on this report cover three time-slices, henceforth named as historical (1971-2000), mid-21st century (2041-2070) and late-21st century (2071-2100) projections. Two different future emission scenarios were also considered, namely the RCP4.5 and RCP8.5 (Riahi *et al.*, 2011).

A few studies in recent scientific literature dealt with the problematic of future extreme sea levels along the European coasts. Vousdoukas *et al.* (2017) presented a dataset of extreme storm surge levels (SSLs) and wave climate projections forced by 6 CMIP5 GCMs for the RCP4.5 and RCP8.5 scenarios, with increased horizontal resolution along the European (and therefore Portuguese) coastlines. This ensemble presents a high degree of coherence between the forcing GCMs, the SSLs and wave outputs, which is scarce. The ACCESS1.0, ACCESS1.3, CSIRO-Mk3.6.0, EC-EARTH, GFDL-ESM2G, and GFDL-ESM2M GCMs were used, according to Perez *et al.* (2014), due to their increased performance in reproducing the synoptic climatologies and inter-annual variability across Europe. The SSLs were estimated using the Delft3D-FLOW model (the reader is referred to section 3.2.1.2). GCM simulations are uncoupled to the waves, thus neglecting the atmosphere-wave-atmosphere feedback. Therefore, the associated wave climate simulations were obtained by forcing the third-generation spectral wave model WaveWatchIII (WW3; Tolman, 2002) using state-of-the-art growth/dissipation source terms (ST4 package; Ardhuin *et al.*, 2010). This ST package, based on Bidlot *et al.* (2007), introduced a term for the dissipation of the long swell as a function of the wind, improving the description of the evolution of waves for long distances, with a positive impact on the model performance at a global scale (Ardhuin *et al.*, 2010; Rascle and Ardhuin, 2013). The horizontal resolution for the southwestern Europe domain is 0.5º. These outputs were compared with the ERA-Interim reanalysis to correct systematic biases in the wave and storm surge projections generated from each GCM (Vousdoukas *et al.*, 2016a).

2.2.2.1. Overcoming challenges

Given the very limited existence of comprehensive and coherent wave and SSL datasets, the number of ensemble members used to force the hydrodynamic models with TWL derived from the referred data was reduced, when compared to the overall available GCM data used, for example, to compute de SLR, or wave data at a global scale (Table 1). Given the absence of RCM-forced wave climate simulations/projections for the Portuguese coastal areas, it was possible to propagate offshore GCM-driven waves to the coast using the spectral wave model SWAN (the reader is referred to section 3.2.1.2). Near the beach, it was then possible to manually compute the TWL and its cumulative density function (CDF), by adding to the SLR values, the local projected tides (Antunes *et al.*, 2007) as well as the projected SSLs from Vousdoukas *et al.* (2017) (the reader is referred to sections 3.1.2.1, 3.1.2.2, and 3.1.2.3). It is relevant to mention that these computations were clearly beyond the project commitments. Nevertheless, they constituted the most coherent approach possible, in order to produce accurate and consistent results.

Wave climate projections are produced using wave models, forced by GCM outputs, such as U_{10}, U_{10D}, $MSLP$ and sea-ice cover. These are computational- and time-costly simulations, which need to be produced by specialists in the area. Therefore, the number of available wave climate projections, in comparison to the number of direct GCM outputs, is very limited. Considering the RCP2.6 climate scenario, there are currently no dynamic wave climate (as well as TWL) projections covering the Portuguese coastal areas available in scientific literature. There is, however, one study that focuses on the RCP2.6 scenario using statistical wave climate projections and a downscaling method for Europe (Pérez *et al.*, 2015). This study concludes that the overall RCP2.6 projections, for H_S, T_m and wave energy flux (P_w) are of lower magnitude, when compared with the RCP4.5 and RCP8.5. In another study, Camus *et al.* (2014), RCP2.6 projections are presented for two locations, one near Ireland, and another offshore of Galicia, Spain. These are consistent with the ones from Pérez *et al.*, (2015). Considering the results from both studies and the relationship between the RCP2.6 and other scenarios, it would be reasonable to assume that the projections under RCP2.6 should be of lower magnitude when compared with the remaining scenarios, both in terms of shoreline retreat and overall extreme coastal flooding.

The strategies presented in this section were considered by the authors as best-practice to deal with the challenges found while conducting the work. Although beyond project commitments, such approaches were required to produce rigorous results.

Table 1 – Summary of the GCMs available to provide relevant climate parameters for the historical and three future experiments (RCP2.6, RCP4.5, and RCP8.5). For the different climate scenarios, the symbol ✓ indicates the availability of SLR, SSL and wave parameters, while the symbols ☁, SLR and ~ indicate the availability of solely SSL, SLR and wave parameters, respectively. The symbol x indicates data unavailability.

GCM (RCM)	Institute	RCP2.6	RCP4.5	RCP8.5
ACCESS1.0	Commonwealth Scientific and Industrial Research Organisation – Bureau of Meteorology (Australia)	x	✓	✓
ACCESS1.3	Commonwealth Scientific and Industrial Research Organisation – Bureau of Meteorology (Australia)	x	~ ☁	~ ☁
BCC-CSM1.1	Beijing Climate Centre (China)	SLR	SLR	SLR
CanESM2	Canadian Centre for Climate Modelling and Analysis (Canada)	x	SLR	SLR
CNRM-CM5	Centre National de Recherches Météorologiques (France)	x	SLR	SLR
CSIRO-Mk3.6.0	Commonwealth Scientific and Industrial Research Organisation - Queensland Climate Change Centre of Excellence (Australia)	SLR	✓	✓
EC-EARTH	EC-EARTH consortium	x	~ ☁	~ ☁
EC-EARTH (HIRHAM5)	EC-EARTH consortium	x	SLR	SLR
GFDL-ESM2G	NOAA Geophysical Fluid Dynamics Laboratory (USA)	SLR	✓	✓
GFDL-ESM2M	NOAA Geophysical Fluid Dynamics Laboratory (USA)	SLR	✓	✓
GISS-E2-R	NOAA Geophysical Fluid Dynamics Laboratory (USA)	SLR	SLR	SLR
HadGEM2-CC	Met Office Hadley Centre (UK)	x	SLR	SLR
HadGEM2-ES	Met Office Hadley Centre (UK)	SLR	SLR	SLR
IPSL-CM5A-LR	Institut Pierre-Simon Laplace (France)	SLR	SLR	SLR
IPSL-CM5A-MR	Institut Pierre-Simon Laplace (France)	SLR	SLR	SLR
INMCM4	Institute for Numerical Mathematics (Russia)	x	SLR	SLR
MIROC-ESM	Agency for Marine-Earth Science and Technology (Japan)	SLR	SLR	SLR

MIROC-ESM-CHEM	Agency for Marine-Earth Science and Technology (Japan)	SLR	SLR	SLR
MIROC5	Agency for Marine-Earth Science and Technology (Japan)	SLR	SLR	SLR
MPI-ESM-LR	Max Planck Institute (Germany)	SLR	SLR	SLR
MPI-ESM-MR	Max Planck Institute (Germany)	SLR	SLR	SLR
MRI-CGCM3	Meteorological Research Institute (Japan)	SLR	SLR	SLR
NorESM1-M	University Corporation for Atmospheric Research (USA)	SLR	SLR	SLR
NorESM1-ME	University Corporation for Atmospheric Research (USA)	SLR	SLR	SLR

2.2.3. Reference data

2.3.3.1. ERA5 reanalysis

The ERA5 (where “ERA” stands for “ECMWF reanalysis”) is the most recent ECMWF reanalysis (Hersbach *et al.*, 2020). It is produced within the Copernicus Climate Change Service (C3S), replacing the previous ECMWF’s reanalysis, the ERA-Interim (Dee *et al.*, 2011), since 2019. The ERA5 provides a detailed record of the global atmosphere, land surface and ocean waves, from 1950 onwards.

ERA5 presents several improvements in model physics, core dynamics and data assimilation, when compared with ERA-Interim, and a considerable increase in horizontal, vertical (model levels) and time resolutions. The horizontal resolution of ERA-5 is 0.25º (31 km) for the atmosphere and 0.36º (40 km) for the waves, being the time resolution 1-hour. The ERA-5 continues to be extended in almost real-time using the ECMWF Integrated Forecast System (IFS) Cy41r2 (ECMWF, 2016), used operationally for forecasting from March to November 2016.

Hourly assimilation of altimeter wave data is carried out in ERA5. Starting from 1991, ERA5 has assimilated data from most missions, except GEOSAT, TOPEX, SENTINEL-3A and B, and JASON-3. The scheme used is a simple Optimum Interpolation scheme that updates hourly the wave fields in the last forward integration (trajectory) of the atmospheric 4-dimensional variational (4D-Var) analysis system. Therefore, ERA5 data are fully synchronous in time with real-world observations.

The ERA5 data are freely available from the Copernicus Climate Data Store (https://cds.climate.copernicus.eu/cdsapp#!/home). In this work, TWL and wave data from the ERA5 were used as reference to evaluate the performance of the hydro-morphodynamic models in simulating real storm events (extreme events) that took place during the present climate period, starting in 1971.

2.3.3.2. In-situ buoy observations

In-situ buoy observations were used near the five key-locations to assess the performance of the ERA5 reanalysis in depicting the H_S, T_m and MWD climate, considering the available observational periods. Despite being a reanalysis, built using advanced assimilation methods based on *in-situ* observations and satellite altimetry measurements, the ERA5 is not able to capture local phenomena as accurately as the buoys. Therefore, to promote a more correct representation of local features, such as changes in MWD driven by nearshore bathymetry, *in-situ* wave observations were used to correct the ERA5, using a quantile mapping bias correction methodology (the reader is referred to section 3.1.1).

In a later stage of the work, buoy observations were also used to correct the large-scale wave climate projections used in the transfer functions for the national scale vulnerability assessment. Given that the wave propagation to the coast at the five key-locations is only valid in a small area, due to the local bathymetry, and that ERA5 is not able to fully capture the wave characteristics at the coast, the offshore wave climate projections from the 6-member ensemble presented in section 2.2.2 and Table 1 were also corrected using *in-situ* wave observations.

Six buoys were used in the present assessment. These correspond to the Leixões buoy (IH), Costa Nova buoy (RAIA project), Cova Gala buoy (IH), Lisbon buoy ("Administação do Porto de Lisboa"; APL), Sines buoy (IH) and Faro buoy (IH). The geographical location and time period covered by each buoy can be found in Table 2.

Table 2 – Details regarding the *in-situ* buoy observations.

Buoy	**Institution**	**Latitude (º)**	**Longitude (º)**	**Period**
Leixões	IH	41.32ºN	8.98ºW	28-07-1993 – 05-04-2018
Costa Nova	RAIA project	41.15ºN	9.58ºW	23-10-2010 – 19-03-2020
Cova Gala	IH	40.13ºN	8.90ºW	06-07-1984 – 05-02-1996
Lisboa	APL	38.62ºN	9.38ºW	31-07-2005 – 27-06-2011
Sines	IH	37.92ºN	8.93ºW	01-01-1990 – 31-12-2011
Faro	IH	36.90ºN	7.88ºW	19-03-2009 – 05-04-2018

Table 3 – Summary of datasets required for the coastal vulnerability assessment.

Data Type		**Data source**	**Spatial Res.**	**Time Res.**	**Coordinate System**	**Observations**
Digital Terrain Model (DTM)	Aero-photogrammetric	DGT, 2015	2 m	N/A	PT-TM06 / ETRS89	Digital Terrain Model of Portugal's Coastal Zones.
	LiDAR	DGT, 2011	2 m	N/A	PT-TM06 / ETRS89	600 m bathymetry cover and 400 m on land.
Administrative Units	CAOP 2020	DGT, 2021	Scale: 1:25000	N/A	PT-TM06 / ETRS89	Delimitation and demarcation of the country's administrative circumscriptions.
	Statistical Subsection	INE, 2011	Scale: 1:10000	N/A	PT-TM06 / ETRS89	Territorial unit that identifies the smallest homogeneous area of construction or not, existing within the statistical section.
	POOC	APA	N/A	N/A	PT-TM06 / ETRS89	Delimitation of coastal protection zones along the Portuguese coast (500 m inland down to 30 m depth).
Wave variables	H_S, mean wave period (T_m), peak wave period (T_p) and mean wave direction (MWD)	WW3 wave model forced by CMIP5 GCMs	Coastal locations (~ 0.5º grid)	6 hours	N/A	Availability: Historical (1971-2005) and future (2006-2100), under RCP4.5 and RCP8.5
		ERA5 reanalysis	0.36º grid	1 hour	N/A	Availability: ERA5: 1950 onwards
		Buoy data	5 buoys on the coast	Hourly based	N/A	Leixões Costa Nova Cova Gala Lisboa Sines Faro
Coastal Flooding	Tide	FCUL, 2015	Regional	1 hour	Mean sea level	N/A
	Sea Surface Height	CMIP5 GCMs	1º grid	Monthly	N/A	Availability: Historical (1971-2005) and future (2006-2100), under RCP2.6, RCP4.5, RCP8.5.

	Storm Surge	LISCOAST project / FCUL, 2015	Coastal locations	6 hours	N/A	N/A
	Wave run-up	XBeach model	Key-locations	N/A	N/A	N/A
	Wave set-up	XBeach model	Key-locations	N/A	N/A	N/A
Coastal Erosion	Sedimentological & geomorphological characterization	Coastal sediment budget evaluation	Each coastal sedimentary cell	N/A	N/A	Based on GTL (Santos *et al.*, 2014)
	Coastal erosion model	ShorelineS	50-100 m	Yearly	PT-TM06 / ETRS89	Wave parameters (H_S, T_p and MWD)
	Hydro- and morphodynamic model	SWAN (Delft3D-Wave) and XBeach	2-10 m	Exreme events	PT-TM06 / ETRS89	Storm impact: Total water levels (SLR, tide, storm-surge, wave set-up and run-up)
Physical	Hydrographic Network	CiGeoE, 2016	Scale: 1:250000	N/A	WGS84	N/A
	Coastline	IH, 2011	Scale: 1:250000	N/A	WGS84	The World Vector Shoreline (WVS) / DTM 2008-2015
	Lithological Chart	APA, 2015	Scale: 1:1000000	N/A	Esri code: 20790	Vector format, referring to Charter I.13 of the Atlas of the Environment (physical environment).
	Coastal Defence	APA, 2020	N/A	N/A	Esri code: 102164	Location and Characterization of coastal structures.
	Land Use [COS2018]	DGT, 2019	20 m	N/A	PT-TM06 / ETRS89	Cartography with a defined minimum cartographic unit (1 ha) with a distance between lines greater than or equal to 20 m.
Socioeconomic	Population	INE, 2021	N/A	N/A	N/A	CENSOS2021
	Infrastructures	Municipality	N/A	N/A	PT-TM06 / ETRS89	Requested at each key-location's municipality.

		OpenStreetMap	N/A	N/A	WGS84	To complement the official information from each municipality.
	Communication routes	Municipality	N/A	N/A	PT-TM06 / ETRS89	Requested at each key-location’s municipality.
		OpenStreetMap	N/A	N/A	WGS84	To complement the official information from each municipality.
	Ecological Areas	ICNF, 2017	N/A	N/A	PT-TM06 / ETRS89	SNAC – National System of Classified Areas.
	Property value	Decree-Law no. 287/2003, of November 12th.	N/A	N/A	N/A	Possibly based on CIMI – Municipal Property Tax Code.

3. Methodology

3.1. General Overview

The conceptual framework of the coastal impact assessment relied on a set of CMIP5 GCM projections, as in Table 1 and Table 3. These provided the necessary forcing to the EURO-CORDEX RCM multi-model ensemble (a dynamical downscaling experiment of the coarse-gridded GCMs), and to wave models that generate wave climate simulations and projections for several parameters (*e.g.*, H_S, T_m, T_p, MWD). Figure 12 summarizes the adopted framework for the assessment of physical and socioeconomic impacts driven by climate change on the coastal risk zones for the 2041-2070 and 2071-2100 future reference periods.

Numerical hydro-morphodynamic and wave modelling relied, to the maximum possible extent, on field data (*e.g.*, grain-size information and information on historical events and patterns), and on reference datasets, such as the ERA5 reanalysis and the Portuguese tide gauge network. To model such a complex natural setting, with an almost countless number of variables, an approach validated by reference data was crucial to increase our confidence in the results. An extensive evaluation process was carried out, first along the five key-locations (please refer to section 2.1), and later along the chosen coastal sections (please refer to section 3.2.2), before employing the methodology at a national scale.

The time and computational-costly downscaling modelling using the SWAN (Delft3D-Wave) and XBeach models (please refer to sections 3.2.1.2 and 3.2.1.3) was first carried out along the five key-locations. Using these results, semi-empirical models were generated and validated for each coastal section along Mainland Portugal's coast. This simplification was needed since it would not be possible to perform such a detailed assessment along the entire coastline with the enhanced horizontal resolution used at the key-locations. Such semi-empirical Parametric Coastal Retreat (PCR) models, developed by the FCUL team, will also be useful for future national and international assessments of coastal vulnerability.

The final results consist of a large set of Coastal Vulnerability Index (CVI) cartography, obtained through the combination of the Extreme Flood Hazard Index (EFHI) and the Physical Susceptibility Index (PSI), which translate the hazard, as represented by the external forcing on the coast, by the influence of SLR, tides, storm surges and waves, and the physical susceptibility of the coast, as represented by its topographic features (the digital terrain model – DTM). The combination of those two types of data, for the entirety of the Portuguese coastline, implied the use of Geographical Information System (GIS) tools.

3.1.1. Wave bias correction

Modelling efforts exhibit systematic errors (biases) when compared to observations or reanalyses and hindcasts. These arise from simplified physics or numerical parameterizations within the models (Rocheta *et al.*, 2017), which can be inherited in downscaling processes or in offline modelling. Biases in GCMs have been a concerning issue, especially in the past two decades, for both CMIP3 (van Ulden and van Oldenborgh, 2006; Vial and Osborn, 2012) and CMIP5 (Brands *et al.*, 2013; Jury *et al.*, 2015; Maraun *et al.*, 2017) climate simulations. Attempting to correct these systematic errors, bias correction (BC) methodologies have become a standard procedure in climate change studies. These post-processing tools aim to improve the model agreement with reference data (*e.g.*, observations, reanalyses, hindcasts), assuming that the bias behaviour does not change in time (*i.e.*, the bias remains stationary between historical simulations and future projections; Haerter *et al.*, 2011). The main purpose of BC is to promote greater consistency between the reference and simulated climates.

Here, two bias correction methods, namely the Empirical Gumbel Quantile Mapping (EGQM) and the Empirical Quantile Mapping (EQM), were applied to the wave climate simulations and projections, following Lemos *et al.* (2020a) and Lemos *et al.* (2020b), in an attempt to better characterize the local wave climate features at each of the five key-locations. On a first stage, the entire ERA5 reanalysed period (1971-2020), propagated from offshore to the buoy locations, was corrected, for H_S, T_m, T_p (EGQM) and MWD (EQM), using observed information from each of the five buoys. Then, the ERA5 reanalysis, propagated towards the coast (until approximately 20 m depth) was used to correct the (also propagated) wave climate simulations, both during present and future projected periods. Additional information regarding the propagation method can be found in section 3.2.1.2.

The EGQM method consists of correcting a simulated empirical cumulative distribution function (ECDF; Wilks, 1995), by adding a correction term to each individual (pre-selected) quantile. The quantiles where this correction term is applied are defined by a standard Gumbel distribution (SGD; Gumbel, 1934), with a better representation of the upper tail of the distribution. This method was used to correct the H_S, T_m and T_p parameters, during 1971-2020 for ERA5, and 1971-2000, 2041-2070 and 2071-2100 (under RCP4.5 and RCP8.5) for the 6-member ensemble of wave climate simulations and projections. A set of $n_q = 20$ quantiles was selected for the application of the EGQM method, following a SGD, being the first and last ones the 1st and the 99.999th quantiles, respectively, where 11 of the 20 selected quantiles are above the 99th one, focusing on the correction of the extreme values, where the higher biases are usually found.

The correction term corresponds to the difference between the inverse ECDFs of the reference data ($ECDF^{REF^{-1}}$), here being the buoy observations, for the correction of ERA5 at the buoy locations, and the

ERA5 itself, for the correction of the 6-member ensemble near the coast, and the inverse ECDFs of the simulated data ($ECDF^{SIM^{-1}}$), here being the ERA5 at the buoy locations and the 6-member ensemble near the coast. This difference is calculated and applied at each at selected quantile, such as in Eqs. (1) and (2):

$$X(q_i) = ECDF^{REF^{-1}}(q_i) - ECDF^{SIM^{-1}}(q_i), i = 1, \dots, n_q, \quad (1)$$

$$SIM^C(q_i) = SIM(q_i) + X(q_i), i = 1, \dots, n_q, \quad (2)$$

… where SIM is the original wave parameter simulation and SIM^C is the bias corrected one, at each selected quantile. The correction terms were linearly interpolated between the selected quantiles, and all data outside the defined quantile range was extrapolated using the same correction terms found for the first and last selected quantiles.

A simplified version of the EGQM, the EQM, method, was used to correct the simulated MWD, since this is a circular parameter. All MWD data were transformed into zonal (u) and meridional (v) components, being each one corrected individually. For the EQM method, a linearly spaced set of quantiles was chosen, from the 1st to the 99th quantile ($n_q = 99$). The implementation then followed the EGQM method, by solving Eqs. (1) and (2). The bias corrected u and v components were finally used to reconstruct the bias corrected MWD parameter.

3.1.2. Coastal flood hazard

The present work used the probabilistic approach, rather than a deterministic approach, based on Antunes *et al.* (2019). The reason why a probabilistic approach was applied to produce cartography is that the generated hazard maps serve to combine physical susceptibility and socioeconomic exposure maps to produce coastal risk maps on a standardized basis with three risk classes from 1 (low) to 3 (high). Moreover, this approach also allowed to reveal the most likely areas to be flooded, which is important for territory management and planning concerning climate adaptation. Through the probabilistic combination of each extreme coastal flooding component (SLR, tide, storm surge, wave set-up and wave run-up), the flood hazard probability was obtained. This probabilistic representation relied on multi-parameter combined CDFs and shown using different hazard levels related to extreme flooding, achieved over a given coastal DTM with a 2 m resolution (Figure 12). Given the climate-change-driven forcing on the coastal topography, the DTM was modified (especially along the sandy coastal sections) by morphodynamic modelling (please refer to section 3.2.1.1) due to shoreline retreat.

As mentioned, the assessment of the coastal flood hazard, and, finally, of the coastal vulnerability, depends on several components. These, and the methodologies needed for their computation and analysis, are described below.

3.1.2.1. Sea level rise (SLR)

It is estimated that, since the 19th century, the sea level has already risen approximately 20 cm (Nerem *et al.*, 2010; Church *et al.*, 2011; Hay *et al.*, 2015; Sweet *et al.*, 2017; IPCC, 2022). Although there is a very low rate of regional uplifting (Cabral, 1995; Figueiredo *et al.*, 2014), the SLR along the Portuguese coastlines is in line with the global mean values, showing a slow but progressive response to global warming. Two sources of SLR can be identified: the first, due to the ocean's thermal expansion related to the increasing temperature, and the second, due to the increase in the global amount of liquid water resulting from the melting of both the Arctic and Antarctic ice caps, and continental glaciers. Recent data has shown that since the beginning of the 21st century, the contribution of the melting of the ice caps to the SLR surpassed the thermal expansion (Sweet *et al.*, 2017; Leuliette and Scharroo, 2010; Johnson and Chambers, 2013; Roemmich and Gilson, 2009; Watkins *et al.*, 2015).

The SLR projections were obtained from the CMIP5 GCMs outputs, through the sea surface height (SSH) parameter (Table 1 and Table 3). Following Church *et al.* (2013) the global average of SSH from each GCM is forced to be the global thermal expansion, obtained by subtracting the globally averaged regional SSH field at each time step from each grid box, and then adding the global thermal expansion time-series to each grid box (a single global value, at a given time step). Additionally, SLR projections comprise information from several geophysical sources that drive long-term changes in SSH, such as the ice components (Greenland and Antarctic dynamic ice and surface mass balance, and glaciers), land water storage and glacial isostatic adjustment (GIA).

The complete SLR dataset includes simulations from 4 GCMs for the historical period, and 16, 22 and 22 GCMs for the RCP2.6, RCP4.5 and RCP8.5 future periods, respectively. The methodology used to extract relevant information from this dataset, using a CDF at each coastal section, is detailed in section 3.3.1.

3.1.2.2. Tides

Tides are dominated by astronomical forcing, such as the influence of the Sun and the Moon, and, to a smaller extent, by atmospheric forcing, due to the winds and changes in the air pressure (for more information, the reader is referred to section 3.1.2.3). Tides vary on timescales ranging from hours to years due to a number of factors, which determine the lunitidal interval. To generate accurate records, tide gauges (TGs) at fixed locations measure water level over time. Gauges ignore variations caused by wind waves with periods shorter than minutes, however, the records are influenced by infragravity waves with periods of couple to tens of minutes and storm surge waves.

Portuguese long tide time-series are only available for the Cascais and Lagos TG, under the responsibility of the DGT. For the rest of the country, except for the Leixões harbour (North), the tides have only been observed for short periods of a few years up to two decades in the TGs under the responsibility of the Portuguese Hydrographic Institute (IH).

All tidal data, by convention, are referred to the vertical reference used in hydrography, the chart datum (CD), defined in Portugal as the lowest low-tide (minimum low water) observed during a period longer than 19 years (the Moon's 18.6-year nodal period), plus an additional safety margin (one foot). For all Portuguese tide ports, the CD is 2.00 m relative to the national vertical reference, the 1938 Cascais Vertical Datum (CASCAIS1938), except for the Tagus River estuary, where the CD is 2.08 m. The CD was removed from the hydrographic tide heights to obtain the tide elevation, which corresponds to the tide orthometric height relative to the national vertical reference of CASCAIS1938.

To accurately project tides into the future, numerical modelling was employed, based on harmonic analysis considering long time-series of tidal observations. Local tide simulations and projections, generated using models based on the national tide gauge (TG) network data, are available at Faculdade de Ciências da Universidade de Lisboa (FCUL). These employ state-of-the-art harmonic analysis (Antunes, 2007). Through the harmonic tide models, a long-term-based CDF was generated for each coastal key-location and coastal section (the reader is referred to section 2.2.1).

3.1.2.3. Storm surge

The storm surge (SS) is the abnormal water level rise above the predicted astronomical tides, caused by meteorological forcing due to storm events, through the joint effect of a lower atmospheric pressure, with an approximated ratio of −1 cm/hPa, and the persistent effect of wind friction on the sea surface, depending on its direction and intensity. The SS, as a tide level disturbance, is usually positive, but it can also be negative when high atmospheric pressure occurs, ranging from a few centimetres to several meters, and lasting from a few hours to more than a day.

In Portugal, according to Vieira *et al.* (2012), based on the analysis of tide gauge data series from 1960 to 2010, the maximum observed storm surge along the west coast of Portugal's mainland exhibited average values ranging from 50 to 70 cm for the different TGs, and maximum values of 80 cm to 1 m for long return periods (100 years or more). The maximum value detected by harmonic analysis was 82 cm in the Viana do Castelo TG on October 15, 1987, and 83 cm in the Lagos TG on March 4, 2013. In the latter, such a magnitude is only explained by the additional wave set-up effect due to the TG location and the SW wave direction of the storm event.

The storm surge component can be calculated using models, such as the Delft3D-FLOW (please refer to the section 3.2.1.2) or the GTSM (please refer to section 2.2.2), or using semi-empirical formulas (WMO, 2011). For the local scale assessment across the five key-locations, the SSL series described in section 2.2.2 were used to manually compute the TWL. Extreme events selected from these time-series integrated the future projected extreme TWL scenarios. For the national scale assessment, a statistical analysis based on long storm surge return periods based on the SSLs series was conducted using a Generalized Extreme Value (GEV) distribution for both the historical simulations and future projections. The 4-, 10-, 25- and 100-year return levels were then used to manually compute the TWL ones. Note that the original SSL simulations and projections were corrected considering the biases found in comparison with the measurements from the Cascais TG during the historical climate, using a simple "delta" method (Hay *et al.*, 2000), consisting of homogeneously adjusting the SSL simulated distributions by adding the mean difference between the Cascais TG measurements and the original SSL simulations. The same correction terms were applied to the future SSL projections.

3.1.2.4. Wave set-up and run-up

Due to extreme atmospheric events, besides storm surge effects, high energy ocean waves forced by storm events induce coastal set-up and run-up levels that additionally raise the sea level nearshore, which reinforces the coastal flooding level. The wave run-up is the sum of wave set-up and swash uprush (upwards propagation of bores formed after wave breaking over the beach). Therefore, sea level extremes are also influenced by settling effects resulting either from waves in coastal breaking zones or from strong winds, particularly in inland waters and sheltered locations in the absence of swell waves. Thus, to estimate sea surface extreme values near the coast, the wave set-up and run-up was also considered. Coastal wave set-up and run-up were computed using the XBeach model forced by TWL plus waves time-series during the considered periods, along the five key-locations (please refer to section 3.2.1.2) and using one dimensional (1D) equations for the total run-up through semi-empirical methods, to calculate the overtopping over the longitudinal adherent structures across the entire coastal range (the reader is referred to section 3.3.2).

For the PCR algorithm, the determination of the total wave set-up and run-up levels (TWRup) followed Antunes (2014) and Antunes *et al.* (2019), by adding to the TWL (SLR plus tide plus storm surge) the sum of the set-up and the incident run-up. The set-up (S_o) is composed by two components, the static ($\bar{\eta}$) and the dynamic ($\hat{\eta}$), being computed following Eq. (3):

$$\boldsymbol{S_o = \bar{\eta} + \hat{\eta}} \tag{3}$$

… where the static component is given by Eq. (4):

$$\bar{\eta} = 0.189H_S \tag{4}$$

… and the dynamic component is defined by the combination of the standard deviation of the set-up oscillation, σ_1, and the standard deviation of incident run-up, σ_2, as in Eq. (5):

$$\hat{\eta} = 2.0\sqrt{\sigma_1^2 + \sigma_2^2} \tag{5}$$

… with…

$$\sigma_1 = 0.3\frac{mH_S}{\sqrt{2\pi H_S/gT_m}} \tag{6}$$

… and…

$$\sigma_2 = 2.7\left(\frac{H_S}{26.2}\right)^{0.8}\left(\frac{T_m}{20.0}\right)^{0.4}3^{0.16}\left(\frac{m}{0.01}\right)^{0.2} \tag{7}$$

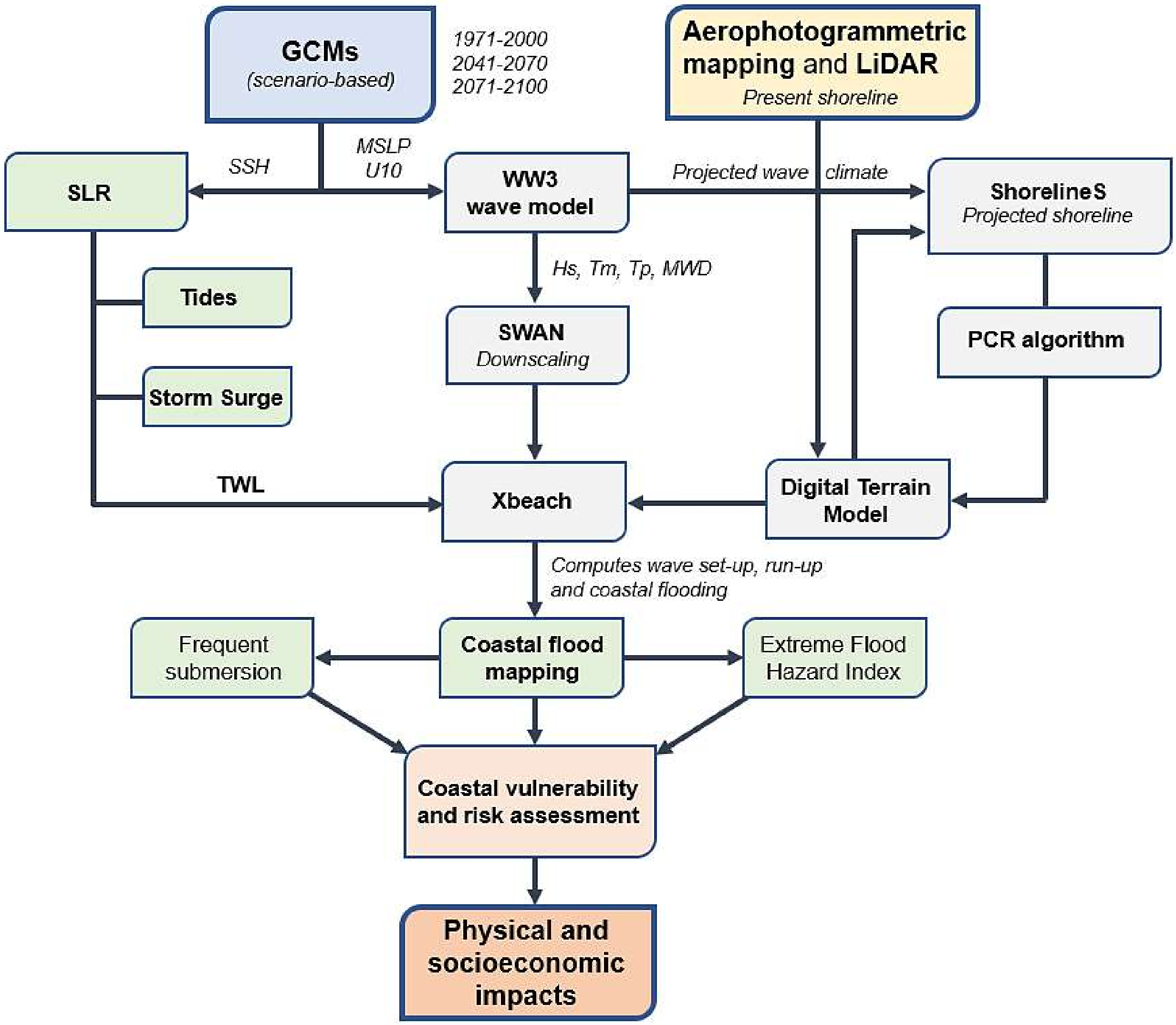

Figure 12 – Coastal impact assessment framework for each climate change scenario, considering the 1971-2000 historical and 2041-2070 and 2071-2100 future reference periods applied at the five key-locations used as reference.

3.2. Coastal Erosion and Flood Hazard

The modelling approach to assess future scenarios of coastal erosion consisted of first analysing the coastal sedimentary budget on each coastal section and identifying the main sources and sinks to be accounted for shoreline evolution (GTL report, Santos *et al.*, 2014), forced by wave parameters, using a shoreline evolution model (ShorelineS; the reader is referred to section 3.2.1). The aim was to produce results with enhanced spatial resolution, under 10 m on land, and to extend them offshore until reaching a bedrock outcrop, an anthropogenic structure or depth of closure. The definition of horizontal extension constraints was assessed locally at each key-location.

The Digital Terrain Models (DTMs) for the present climate period were based on the European Marine Observation and Data Network (EmodNET), Copernicus Programme, the Planning and Management of Coastal Zones Programme of Portugal – with vertical datum adjusted to mean sea level at the Cascais TG, and LiDAR data, providing an accurate elevation surface for sea-land transition areas. The evaluation of the modelled shoreline evolution during present climate, subjected to climate forcing, consisted of comparison with recent shoreline data. The historical time-slice defined for climate change assessment (1971-2000) was not considered here, since shoreline data is not available for most of its period (the evaluation is therefore conducted for the 2008-2018 period).

The future projected shoreline, obtained with the application of the ShorelineS, together with an equilibrium coastal profile, resulted in a new coastal topo-bathymetric configuration, generated by the PCR algorithm applied with 1D approach to each individual topo-bathymetric profile. The resulting DTM was then used as input to the XBeach numerical model, to assess the impact of future extreme events on this projected shoreline. Overall, the modelling approach consisted of first propagating the wave conditions towards the coast, using the SWAN (Delft3D-Wave) hydrodynamic model, and then locally assessing the impact of the extreme wave events and TWL onshore using the XBeach model, allowing to obtain projected wave set-up and run-up, and the consequent overtopping and flooding.

3.2.1. Hydro- and morpho-dynamic modelling

To model the coastal geomorphological response to wave regime and overtopping under extreme events, a sedimentary budget analysis was firstly performed for each study area (mainly based in Santos *et al.*, 2014), in order to evaluate the main processes driving coastline evolution and identify sedimentary sources and sinks for modelling the long-term coastal evolution. The particular dynamics affecting each coastal area, as well as the distinct geomorphological configurations, can lead to different approaches on coastline evolution modelling. Some of the most complex areas correspond to highly artificialized coastal stretches, where strong coastal sedimentary imbalances were identified, and barrier islands (as in the Praia de Faro key-location, in section 2.1.5) that can experience rollover mechanisms (landward migration) in response to SLR.

The shoreline evolution modelling was performed for each key-location, considering the sediment budget analysis for the different future time periods and scenarios. Boundary forcing conditions consisted of SLR and wave climate projections from GCM-forced outputs (the reader is referred to section 2.2.2). The projected shoreline was used to reconstruct the DTMs at each key-location, to assess the impact of future expected extreme wave conditions along the “new” coastal configuration (Figure 13). The results from the shoreline evolution at each of the key-locations were then used to define a semi-empirical shoreline model, applied to all coastal areas throughout Mainland Portugal.

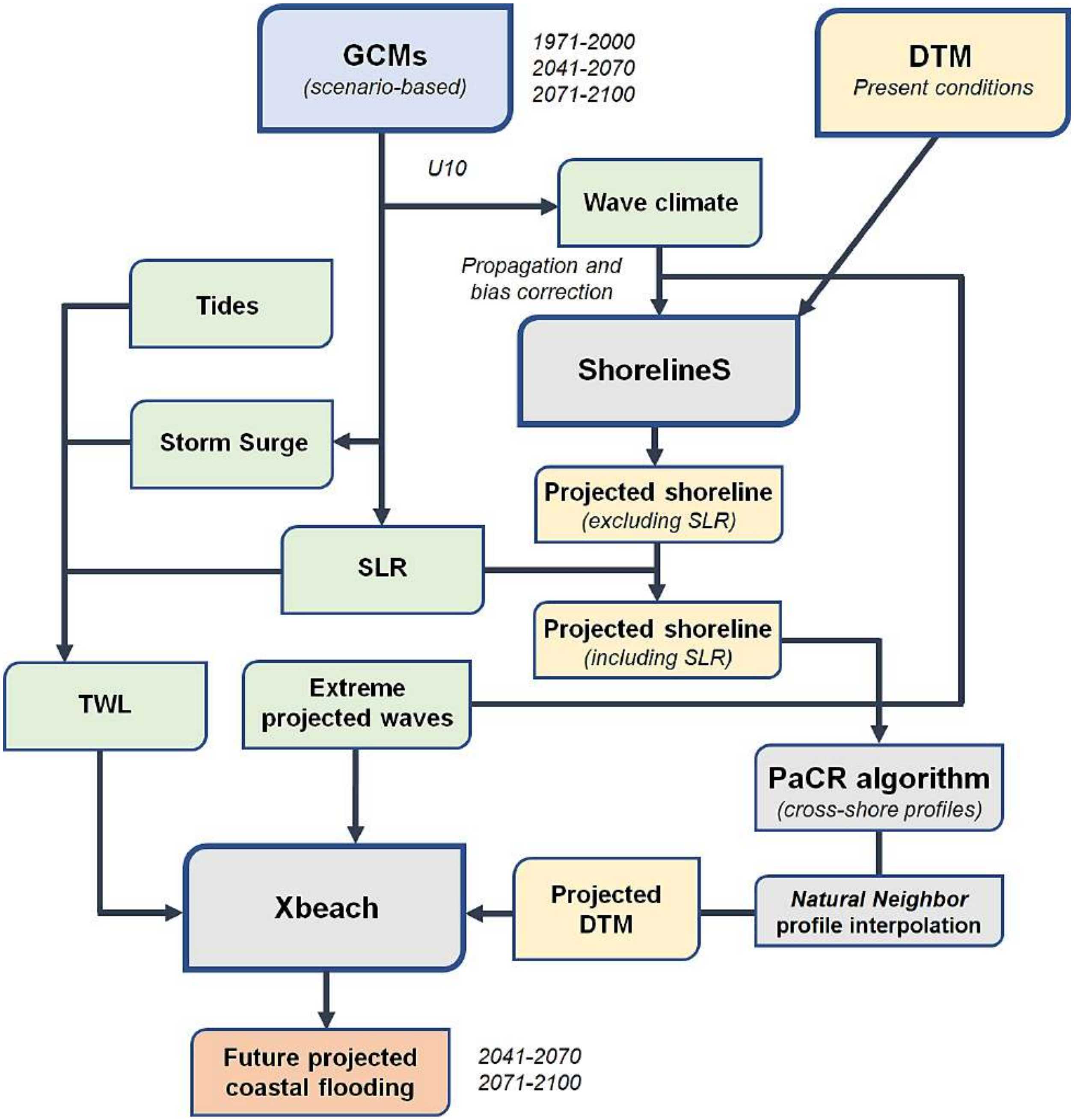

Figure 13 – Framework to model the evolution of the coastline subjected to long-term erosion mechanisms using the ShorelineS, for each climate change scenario, considering the 1971-2000 present and 2041-2070 and 2071-2100 future reference periods.

3.2.1.1. The ShorelineS model

Shoreline evolution models are useful tools in analysing and projecting the coastal morphological evolution from seasonal to decadal time scales, especially due to the inefficiency of process-based models in multi-year coastal area applications. The ShorelineS model is a free-form coastline model capable of describing drastic coastal transformations based on relatively simple principles borrowed from general coastline theory (Pelnard-Considere, 1956). This open-source MATLAB-based model describes the coastline like a freely moving string of points with for an arbitrary number of coastal sections (open/closed) that can interact with rocky parts and/or structures.

The ShorelineS model was employed here to project the future shoreline evolution under the different RCPs, according to the associated future projected wave climates. The model was first validated, and its performance in simulating the evolution of the shoreline was evaluated using the bias corrected ERA5 wave data at the five key-locations, from 2008 to 2018, corresponding to the overlapping temporal availability of the latest high-resolution aero-photogrammetry datasets. Then, the 6-member bias corrected ensemble of wave climate projections was used to force ShorelineS, towards the end of the 21st century. Since shoreline evolution is a continuous process, the moment in time considered for the future projected 2041-2070 (2071-2100) time-slice is the year 2070 (2100), corresponding to the end of the time-slice. The final projected shoreline was set to be the average of the 6 independent ensemble member projections. A range of natural inter-member uncertainty was also identified. It should be noted that the ShorelineS is not able to account for changes in the sea level during the simulation periods, therefore, not representing SLR and tide oscillations. Hence, the additional effects of SLR were included *a posteriori*, using a Bruun's rule, accounting for the available accommodation space at each location.

3.2.1.2. The SWAN (Delft3D-Wave) model

The Delft3D is a 3D hydro-morpho-dynamic modelling system designed to simulate wave propagation, currents, sediment transport, morphological developments and water quality aspects in coastal, river and estuarine areas (Roelvink and Van Banning, 1994). Delft3D is open-source for the hydrodynamic (Flow), Morphodynamic (Mor), and waves (Wave; SWAN) modules. SWAN is a third-generation wave model designed especially for coastal waters, lakes and estuaries, to obtain a wide range of wave parameters from forcing winds, bathymetry and current conditions (Booij et al, 1999). The model is based on the wave action balance equation with sources and sinks. SWAN was used to propagate the offshore waves to nearshore, at approximately 20 m depth, allowing to consider the effects of local bathymetry changes while approaching the coast using a high-resolution bathymetry dataset. These effects were not contemplated in the original lower-resolution datasets (please refer to section 2). The ShorelineS and XBeach models were then forced with the propagated and bias corrected waves at 20 m depth.

To promote a rigorous correction of the waves, first, the ERA5 data was propagated from the offshore grid-point to the closest *in-situ* location (from the five available and described in section 2.2.1). The ERA5 was then bias corrected using two quantile mapping strategies (section 3.1.1), and finally propagated to nearshore, at approximately 20 m depth. Simultaneously, the GCM-driven wave climate simulations and projections were propagated from their original grid-points, offshore, towards the same final location, being then bias corrected using the corrected ERA5 data based on buoy observations. Additional details are shown in Figure 14.

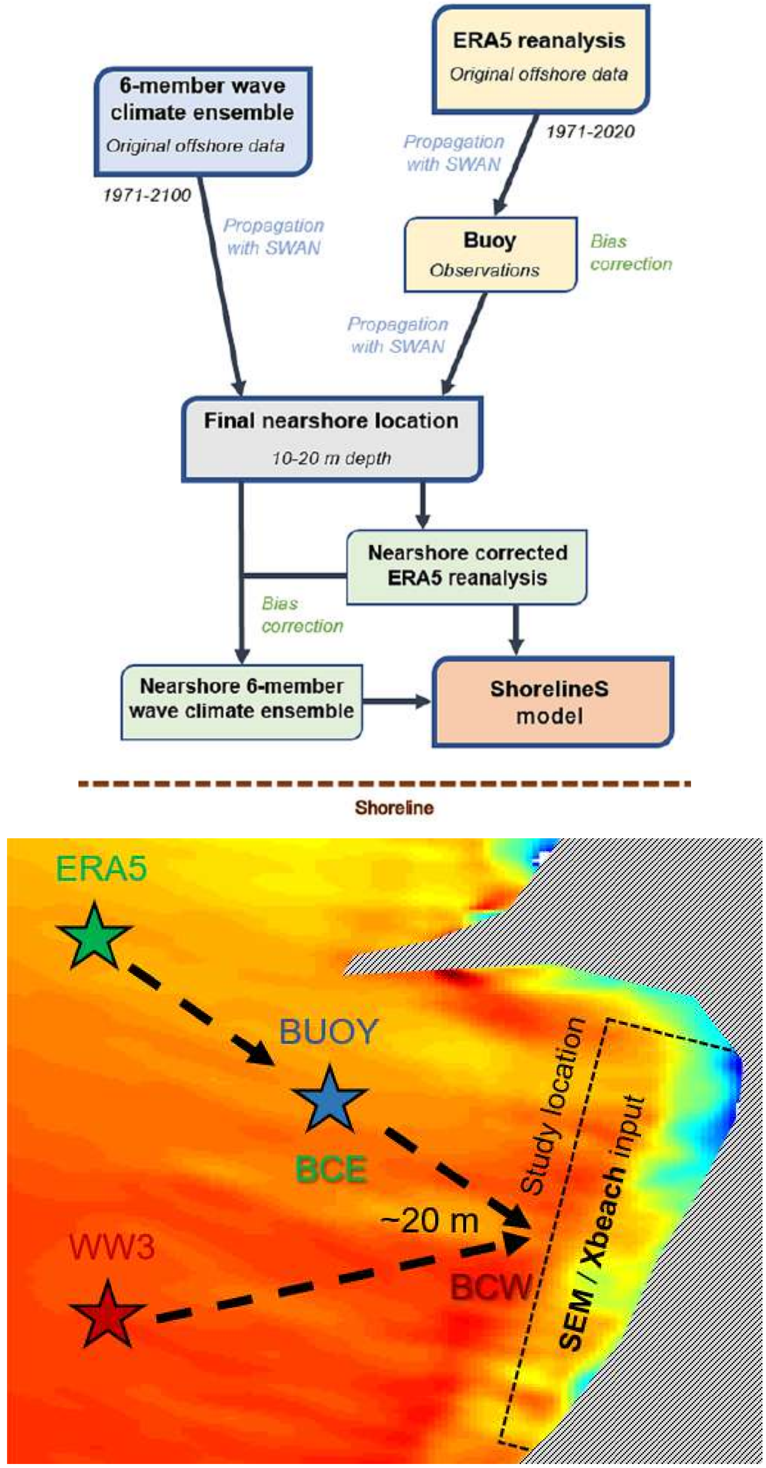

Figure 14 – Scheme for offshore wave propagation and bias correction in order to drive the ShorelineS and XBeach models nearshore. The green star corresponds to a generic ERA5 offshore grid-point, the blue to the buoy location, where ERA5 is corrected (BCE) and the red to a generic offshore grid-point for the GCM-driven wave climate simulation and projections (WW3). Both the corrected ERA5 and the WW3 waves were propagated to a final location in the boundary of the key-location, to finally force the ShorelineS and XBeach models.

3.2.1.3. The XBeach model

The XBeach (Roelvink *et al.*, 2009) is a two-dimensional model for wave propagation, long waves and mean flow, sediment transport and morphological changes of the nearshore area, beaches, dunes and backbarrier during storms. It was originally developed as a two-dimensional process-based storm impact model but shown to be applicable in a wide range of conditions. Good agreement with flood extent was found for XBeach using a combination of non-linear shallow water equations and an advection-diffusion equation for sediment and dynamic bed updating. A recently implemented functionality in XBeach, the one-layer non-hydrostatic model, was applied here. Overall, the XBeach was used to compute nearshore wave conditions, wave set-up, run-up and overtopping, by receiving TWL and wave parameters propagated from offshore to nearshore by the SWAN model. The XBeach was run under 2DH mode with absorbing-generating boundary conditions at the offshore forcing. The advanced default parameter values recommended by the developers were considered to run a wave-resolving non-hydrostatic model. Additionally, the formulations considered non-stationary shallow water equations and a pre-defined JONSWAP wave spectrum. Note that since the TWL was computed "offline" using a joint probability approach at each location and given the particular interest of the study on the extreme events, the XBeach was run considering extreme TWLs resulting from the probabilistic combination of extreme SSLs and tides (under a mean SLR). Extreme wave conditions were selected according to the nearshore total wave energy. All modelling domains were represented by regular grids with spatial-varying resolution (from 20 m offshore up to 3 m onshore). The landward expression of coastal flooding is finally given by the interception between the "water level" parameter and the DTM (run-up limit).

Figure 15 shows an example of the XBeach modelling capabilities in shallow waters, close and/or within the surf zone, depicting also the interface between water and land (shoreline) at Praia de Cova Gala – Praia da Leirosa key-location (the reader is referred to section 2.1.3). Figure 15 is a frame of a video showing the rough sea states caused by the Hercules storm, in January 2014. The full video can be assessed through this link: https://i.imgur.com/skUT4MO.mp4. Here, the XBeach used as input the TWL and waves from ERA5 propagated from offshore to 15 m depth using the SWAN (Delft3D) model. The XBeach was run in stationary and non-hydrostatic mode, and the topo-bathymetry was given by the combination of the EmodNET, COSMO and LiDAR 2011 datasets.

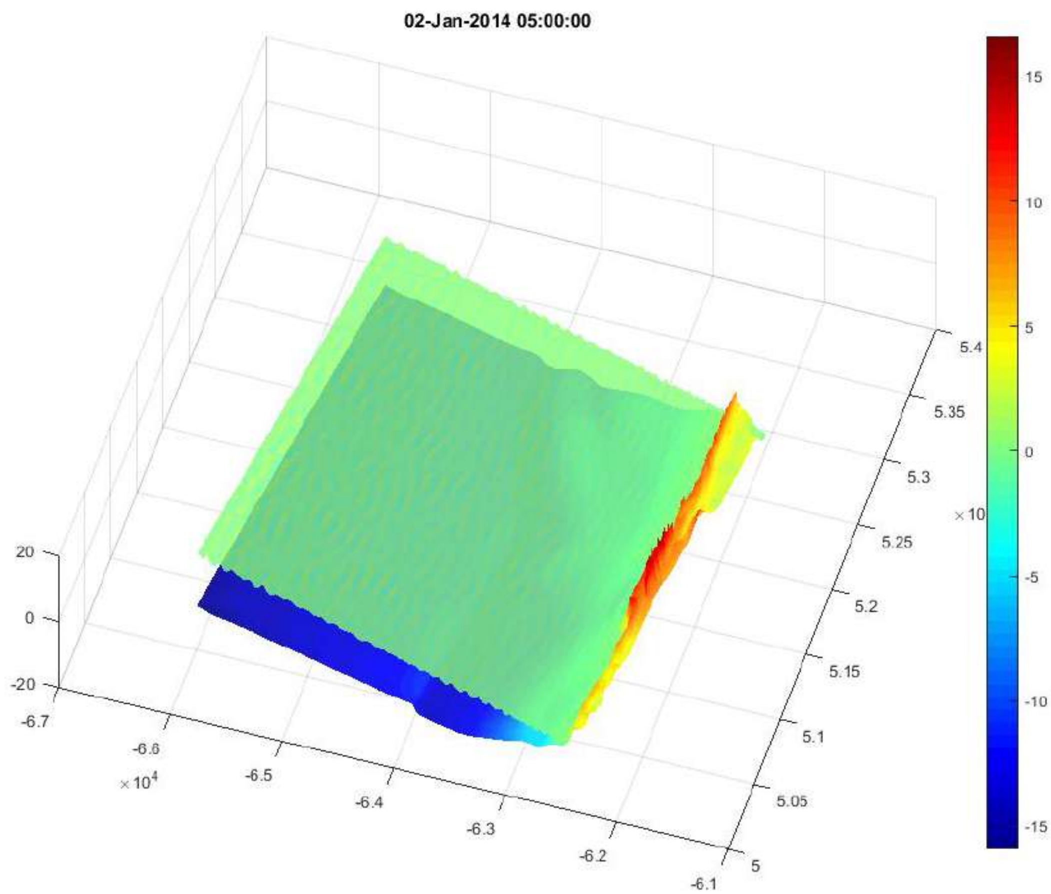

Figure 15 – Example of the application of the XBeach model for January 2nd, 2014, 05:00, at Praia de Cova Gala – Praia da Leirosa key-location.

3.2.2. Modelling of large-scale geomorphologically-similar areas

The identification and characterization of the Portuguese coastal areas more prone to suffer direct impacts from climate change (*e.g.*, low lying sandy and artificialized coastal zones) was essential, using topographic profiling dynamical methods combined with semi-empirical models that allow the computation of future extreme scenarios based on the projected SLR, tides, waves (wave parameters, set-up and run-up) and storm surges. From the five key-locations to a national scale assessment of coastal vulnerability, similarity assumptions were made to simplify the processes and allow the implementation of large-scale semi-empirical models. These were based on the complete time- and computational-costly hydro- and morphodynamic parametric modelling frameworks, adopted for the key-locations. Mainland Portugal's coastline was, therefore, divided into four categories, comprising all the coastal sections with similar characteristics. These are: low sandy and sandy cliff coastlines, rocky coastlines or with longitudinal adherent structures, urban artificial coastlines and urban/sheltered beaches.

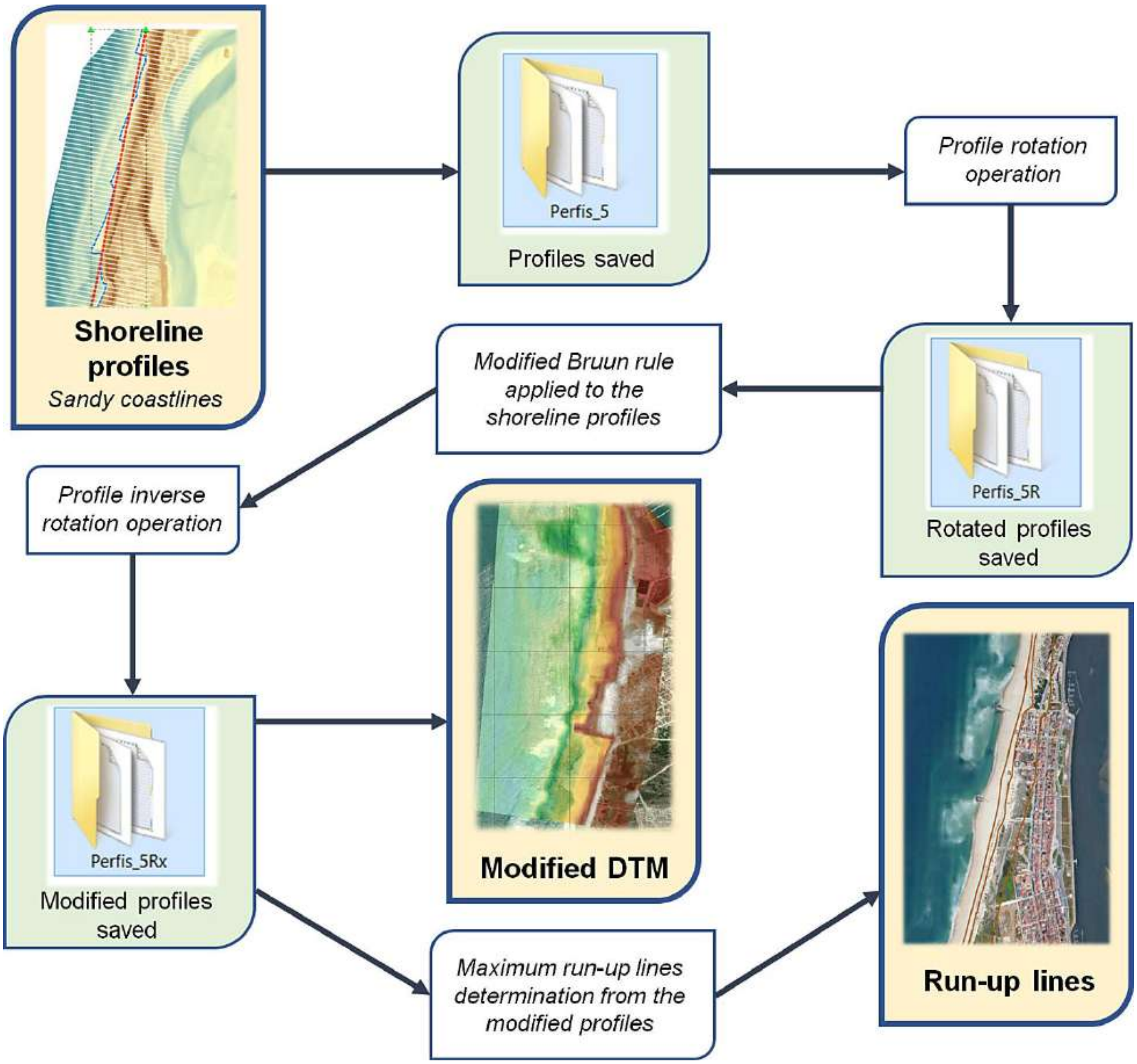

Figure 16 – Framework to model the semi-empirical approach for coastal retreat and setback lines determination in a semi-automatic supervised process for a given sandy coastal section.

A semi-automatic process, to run in a GIS (Geographic Information System) environment, for the application of a semi-empirical approach for coastal retreat (PCR parametric coastal retreat method), based on the modified Bruun rule (MBR; Rosati *et al.*, 2013), has been developed (Figure 16). The Parametrical Coastal Retreat (PCR) method, developed by Antunes (2017), applies an elasticity function ($E(X)$ in Eq. (9)) to a beach profile, a scaled function to the shoreline retreat value (R), estimated by MBR. Eq. (8) and Figure 17 present the MBR, where Y_L represents the landward sediment transport, $W*$ the baseline from the closure profile depth to the maximum of the total run-up level (considering a long period from 10 to 30 years), and $B = B_0 + h*$, with B_0 as the topographic height of the maximum total water run-up (TWRup; for a given SLR) and $h*$ the depth of closure of the topo-bathymetric profile. In Eq. (9), H corresponds to the orthometric height of both the original and the modified DTMs, at each X (cross-shore) coordinate, with origin at H = 0 m, being positive (negative) for positive (negative) H. The n-scaled elasticity function E is applied around X_{MLW}, which corresponds to the reference minimum low water (MLW) position, for the lowest recorded tide at the location. Finally, $E(X)$ corresponds to the modified X coordinate. The scale factor n is a parameter calibrated with historical shoreline retreat data. It depends on the erosion dynamics and shoreline response to erosion forcing factors. Usually, n ranges from 3 to 9, from low to high erosion dynamics.

$$R = (W * + Y_L) \cdot log\left(\frac{B}{B - SLR}\right) \tag{8}$$

$$E(X) = n \cdot R \cdot \frac{X - X_{ref}(LW_{max})}{W *} \ \& \ H(X) = H(X) \cdot (1 - SLR^{2.0}), \qquad if \quad X > 0$$
$$E(X) = X \ \& \ H(X) = H(X) \cdot (1 - SLR^{2.7}), \qquad if \ X < 0 \tag{9}$$

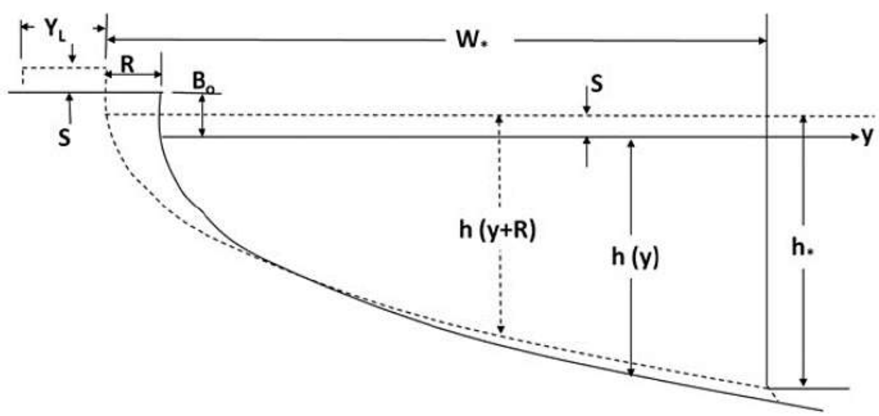

Figure 17 – Variables in the Modified Bruun Rule (extracted from Rosati *et al.*, 2013), where the Y-axis represents the X-variable in Eq. (7).

Before applying the PaCR algorithm, a coordinate system rotation transformation was conducted. The original DTM is defined in the cartographic coordinate system PT-TM06/ETRS89 (Portuguese Transverse Mercator of 2008 with the European Terrestrial Reference System 1989), with three-dimensional coordinates (X, Y, H). From this DTM, for a coastal stretch of generally the same orientation, a set of cross-shore profiles spaced by 50 m are obtained. Each individual profile, with 2 m resolution, is transformed into a local coordinate system (X, H), where transformed X-coordinate corresponds to the transverse position relative to shoreline defined by the mean sea level (H = 0 m), or the profile length component, and H-coordinate is the original orthometric height. After the PaCR algorithm is applied, the local coordinates, modified by the algorithm, are inversely transformed to the original cartographic coordinates, obtaining the modified DTM. After all topo-bathymetric profiles were modified accounting for SLR, two outputs can be derived, which are used in a later stage to produce the national-scale coastal vulnerability assessment: 1) the new retreated shoreline, based on the maximum wave run-up for a projected SLR, following Antunes (2014) and Antunes et al. (2019), considering the sum of the set-up and the incident run-up; 2) a modified DTM, built from the total profile dataset, consisting of a set of points, through spatial interpolation. This process is performed in a Geographic Information System software, by first building a TIN model, and then interpolating the grid points using the Natural Neighbor interpolation method.

The resulting DTMs are used as forcing to the XBeach model, over which extreme coastal flooding projections are obtained.

Figure 18 – Example of shoreline retreat modelling for 2071-2100 under RCP8.5 at Costa Nova, considering only SLR and wave run-up. This example does not correspond to the final result, being used here to demonstrate the concept.

An example of the application of the PCR method to the scheme presented in Figure 16 at Praia da Costa Nova is presented in Figure 18, considering SLR and the maximum TWRup, from the combined extreme flood level under the RCP8.5 scenario for the 2071-2100 period (divided into three levels of coastal vulnerability index – CVI), using a sequential process applied with a 10-year step. The three vulnerability levels (1 – Low; 2 – Moderate; and 3 – High) resulted from applying the PCR method to the low (5%), medium (50%) and high (95%) percentile of the SLR ensemble composed CDF function, for a given scenario, and the respective minimum, medium and maximum of TWRup, both considered at the end of each future projected 30-year long climate period (2070 for the 2041-2070 period, and 2100 for the 2071-2100 period).

3.3. Coastal Vulnerability Assessment and Risk Zones

The present work follows a methodology to assess, at a national scale, both the coastal vulnerability and the coastal risk at the most vulnerable and exposed areas. Based on the combination of different types of information, including GCM/RCM-driven wave climate and TWL projections (including SLR, tides and storm surges), geomorphological characteristics, extreme flooding scenarios, erosion and coastline retreat models of the Portuguese mainland's coastlines, and socioeconomic data related to the population, infrastructures, communication routes and real estate property value along the areas of interest, vulnerability and risk were assessed.

For the SLR hazard determination, vulnerability, and risk assessment, most of the work published in scientific literature is based on the deterministic flooding cartography approach (Poulter and Halpin, 2007; Gesch, 2009; Marcy *et al.*, 2011). However, there are many unknowns and empirical assumptions when mapping future flood scenarios, including the evolution of coastal landforms (by erosion or sedimentation, or even man-made for building and protection), as well as the data used to produce the DTMs models and to predict flooding levels. Partly based on the probabilistic mapping of Antunes *et al.* (2019), the present developed methodology is an innovative approach to produce the probabilistic cartography of different coastal flooding scenarios, with different extreme event return periods and maximum water levels. The probabilistic cartography for the coastal vulnerability assessment was conducted with enhanced horizontal resolution (up to 2 m), for areas along the Atlantic coast of Mainland Portugal that are susceptible to extreme erosion and flooding due to future extreme events.

The developed probabilistic methodology for flooding cartography and vulnerability assessment was mainly based on the uncertainties associated with the numerous variables (DTMs, CDFs of SLR, tides, SSLs, waves) that were used in the modelling process. The flooding hazard of a certain location for a given flood level increases with decreasing terrain height, since it returns higher water columns and higher flooding. Due to the extreme flooding level (EFL) uncertainty, the flooding occurrence probability in a certain location for a given flood level is also higher in terrain below EFL and lower in terrain above EFL (Figure 22). Therefore, contrary to the usual natural hazard probability, in which higher hazard has a low occurrence probability and vice versa, in this case high flooding hazard corresponds to a high occurrence probability and low flooding hazard corresponds to a low occurrence probability.

Across the different key-locations and coastal sections analysed, the EFL was computed differently, depending on the exposure to the open ocean and to the coastal processes, such as erosion and coastal retreat. When the coastline is sheltered, such as in lagoon systems and estuaries, the EFL is similar to the TWL parameter, namely SLR plus tide plus storm surge. Nevertheless, when the coastline faces the open ocean and is impacted by the ocean waves and coastal dynamics (currents, coastal drift, sediment deficit, etc.), the EFL needs to contemplate the wave set-up and incident run-up components. In such cases, besides probabilistic EFL, vulnerability is complemented with coastal retreat due to the erosion effects and maximum overtopping as well.

In order to make a national scale analysis suitable, three separate indices were generated (Figure 19): the Extreme Flood Hazard Index (EFHI), the Coastal Vulnerability Index (CVI) and the Exposure Vulnerability Index (EVI). All indices were classified into three levels of relevance (levels 1 to 3) and obtained by weighing the parameters, through the weight's assigned by a multicriteria analysis process (*e.g.*, Analytic Hierarchy Process - AHP; Taherdoost, 2017).

The assessment of the coastal risk zones (*i.e.*, vulnerability times exposure) was articulated with the information on critical risk zones identified in the Shoreline Management Plans (*Programas da Orla Costeira* – POCs), which define setback lines, hazard areas and buffer zones for coastal erosion and coastal overtopping/flooding.

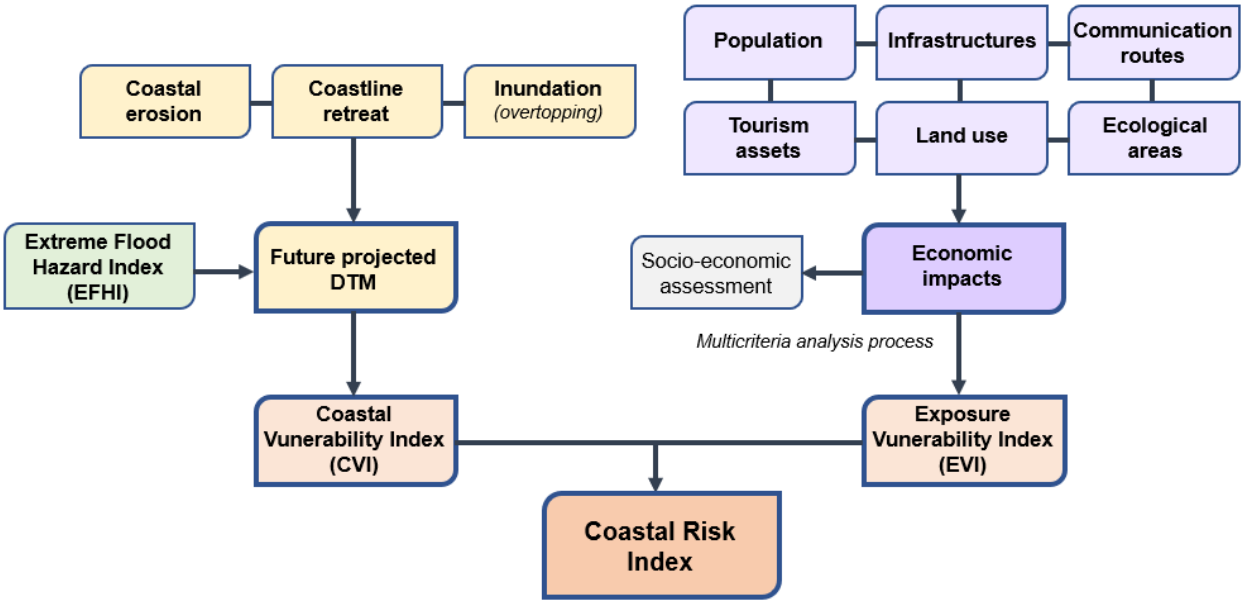

Figure 19 – Coastal vulnerability assessment framework, considering each climate change scenario and the 1971-2000 present, 2041-2070 and 2071-2100 future reference periods.

3.3.1. Extreme Flood Hazard Index (EFHI)

To incorporate the EFL, based on the variability of tides, sea level and storm surge, into the vulnerability and risk assessment, the EFHI was defined based on a combined probability from the three independent variables. Contrasting with the probabilistic approach of Antunes *et al.* (2019), where the EFHI was calculated considering the uncertainty of the submersion frequency, in the present approach, the EFHI corresponds to the exceeding probability for extreme flood levels, evaluated from the CDF (Table 4), resulting in TWL return periods (RPs). Using Eq. (8), the combined flood CDF was obtained through the integration of product between of the three (tides, sea level and storm surge) individual probabilities.

$$P(Flood_{Level}) = P(tide) \cap P(sea\ level) \cap P(storm\ surge) \tag{8}$$

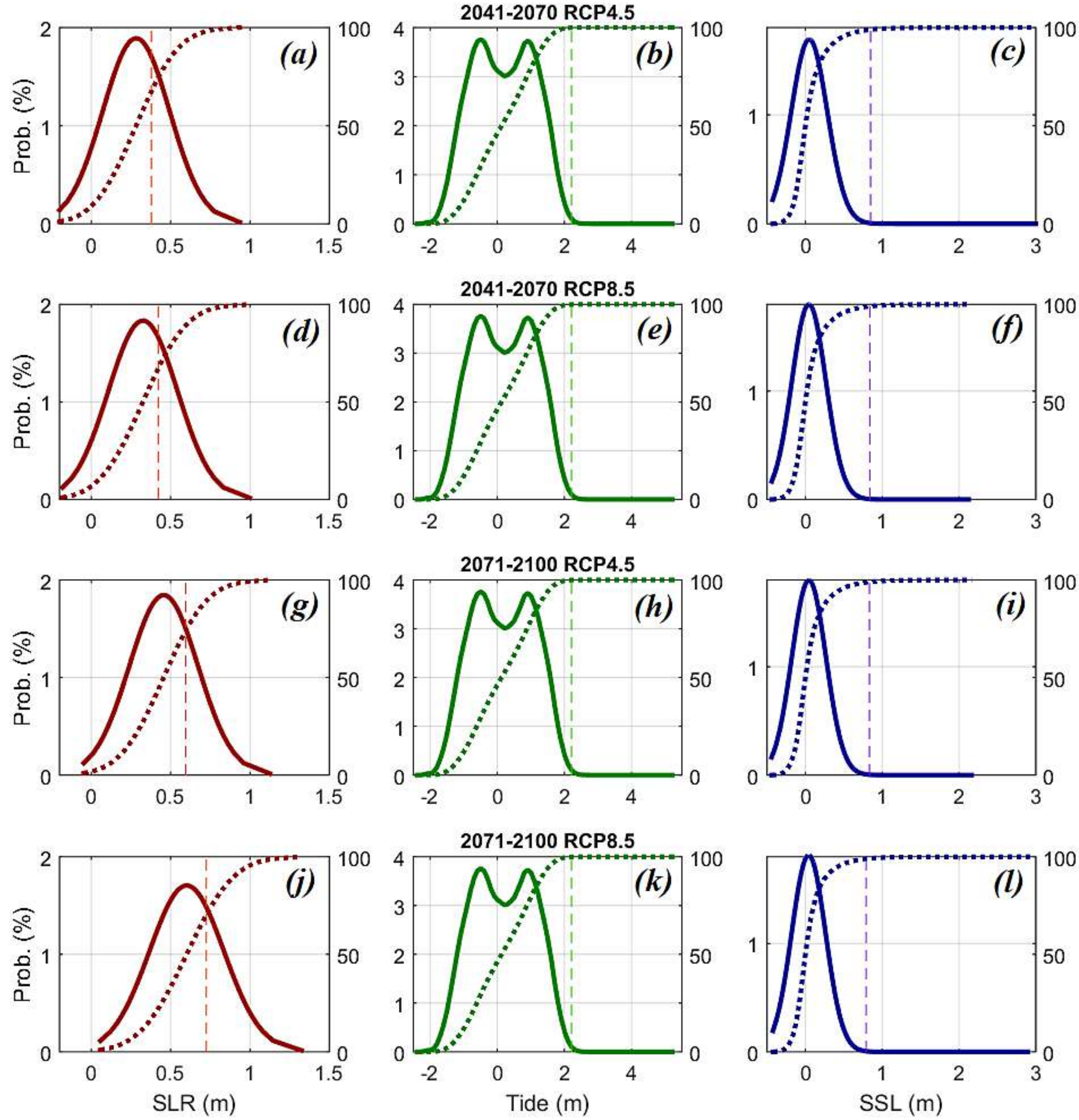

Figure 20 – (full lines) PDFs and (dotted lines) CDFs of the projected (a,d,g,j) SLR, (b,e,h,k) tide and (c,f,I,l) storm surges at Cascais harbor, for the 2041-2070 and 2071-2100 future periods, under the RCP4.5 and RCP8.5 scenarios.

Departing from the harmonic tide projections, random (non-synchronized) SS levels and SLR values are superimposed, extracted from the respective CDFs (ranging from 0.01% to 99.9% probability), resulting in a large set of TWL values for each future period (~2.6 x 10^8), from which a representative TWL PDFs can be computed. The complete sample allows the extraction of representative TWL RPs, avoiding a deterministic approach (*i.e.*, by simply adding the independent TWL components).

By applying Eq. (8), as an example, to the combination of probabilities referring to the Cascais astronomical tide, SLR under RCP8.5 for the 2071-2100 period, and current storm surge conditions, the combined flood CDF was obtained (Figure 21), by considering a simple variable-independent model. In this simple numerical model, Eq. (8) was replaced by simple scalar product and determined as a combinatory calculation with tens of thousands of combinations between 30-year projections of SLR, tides and storm surge frequencies of occurrence.

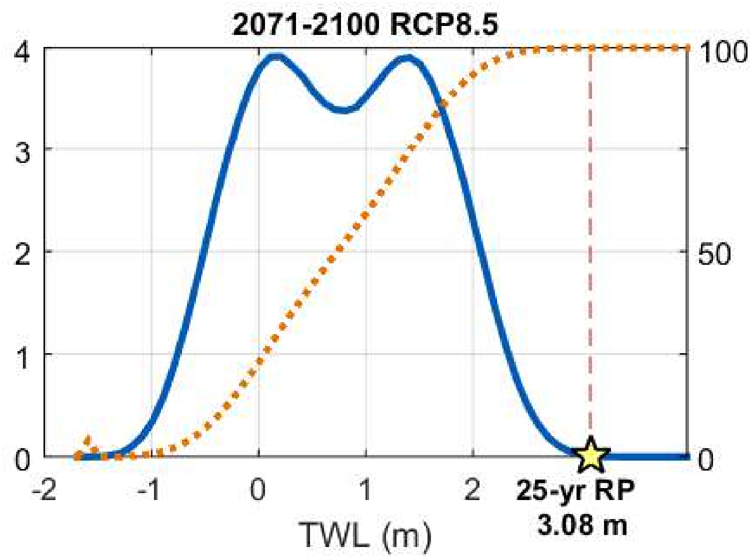

Figure 21 – Combined flood PDF at Cascais, using the tide, storm surge and future projected SLR conditions (2071-2100 under RCP8.5; blue line), and respective CDF (orange line), with the 0.005% exceeding probability of 3.08 m flood height and a mean sea level of 0.88 m.

Table 4 – EFHI classification levels and respective conditional probability intervals for an extreme flooding scenario.

Hazard Index Level	**Moderate**	**High**	**Extreme**
	1	**2**	**3**
Exceeding Flood Probability	0.05%	0.005%	0.001%
Return Period	4-year	25-year	100-year

For the present application, a probabilistic combination of PDFs from SLR, tide and storm surge maximum frequency was applied, instead of a standard error distribution centred at the deterministic EFL. The result was a combined PDF, or a CDF, from which the exceeding probability of extreme flooding was extracted. Figure 22 shows a scheme of the present approach of low frequent flooding levels, corresponding to extreme flood levels of 100-year return period (RP; very low frequency), 25-year RP (low frequency) and 4-year RP (frequent flood, the frequency of quarter-nodal tide period)

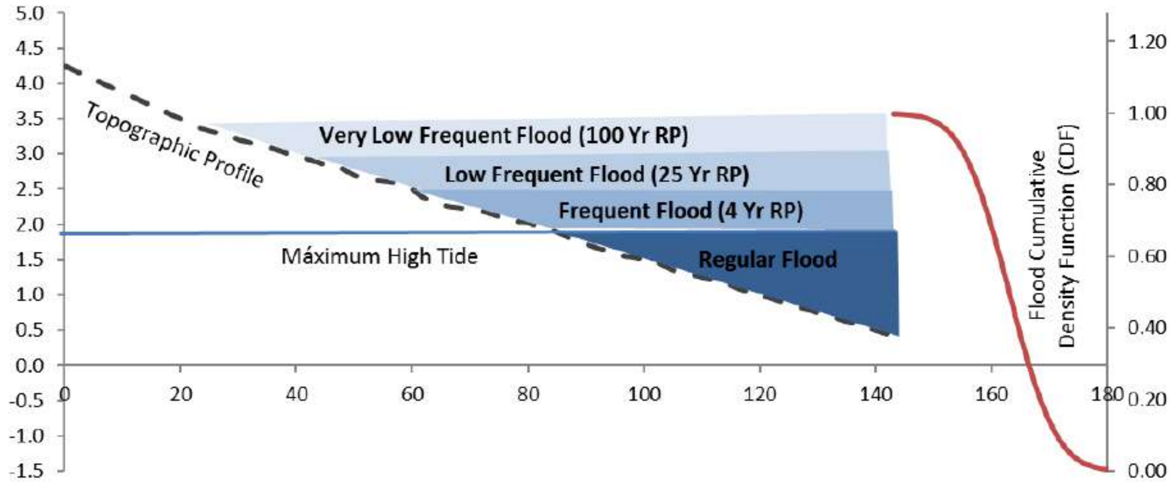

Figure 22 – Method schematization for the Extreme Flood Hazard Index (EFHI) on a generic topographic profile (left axis) based on the combined flooding CDF (right axis), from a given future projected SLR scenario, and tide and storm surge frequency models.

Each CDF represents the extreme flooding level probability (considering the uncertainty between the GCMs, the variability of tide level and the frequency of storm surge) and is centred at the analysed 30-year period mean sea level (MSL) of the ensemble. This PDF intersects the topographic profile to determine the EFHI (Figure 22), evaluating occurrence probability level at a certain topographic location for a given EFL. Since the EFL is conditioned by the forcing GCM-driven projections, the respective probability corresponds to a combined conditional probability. This probabilistic distribution function contains a conditional flood probability for the dimension of the topographic profile, which enables the determination of the probabilistic EFL for different topographic locations (Figure 23).

Figure 23 – Example of the EFHI applied using the described probabilistic approach of a combined flood CDF, focusing on the inland waters at the Costa Nova key-location. This example does not correspond to the final result, being used here to demonstrate the concept.

3.3.2. Coastal Vulnerability Index (CVI)

The EFHI was obtained from the direct use of the coastal forcing parameters, directly related to extreme coastal flooding (TWL and wave parameters) and represents the flood hazard through the flood probability. The CVI, on the other hand, focuses on determining geographical susceptibility to a certain hazard, depending on the TWL, extreme coastal erosion and flooding in the actual (historical) coastal environment, which includes the internal and external physical characteristics of the system, defined for each of the analysed coastal sections.

Figure 24 – Example of the CVI at a low-lying sandy coast section (Costa Nova), resulting from the combination of the probabilistic approach of the EFHI (from Figure 22) and the maximum TWRup (contribution of ocean waves) applied to the PCR method of shoreline retreat (from Figure 17). This example does not correspond to the final result, being used here to demonstrate the concept.

Considering the methodology presented in Rocha *et al.* (2020), the CVI was obtained through the weighted average of the EFHI and the Physical Susceptibility Index (PSI), given by a set of parameters considering the hydrographic network, distance to the coastline, coastal type, solid geology, drift geology, and land use, weighted through a multicriteria analysis process (*e.g.,* AHP). Here, a numerical projections of potential coastline retreat (the ShorelineS model and the PCR method; please refer to sections 3.2.1.1 and 3.2.2) were added and combined with the EFHI to generate the CVI (Figure 24). Since there are four different types of coastal sections (the reader is referred to section 3.2.2), the CVI was evaluated by different combinations of coastline retreat, flood projections and flood overtopping. Each combination solution depends on the coastal process involved in the hazard: 1) for an open, low sandy coastal section, the CVI combined erosion with extreme flood hazard; 2) for a coastal section with adherent and/or urban artificial structures, the CVI combined extreme flood hazard with overtopping; and finally 3), for inland waters, such as estuaries or lagoon systems, the CVI was defined only by the EFHI given by the extreme TWL. Such combinations were obtained using spatial functions of map's algebra through the GIS application.

3.3.3. Exposure Vulnerability Index (EVI)

Through the coastal sections assessed and classified by the CVI, a set of exposure parameters such as population, infrastructures (maritime ports, factories, large commercial hubs, monuments, etc.), buildings (domestic, homes, small commerce and services), tourism assets (beach, parks, restaurants and hotels, etc.), communication routes (roads, railways, bridges), land-use and ecological areas (natural parks and reserves, salt marshes, coastal meadows, salt flats, avifauna ecosystems, etc.) were considered for the socioeconomic vulnerability assessment and to compute the EVI. This index was computed for the most vulnerable identified areas, mapping the exposed elements and potential associated damage (based on land-use and occupation charts, the equity and real-estate value and the socio-demographic data per census tract or statistical subsection (Table 3), to finally map Mainland Portugal's coastal risk zones.

Finally, based on damage and cost functions applied on the assets exposed to the future potential coastal flooding hazards, the economic damage levels were estimated over the risk zones, and the respective risk assessment was obtained.

3.4. Physical and Socioeconomic Impacts

The climate-change-driven physical and socioeconomic impacts at the coast were evaluated and quantified along the previously defined risk zones. The assessment of socioeconomic vulnerability and economic damage was then used to evaluate the potential socioeconomic impacts due to climate change, related with the combination of coastline recession with SLR, tides, future projected storm surges and extreme run-up, through the CVI, allowing to identify and quantify losses and damages (the reader is referred to the "WP5 – Adaptation Needs" report).

The economic damage assessment evaluated the costs associated with the losses, partial damages suffered on assets such as the infrastructures, communication routes, land use and ecological areas, and real estate depreciation. On a wider scale, this assessment was based on the land and real estate value database from the Portuguese financial authority, per administrative unit. The economic impact of future extreme flooding in a certain region was directly assessed considering the area projected to become permanently inundated or frequently flooded according to Table 4 (the reader is referred to section 3.1.2), considering a "no-action" scenario until the end of the projection.

The output of the physical and socioeconomic impact assessment consists of listing the assets expected to be exposed to losses and damages, and the quantification of the respective economic costs within the referred "no-action" scenario.

4. Results

The results presented in this section refer to the direct implementation of the previously described methodology to ensure a correct representation of the wave climate and TWLs along the five key-locations. Focus is given to the impacts of local bathymetry on the ocean wave fields, as well as on the correction of systematic errors in the ERA5 reanalysis and 6-member ensemble datasets (the reader is referred to section 3.2.1.2). Accurate wave fields at the coast are essential for a rigorous projection of the future shorelines as well as for the assessment of extreme coastal flooding and associated vulnerability of the inland areas, in which extreme TWL given by a probabilistic approach are also of the upmost importance.

4.1. The relevance of the iterative propagation-correction-propagation scheme on the coastal wave climate and longshore sediment transport rates

An innovative methodology focusing on an iterative propagation-correction scheme has been applied to the ERA5 reanalysis wave dataset, using "ground-truth" *in-situ* observations from five buoys located near the study areas, and a high-resolution coastal bathymetry. Such procedure ensured the obtention of a local, long-term corrected reanalysis dataset backed up by observations spanning for 50 years, from 1971 to 2020. Figure 25 to Figure 29 show the relevance of this methodology on the transformation of the wave fields from the offshore original data to the local wave climate datasets. Although timely, the process led to significant changes in the original H_S and MWD patterns, compatible with the real ones at the coast.

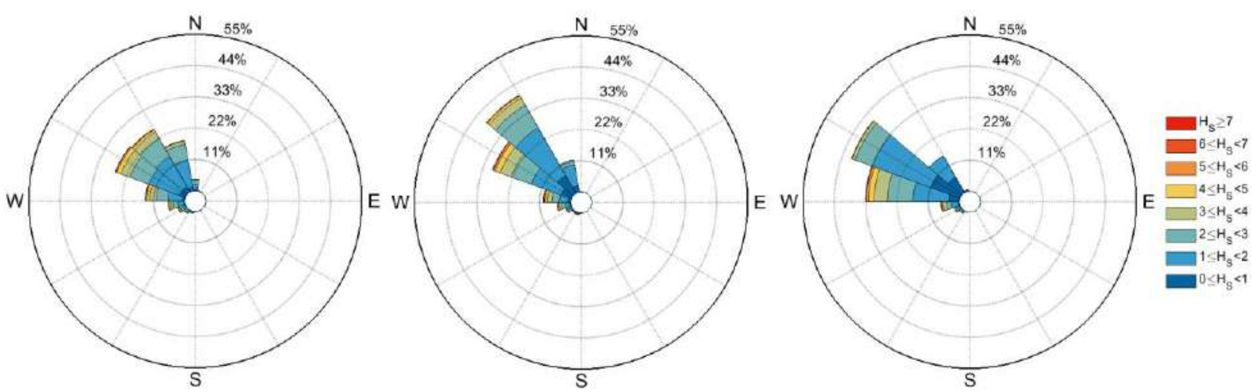

Figure 25 – ERA5 1971-2020 wave field transformation using the propagation-correction-propagation methodology, at the Ofir key-location: (left) original ERA5 data, (center) propagated-corrected ERA5 at buoy location, (right) propagated-corrected-propagated ERA5 near the coast.

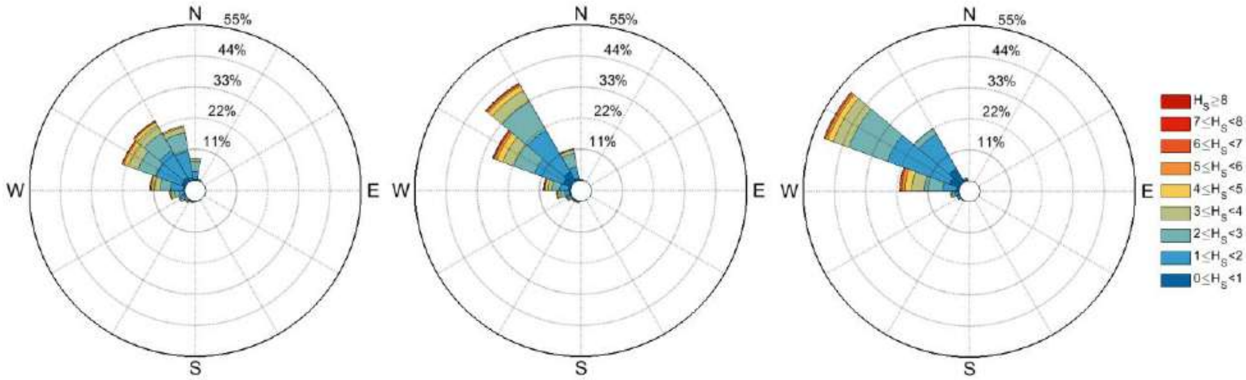

Figure 26 – Same as in Figure 25, but for the Costa Nova key-location.

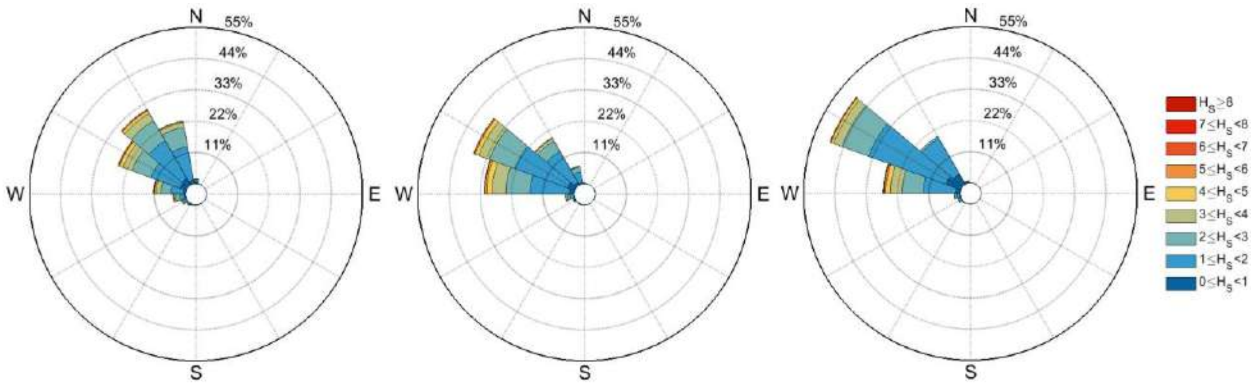

Figure 27 – Same as in Figure 25, but for the Cova Gala key-location.

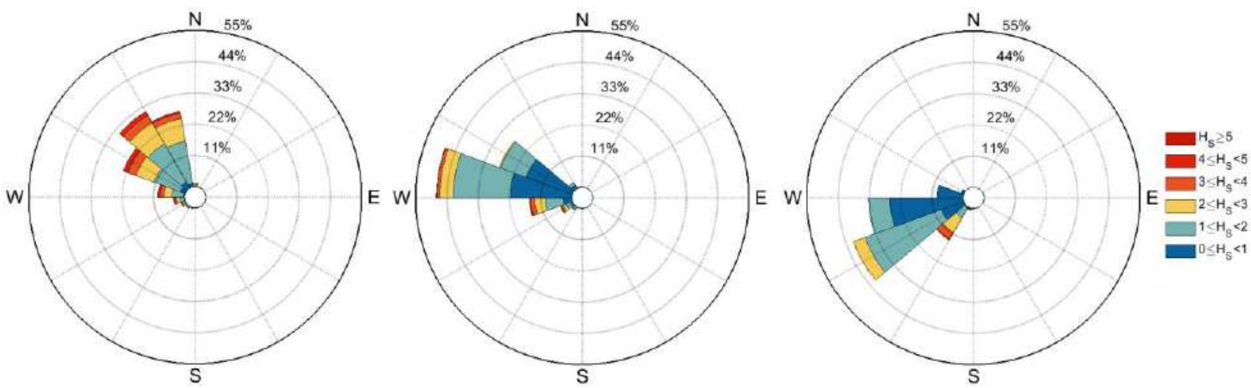

Figure 28 – Same as in Figure 25, but for the Costa da Caparica key-location.

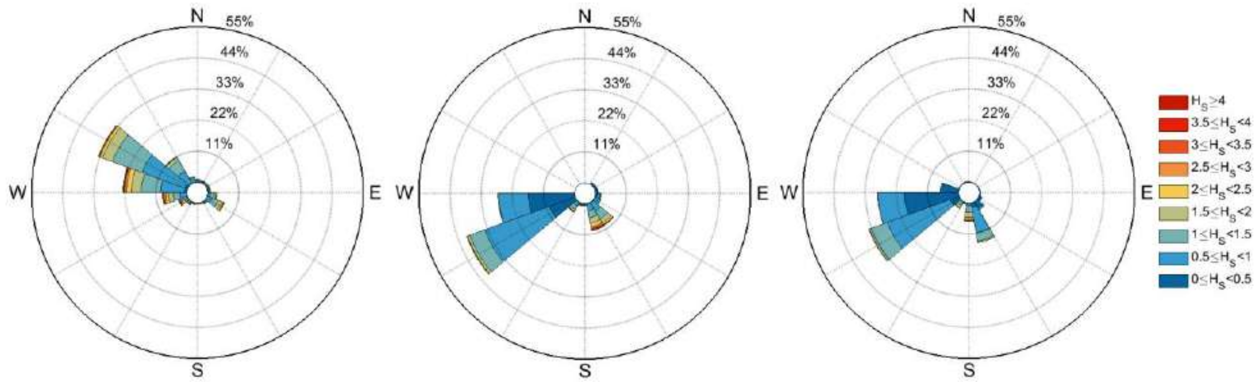

Figure 29 – Same as in Figure 25, but for the Praia de Faro key-location.

Figure 25 to Figure 29 show a consistent transformation of the wave fields while approaching the coast under correction using observations. While Figure 25 to Figure 27 depict a smooth transformation, essentially modifying the frequencies of occurrence of certain H_S values along a consistent range of directions, Figure 28 and Figure 29 should, nevertheless, be highlighted, since a complete change in the wave climate characteristics is found after the propagation-correction process. At Costa da Caparica, the original ERA5 H_S data has a strong northwesterly component (Figure 29a), with values often surpassing 3 m in a wide range of MWDs, from approximately 270º to 350º. Such behaviour is related to an offshore location of the grid-point (the closer to coast, nevertheless), as well as to an inaccurate depiction of the coastal bathymetry and coastlines due to the relatively coarse resolution of ERA5 of approximately 40 km. The *in-situ* observations used for the bias correction procedure were obtained in the Tagus River mouth, where the wave fields suffer the effects from the Lisbon peninsula, blocking the most energetic northwesterly swells (Figure 29b) and diffracting the incident MWD, and from the Tagur River ebb delta, inducing further wave refraction. Upon propagation towards the final location near the coast, at 13 m depth, the inclusion of the bathymetric effects lead to a wave climate characterized by an enhanced southwesterly component, with almost no waves exhibiting MWDs over 270º (Figure 29c). A similar wave field transformation is visible for Praia de Faro (Figure 30), where the main directions of propagation shift from westerly (270º–310º; Figure 30a) to southwesterly (230º –270º; Figure 30b) and south-southeasterly (160º–190º; Figure 30c).

Given the dependence of the shoreline evolution process on the local wave fields, the transformations shown in Figure 26 to Figure 30 are expected to have a clear impact on the longshore sediment transport (LST) rates. Figure 31 to Figure 35 show the potential LST rates at each of the five study areas, considering the original ERA5 wave fields, the propagated-corrected ones at the in-situ locations, and the final propagated-corrected-propagated ones close to the coast. Similarly to Figure 26 to Figure 30, the following examples aim to highlight the relevance of the employed methodology on the accuracy of the final input data for the morpho-dynamic modelling.

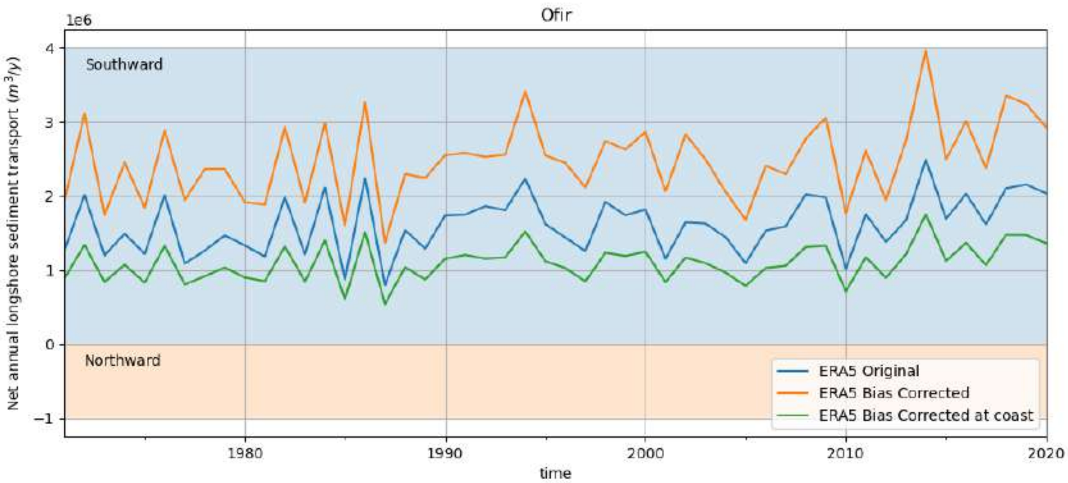

Figure 30 – LST rates (in m^3/year) at the Ofir key-location, considering forcing wave fields from the (blue) original offshore ERA5, (orange) propagated-corrected ERA5 at the *in-situ* location and (green) propagated-corrected-propagated ERA5 near the coast. REF: 1.0 x 10^6 m^3/year.

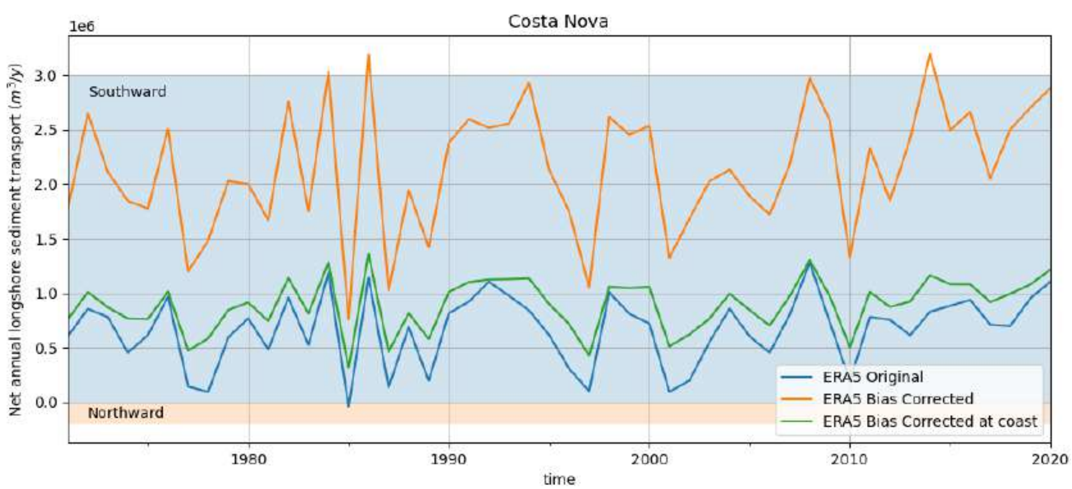

Figure 31 – Similar to Figure 30, but for the Costa Nova key-location. REF: 0.97 x 10^6 m^3/year (Pinto *et al.*, 2022).

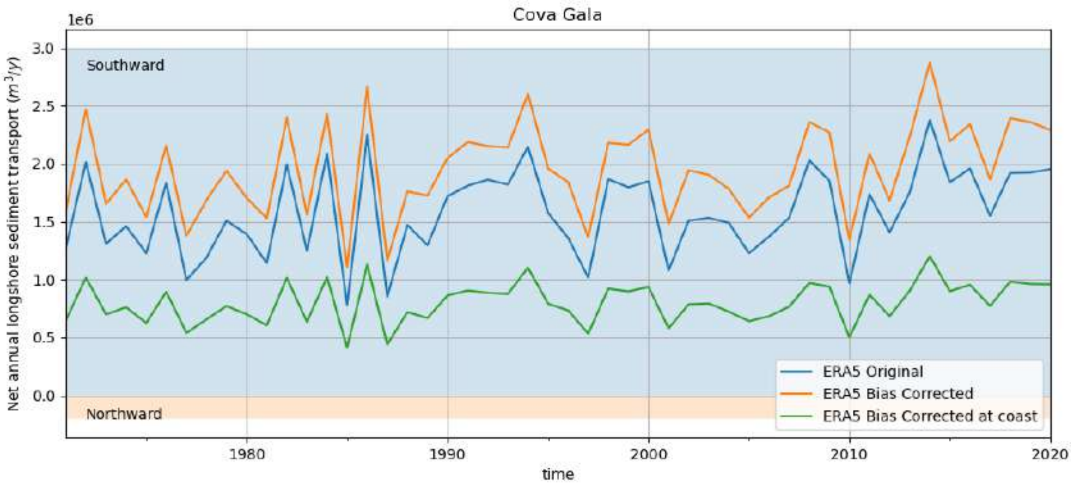

Figure 32 – Similar to Figure 30, but for the Cova Gala key-location. REF: 1.0 x 10^6 m^3/year.

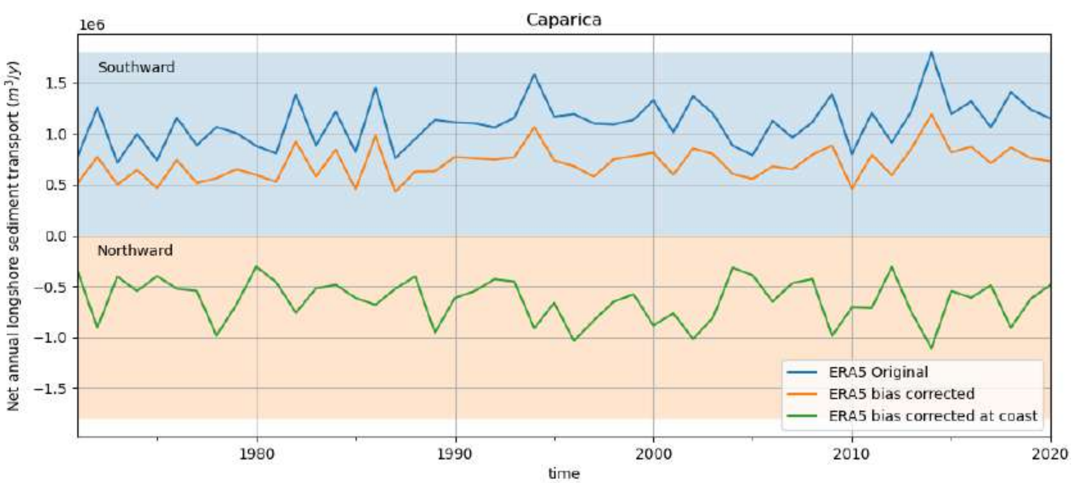

Figure 33 – Similar to Figure 30, but for the Costa da Caparica key-location. REF: -0.5 to -1.0 x 10^6 m^3/year (Taborda *et al.*, 2019).

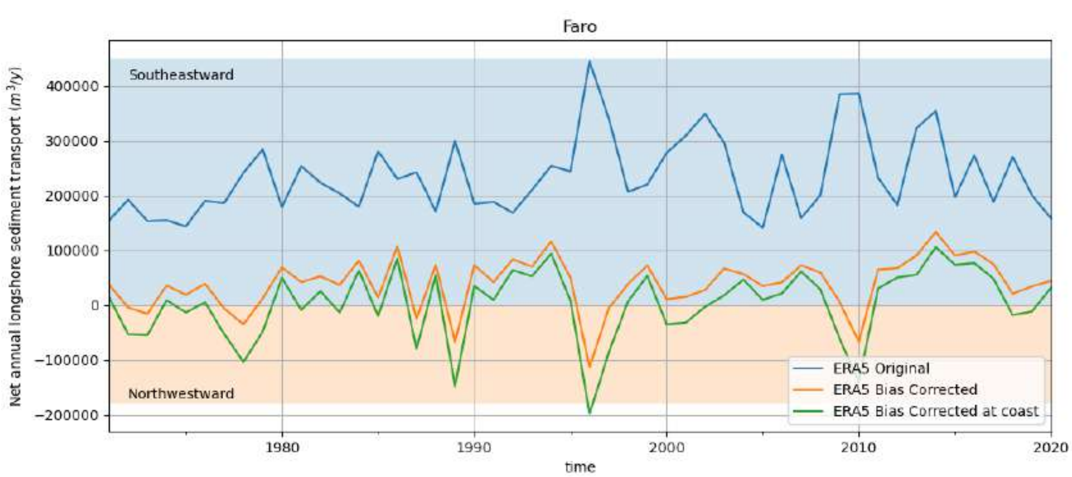

Figure 34 – Similar to Figure 30, but for the Praia de Faro key-location. REF: -1 x 10^5 m^3/year.

While all the key-locations show LST rates compatible with other references in scientific literature, the behaviour of the LST rates during the propagation-correction-propagation scheme varies between locations. For the two northernmost ones (Ofir and Costa Nova, in Figure 30 and Figure 31), the LST rates obtained using the propagated-corrected-propagated ERA5 dataset are found to be similar to the ones obtained using the original offshore data, as well as closer to the reference than the ones obtained using the propagated-corrected dataset at the *in-situ* locations. This is possibly due to the general underestimation of the H_S and T_m values by the original ERA5 at these locations, which, upon correction, are enhanced, thus producing higher LST rates. Near the coast, as part of the energy dissipates due to bottom friction, the propagated-corrected-propagated rates return to lower values, which are coincidently closer to the original ones.

Nevertheless, for the most challenging locations, where the wave fields were shown to suffer the greatest transformations from the offshore locations towards the coast (Cova Gala in Figure 27, Costa da Caparica in Figure 28 and Praia de Faro in Figure 29), the LST rates also show quite different patterns depending on the dataset used. For Cova Gala, in Figure 32, the LST rates get progressively reduced while approaching the coast, stabilizing at 0.5–1 x 10^6 m^3/year, closer to the reference of 1 x 10^6 m^3/year when forced by the propagated-corrected-propagated data. For Costa da Caparica and Praia de Faro, the changes induced by local conditions to the wave climate are visible in Figure 33 and Figure 34. Using the original ERA5 wave data would lead to the obtention of erroneous LST rates, not only in terms of magnitude, but also signal (direction of coastal drift). And while it can be argued that in Praia de Faro a more simple propagation-correction scheme would yield reasonable results, in Costa da Caparica, however, the effects of local bathymetry between the *in-situ* location and the final location at 13 m depth are more intensely felt, leading to a complete overturn of the local sediment circulation, compatible with reference studies such as Taborda *et al.* (2019), and solely visible after the complete implementation propagation-correction-propagation methodology.

4.2. Performance evaluation of the propagated-corrected ensemble of wave climate simulations at the coast during present climate

As described in Figure 14, the GCM-driven 6-member ensemble of wave climate simulations, spanning over the historical period 1971-2000, were also subjected to a propagation-correction scheme to ensure both the inclusion of the bathymetric effects near the coast, as well as a correction of the systematic biases, using ERA5, at exactly the same location (*i.e.*, both the WW3 wave climate simulations and the

ERA5 are equally transformed). This methodology is simpler than the one conducted for ERA5, given that only the reference data in the final location near the coast is needed.

Figure 35 shows the wave field transformation, by member, for the 6-member ensemble of wave climate simulations during the historical period at the Costa da Caparica key-location, showing the "wave rose" of the raw offshore H_S and MWD data in the left column, the propagated data in the middle one (towards 13 m depth using the SWAN wave model; the reader is referred to section 3.2.1.2), and finally, the propagated and corrected data (using ERA5 at the same location). The Costa da Caparica location was chosen for this example given the greater differences found between each step of the methodology, explained by the local geography and morphology (as seen in Figure 25 to Figure 29). The original wave fields for the 6 members show a dominating northwesterly component, exhibiting extreme H_S values surpassing 5 m (especially for the CSIRO-Mk3-6-0 and GFDL-ESM2G members). The expression of the westerly component is, nevertheless, distinct between ensemble members, with the frequencies of occurrence for the 270º-290º bin ranging between 12% for the GFDL-ESM2G and approximately 30% for the CSIRO-Mk3-6-0. Similarly to what was shown in Figure 28, upon propagation to the coastal location, the wave field displays a strong southwesterly to westerly component (230º to 270º), with reduced H_S values, yet occasionally surpassing 4 m (approximately 5% of the time between 230º and 250º). Finally, the correction with the propagated-corrected-propagated ERA5 reference data depicts a generalized cut for MWD values above 270º and an enhancement of the 210º-250º range, including a shift of the highest wave heights from the 230º-250º towards the 210º-230º bin.

The application of the described methodology, although providing a more realistic depiction of the wave fields near the coast, leads to a reduction of the natural uncertainty between ensemble members. While this can be viewed as a disadvantage, we are confident that the benefits of a correct representation of the wave climate near the coast far outweigh the shortcomings of reducing the ensemble spread.

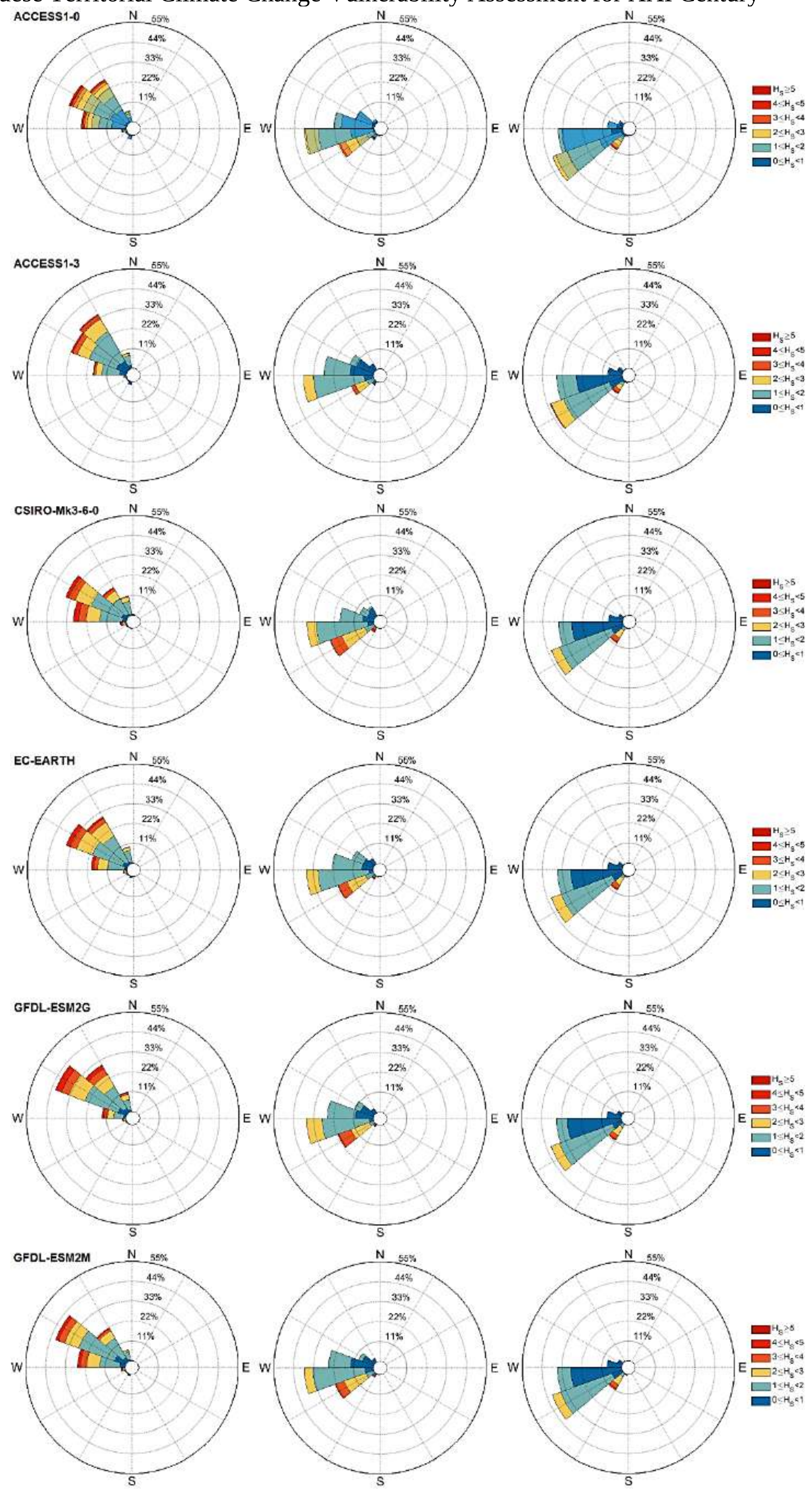
ACCESS1-0
ACCESS1-3
CSIRO-Mk3-6-0
EC-EARTH
GFDL-ESM2G
GFDL-ESM2M
N
S
W
E
55%
44%
33%
22%
11%
$H_s \geq 5$
$4 \leq H_s < 5$
$3 \leq H_s < 4$
$2 \leq H_s < 3$
$1 \leq H_s < 2$
$0 \leq H_s < 1$

Figure 35 – Wave field transformation of the 6-member ensemble using the PCP methodology at Costa da Caparica location.

Figure 36 to Figure 40 show the wave field transformation for the 6-member ensemble (all members pulled together) wave climate simulations during the historical period at each of the key-locations, similarly to Figure 25 to Figure 29. Overall, while the offshore ensemble is able to capture the major directional characteristics of the coastal wave fields at the Ofir (Figure 36), Costa Nova (Figure 37) and Cova Gala (Figure 38) key-locations, its performance is quite low at Costa da Caparica (Figure 39) and Praia de Faro (Figure 40), given their complex geographical and morphologic context, which is not well represented by a global product. At the first three locations, upon propagation and correction, the northwesterly component is enhanced, especially at Costa Nova. Possibly due to local conditions, the highest H_S values at the coast occur there as well, surpassing 4 m during 7.74% of the historical period (Table 6). At the Praia de Faro location, the coastal wave fields exhibit perhaps the most considerable change from their original offshore characteristics. Near the shore, while low waves (H_S below 1.5 m) are often from WSW (230º–270º; approximately 65% dominance), the highest H_S values are originated by waves from SSE (150º–170º), with a frequency of occurrence of values in excess of 2 m of 1.96% (

Table 9).

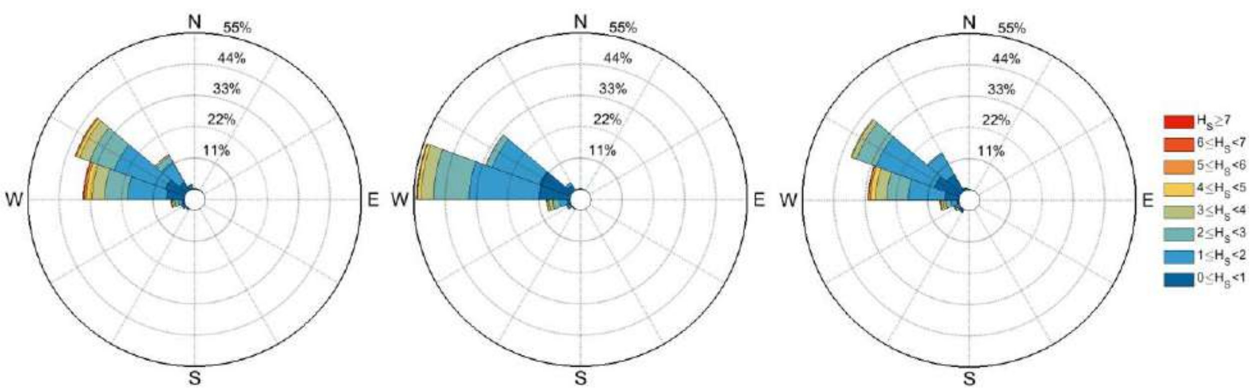

Figure 36 – Wave field transformation for the 6-member ensemble using the propagation-correction methodology, at the Ofir key-location. Original ensemble wave field (left), propagated ensemble wave field (center) and propagated-corrected ensemble wave field (right).

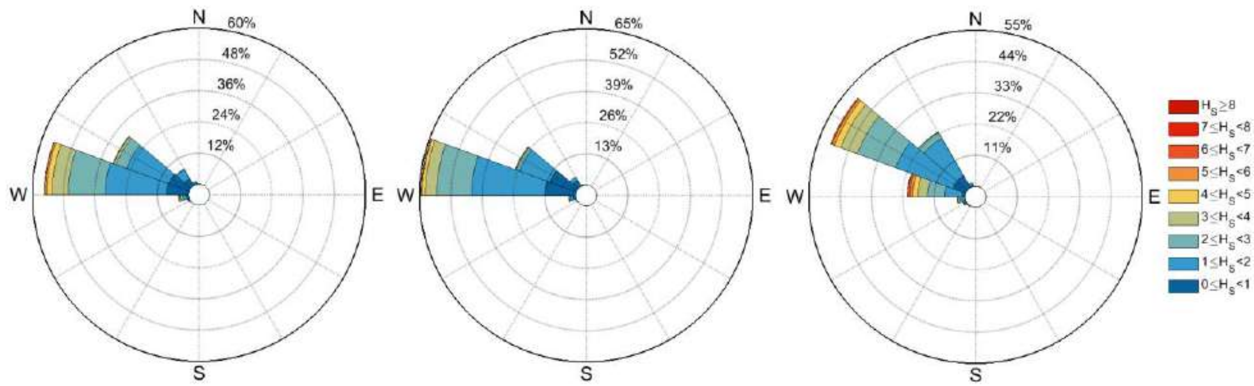

Figure 37 – Same as in Figure 36, but for the Costa Nova key-location.

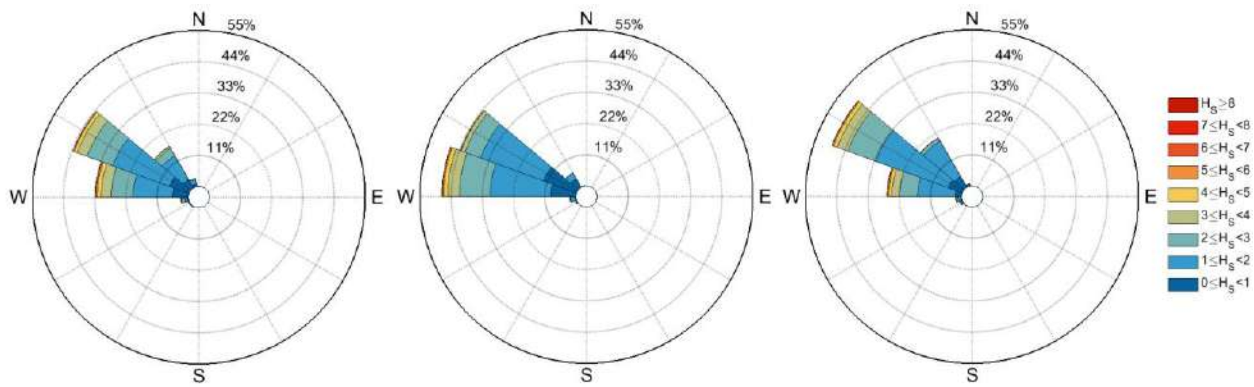

Figure 38 – Same as in Figure 36, but for the Cova Gala key-location.

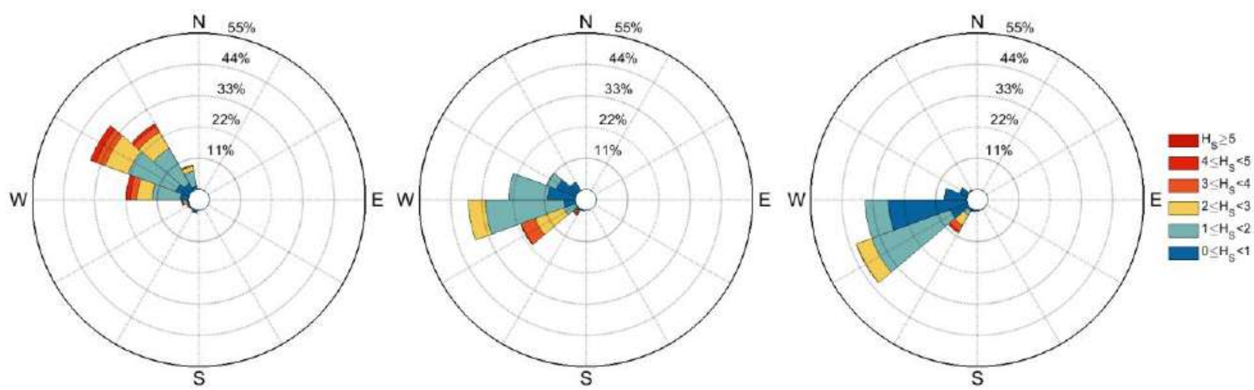

Figure 39 – Same as in Figure 36, but for the Costa da Caparica key-location.

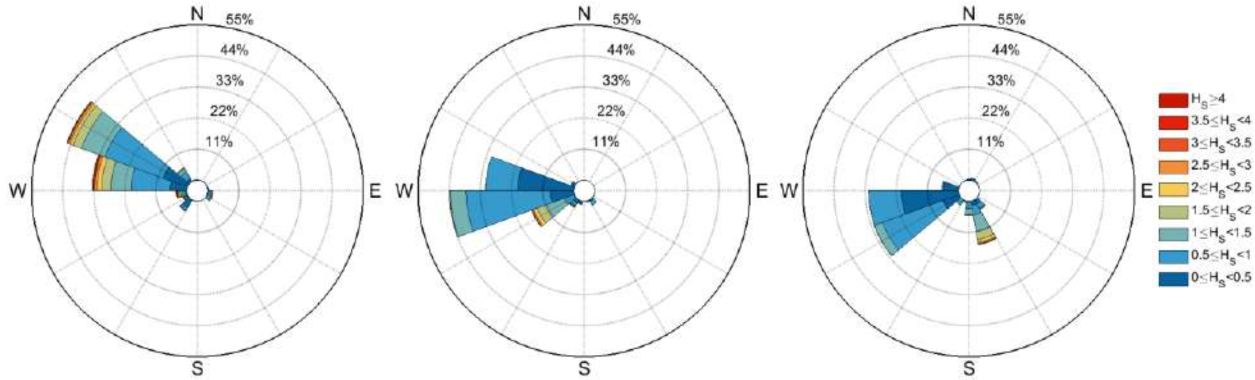

Figure 40 – Same as in Figure 36, but for the Praia de Faro key-location.

Table 5 to

Table 9 show the distribution of the ERA5 and ensemble H_S and MWD data in detail, during the 1971-2000 historical period, at the final coastal locations, post propagation-correction-propagation (ERA5, backed up by *in-situ* observational records) and propagation-correction (ensemble), respectively. Frequencies below 0.01% are considered negligible and are not shown. The differences between the ensemble and the reference data are highlighted using green (< 1%), yellow (< 2%), orange (< 3%), dark orange (< 4%), red (< 5%) and dark red (> 5%). The similarity between the distributions is clearly visible at the five key-locations, due to the application of the EGQM (H_S) and EQM (MWD) bias correction methods. Nevertheless, while the total frequencies of occurrence for a given H_S bin generally present differences below 0.4%, the ensemble tends to present a slightly stronger westerly component, especially for the lower wave heights, with localized differences for the same MWD bin exceeding 2% in Table 5 to Table 8. In

Table 9, for the Praia de Faro key-location, the ensemble shows an underestimation of the amount of small waves (H_S values between 0.5 m and 1 m) coming from the SSE (150º–170º), of about 6%, overestimating the number of higher waves (above 1 m). In fact, at this location, even after bias correction, the highest simulated waves (H_S above 3.5 m) show MWDs within 130º–170º, in contrast with ERA5's MWD range (170º–230º).

Table 5 – ERA5 (E) and 6-member ensemble (W) frequencies of occurrence (in %) per bin of propagated-corrected coastal H_S and MWD, considering the historical period at the Ofir key-location. Errors: green (0-1%), yellow (1-2%), orange (2-3%), dark orange (3-4%), red (4-5%), dark red (above 5%).

Dir (º)	**[0 – 1 [m**		**[1 – 2 [m**		**[2 – 3 [m**		**[3 – 4 [m**		**[4 – 5 [m**		**[5 – 6 [m**		**[6 – ∞ [m**	
	E	**W**	**E**	**W**	**E**	**W**	**E**	**W**	**E**	**W**	**E**	**W**	**E**	**W**
[350-10[	0.04	0.06	-	0.01	-	-	-	-	-	-	-	-	-	-
[10-30[	0.07	0.07	-	0.02	-	-	-	-	-	-	-	-	-	-
[30-50[	0.04	0.12	-	0.02	-	-	-	-	-	-	-	-	-	-
[50-70[	0.03	0.01	-	-	-	-	-	-	-	-	-	-	-	-
[70-90[	0.05	-	0.01	-	-	-	-	-	-	-	-	-	-	-
[90-110[	0.01	-	-	-	-	-	-	-	-	-	-	-	-	-
[110-130[	0.01	-	-	-	-	-	-	-	-	-	-	-	-	-
[130-150[	0.01	-	0.01	-	-	-	-	-	-	-	-	-	-	-
[150-170[	0.01	-	0.01	-	-	-	-	-	-	-	-	-	-	-
[170-190[	-	-	0.02	-	-	-	-	-	-	-	-	-	-	-
[190-210[	0.04	0.06	0.13	-	0.01	0.01	0.01	-	-	-	-	-	-	-
[210-230[	0.10	0.67	0.45	0.37	0.44	0.19	0.15	0.05	0.03	0.01	-	-	-	-
[230-250[	0.17	0.29	0.79	0.79	0.60	0.59	0.37	0.31	0.15	0.14	0.05	0.05	0.05	0.01
[250-270[	0.65	0.62	2.30	2.18	1.69	1.84	1.13	1.03	0.55	0.60	0.29	0.32	0.16	0.20
[270-290[	3.92	5.01	12.1	12.8	8.68	7.57	4.42	3.94	1.86	1.71	0.72	0.66	0.26	0.25
[290-310[	11.1	9.37	21.8	21.9	6.50	7.38	1.13	1.74	0.18	0.34	0.03	0.04	-	-
[310-330[	6.69	6.73	9.18	8.46	0.05	0.52	-	0.01	-	-	-	-	-	-
[330-350[	0.70	0.68	0.05	0.17	-	-	-	-	-	-	-	-	-	-
TOTAL	**23.7**	**23.7**	**46.8**	**46.8**	**18.0**	**18.1**	**7.21**	**7.09**	**2.77**	**2.80**	**1.09**	**1.07**	**0.47**	**0.47**

Table 6 – Same as in Table 5, but for the Costa Nova key-location.

Dir (º)	**[0 – 1 [m**		**[1 – 2 [m**		**[2 – 3 [m**		**[3 – 4 [m**		**[4 – 5 [m**		**[5 – 6 [m**		**[6 – 7 [m**		**[7 – ∞ [m**	
	E	**W**	**E**	**W**	**E**	**W**	**E**	**W**	**E**	**W**	**E**	**W**	**E**	**W**	**E**	**W**
[350-10[	0.02	0.04	0.02	0.02	-	-	-	-	-	-	-	-	-	-	-	-
[10-30[	0.01	0.06	0.02	0.03	-	-	-	-	-	-	-	-	-	-	-	-
[30-50[	0.01	0.07	0.02	0.04	-	-	-	-	-	-	-	-	-	-	-	-
[50-70[	-	-	0.01	-	-	-	-	-	-	-	-	-	-	-	-	-
[70-90[	-	-	0.01	-	-	-	-	-	-	-	-	-	-	-	-	-
[90-110[	-	-	0.03	-	-	-	-	-	-	-	-	-	-	-	-	-
[110-130[	0.01	-	0.02	-	-	-	-	-	-	-	-	-	-	-	-	-
[130-150[	-	-	0.03	-	-	-	-	-	-	-	-	-	-	-	-	-
[150-170[	-	-	0.01	-	-	-	-	-	-	-	-	-	-	-	-	-
[170-190[	-	-	0.02	-	-	-	-	-	-	-	-	-	-	-	-	-
[190-210[	0.05	-	0.03	-	-	-	-	-	-	-	-	-	-	-	-	-
[210-230[	0.10	0.13	0.30	0.21	-	0.07	-	-	-	-	-	-	-	-	-	-
[230-250[	0.20	0.41	0.67	0.38	0.20	0.29	0.01	0.11	-	0.02	-	-	-	-	-	-
[250-270[	0.28	0.29	1.27	0.99	0.86	0.88	0.43	0.53	0.13	0.23	0.05	0.11	0.01	-	-	0.01
[270-290[	1.17	0.97	4.61	6.36	6.37	5.89	4.13	3.49	2.28	1.82	1.09	0.98	0.67	0.06	0.12	0.13
[290-310[	3.92	4.87	23.1	21.4	14.3	14.3	5.93	6.27	1.96	2.28	0.80	0.89	0.57	0.73	0.05	0.03
[310-330[	6.03	4.85	14.5	15.3	2.09	2.40	0.09	0.19	-	0.02	-	-	-	0.45	-	-
[330-350[	0.65	0.55	0.71	0.81	-	0.01	-	-	-	-	-	-	-	-	-	-
TOTAL	**12.5**	**12.2**	**45.4**	**45.5**	**23.8**	**23.9**	**10.6**	**10.6**	**4.36**	**4.36**	**1.94**	**1.99**	**1.25**	**1.23**	**0.17**	**0.17**

Table 7 – Same as in Table 5, but for the Cova Gala key-location.

Dir (º)	**[0 – 1 [m**		**[1 – 2 [m**		**[2 – 3 [m**		**[3 – 4 [m**		**[4 – 5 [m**		**[5 – 6 [m**		**[6 – 7 [m**		**[7 – ∞ [m**	
	E	**W**	**E**	**W**	**E**	**W**	**E**	**W**	**E**	**W**	**E**	**W**	**E**	**W**	**E**	**W**
[350-10[	-	-	-	-	-	-	-	-	-	-	-	-	-	-	-	-
[10-30[	-	0.01	-	-	-	-	-	-	-	-	-	-	-	-	-	-
[30-50[	-	0.01	-	-	-	-	-	-	-	-	-	-	-	-	-	-
[50-70[	-	0.01	-	-	-	-	-	-	-	-	-	-	-	-	-	-

[70-90[	-	-	-	-	-	-	-	-	-	-	-	-	-	-	-	-
[90-110[	-	-	-	-	-	-	-	-	-	-	-	-	-	-	-	-
[110-130[	-	-	-	-	-	-	-	-	-	-	-	-	-	-	-	-
[130-150[	-	-	-	-	-	-	-	-	-	-	-	-	-	-	-	-
[150-170[	-	-	-	-	-	-	-	-	-	-	-	-	-	-	-	-
[170-190[	-	-	-	-	-	-	-	-	-	-	-	-	-	-	-	-
[190-210[	-	-	-	-	-	-	-	-	-	-	-	-	-	-	-	-
[210-230[	0.18	0.18	0.10	0.08	-	-	-	-	-	-	-	-	-	-	-	-
[230-250[	0.18	0.24	0.80	0.57	0.14	0.22	-	0.04	-	0.01	-	-	-	-	-	-
[250-270[	0.17	0.20	1.18	1.07	0.56	0.66	0.26	0.26	0.05	0.09	0.02	0.02	-	0.01	-	-
[270-290[	1.63	2.31	11.3	13.3	7.17	6.28	3.87	2.73	1.53	1.12	0.59	0.45	0.16	0.12	0.12	0.09
[290-310[	6.04	5.27	28.2	27.3	10.1	10.4	3.02	3.91	0.95	1.35	0.31	0.44	0.05	0.09	0.03	0.06
[310-330[	4.52	4.46	14.9	14.4	0.74	1.19	-	0.12	-	0.01	-	-	-	-	-	-
[330-350[	0.70	0.60	0.29	0.36	-	-	-	-	-	-	-	-	-	-	-	-
TOTAL	**13.4**	**13.3**	**56.8**	**57.1**	**18.8**	**18.7**	**7.15**	**7.06**	**2.54**	**2.58**	**0.92**	**0.91**	**0.21**	**0.22**	**0.15**	**0.15**

Table 8 – Same as in Table 5, but for the Costa da Caparica key-location.

Dir (º)	**[0 – 1 [m**		**[1 – 2 [m**		**[2 – 3 [m**		**[3 – 4 [m**		**[4 – ∞ [m**	
	E	**W**	**E**	**W**	**E**	**W**	**E**	**W**	**E**	**W**
[350-10[	0.01	0.01	-	-	-	-	-	-	-	-
[10-30[	0.00	0.01	-	-	-	-	-	-	-	-
[30-50[	0.00	0.01	-	-	-	-	-	-	-	-
[50-70[	0.02	0.02	-	-	-	-	-	-	-	-
[70-90[	0.08	-	-	-	-	-	-	-	-	-
[90-110[	0.12	-	-	-	-	-	-	-	-	-
[110-130[	0.06	-	-	-	-	-	-	-	-	-
[130-150[	0.06	0.22	-	0.07	-	0.01	-	-	-	-
[150-170[	0.11	0.13	0.01	0.01	-	-	-	-	-	-
[170-190[	0.08	0.12	0.06	0.01	-	-	-	-	-	-
[190-210[	0.10	0.48	0.29	0.05	0.10	0.03	0.05	0.02	0.31	0.05
[210-230[	0.62	0.65	3.83	1.92	5.57	4.12	2.53	2.37	0.38	0.65
[230-250[	8.33	6.40	28.2	29.5	4.21	5.70	0.01	0.14	-	-
[250-270[	26.2	27.7	7.28	8.17	-	-	-	-	-	-
[270-290[	10.0	7.91	0.07	0.07	-	-	-	-	-	-
[290-310[	1.19	3.01	-	-	-	-	-	-	-	-
[310-330[	0.05	0.41	-	-	-	-	-	-	-	-
[330-350[	0.02	0.01	-	-	-	-	-	-	-	-
TOTAL	**47.1**	**47.1**	**39.8**	**39.8**	**9.88**	**9.86**	**2.59**	**2.54**	**0.69**	**0.70**

Table 9 – Same as in Table 5, but for the Praia de Faro key-location.

Dir (º)	**[0 – 0.5 [m**		**[0.5 – 1 [m**		**[1 – 1.5 [m**		**[1.5 – 2 [m**		**[2 – 2.5 [m**		**[2.5 – 3 [m**		**[3 – 3.5 [m**		**[3.5 – ∞ [m**	
	E	**W**	**E**	**W**	**E**	**W**	**E**	**W**	**E**	**W**	**E**	**W**	**E**	**W**	**E**	**W**
[350-10[	0.17	0.44	-	0.01	-	-	-	-	-	-	-	-	-	-	-	-
[10-30[	0.11	0.89	-	0.04	-	-	-	-	-	-	-	-	-	-	-	-
[30-50[	0.17	0.54	-	0.01	-	-	-	-	-	-	-	-	-	-	-	-
[50-70[	0.16	0.07	-	-	-	-	-	-	-	-	-	-	-	-	-	-
[70-90[	0.24	-	-	-	-	-	-	-	-	-	-	-	-	-	-	-
[90-110[	0.58	-	-	-	-	-	-	-	-	-	-	-	-	-	-	-
[110-130[	1.23	0.01	-	-	-	-	-	-	-	-	-	-	-	-	-	-
[130-150[	2.67	1.71	0.72	1.84	-	0.41	-	0.13	-	0.05	-	0.03	-	0.03	-	0.01
[150-170[	1.92	1.55	9.21	3.49	2.91	5.86	0.49	2.95	0.07	1.07	-	0.43	-	0.23	-	0.09
[170-190[	0.03	0.09	0.79	2.46	2.59	2.17	1.74	0.31	0.71	0.02	0.41	-	0.21	-	0.09	-
[190-210[	0.03	0.01	0.18	0.28	0.22	0.19	0.11	0.02	0.05	-	-	-	-	-	-	-
[210-230[	0.05	0.05	0.47	1.38	1.02	0.74	0.70	0.06	0.15	-	0.04	-	0.03	-	0.01	-
[230-250[	3.76	6.20	23.4	22.7	5.73	3.09	0.54	0.11	0.13	-	0.02	-	0.01	-	-	-
[250-270[	19.7	20.3	8.90	11.6	0.05	0.08	-	-	-	-	-	-	-	-	-	-
[270-290[	6.29	5.43	0.57	0.53	-	-	-	-	-	-	-	-	-	-	-	-
[290-310[	0.20	0.09	-	-	-	-	-	-	-	-	-	-	-	-	-	-

[310-330[	0.10	0.09	-	-	-	-	-	-	-	-	-	-	-	-	-	-
[330-350[	0.30	0.15	-	0.01	-	-	-	-	-	-	-	-	-	-	-	-
TOTAL	**37.8**	**37.6**	**44.2**	**44.2**	**12.5**	**12.5**	**3.59**	**3.58**	**1.12**	**1.14**	**0.48**	**0.46**	**0.25**	**0.26**	**0.10**	**0.10**

Table 10 shows the overall performance of the coastal propagated-corrected 6-member ensemble wave fields at the key-locations, in comparison with the coastal propagated-corrected-propagated ERA5 reference data, in terms of the joint frequency of occurrence of all waves for each MWD bin (values corresponding to the ones displayed in Figure 25 to Figure 29 and Figure 36 to Figure 40). The differences between the ensemble and the reference data are highlighted using green (< 1%), yellow (< 2%), orange (< 3%), dark orange (< 4%), red (< 5%) and dark red (> 5%). Not surprisingly, at the coast, the overall ensemble's performance is better at the Ofir, Costa Nova and Cova Gala key-locations, with differences below 0.2% for all directional bins. At Costa da Caparica and Praia de Faro, the differences tend to be slightly greater, however, not exceeding 3.3% in both cases. While the ensemble tends to underestimate the southwesterly components at Costa da Caparica and Praia de Faro, it overestimates the westerly ones. Note that this feature was also apparent before the correction at the coast, as it shows in Figure 39 and Figure 40, being, nevertheless, smoothed after the procedure.

Table 10 – Near the coast H_S frequency of occurrence for each directional bin (20º) for the 6-memb. ens. and ERA5. Errors: green (0-1%), yellow (1-2%), orange (2-3%), dark orange (3-4%), red (4-5%), dark red (above 5%).

Directions (º)	F. ERA5 Ofir (%)	F. WW3 Ofir (%)	F. ERA5 Costa Nova (%)	F. WW3 Costa Nova (%)	F. ERA5 Cova Gala (%)	F. WW3 Cova Gala (%)	F. ERA5 Costa da Caparica (%)	F. WW3 Costa da Caparica (%)	F. ERA5 Praia de Faro (%)	F. WW3 Praia de Faro (%)
[350-10[	0.04	0.08	0.04	0.06	-	0.01	0.01	0.01	0.17	0.45
[10-30[	0.07	0.09	0.03	0.10	-	0.01	0.00	0.01	0.11	0.94
[30-50[	0.04	0.14	0.03	0.11	-	0.01	0.00	0.01	0.17	0.55
[50-70[	0.03	0.01	0.01	-	-	0.01	0.02	0.02	0.16	0.07
[70-90[	0.06	-	0.01	-	-	-	0.08	-	0.24	-
[90-110[	0.01	-	0.03	-	-	-	0.12	-	0.58	-
[110-130[	0.02	-	0.03	-	-	-	0.06	-	1.23	0.01
[130-150[	0.01	0.01	0.04	-	-	-	0.06	0.30	3.39	4.21
[150-170[	0.02	-	0.01	-	-	-	0.16	0.15	14.6	15.7
[170-190[	0.02	-	0.02	-	-	-	0.14	0.14	6.57	5.04
[190-210[	0.19	0.09	0.08	-	-	-	0.86	0.62	0.60	0.49
[210-230[	1.17	1.30	0.40	0.41	0.28	0.26	12.9	9.70	2.47	2.24
[230-250[	2.17	2.17	1.08	1.21	1.14	1.06	40.7	41.8	33.6	32.1
[250-270[	6.78	6.80	3.03	3.10	2.24	2.31	33.5	35.9	28.7	32.0
[270-290[	32.0	32.0	20.4	20.4	26.4	26.4	10.1	7.99	6.86	5.96
[290-310[	40.7	40.7	50.6	50.5	48.7	48.8	1.19	3.01	0.21	0.09

[310-330[	15.9	15.7	22.7	22.8	20.2	20.2	0.05	0.41	0.10	0.09
[330-350[	0.75	0.86	1.36	1.38	0.99	0.95	0.02	0.01	0.30	0.16

4.3. Propagated-corrected wave climate projections at the coast

The performance evaluation conducted for the propagated-corrected wave climate simulations during present climate at the 5 key-locations provided the necessary confidence in the ability of the ensemble to accurately simulate the local wave climatology and therefore provide a realistic climate change signal until 2100. Therefore, Figure 41 to Figure 45 describe the projected changes in each study area's wave fields (here depicted by H_S and MWD) for four future periods, under two scenarios: 2041-2070 (RCP4.5), 2071-2100 (RCP4.5), 2041-2070 (RCP8.5) and 2071-2100 (RCP8.5). The differences in the mean and 95% percentile H_S for each future period are also shown. Additionally, Table 11 to

Table 15 describe the projected frequencies of occurrence for each H_S bin ("F"; of 1 m for all locations except Praia de Faro, for which it is 0.5 m), in comparison with the present climate ("H") ones, consider each MWD bin (of 20º), and the entire directional range.

The projected changes at the Ofir key-location (Figure 41 and Table 11) show an overall increase in the frequency of occurrence of lower H_S values (below 1 m), ranging between 1.4% and 3.3% considering both RCPs after 2041. Such projected increase assumes greater values for the RCP8.5, nevertheless, consistent with enhanced projected decreases in the mean H_S values along the eastern North Atlantic, as described by Lemos *et al.* (2021a) and others (*e.g.* Semedo *et al.*, 2013; Hemer *et al.*, 2013, 2013a; Fan *et al.*, 2013; Shimura *et al.*, 2014; Wang *et al.*, 2014; Dobrynin *et al.*, 2015; Pérez *et al.*, 2015; Gallagher *et al.*, 2016; Aarnes *et al.*, 2017; Camus *et al.*, 2017; Casas-Prat *et al.*, 2018; Webb *et al.*, 2018; Morim *et al.*, 2018, 2019; Lemos *et al.*, 2019; 2020a). For H_S values above 1 m, frequencies are projected to decrease by the same order of magnitude as the increases expected for the first bin, however these are shown to be greater up to the 3 m mark (between 0.6% and 1.4% for 1-2 m, and 0.6% to 1.2% for 2-3 m). Events with H_S above 6 m are projected to decrease only marginally (from 0.47% down to 0.43% during 2071-2100 under RCP8.5). Regarding the mean and 95% percentile H_S associated with each MWD bin, differences are usually small (below 0.2 m), corresponding to normalized projected changes between 2% and 5%, which are also consistent with previous studies conducted for the eastern North Atlantic. Nevertheless, such projections vary in signal between scenarios. While during 2041-2070 under RCP4.5 projected increases are visible between 230º and 270º (W) of up to 0.1 m for the mean (~ 5%) and 0.2 m for the 95% percentile (~ 4%), for the remaining scenarios projected decreases are observable through most of the directional range, despite slight positive changes for the SW-WSW components (~ 2-3%) and NNW (only for the RCP8.5). During 2071-2100 under RCP8.5, extreme H_S values from the 230-240º range are also projected to increase, compatible with enhanced storm events from the SW, possibly associated with higher-latitude tropical and/or post-tropical cyclones in a warmer climate by the end of the 21st century. Note that especially for the RCP8.5, generous projected increases in H_S are visible across the 170-190º range (S), locally as high as 30% (nevertheless the associated frequencies of occurrence are below 0.01% for these instances).

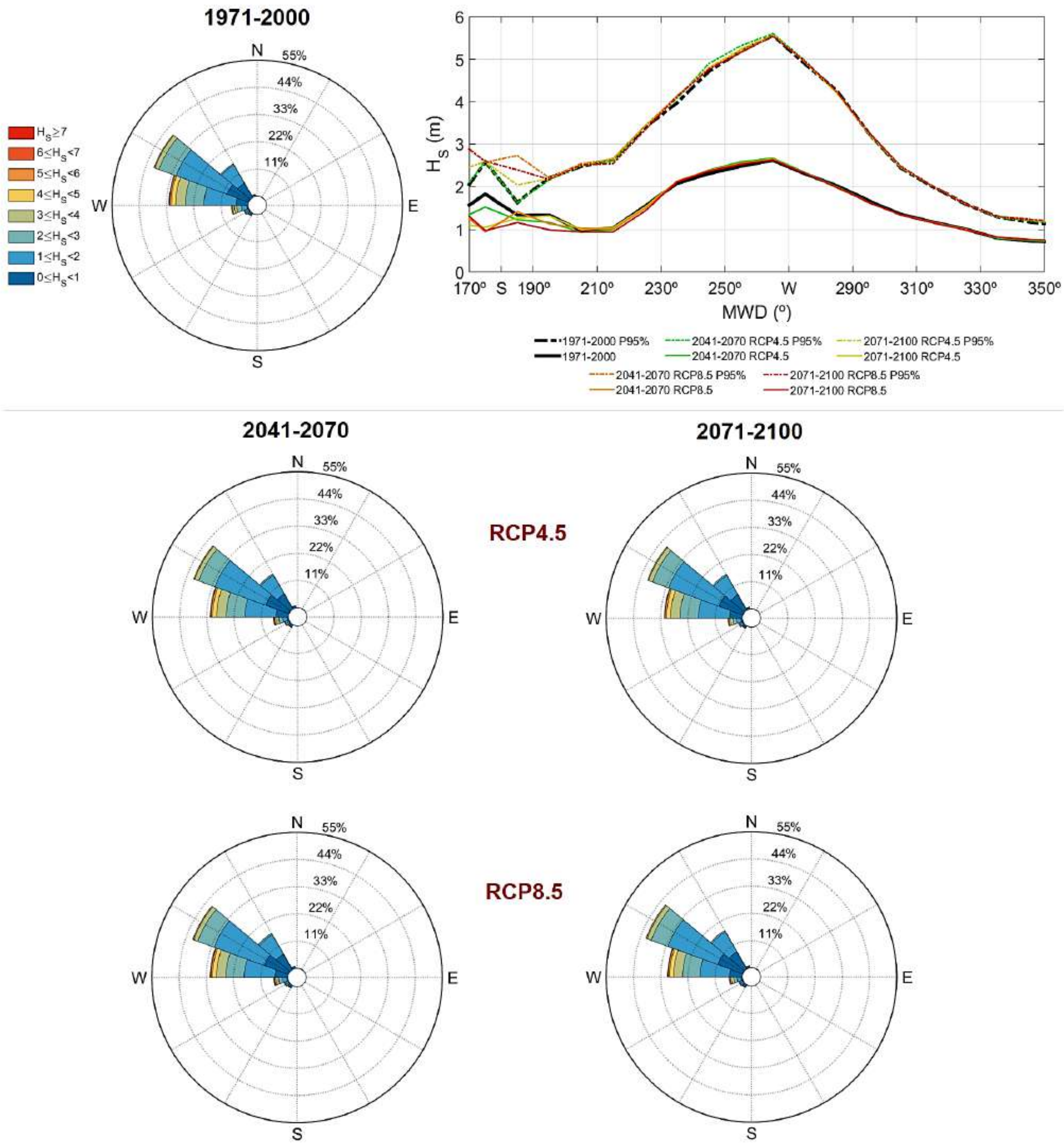

Figure 41 – Ofir 6-member ensemble historical and future projected coastal wave fields (wave roses), and mean H_S and 95% percentile H_S by bin of MWD (10º), along the possible range of incoming directions, per period, per scenario.

Table 11 – 6-member ensemble historical (H) and future projected (F) frequencies of occurrence (in %), considering the RCP4.5 2041-2070, RCP4.5 2071-2100, RCP8.5 2041-2070 and RCP8.5 2071-2100 time-slices per bin of propagated-corrected coastal H_S and MWD, at the Ofir key-location.

Dir (º)	[0 – 1 [m		[1 – 2 [m		[2 – 3 [m		[3 – 4 [m		[4 – 5 [m		[5 – 6 [m		[6 – ∞ [m	
	H	F	H	F	H	F	H	F	H	F	H	F	H	F
[350-10[	0.06	0.08 0.07 0.07	0.01	0.01 0.02 0.02	-	- - -	-	- - -	-	- - -	-	- - -	-	- - -

		0.08		0.02		-		-		-		-		-
[10-30[	0.07	0.08 0.09 0.09 0.09	0.02	0.02 0.02 0.01 0.02	-	- - - -	-	- - - -	-	- - - -	-	- - - -	-	- - - -
[30-50[	0.13	0.15 0.16 0.16 0.16	0.02	0.03 0.03 0.03 0.03	-	- - - -	-	- - - -	-	- - - -	-	- - - -	-	- - - -
[50-70[	0.01	- 0.01 - 0.01	-	- - - -	-	- - - -	-	- - - -	-	- - - -	-	- - - -	-	- - - -
[70-90[	-	- - - -	-	- - - -	-	- - - -	-	- - - -	-	- - - -	-	- - - -	-	- - - -
[90-110[	-	- - - -	-	- - - -	-	- - - -	-	- - - -	-	- - - -	-	- - - -	-	- - - -
[110-130[	-	- - - -	-	- - - -	-	- - - -	-	- - - -	-	- - - -	-	- - - -	-	- - - -
[130-150[	-	- - - -	-	- - - -	-	- - - -	-	- - - -	-	- - - -	-	- - - -	-	- - - -
[150-170[	-	- - - -	-	- - - -	-	- - - -	-	- - - -	-	- - - -	-	- - - -	-	- - - -
[170-190[	-	- - - -	-	- - - -	-	- - - -	-	- - - -	-	- - - -	-	- - - -	-	- - - -
[190-210[	0.06	0.06 0.05 0.05 0.06	0.02	0.02 0.02 0.02 0.02	0.01	0.01 0.01 0.01 0.01	-	- - - -	-	- - - -	-	- - - -	-	- - - -
[210-230[	0.67	0.75 0.69 0.74 0.84	0.37	0.35 0.34 0.32 0.31	0.19	0.19 0.18 0.18 0.17	0.05	0.05 0.05 0.05 0.05	0.01	0.01 0.01 0.01 0.01	-	- - - -	-	- - - -
[230-250[	0.29	0.27 0.27 0.26 0.25	0.79	0.71 0.67 0.65 0.63	0.59	0.59 0.57 0.56 0.52	0.31	0.31 0.31 0.31 0.29	0.14	0.13 0.12 0.13 0.12	0.04	0.06 0.05 0.05 0.04	0.01	0.02 0.02 0.02 0.02
[250-270[	0.62	0.56 0.55 0.54 0.53	2.18	1.84 1.80 1.72 1.62	1.84	1.63 1.61 1.56 1.45	1.04	1.00 0.96 0.94 0.88	0.60	0.58 0.55 0.53 0.50	0.32	0.30 0.29 0.26 0.24	0.20	0.19 0.18 0.17 0.16
[270-290[	5.01	5.16 5.29 5.29 5.30	12.9	12.6 12.6 12.5 11.9	7.58	7.46 7.40 7.37 7.07	3.94	3.81 3.74 3.76 3.59	1.72	1.68 1.65 1.66 1.59	0.65	0.65 0.61 0.62 0.61	0.25	0.25 0.24 0.25 0.25
[290-310[	9.37	10.1 10.3 10.5 10.9	21.9	21.7 21.6 21.5 21.4	7.38	7.07 6.99 7.07 7.14	1.74	1.71 1.73 1.74 1.78	0.34	0.35 0.36 0.36 0.39	0.04	0.05 0.05 0.05 0.07	-	- - 0.01 0.01

[310-330[	6.73	7.12 7.31 7.33 8.10	8.46	8.70 8.91 9.00 9.25	0.52	0.55 0.56 0.57 0.59	0.01	0.01 0.01 0.01 0.02	-	- - - -	-	- - - -	-	- - - -
[330-350[	0.68	0.75 0.74 0.74 0.74	0.17	0.20 0.22 0.23 0.24	-	- - - -	-	- - - -	-	- - - -	-	- - - -	-	- - - -
TOTAL	**23.7**	**25.1 25.6 25.8 27.0**	**46.8**	**46.2 46.2 46.0 45.4**	**18.1**	**17.5 17.3 17.3 16.9**	**7.09**	**6.89 6.81 6.82 6.60**	**2.80**	**2.75 2.69 2.69 2.61**	**1.07**	**1.05 1.00 0.99 0.97**	**0.47**	**0.47 0.44 0.44 0.43**

For the Costa Nova key-location (Figure 42 and

Table 12), while the general behaviour of the future projected wave climate at the coast (in terms of H_S and MWD) is similar to Ofir, some peculiarities may be highlighted. Regarding frequencies of occurrence, projections indicate more common lower H_S values (below 2 m), essentially incoming from northwards of 270º (W), compatible with the arrival of older swells generated at higher latitudes, due to the projected poleward displacement of the storm tracks. Differences in these projected frequencies, in comparison with the historical period, range between 1.9% (2041-2070 under RCP4.5) and 3.4% (2071-2100 under RCP8.5). In terms of mean and 95% percentile H_S, values are generally projected to decrease (increase) northwards (southwards) of 280º (WNW). These projections are below 0.2 m, or ~10% (0.3 m, or ~7%) for the mean (95% percentile) H_S, except for the SSW-SW range (200º-230º), where differences between 0.1-0.3 m, or up to 50% (0.3-0.8 m, or up to 70%) are projected to occur. Note, however, that the SSW-SW MWD range corresponds to the incoming directions of less than 1% of the total sample.

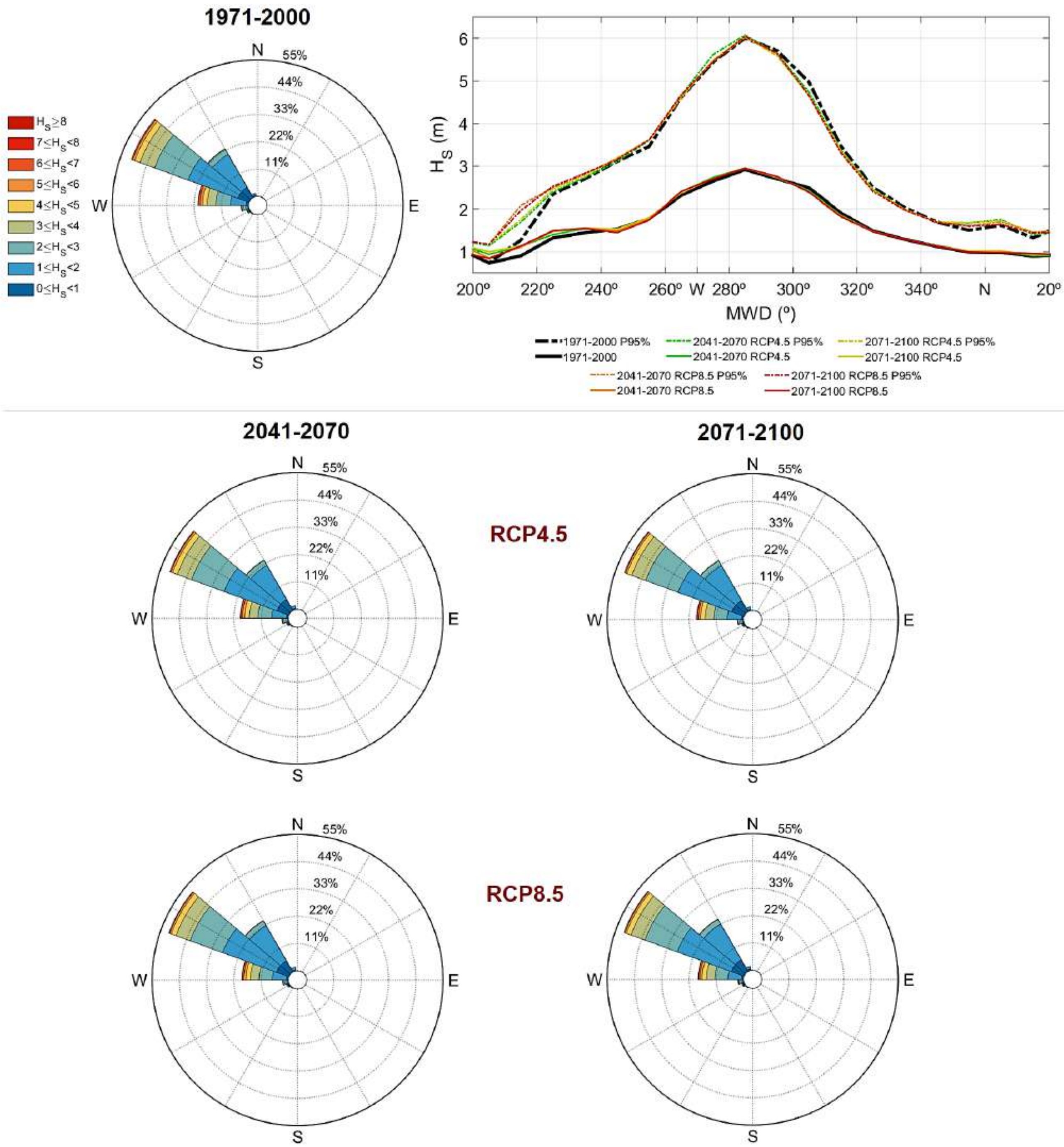

Figure 42 – Same as in Figure 41, but for the Costa Nova key-location.

Table 12 – Same as in Table 11, but for the Costa Nova key-location.

Dir (º)	[0 – 1 [m		[1 – 2 [m		[2 – 3 [m		[3 – 4 [m		[4 – 5 [m		[5 – 6 [m		[6 – 7 [m		[7 – ∞ [m	
	H	F	H	F	H	F	H	F	H	F	H	F	H	F	H	F
[350-10[	0.04	0.03 0.03 0.03 0.03	0.02	0.02 0.02 0.02 0.02	-	- - - -	-	- - - -	-	- - - -	-	- - - -	-	- - - -	-	- - - -
[10-30[	0.06	0.06 0.06 0.05 0.06	0.03	0.03 0.03 0.03 0.03	-	- - - -	-	- - - -	-	- - - -	-	- - - -	-	- - - -	-	- - - -
[30-50[	0.07	0.06 0.06 0.05 0.05	0.01	0.04 0.04 0.04 0.04	-	- - - -	-	- - - -	-	- - - -	-	- - - -	-	- - - -	-	- - - -
[50-70[	-	- - - -	-	- - - -	-	- - - -	-	- - - -	-	- - - -	-	- - - -	-	- - - -	-	- - - -
[70-90[	-	- - - -	-	- - - -	-	- - - -	-	- - - -	-	- - - -	-	- - - -	-	- - - -	-	- - - -
[90-110[	-	- - - -	-	- - - -	-	- - - -	-	- - - -	-	- - - -	-	- - - -	-	- - - -	-	- - - -
[110-130[	-	- - - -	-	- - - -	-	- - - -	-	- - - -	-	- - - -	-	- - - -	-	- - - -	-	- - - -
[130-150[	-	- - - -	-	- - - -	-	- - - -	-	- - - -	-	- - - -	-	- - - -	-	- - - -	-	- - - -
[150-170[	-	- - - -	-	- - - -	-	- - - -	-	- - - -	-	- - - -	-	- - - -	-	- - - -	-	- - - -
[170-190[	-	- - - -	-	- - - -	-	- - - -	-	- - - -	-	- - - -	-	- - - -	-	- - - -	-	- - - -
[190-210[	-	- - - -	-	- - - -	-	- - - -	-	- - - -	-	- - - -	-	- - - -	-	- - - -	-	- - - -
[210-230[	0.13	0.10 0.09 0.09 0.09	0.21	0.21 0.20 0.18 0.17	0.07	0.08 0.08 0.07 0.07	0.01	0.01 0.01 0.01 0.01	-	- - - -	-	- - - -	-	- - - -	-	- - - -
[230-250[	0.41	0.41 0.35 0.38 0.39	0.38	0.35 0.32 0.31 0.30	0.29	0.27 0.24 0.24 0.22	0.11	0.10 0.09 0.09 0.09	0.02	0.02 0.02 0.02 0.02	-	- - - -	-	- - - -	-	- - - -
[250-270[	0.29	0.23 0.23 0.22 0.21	0.99	0.81 0.77 0.71 0.70	0.88	0.77 0.77 0.72 0.69	0.53	0.49 0.47 0.45 0.44	0.23	0.20 0.19 0.19 0.18	0.11	0.10 0.09 0.08 0.08	0.06	0.06 0.05 0.04 0.04	0.01	0.01 0.01 0.01 0.01
[270-290[	0.97	0.89 0.87 0.87 0.85	6.36	5.92 5.78 5.69 5.56	5.89	5.58 5.47 5.39 5.25	3.49	3.42 3.41 3.40 3.33	1.82	1.89 1.84 1.83 1.79	0.98	0.94 0.90 0.90 0.88	0.73	0.65 0.59 0.59 0.60	0.13	0.13 0.13 0.13 0.13

[290-310[	4.87	5.21 5.38 5.42 5.53	21.4	22.6 23.0 23.1 23.2	14.3	14.0 13.9 13.9 13.9	6.27	6.08 5.99 6.03 5.93	2.28	2.11 2.12 2.12 2.06	0.89	0.74 0.69 0.70 0.67	0.45	0.32 0.27 0.27 0.25	0.03	0.02 0.02 0.02 0.01
[310-330[	4.85	5.20 5.22 5.28 5.52	15.3	15.9 16.3 16.4 16.6	2.40	2.23 2.20 2.21 2.17	0.19	0.16 0.16 0.15 0.14	0.02	0.01 0.01 0.01 0.01	-	- - - -	-	- - - -	-	- - - -
[330-350[	0.55	0.61 0.61 0.60 0.65	0.81	0.91 0.95 0.96 0.99	0.01	0.01 0.01 0.01 0.01	-	- - - -	-	- - - -	-	- - - -	-	- - - -	-	- - - -
TOTAL	**12.2**	**12.8 12.9 13.0 13.4**	**45.5**	**46.8 47.4 47.4 47.7**	**23.9**	**22.9 22.7 22.6 22.3**	**10.6**	**10.3 10.1 10.1 9.93**	**4.36**	**4.24 4.17 4.15 4.05**	**1.99**	**1.79 1.68 1.68 1.63**	**1.23**	**1.02 0.90 0.90 0.89**	**0.17**	**0.16 0.15 0.15 0.15**

At the Cova Gala key-location, while the absolute mean and 95% percentile values are shown to be lower than for Ofir and Costa Nova (Figure 43), projections show similar patterns to those of Figure 41 and Figure 42. Overall, as shown in

Table 13, H_S values below 1 m are projected to become more common, between 1.3% (2041-2070 under RCP4.5) and 2.5% (2071-2100 under RCP8.5), while higher wave heights are projected to become scarcer. Nevertheless, similarly to the previous locations, the frequency of the most extreme H_S values is projected to remain almost unaltered (from 0.15% to 0.13-0.14% for H_S above 7 m). While a consistent increase in the frequency of waves incoming from S-W (190º-270º) is projected to occur for all wave heights, above 270º this behaviour is generally limited to H_S below 1 m. Regarding the mean H_S, future projections show slight decreases between 250º and 330º (WSW-NNW), generally below 0.1 m (3-7%), except for the 2041-2070 period under RCP4.5, for which a projected increase is visible between 250º and 290º (WSW-WNW) up to 0.2 m (~10%). In contrast, the remaining scenarios show mean H_S projected increases between 230º and 250º (SW-WSW) and 330º and 360º (NNW-N). For the 95% percentile H_S, a similar pattern is visible northwards of 290º (WNW). Nevertheless, all scenarios project an increase of the extreme H_S southwards of 290º, generally within 0.1-0.3 m (5-20%). In fact, the 95% percentile H_S for the 2041-2070 period under the RCP4.5 scenario is projected to be higher than the historical value by 0.25 m (5.7%). Furthermore, between WSW-WNW, an increase from 0.2 m to 0.4 m (7-12%) is also expected during this period/scenario.

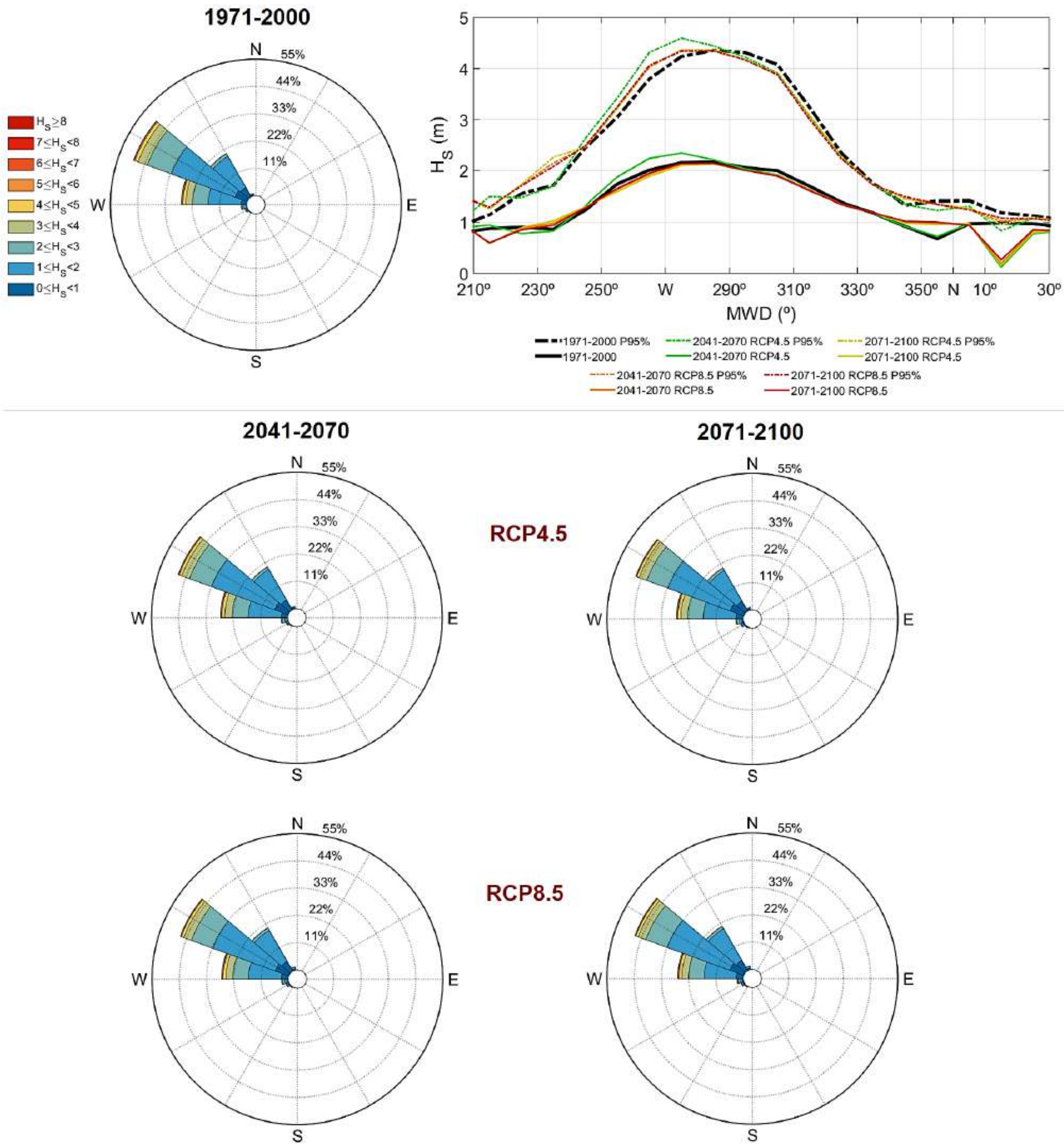

Figure 43 – Same as in Figure 41, but for the Cova Gala key-location.

Table 13 – Same as in Table 11, but for the Cova Gala key-location.

Dir (º)	[0 – 1 [m		[1 – 2 [m		[2 – 3 [m		[3 – 4 [m		[4 – 5 [m		[5 – 6 [m		[6 – 7 [m		[7 – ∞ [m	
	H	**F**	**H**	**F**	**H**	**F**	**H**	**F**	**H**	**F**	**H**	**F**	**H**	**F**	**H**	**F**
[350-10[	-	0.04 0.03 0.02 0.02	-	- 0.01 0.01 0.01	-	- - - -	-	- - - -	-	- - - -	-	- - - -	-	- - - -	-	- - - -
[10-30[	0.01	0.01 0.01 0.01 0.01	-	- - - -	-	- - - -	-	- - - -	-	- - - -	-	- - - -	-	- - - -	-	- - - -
[30-50[	0.01	0.01 0.01 0.01 0.01	-	- - - -	-	- - - -	-	- - - -	-	- - - -	-	- - - -	-	- - - -	-	- - - -
[50-70[	0.01	0.01 0.01 0.01 0.01	-	- - - -	-	- - - -	-	- - - -	-	- - - -	-	- - - -	-	- - - -	-	- - - -
[70-90[	-	0.01 0.01 0.01 0.01	-	- - - -	-	- - - -	-	- - - -	-	- - - -	-	- - - -	-	- - - -	-	- - - -
[90-110[	-	- - - -	-	- - - -	-	- - - -	-	- - - -	-	- - - -	-	- - - -	-	- - - -	-	- - - -
[110-130[	-	- - - -	-	- - - -	-	- - - -	-	- - - -	-	- - - -	-	- - - -	-	- - - -	-	- - - -
[130-150[	-	- 0.02 0.02 0.02	-	- - - -	-	- - - -	-	- - - -	-	- - - -	-	- - - -	-	- - - -	-	- - - -
[150-170[	-	- - - -	-	- - - -	-	- - - -	-	- - - -	-	- - - -	-	- - - -	-	- - - -	-	- - - -
[170-190[	-	- - - -	-	- - - -	-	- - - -	-	- - - -	-	- - - -	-	- - - -	-	- - - -	-	- - - -
[190-210[	-	- 0.10 0.08 0.06	-	- 0.01 0.01 0.01	-	- - - -	-	- - - -	-	- - - -	-	- - - -	-	- - - -	-	- - - -
[210-230[	0.18	0.33 0.29 0.30 0.32	0.08	0.09 0.14 0.12 0.12	-	0.01 0.03 0.02 0.02	-	- - - -	-	- - - -	-	- - - -	-	- - - -	-	- - - -
[230-250[	0.24	0.22 0.45 0.40 0.36	0.57	0.59 0.75 0.67 0.61	0.22	0.26 0.24 0.24 0.22	0.04	0.07 0.06 0.06 0.06	0.01	0.02 0.01 0.01 0.01	-	- - - -	-	- - - -	-	- - - -
[250-270[	0.20	0.21 0.65 0.53 0.46	1.07	1.11 1.08 1.01 0.99	0.66	0.82 0.79 0.74 0.69	0.26	0.40 0.35 0.33 0.32	0.09	0.16 0.14 0.13 0.12	0.02	0.05 0.04 0.04 0.03	0.01	0.01 0.01 0.01 0.01	-	0.01 0.01 0.01 -
[270-290[	2.31	2.60 3.01 2.95 2.89	13.3	13.4 13.2 13.2 13.0	6.28	6.51 6.32 6.29 6.19	2.73	2.94 2.78 2.79 2.74	1.12	1.14 1.09 1.09 1.07	0.45	0.43 0.40 0.39 0.38	0.12	0.11 0.10 0.10 0.10	0.09	0.09 0.09 0.09 0.09

[290-310[	5.27	5.86 5.90 5.89 6.07	27.3	27.1 26.7 26.8 26.9	10.4	9.46 9.14 9.25 9.18	3.91	3.31 3.24 3.25 3.19	1.35	1.09 1.05 1.06 1.03	0.44	0.35 0.32 0.33 0.32	0.09	0.08 0.07 0.07 0.06	0.06	0.04 0.04 0.04 0.04
[310-330[	4.46	4.70 4.64 4.67 4.87	14.4	14.2 14.3 14.4 14.7	1.19	1.06 1.06 1.06 1.02	0.12	0.10 0.09 0.09 0.09	0.01	0.01 0.01 0.01 0.01	-	- - - -	-	- - - -	-	- - - -
[330-350[	0.60	0.62 0.63 0.66 0.73	0.36	0.36 0.57 0.72 0.83	-	- - - -	-	- - - -	-	- - - -	-	- - - -	-	- - - -	-	- - - -
TOTAL	**13.3**	**14.6 15.8 15.6 15.8**	**57.1**	**56.8 56.7 56.9 57.2**	**18.7**	**18.2 17.6 17.6 17.3**	**7.06**	**6.81 6.54 6.54 6.39**	**2.58**	**2.41 2.30 2.30 2.24**	**0.91**	**0.83 0.76 0.76 0.74**	**0.22**	**0.20 0.18 0.18 0.17**	**0.15**	**0.14 0.14 0.14 0.13**

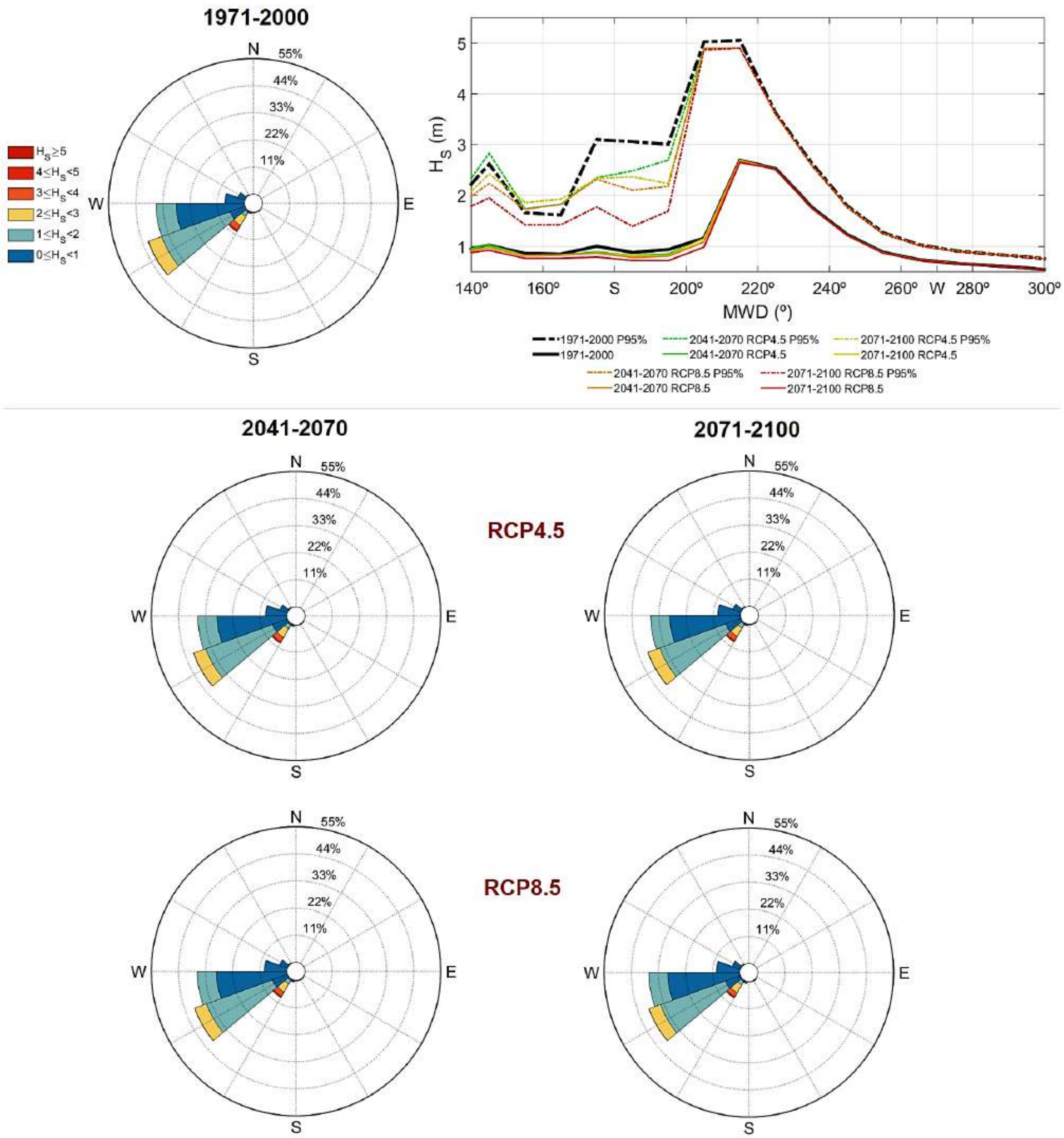

Figure 44 – Same as in Figure 41, but for the Costa da Caparica key-location.

Table 14 – Same as in Table 11, but for the Costa da Caparica key-location.

Dir (º)	[0 – 1 [m		[1 – 2 [m		[2 – 3 [m		[3 – 4 [m		[4 – ∞ [m	
	H	F	H	F	H	F	H	F	H	F
[350-10[	0.01	0.01 0.01 0.01 0.02	-	- - - -	-	- - - -	-	- - - -	-	- - - -
[10-30[	0.01	0.01 0.01 0.01 0.01	-	- - - -	-	- - - -	-	- - - -	-	- - - -
[30-50[	0.01	0.01 0.01 0.01 0.01	-	- - - -	-	- - - -	-	- - - -	-	- - - -
[50-70[	0.02	0.01 0.01 0.01 0.01	-	- - - -	-	- - - -	-	- - - -	-	- - - -
[70-90[	-	- - - -	-	- - - -	-	- - - -	-	- - - -	-	- - - -
[90-110[	-	- - - -	-	- - - -	-	- - - -	-	- - - -	-	- - - -
[110-130[	-	- - - -	-	- - - -	-	- - - -	-	- - - -	-	- - - -
[130-150[	0.22	0.23 0.26 0.26 0.28	0.07	0.08 0.08 0.08 0.08	0.01	0.01 0.01 0.01 0.01	-	- - - -	-	0.01 - - -
[150-170[	0.13	0.16 0.15 0.17 0.21	0.01	0.02 0.01 0.01 0.01	-	- - - -	-	- - - -	-	- - - -
[170-190[	0.12	0.15 0.15 0.16 0.21	0.01	0.01 0.01 0.01 0.01	-	0.01 - - -	-	- - - -	0.01	- - - -
[190-210[	0.48	0.60 0.58 0.65 0.77	0.05	0.05 0.05 0.05 0.05	0.03	0.03 0.03 0.03 0.03	0.02	0.02 0.02 0.02 0.01	0.05	0.06 0.06 0.06 0.05
[210-230[	0.65	0.63 0.56 0.55 0.57	1.92	1.77 1.76 1.67 1.59	4.12	3.95 3.84 3.82 3.64	2.37	2.19 2.07 2.04 1.95	0.64	0.62 0.57 0.55 0.53
[230-250[	6.40	6.45 6.56 6.52 6.46	29.5	28.8 28.5 28.4 28.0	5.70	5.21 5.07 5.06 4.91	0.14	0.12 0.11 0.11 0.11	-	- - - -
[250-270[	27.7	28.3 28.7 28.7 29.2	8.17	7.85 7.75 7.73 7.64	-	- - - -	-	- - - -	-	- - - -
[270-290[	7.91	8.70 9.11	0.07	0.07 0.08	-	- -	-	- -	-	- -

		9.23 9.51		0.07 0.08		- -		- -		- -
[290-310[	3.01	3.35 3.46 3.50 3.51	-	- - - -	-	- - - -	-	- - - -	-	- - - -
[310-330[	0.41	0.44 0.42 0.44 0.43	-	- - - -	-	- - - -	-	- - - -	-	- - - -
[330-350[	0.01	0.02 0.02 0.02 0.02	-	- - - -	-	- - - -	-	- - - -	-	- - - -
TOTAL	**47.1**	**49.1 50.0 50.2 51.3**	**39.8**	**38.7 38.2 38.1 37.5**	**9.86**	**9.21 8.96 8.92 8.58**	**2.54**	**2.33 2.21 2.17 2.08**	**0.70**	**0.68 0.64 0.62 0.60**

The characteristics of the wave climate and associated projected changes at the Costa da Caparica key-location are shown in Figure 44 and

Table 14. Overall, across the most frequent MWD range (130º-330º), the frequencies of occurrence of low wave heights (H_S below 1 m) are projected to increase, between 2.0% for the 2041-2070 period under the RCP4.5, and 4.2%, for the 2071-2100 period under RCP8.5. For H_S values above 1 m, the opposite behaviour is projected, with enhanced decreases towards the end of the 21st century, and the highest emission scenarios. In contrast with Ofir, Costa Nova and Cova Gala, at Costa da Caparica the mean H_S is projected to decrease throughout the entire directional range for all periods and scenarios, especially for MWD values below 210º (SSW), for which differences between -0.1 m and -0.2 m (10% to 20%) can be expected. Northwards of 210º, projected changes in mean H_S are negligible in comparison with the historical period. In terms of 95% percentile H_S, the general behaviour is similar to the mean H_S, however, the projected decreases tend to be greater, especially between 170º-200º (SSE-SSW), down to -0.75 m or -24% (-1.65 m or -54%) for the 2041-2070 RCP4.5 (2071-2100 RCP8.5) period. It should be noted, however, that incoming MWDs below 210º account for only 1-2% of the total samples.

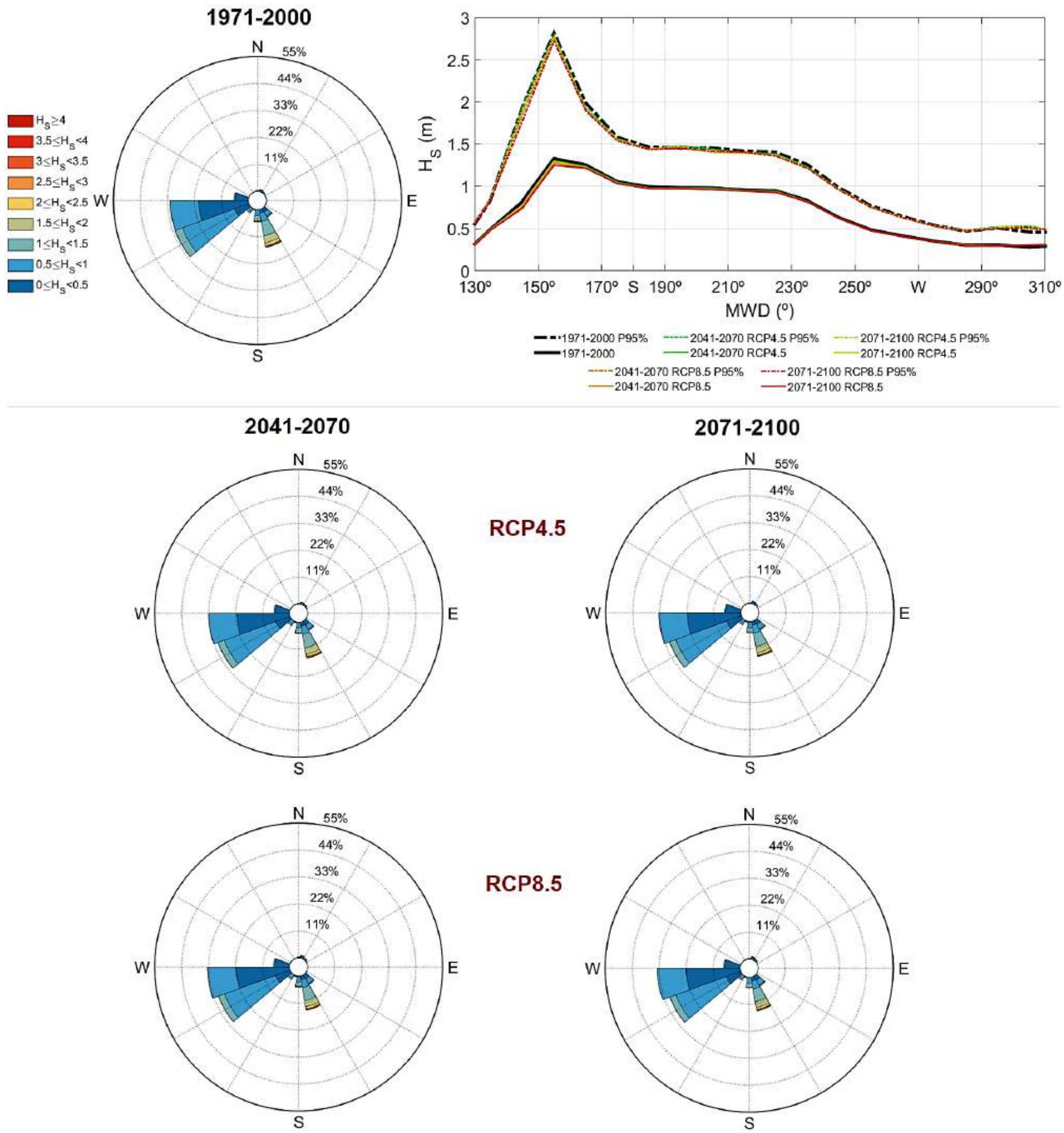

Figure 45 – Same as in Figure 41, but for the Praia de Faro key-location.

Table 15 – Same as in Table 11, but for the Praia de Faro key-location.

Dir (º)	[0 – 0.5 [m		[0.5 – 1 [m		[1 – 1.5 [m		[1.5 – 2 [m		[2 – 2.5 [m		[2.5 – 3 [m		[3 – 3.5 [m		[3.5 – ∞ [m	
	H	**F**	**H**	**F**	**H**	**F**	**H**	**F**	**H**	**F**	**H**	**F**	**H**	**F**	**H**	**F**
[350-10[	0.44	0.41 0.43 0.42 0.44	0.01	0.01 0.01 0.01 0.01	-	- - - -	-	- - - -	-	- - - -	-	- - - -	-	- - - -	-	- - - -
[10-30[	0.89	0.97 1.07 1.10 1.15	0.04	0.05 0.04 0.04 0.05	-	- - - -	-	- - - -	-	- - - -	-	- - - -	-	- - - -	-	- - - -
[30-50[	0.54	0.60 0.67 0.69 0.71	0.01	0.02 0.02 0.02 0.02	-	- - - -	-	- - - -	-	- - - -	-	- - - -	-	- - - -	-	- - - -
[50-70[	0.07	0.09 0.10 0.10 0.11	-	- - - -	-	- - - -	-	- - - -	-	- - - -	-	- - - -	-	- - - -	-	- - - -
[70-90[	-	0.01 0.01 - -	-	- - - -	-	- - - -	-	- - - -	-	- - - -	-	- - - -	-	- - - -	-	- - - -
[90-110[	-	- - 0.01 -	-	- - - -	-	- - - -	-	- - - -	-	- - - -	-	- - - -	-	- - - -	-	- - - -
[110-130[	0.01	0.02 0.02 0.02 0.02	-	- - - -	-	- - - -	-	- - - -	-	- - - -	-	- - - -	-	- - - -	-	- - - -
[130-150[	1.71	1.94 1.98 2.02 2.15	1.84	1.89 1.95 1.99 2.07	0.41	0.35 0.38 0.36 0.36	0.13	0.12 0.13 0.12 0.11	0.05	0.06 0.06 0.05 0.05	0.03	0.03 0.03 0.03 0.02	0.03	0.03 0.03 0.03 0.02	0.01	0.01 0.01 0.01 0.01
[150-170[	1.55	1.63 1.62 1.64 1.73	3.49	3.41 3.29 3.26 3.26	5.86	5.56 5.43 5.32 5.19	2.95	2.72 2.60 2.53 2.41	1.07	0.95 0.89 0.86 0.82	0.43	0.39 0.36 0.35 0.33	0.23	0.21 0.20 0.19 0.18	0.09	0.09 0.07 0.07 0.07
[170-190[	0.09	0.01 0.09 0.09 0.09	2.46	2.32 2.33 2.29 2.26	2.17	1.97 1.87 1.86 1.81	0.31	0.26 0.25 0.24 0.22	0.02	0.01 0.01 0.01 0.01	-	- - - -	-	- - - -	-	- - - -
[190-210[	0.01	0.01 0.01 0.01 0.01	0.28	0.26 0.25 0.25 0.25	0.19	0.17 0.16 0.16 0.15	0.02	0.02 0.01 0.01 0.01	-	- - - -	-	- - - -	-	- - - -	-	- - - -
[210-230[	0.05	0.06 0.06 0.06 0.06	1.38	1.35 1.36 1.35 1.33	0.74	0.69 0.67 0.67 0.66	0.06	0.05 0.05 0.05 0.04	-	- - - -	-	- - - -	-	- - - -	-	- - - -
[230-250[	6.20	6.24 6.35 6.30 6.22	22.7	22.3 22.1 22.2 21.9	3.09	2.70 2.59 2.60 2.50	0.11	0.09 0.08 0.08 0.07	-	- - - -	-	- - - -	-	- - - -	-	- - - -
[250-270[	20.3	21.5 21.8 21.8 22.1	11.6	11.5 11.6 11.6 11.7	0.08	0.06 0.06 0.06 0.05	-	- - - -	-	- - - -	-	- - - -	-	- - - -	-	- - - -
[270-290[	5.43	5.84 6.02 6.11 6.24	0.53	0.52 0.53 0.52 0.53	-	- - - -	-	- - - -	-	- - - -	-	- - - -	-	- - - -	-	- - - -

[290-310[	0.09	0.09 0.09 0.09 0.10	-	0.01 0.01 0.01 0.01	-	- - - -	-	- - - -	-	- - - -	-	- - - -	-	- - - -	-	- - - -
[310-330[	0.09	0.09 0.09 0.09 0.09	-	- - - -	-	- - - -	-	- - - -	-	- - - -	-	- - - -	-	- - - -	-	- - - -
[330-350[	0.15	0.18 0.20 0.21 0.22	0.01	0.01 0.01 0.01 0.01	-	- - - -	-	- - - -	-	- - - -	-	- - - -	-	- - - -	-	- - - -
TOTAL	**37.6**	**39.8** **40.6** **40.8** **41.5**	**44.2**	**43.7** **43.5** **43.5** **43.4**	**12.5**	**11.5** **11.2** **11.0** **10.7**	**3.58**	**3.26** **3.11** **3.03** **2.87**	**1.14**	**1.02** **0.96** **0.93** **0.88**	**0.46**	**0.41** **0.39** **0.38** **0.35**	**0.26**	**0.24** **0.23** **0.22** **0.20**	**0.10**	**0.10** **0.08** **0.08** **0.08**

At the Praia de Faro key-location, in the south-facing coast of Portugal (Figure 45 and

Table 15), similarly to the remaining key-locations, projections show an increase in the frequency of occurrence of lower H_S values (below 0.5 m), at both the main sectors of incoming waves (150º-170º - SSE, and 230º-270º - SW-W). Overall, waves below (above) 0.5 m H_S are projected to become commoner (scarcer) in between 2.2% and 3.9%, for the 2041-2070 RCP4.5 and 2071-2100 RCP8.5 periods, respectively. Projected changes in the mean and 95% percentile H_S follow a similar behaviour at Praia de Faro, showing consistent decreases throughout most of the incoming directional range (except between 300º and 310º; NW). For both cases, projected differences assume similar absolute magnitudes, generally below 0.1 m. From the five key-locations, Praia de Faro exhibits the most constant wave climate features throughout the 21st century projected future periods.

Table 16 shows the overall projected changes as represented by the coastal propagated-corrected 6-member ensemble of wave climate projected at each of the five key-locations, in terms of total frequency of occurrence considering all waves for each MWD bin. At the Ofir and Costa Nova locations (first four rows of Table 16), incoming directions below (above) 290º (WNW) are projected to become less (more) frequent. The frequency increase of northerly waves (above 290º) on the overall balance ranges from 1.08% to 4.22% at Ofir, and 1.45% to 2.97% at Costa Nova, considering the 2041-2070 RCP4.5 and 2071-2100 RCP8.5 projected periods. At Cova Gala, on the other hand, projections also reveal an increase in frequency for MWDs within 190º-290º (SSW-WNW, especially for the 2071-2100 RCP4.5 future period, at 2.15%), in addition to the slight increase for the 310º-350º (NW-N) interval. In Costa da Caparica, directional frequency projected increases are also bimodal, across 130º-210º (SE-SW) and northwards of 250º (WSW). The projected frequency decreases between 210º and 250º range from -1.75% (2041-2070 RCP4.5) to -3.72% (2071-2100 RCP8.5). Finally, at Praia de Faro, the frequency of occurrence of MWDs below 250º (WSW) is generally expected to decrease, except for the 130º-150º range (SE-SSE). Northwards of 250º, projected increases vary between 1.53% (2041-2070 RCP4.5) and 2.80% (2071-2100 RCP8.5). Note, nevertheless, that across Costa da Caparica and Praia de Faro, the ensemble was shown to slightly underestimate the southwesterly components while overestimating the westerly ones, even after the propagation-correction procedure (Table 11).

Table 16 – Near the coast H_S frequency of occurrence for each directional bin (20º) for the 6-member ensemble, considering the RCP4.5 2041-2070, RCP4.5 2071-2100, RCP8.5 2041-2070 and RCP8.5 2071-2100 time-slices per bin of propagated-corrected coastal H_S and MWD.

Directions (º)	F. Hist. Ofir (%)	F. Fut. Ofir (%)	F. Hist. Costa Nova (%)	F. Fut. Costa Nova (%)	F. Hist. Cova Gala (%)	F. Fut. Cova Gala (%)	F. Hist. Costa da Caparica (%)	F. Fut. Costa da Caparica (%)	F. Hist. Praia de Faro (%)	F. Fut. Praia de Faro (%)
[350-10[	0.08	0.09 0.09 0.09 0.09	0.06	0.05 0.05 0.04 0.05	0.01	0.04 0.03 0.03 0.03	0.01	0.01 0.01 0.01 0.02	0.45	0.42 0.44 0.44 0.46
[10-30[	0.09	0.10 0.10 0.10 0.11	0.10	0.09 0.09 0.09 0.09	0.01	0.01 0.01 0.01 0.01	0.01	0.01 0.01 0.01 0.01	0.94	1.02 1.11 1.15 1.19
[30-50[	0.14	0.18 0.19 0.19 0.19	0.11	0.09 0.10 0.10 0.10	0.01	0.01 0.01 0.01 0.01	0.01	0.01 0.01 0.01 0.01	0.55	0.62 0.68 0.70 0.73
[50-70[	0.01	0.01 0.01 - 0.01	-	0.01 - - -	0.01	0.01 0.01 0.01 0.01	0.02	0.01 0.01 0.01 0.01	0.07	0.09 0.10 0.10 0.11
[70-90[	-	- - - -	-	- - - -	-	0.01 0.01 0.01 0.01	-	- - - -	-	0.01 0.01 - 0.01
[90-110[	-	- - - -	-	- - - -	-	- - - -	-	- - - -	-	- - 0.01 0.01
[110-130[	-	- - - -	-	- - - -	-	- - - -	-	- - - -	0.01	0.02 0.02 0.02 0.02
[130-150[	0.01	0.01 0.01 0.01 0.01	-	- - - -	-	- 0.02 0.02 0.02	0.30	0.32 0.35 0.36 0.38	4.21	4.43 4.56 4.61 4.80

[150-170[	-	0.01 0.01 - 0.01	-	- - - -	-	- - - -	0.15	0.18 0.18 0.19 0.24	15.7	15.0 14.5 14.2 14.0
[170-190[	-	- - - -	-	- - - -	-	- - - -	0.14	0.17 0.17 0.18 0.23	5.04	4.66 4.55 4.49 4.39
[190-210[	0.09	0.09 0.08 0.08 0.09	-	- - - -	-	0.01 0.11 0.08 0.07	0.62	0.76 0.75 0.80 0.92	0.49	0.46 0.44 0.44 0.43
[210-230[	1.30	1.35 1.27 1.31 1.39	0.41	0.40 0.38 0.35 0.34	0.26	0.43 0.46 0.45 0.45	9.70	9.15 8.80 8.63 8.28	2.24	2.15 2.13 2.13 2.09
[230-250[	2.17	2.07 2.01 1.97 1.85	1.21	1.14 1.02 1.04 1.02	1.06	1.16 1.53 1.38 1.26	41.8	40.6 40.2 40.1 39.5	32.1	31.3 31.1 31.1 30.7
[250-270[	6.80	6.09 5.93 5.73 5.37	3.10	2.66 2.57 2.42 2.34	2.31	2.79 3.07 2.80 2.62	35.9	36.2 36.4 36.4 36.9	32.0	33.1 33.4 33.5 33.9
[270-290[	32.0	31.6 31.5 31.4 30.3	20.4	19.4 19.0 18.8 18.4	26.4	27.2 27.0 26.9 26.5	7.99	8.77 9.19 9.30 9.59	5.96	6.36 6.55 6.62 6.77
[290-310[	40.7	41.0 41.0 41.2 41.7	50.5	51.1 51.3 51.6 51.5	48.8	47.3 46.4 46.6 46.8	3.01	3.35 3.46 3.50 3.51	0.09	0.09 0.10 0.10 0.10
[310-330[	15.7	16.4 16.8 16.9 17.8	22.8	23.5 23.9 24.0 24.5	20.2	20.1 20.1 20.3 20.7	0.41	0.44 0.42 0.44 0.43	0.09	0.09 0.09 0.09 0.10
[330-350[	0.86	0.94 0.96 0.96 0.98	1.38	1.53 1.58 1.58 1.65	0.95	0.98 1.21 1.38 1.55	0.01	0.02 0.02 0.02 0.02	0.16	0.19 0.21 0.22 0.23

4.4. Shoreline evolution

The permanent wave action along a sandy shoreline modulates its sedimentary balance with the establishment of longshore currents which, in the absence of human action, are responsible for both short- and long-term shoreline evolution. The evolution of the shoreline depending exclusively on waves may consist of a retreat or advance depending on the MWD. The effect of SLR, on the other hand, promotes a long-term consistent retreat, due to the increasing accommodation space, which forces the equilibrium profile landward and upward to preserve its shape relative to the sea level. At a global scale, Luijendijk *et al.* (2018) showed that, since 1984, 24% of the world's sandy beaches are eroding at rates exceeding 0.5 m/year, 48% are stable and 28% are accreting. It was also shown that the majority of the sandy shorelines in marine protected areas are eroding. Although the global distribution of eroding and accreting sandy beaches may be considered irregular, greatly depending on the local wave climate characteristics and shoreline orientation, the Iberian Peninsula, and consequently Portugal, are shown to be in an area of relatively high sandy beach erosion (Figure 46). In fact, erosion in Portugal has been thoroughly studied over the last decades (*e.g.*, Santos *et al.*, 2014; Pinto *et al.*, 2016; Ponte Lira *et al.*, 2016; Ferreira *et al.*, 2020). It has been concluded that from 1958 to 2021, the total area lost to the sea, at national scale, amounted to 13.5 km^2, with 45% of the Portuguese low sandy beaches under erosion (APA's database, updated from Pinto *et al.*, 2020).

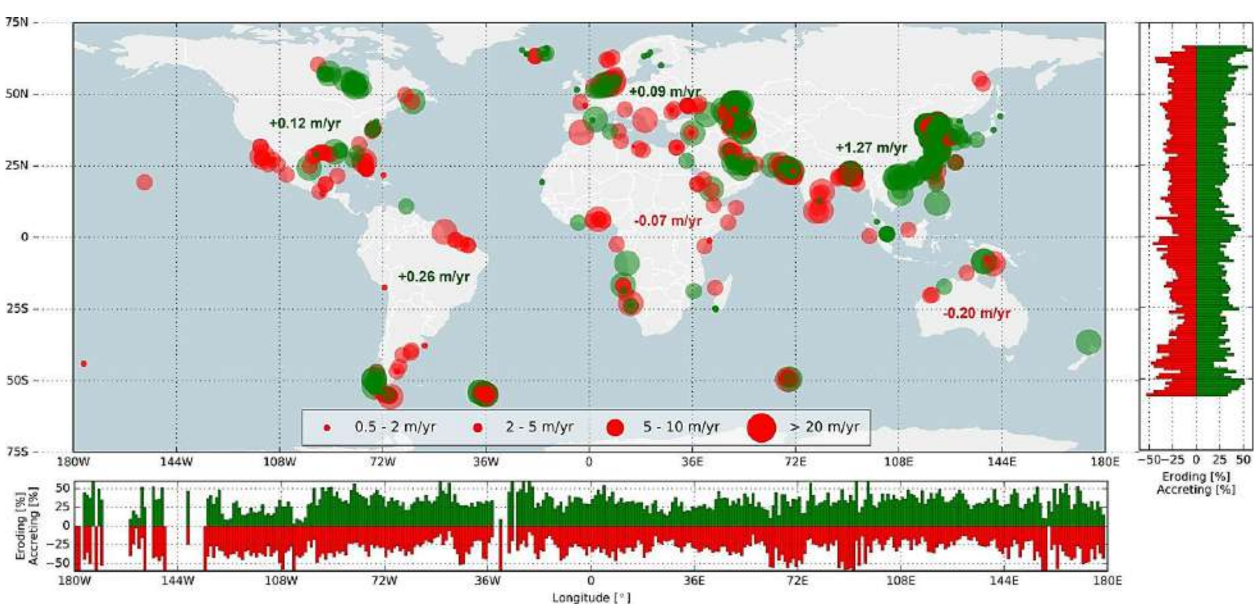

Figure 46 – Global hotspots of beach erosion and accretion; the red (green) circles indicate erosion (accretion) for the four relevant shoreline dynamic classifications (see legend). The bar plots to the right and at the bottom present the relative occurrence of eroding (accreting) sandy shorelines per degree latitude and longitude, respectively. The

numbers presented in the main plot represent the average change rate for all sandy shorelines per continent. From Luijendijk *et al.* (2018).

In this study, ShorelineS model is first evaluated, at each of the five key-locations, in terms of its ability to depict a correct shoreline evolution between 2008 and 2018, using observations from aerophotogrammetry together with a simulation forced by the propagated-corrected-propagated ERA5 wave data near the coast (no SLR or tides are considered during this period). Parameterizations are tuned within the shoreline evolution model to find the better fit to the observations throughout the 2008-2018 period (focusing essentially on the sectors without human intervention, whenever possible). These parameterizations are then used to project shoreline evolution towards 2100 following both the RCP4.5 and RCP8.5 scenarios of the 6-member ensemble of propagated-corrected wave climate projections. For each key-location, future period and scenario, a 6-member ensemble of projected shorelines is obtained. This ensemble approach may help to better quantify the uncertainty associated with the wave climate projections in terms of their further applicability using ShorelineS. SLR is considered when projecting future shorelines, as the average estimate of the associated 21-member ensemble. Note that SLR data is adjusted to the national vertical datum, the MSL of Cascais 1938, which corresponds to a MSL of 13 cm by the year 2000. This means that 75 cm of SLR, from 2000 to 2100, will lead to a MSL, at the end of the century, corresponding, in fact, to 88 cm relative to the national elevation reference system (Cascais MSL1938). The final output consists of a single future projected shoreline, based on the mean of the 6-member ensemble forced by future projected wave climate conditions combined with the retreat associated to the 21-member average SLR estimate using Bruun's rule (Bruun, 1988), that accounts only for the possible accommodation space available upon retreat.

Table 17 summarizes the ensemble mean LST projections for both the RCP4.5 and RCP8.5 scenarios across each of the key-locations, during the entire 21st century (2011-2100), divided into three time-slices (2011-2040, 2041-2070 and 2071-2100), showing also the mean yearly trend throughout this 90-year period. Values are shown in 10^6 m^3/year, positive (negative) for southward (northward) transport.

Table 17 – Ensemble mean LST projections at each of the key-locations for the RCP4.5 and RCP8.5 scenarios throughout the 21st century, and ensemble mean yearly trend during 2011-2100 (10^6 m^3/year).

Longshore Sediment Transport Ensemble Mean (10^6 m^3/year)				
RCP4.5				
	2011-2040	**2041-2070**	**2071-2100**	**Trend**
Ofir	1.251	1.166	1.127	-0.0020
Costa Nova	0.820	0.783	0.805	-0.0003
Cova Gala	0.960	0.880	0.858	-0.0017
Costa da Caparica	-0.527	-0.489	-0.435	0.0014
Praia de Faro	-0.083	-0.078	-0.066	0.0030
RCP8.5				
	2011-2040	**2041-2070**	**2071-2100**	**Trend**
Ofir	1.247	1.190	1.205	-0.0007
Costa Nova	0.861	0.855	0.803	-0.0008
Cova Gala	0.838	0.805	0.748	-0.0015
Costa da Caparica	-0.511	-0.438	-0.378	0.0024
Praia de Faro	-0.079	-0.062	-0.053	0.0005

4.4.1. Ofir

At first instance, the ability of the ShorelineS model to accurately represent the complex processes driving shoreline evolution is evaluated. To do so, the model is forced with hydrodynamic conditions from ERA5 (H_S, T_m and MWD) from 2008 to 2018. This time window corresponds to two moments where aerophotogrammetric data is available and can be used to produce initial and final target conditions for the shoreline, based on real observations. ShorelineS simulated free shoreline evolution from 2008 until 2018, not accounting for human intervention processes, SLR (which was measured at 3.5 cm in Cascais and 4.8 cm offshore using satellite altimetry, or simulated as approximately 4.5 cm by GCMs) or tides. In this particular key-location, the effective littoral drift is significantly lower than the potential drift, and therefore a manual calibration based on the coastline retreat rates described by Lira *et al.* (2016) was performed in order to achieve realistic results. Naturally, the performance of the model is expected to be reduced along greatly artificialized coastal segments. At the Ofir key-location, the evaluation process revealed very reasonable results in all coastal segments (between each set of groins), in Figure 47, providing the necessary confidence in the ability of the ShorelineS model to represent an accurate evolution of the shoreline towards the end of the 21st century.

Figure 47 – Ofir's observed shoreline (2018; black dashed line) versus modelled shoreline in 2018 from 2008 initial conditions, forced by the propagated-corrected-propagated ERA5 reanalysis (red line).

Besides the visual representation of the shoreline evolution, it is also useful to analyse the projected changes in the LST rates in the Ofir key-location towards 2100 (Figure 48). In fact, such analysis provides an indication of the amount of sediment that is being carried off the study area each year, which in turn serves as a tool for future, long-term beach nourishment planning. The projected (potential) LST rates at Ofir until the end of the 21st century are shown in Figure 48. Note that the effective LST rates are generally lower. The projected rates are positive (*i.e.*, southwards net transport), with an ensemble mean value of 1.251 x 10^6 m^3/year (1.247 x 10^6 m^3/year) for the RCP4.5 (RCP8.5) scenario during the first three decades of the future projected period (2011-2040). For the medium- and long-term, the ensemble mean (potential) LST rates are projected to decrease for both scenarios, towards 1.166 x 10^6 m^3/year (1.190 x 10^6 m^3/year) during 2041-2070 and 1.127 x 10^6 m^3/year (1.205 x 10^6 m^3/year) during 2071-2100. Throughout the 21st century, the higher mean projected LST rates for the RCP8.5 are compatible with an enhancement of the northward component in the local wave climate, associated to most sea state conditions (Figure 41 and Table 11). From 2011 to 2100, a mean trend of -2000 m^3/year (-700 m^3/year) is identified, for the RCP4.5 (RCP8.5) scenario (Table 17).

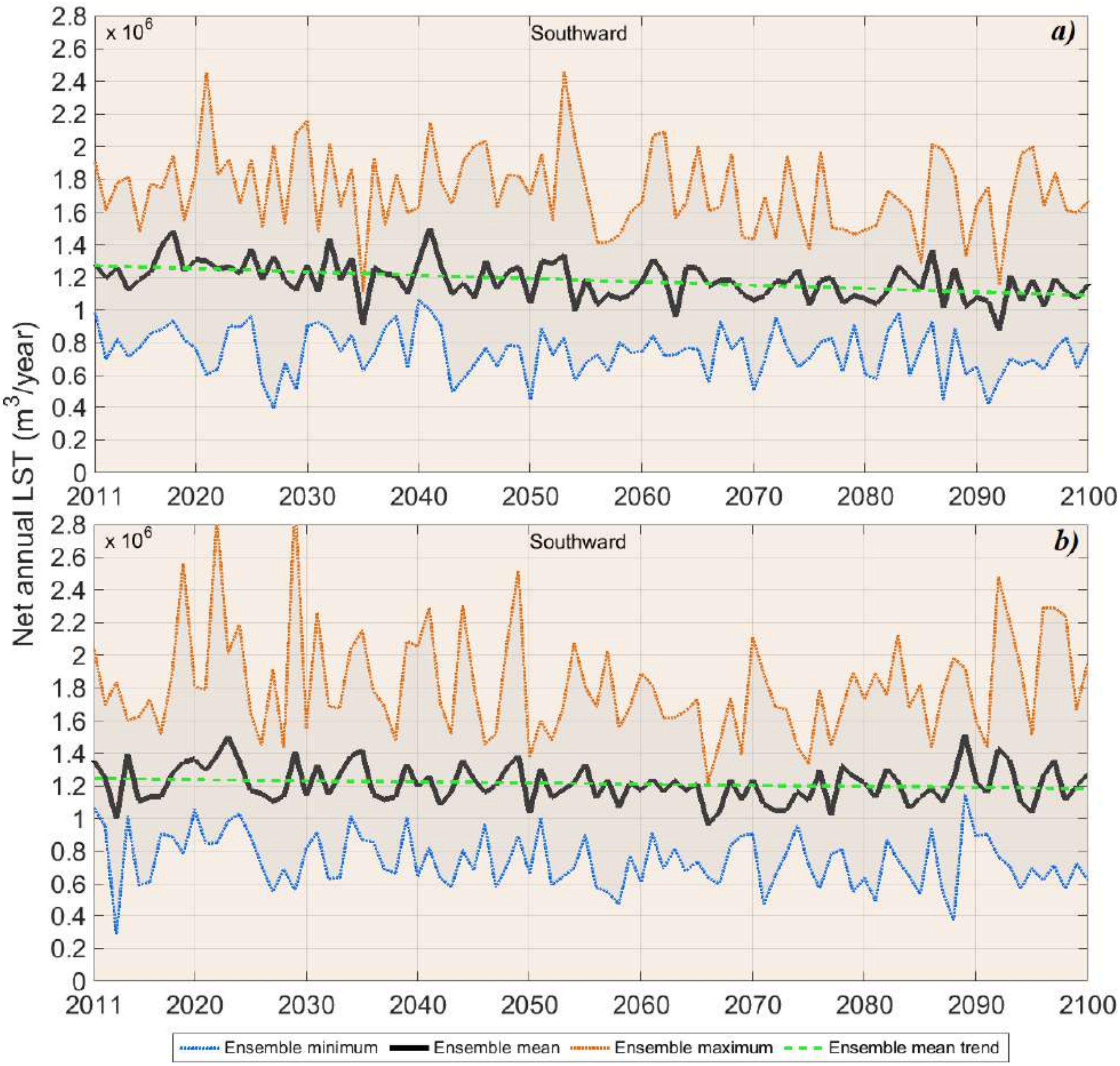

Figure 48 – LST yearly rates (m3/year) at the Ofir key-location for the (a) RCP4.5 and (b) RCP8.5 scenarios.

At the end of the first future period (2041-2070), the projected shorelines forced exclusively by wave climate projections (excluding the additional effects of SLR) are depicted in Figure 49 (RCP4.5) and Figure 50 (RCP8.5). Future projected shoreline behavior at Ofir is marked by different characteristics. In the northern sector (North of the first groin), a slight northwards rotation is visible, with areas of consistent accretion (retreat) between ensemble members, especially for the RCP8.5 (60 m in both directions throughout the sector) scenario, compatible with the mean projected MWD change in this period. In the central sector (Praia de Ofir), rotation is not so evident (very slight accretion for RCP8.5 – Figure 49, and none for RCP4.5 – Figure 50), nevertheless, enhanced erosion is projected to occur south of the first groin, up to 40 m (70 m) under the RCP4.5 (RCP8.5). In the southern sector (Praia da Bonança and Praia de Fao), shoreline retreat is also projected to be dominant, especially for the RCP4.5 scenario (up to 60 m, whereas for the RCP8.5 it does not exceed 50 m).

At the end of the second future period (2071-2100), the projected shorelines forced exclusively by wave climate projections (no SLR) are shown in Figure 51 and Figure 52. While the main shoreline behavior towards 2100 is comparable to the one by 2070, a set of differences can be enumerated. In the northern sector, rotation is now projected to be greater for the RCP4.5 scenario, while for the RCP8.5 it slightly dissipates. At Praia de Ofir (central sector), shoreline retreats assume greater values for both scenarios, peaking at 60 m and 80 m, respectively. In the southern sector, for the RCP4.5, shoreline retreat remains stable at Praia da Bonança, while a slight accretion is visible at Praia de Fao, in comparison with 2070. Under the RCP8.5, shoreline retreat is consistently enhanced, up to 90 m south of the first groin. It is worth noticing that several facilities are located in this area, although not heavily urbanized, including a beach resort, restaurants, a tennis school and a mini-market.

Figure 49 – Projected shorelines at the Ofir key-location forced by the 6-member ensemble of wave climate projections in 2070 (snapshot) under the RCP4.5 scenario, excluding the effects of SLR (wave forcing only). The black dashed line represents the present (2018) shoreline.

Figure 50 – Same as in Figure 49 but for 2070 under the RCP8.5 scenario.

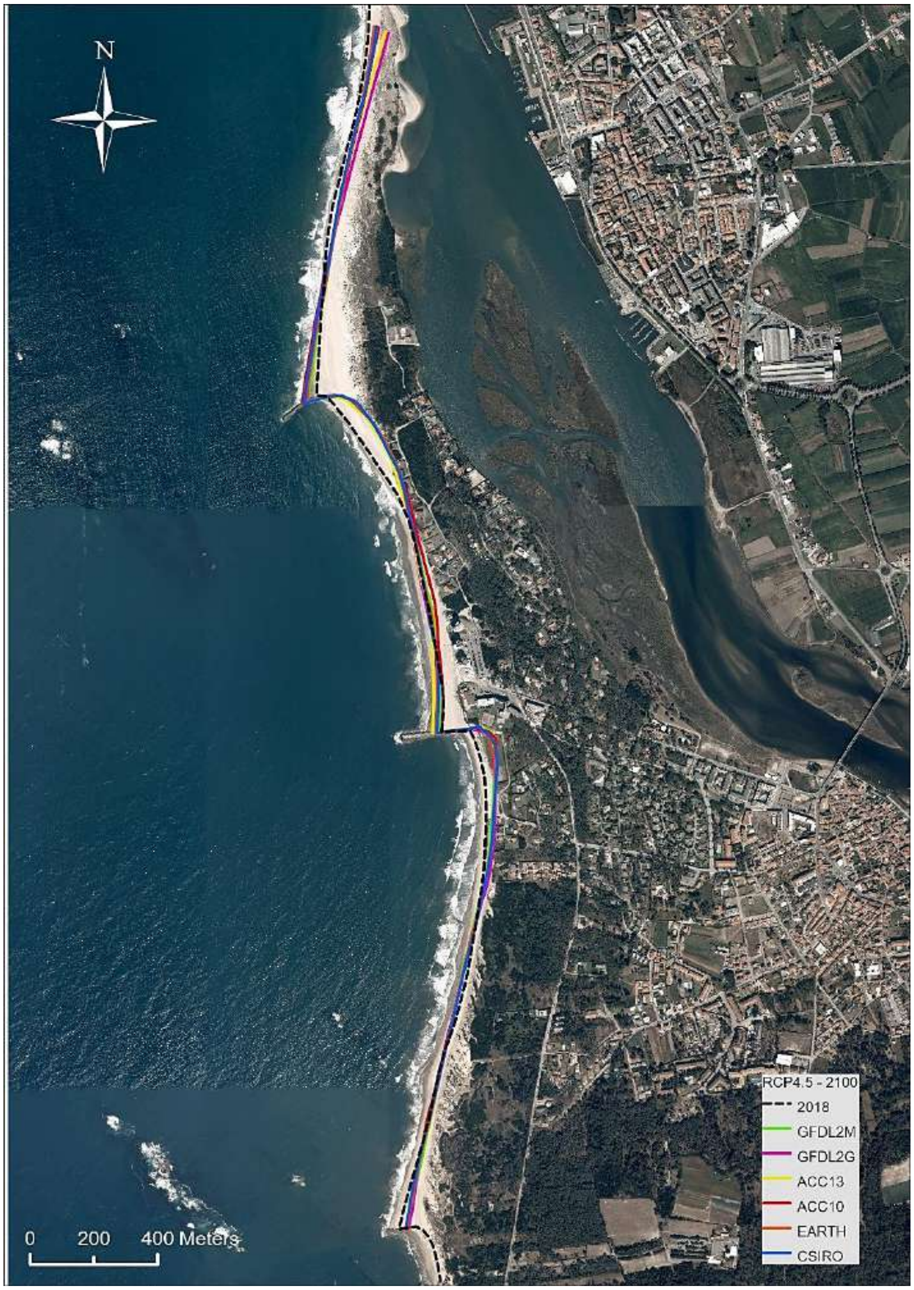

Figure 51 – Same as in Figure 49 but for 2100 under the RCP4.5 scenario.

Figure 52 – Same as in Figure 49 but for 2100 under the RCP8.5 scenario.

The inclusion of SLR in the projection of shoreline followed Bruun's rule, accounting for the available accommodation space at each location along the study area. The final projected shorelines, considering both the effects of the projected wave climate (ensemble mean shoreline) and SLR under the RCP4.5 and RCP8.5 scenarios are depicted in Figure 53 and Figure 54, respectively. The inclusion of SLR unequivocally suppresses all shoreline accretion zones visible throughout the area (especially north of the first groin) in Figure 49 to Figure 52, leading to a robust projected shoreline retreat along most of the Ofir key-location domain extension (the areas showing no retreat represent no accommodation space), assuming no human intervention or beach nourishment during the 21st century.

In Figure 53, the mean projected SLR value from the 21-member ensemble at the closest grid-point (41ºN, 10ºW) is used, at 0.48 m (0.65 m) in 2070 (2100), considering the RCP4.5 scenario. This leads to retreats, from the 2018 reference lines, of up to 60 m (100 m) at Praia de Ofir, south of the first groin, 80 m (100 m) at Praia da Bonança, south of the second groin, and 70 m (70 m) at Praia de Fao, north of the third groin. Note that even considering the RCP4.5 moderate scenario, projections indicate that the shoreline may retreat towards urbanized area, as shown in Figure 53, especially in Praia de Ofir and Praia da Bonança.

In Figure 54, for the RCP8.5, the inclusion of SLR considered mean values of 0.55 m by 2070 and 0.84 m by 2100. Considering no human intervention, shoreline retreats of up to 80 m (120 m) at Praia de Ofir in 2070 (2100) and no less than 30 m (60 m) north of the second groin are projected to occur, from the 2018 reference lines. At Praia da Bonança, directly south of the second groin, 90 m (120 m) retreats can be expected. North of the third groin, at Praia de Fao, values are slightly lower, but still ranging between 50 m (2070) and 80 m (2100). Especially in Praia de Ofir and Praia da Bonança, under the RCP8.5, the shoreline is likely to retreat towards urban areas. Note that these results do not account for the additional effects of wave run-up, which could potentially lead to flooding further inland.

Figure 53 – Projected mean shorelines at the Ofir key-location forced by the 6-member ensemble of wave climate projections in (green) 2070 and (red) 2100 (snapshots) under the RCP4.5 scenario, including the effects of SLR (mean projection). The black dashed line represents the present (2018) shoreline.

Figure 54 – Same as in Figure 53 but for the RCP8.5 scenario.

4.4.2. Costa Nova

At the Costa Nova key-location, the evaluation of the ShorelineS model produced good results between 2008 and 2018 (Figure 55), especially south of the first groin, where human intervention is less frequent. Northwards of this structure, performance is reduced, due to the numerous beach nourishment activities conducted there during the analysed time-window (Pinto *et al.*, 2020). Nevertheless, the overall model performance is considered reasonable for the adopted parameterization, providing the necessary confidence in the ShorelineS model to accurately project the natural evolution of the shoreline in this coastal stretch throughout the 21st century.

Figure 55 – Costa Nova's observed shoreline (2018; black line) versus modelled shoreline in 2018 from 2008 initial conditions, forced by the propagated-corrected-propagated ERA5 reanalysis (red line).

The projected LST rates at Costa Nova towards 2100 are shown in Figure 56. These projections assume mostly positive values (*i.e.*, southwards net transport), with an ensemble mean of 0.820 x 10^6

m^3/year (0.861×10^6 m^3/year) for the RCP4.5 (RCP8.5) scenario at the beginning of the 21st century (2011-2040). Ensemble mean LST rates are projected to decrease for both scenarios, towards 0.783×10^6 m^3/year (0.855×10^6 m^3/year) during 2041-2070 and 0.805×10^6 m^3/year (0.803×10^6 m^3/year) during 2071-2100. Throughout the 21st century, the higher mean projected LST rates for the RCP8.5 are compatible with an enhancement of the northward component in the local wave climate, associated to most sea state conditions (Figure 42 and

Table 12). From 2011 to 2100, a mean trend of -300 m^3/year (-800 m^3/year) is identified, for the RCP4.5 (RCP8.5) scenario (Table 17).

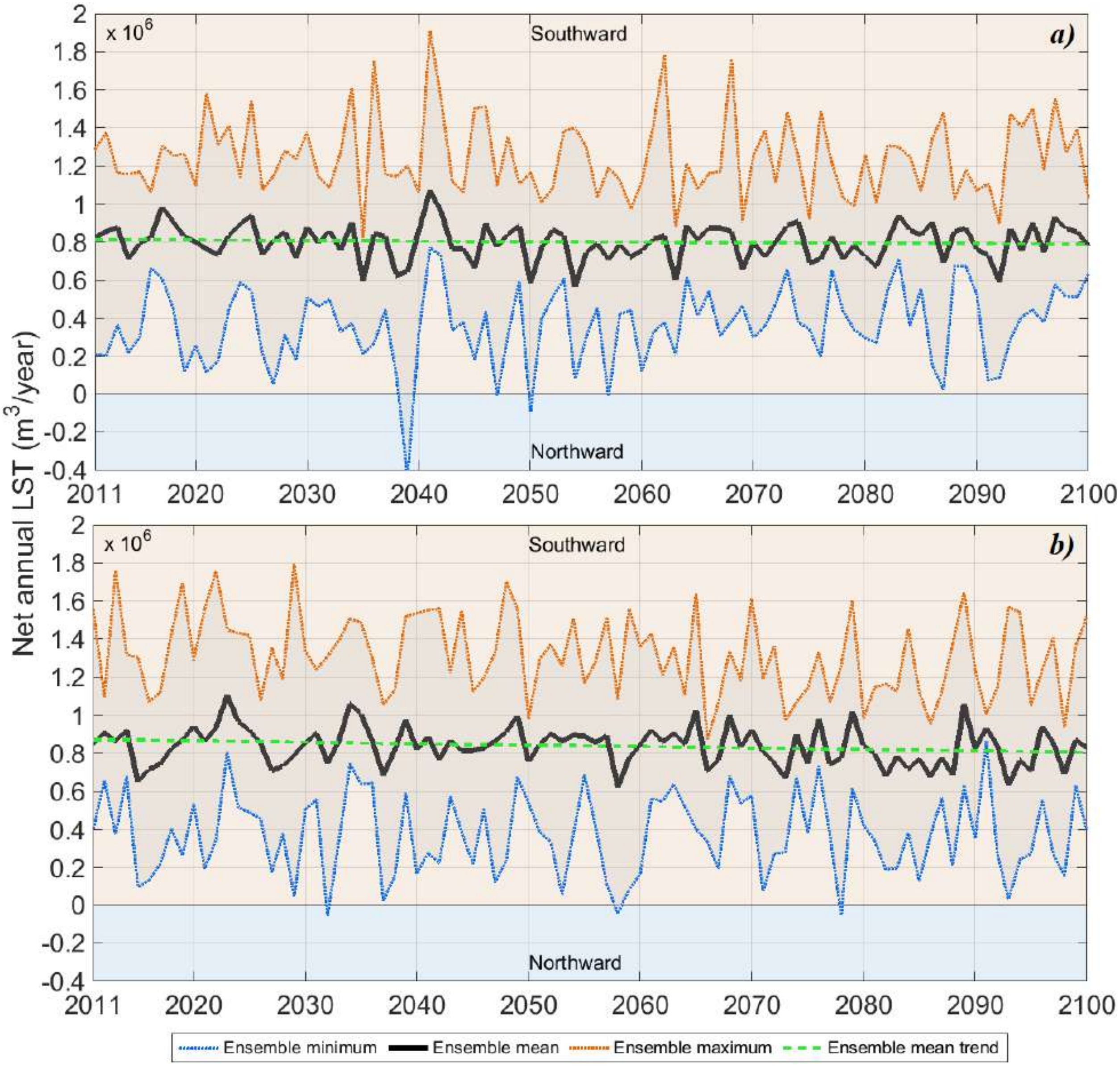

Figure 56 – LST yearly rates (m^3/year) at the Costa Nova key-location for the (a) RCP4.5 and (b) RCP8.5 scenarios.

The projected shorelines, considering exclusively the forcing conditions of the 6-member ensemble of wave climate projections (excluding the additional effects of SLR), at the end of the first future period (2041-2070), are shown in Figure 57 and Figure 58, for the RCP4.5 and RCP8.5, respectively. Overall, the shoreline behavior is marked by a slight northwards rotation, compatible with the projected change in MWD throughout the 21st century (here only until 2070). The impact of the groins is clearly visible, with areas of consistent accretion (retreat) North (South) of each structure. This behavior is observable for all ensemble members, showing therefore increased robustness. Focusing on shoreline retreat, with direct socioeconomic impacts, the most affected area along the Costa Nova key-location lies on the top of the domain, North of Praia da Barra, at Praia Velha. There, considering a no-action (*i.e.*, no human intervention) scenario until 2070, a robust retreat between 100 m and 150 m (110 m and 170 m; inter-member range) for the RCP4.5 (RCP8.5) can be expected, from the 2018 reference shoreline.

At the end of the second future period (2071-2100), the projected shorelines forced exclusively by wave climate projections (no SLR) are shown in Figure 59 and Figure 60. While the main shoreline behavior towards 2100 is comparable to the one by 2070, the overall displacements assume higher values, with consistent retreats peaking between 120 m and 170 m (130 m and 190 m) at the Praia Velha area.

Figure 57 – Projected shorelines at the Costa Nova key-location forced by the 6-member ensemble of wave climate projections in 2070 (snapshot) under the RCP4.5 scenario, excluding the effects of SLR (wave forcing only). The black dashed line represents the present (2018) shoreline.

Figure 58 – Same as in Figure 57 but for 2070 under the RCP8.5 scenario.

Figure 59 – Same as in Figure 57 but for 2100 under the RCP4.5 scenario.

Figure 60 – Same as in Figure 57, but for 2100 RCP8.5 scenario.

The final shoreline projections for the RCP4.5 and RCP8.5 scenarios, considering both the effects of the projected wave climate (ensemble mean shoreline) and SLR, are shown in Figure 61 and Figure 62, respectively. The addition of SLR unequivocally suppresses all shoreline accretion zones visible North of the groins in Figure 57 to Figure 60, leading to consistent projected shoreline retreat along the entire extension of the Costa Nova study area domain.

In Figure 61, the mean projected SLR value from the 21-member ensemble at the closest grid-point (41ºN, 10ºW) is used, at 0.48 m (0.65 m) in 2070 (2100) for the RCP4.5 scenario. This leads to retreats of up to 170 m (210 m) at Praia Velha, 80 m (110 m) south of the first groin (Praia da Costa Nova - Norte), 60 m (90 m) south of the second groin (Praia da Costa Nova - Sul) and 80 m (110 m) south of the third groin (Praia Nova), from the 2018 reference lines. Note that even considering the RCP4.5 moderate scenario, projections indicate that the shoreline may retreat towards urban areas, as shown in Figure 61.

In Figure 62, for the RCP8.5, the effects of the SLR uncertainty were also explored, considering three different SLR values, one “minimum”, corresponding to the percentile 2.5% of the 21-member ensemble by 2100 (0.62 m), the mean (0.55 m by 2070 and 0.84 m by 2100), and the “maximum” (2100 percentile 97.5%, 1.07 m). The different SLR values were applied only for the most extreme projection (2100 under the RCP8.5) to investigate the impact of SLR uncertainty in the shoreline retreat values. Assuming no human intervention towards 2100 and a high SLR projection (“maximum” of 1.07 m), maximum shoreline retreats of 250 m, 150 m, 100 m and 150 m are expected at Praia Velha and south of the first, second and third groins, respectively. The results from Figure 62 indicate that, assuming no human intervention, by the end of the 21st century, the shoreline is likely to be deep inside urban areas at several locations along the Costa Nova key-location. It should be noted that these results do not account for the additional effects of wave run-up, which could potentially lead to flooding further inland.

Figure 61 – Projected mean shorelines at the Costa Nova key-location forced by the 6-member ensemble of wave climate projections in (green) 2070 and (red) 2100 (snapshots) under the RCP4.5 scenario, including the effects of SLR (mean projection). The black dashed line represents the present (2018) shoreline.

Figure 62 – Same as in Figure 61, but for the RCP8.5 scenario.

4.4.3. Cova Gala

The ShorelineS model ability to accurately represent the complex processes driving shoreline evolution is evaluated in Figure 63 for the Cova Gala key-location, by forcing the model with ERA5 hydrodynamic conditions from 2008 to 2018. Note that this free evolution does not account for human intervention processes (*e.g.*, artificial beach nourishments). At Cova Gala, it is shown that the ShorelineS is able to represent the observed shoreline evolution reasonably, in both the northerly (open sandy beaches) and southerly (enclosed beaches limited by groins and adherent structures) portions of the study area. The performance is, nevertheless, lower in the top North of the domain, possibly due to the beach nourishment interventions conducted in that location during the analysed time-window (Pinto *et al.*, 2020). Overall, the ShorelineS performance is considered good for the adopted parameterization, providing the necessary confidence in the model to reasonably project the natural evolution of the shoreline in this coastal stretch throughout the 21st century.

Figure 63 – Cova Gala’s observed shoreline (2018; black dashed line) versus modelled shoreline in 2018 from 2008 initial conditions, forced by the propagated-corrected-propagated ERA5 reanalysis (red line).

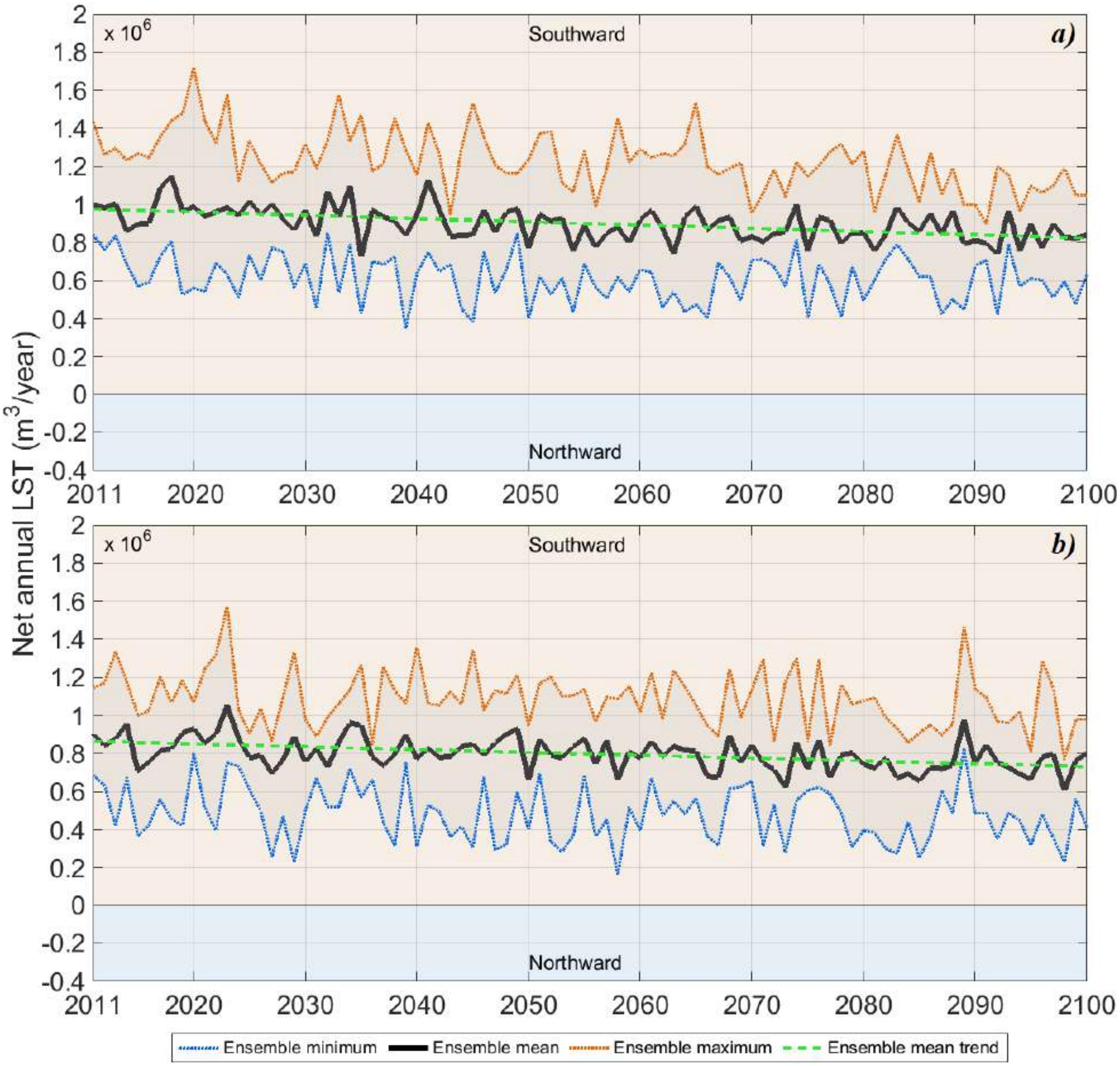

Figure 64 – LST yearly rates (m^3/year) at the Cova Gala key-location for the (a) RCP4.5 and (b) RCP8.5 scenarios.

At the Cova Gala key-location, the LST rates throughout the 21st century follow a similar trend to the ones of Costa Nova, showing a slight projected decrease towards 2100 (Figure 64), from a mean ensemble value of 0.960 x 10^6 m^3/year (0.838 x 10^6 m^3/year) during 2011-2040, to 0.880 x 10^6 m^3/year (0.805 x 10^6 m^3/year) during 2041-2070 and 0.858 x 10^6 m^3/year (0.748 x 10^6 m^3/year) during 2071-2100 under the RCP4.5 (RCP8.5) scenario. The overall trend is slightly more expressive for the RCP4.5 scenario, at -1700 m^3/year, in comparison with -1500 m^3/year found for the RCP8.5. While the inter-member uncertainty range is lower for the Cova Gala key-location, these projections cannot be considered statistically significant, and therefore, the LST rates are projected to remain statistically unaltered during the 21st century. Such projection is compatible with a continued erosion process at Cova Gala, with a main southward LST.

Figure 65 – Projected shorelines at the Cova Gala key-location forced by the 6-member ensemble of wave climate projections in 2070 (snapshot) under the RCP4.5 scenario, excluding the effects of SLR (wave forcing only). The black dashed line represents the present (2018) shoreline.

The projected Cova Gala shorelines, from the 6-member ensemble of wave climate projections (excluding the additional effects of SLR), at the end of the 2041-2070 time-slice, are shown in Figure 65 and Figure 66, for the RCP4.5 and RCP8.5, respectively. Similarly to Costa Nova, a slight northwards shoreline rotation is visible, especially in the northern half of the study area. The five groins positioned directly off Cova Gala village (roughly in the center of the figures) offer additional protection against extreme coastal erosion and rotation associated to the wave climate, and particularly to the projected changes in MWD. This robust behavior is observable for all ensemble members. In terms of shoreline retreat, the most affected area is located in the top of the domain, at Praia do Cabedelo, where a loss of land area between 40 m and 90 m (50 m and 90 m) is expected to occur for the RCP4.5 (RCP8.5) scenario by 2070. Nevertheless, near the Cova Gala village (Praia de Cova Gala Norte), retreats are projected to be lower, not exceeding 30 m (40 m). Not surprisingly, in the areas where a fixed barrier already exists, shoreline is not projected to change significantly.

By 2100, the projected shorelines forced exclusively by wave climate projections (no SLR) are shown in Figure 67 and Figure 68. While the main shoreline behaviors in 2100 is comparable to the ones by 2070, the overall displacements assume higher values, with consistent retreats up to 100 m (110 m) and 40 m (40 m) at Praia do Cabedelo and Praia de Cova Gala Norte for the RCP4.5 (RCP8.5) scenario.

Figure 66 – Same as in Figure 65 but for 2070 under the RCP8.5 scenario.

Figure 67 – Same as in Figure 65 but for 2100 under the RCP4.5 scenario.

Figure 68 – Same as in Figure 65 but for 2100 under the RCP8.5 scenario.

The final shoreline projections for the RCP4.5 and RCP8.5 scenarios, considering both the effects of the projected wave climate (ensemble mean shoreline) and SLR (through a Bruun's rule accounting for the available accommodation space), are shown in Figure 69 and Figure 70, respectively. Similarly to what was observable in the Costa Nova key-location, sediment accretion is no longer projected North of the first groin with the inclusion of SLR, and the remaining retreat values become higher.

In Figure 69, the mean projected SLR value from the 21-member ensemble at the closest grid-point (39ºN, 10ºW) considering the RCP4.5 scenario is used, at 0.48 m (0.65 m) in 2070 (2100). This leads to retreats (from the 2018 reference values) of up to 90 m (140 m) at Praia do Cabedelo, 60 m (80 m) at Praia de Cova Gala Norte (directly affecting urbanized area near "Hospital Distrital da Figueira da Foz"), and 80 m (110 m) in the northern portion of Praia de Cova Gala Sul (also directly affecting urbanized area).

In Figure 70, the mean SLR projected under the RCP8.5 scenario is used, at 0.56 m (0.86 m) in 2070 (2100). Considering absence of human intervention towards 2100, shoreline retreats up to 110 m (150 m) at Praia do Cabedelo, 70 m (90 m) at Praia de Cova Gala Norte and 90 m (120 m) at Praia de Cova Gala Sul are expected. Such projected evolution represents a major risk for Cova Gala, in the case of no human intervention, with the shoreline expected to lay inside urban areas in several locations along the domain. Note that these results do not account for the additional effects of wave run-up, which could potentially lead to flooding further inland.

Figure 69 – Projected mean shorelines at the Cova Gala key-location forced by the 6-member ensemble of wave climate projections in (green) 2070 and (red) 2100 (snapshots) under the RCP4.5 scenario, including the effects of SLR (mean projection). The black dashed line represents the present (2018) shoreline.

Figure 70 – Same as in Figure 69 but for the RCP8.5 scenario.

4.4.4. Costa da Caparica

Figure 70 shows the ShorelineS performance is representing shoreline evolution at Costa da Caparica key-location from 2008 to 2018, using the propagated-corrected-propagated ERA5 wave data. At

Costa da Caparica, the ShorelineS model is able to reasonably depict the historical evolution of the shoreline, with very small differences overall, especially South of Praia de São João da Caparica, where the observed 2018 shorelines are generally very close to the simulated ones, after 10 years (differences below 10 m). In the northern portion of the area, however, differences attain greater values, possibly due to the higher nartural variability range of the system there, related to greater sedimentary availability and shoreline accomodation space. There, the results show positive differences (*i.e.*, advanced shoreline, in comparison with the 2018 observation) of up to 30 m. Nevertheless, it should be noted that this free evolution does not account for human intervention processes (*e.g.*, artificial beach nourishments), which took place in Costa da Caparica during the 2008-2018 evaluation period, namely in 2008, 2009 and 2014. All considered, the ShorelineS performance is considered good for the adopted parameterization, providing the necessary confidence in the model to reasonably project the natural evolution of the shoreline in this coastal stretch throughout the 21st century.

Figure 71 – Costa da Caparica's observed shoreline (2018) versus modelled shoreline in 2018 from 2008 initial conditions, forced by the propagated-corrected-propagated ERA5 reanalysis.

Figure 71 shows the projected LST rates throughout the 21st century, at the Costa da Caparica key-location, for the 6-member ensemble (mean and IQR) under the RCP4.5 and RCP8.5 scenarios. At Costa da Caparica, the LST rates are projected to be negative throughout the 21st century (representing an overall northwards sediment transport), showing, nevertheless, a slight projected decrease in magnitude towards 2100, especially for the RCP8.5 scenario (Figure 71), from a mean ensemble value of -0.527 x 10^6 m^3/year (-0.511 x 10^6 m^3/year) in the 2011-2040 period, to -0.489 x 10^6 m^3/year (-0.438 x 10^6 m^3/year) during 2041-2070 and -0.435 x 10^6 m^3/year (-0.378 x 10^6 m^3/year) during 2071-2100. As mentioned, this trend is especially noticeable for the RCP8.5 scenario, at 2400 m^3/year, in comparison with 1400 m^3/year found for the RCP4.5. In this particular instance, the RCP8.5 scenario would produce lower LST rates in the Costa da Caparica key-location, which could potentially alleviate the local need for beach nourishment interventions. Note, however, that due to the overall geomorphology and dynamic nature of the system, this possibility requires further evaluation at specific locations, and would be more likely where the natural positioning of the future projected shoreline matches the mean projected incoming MWD.

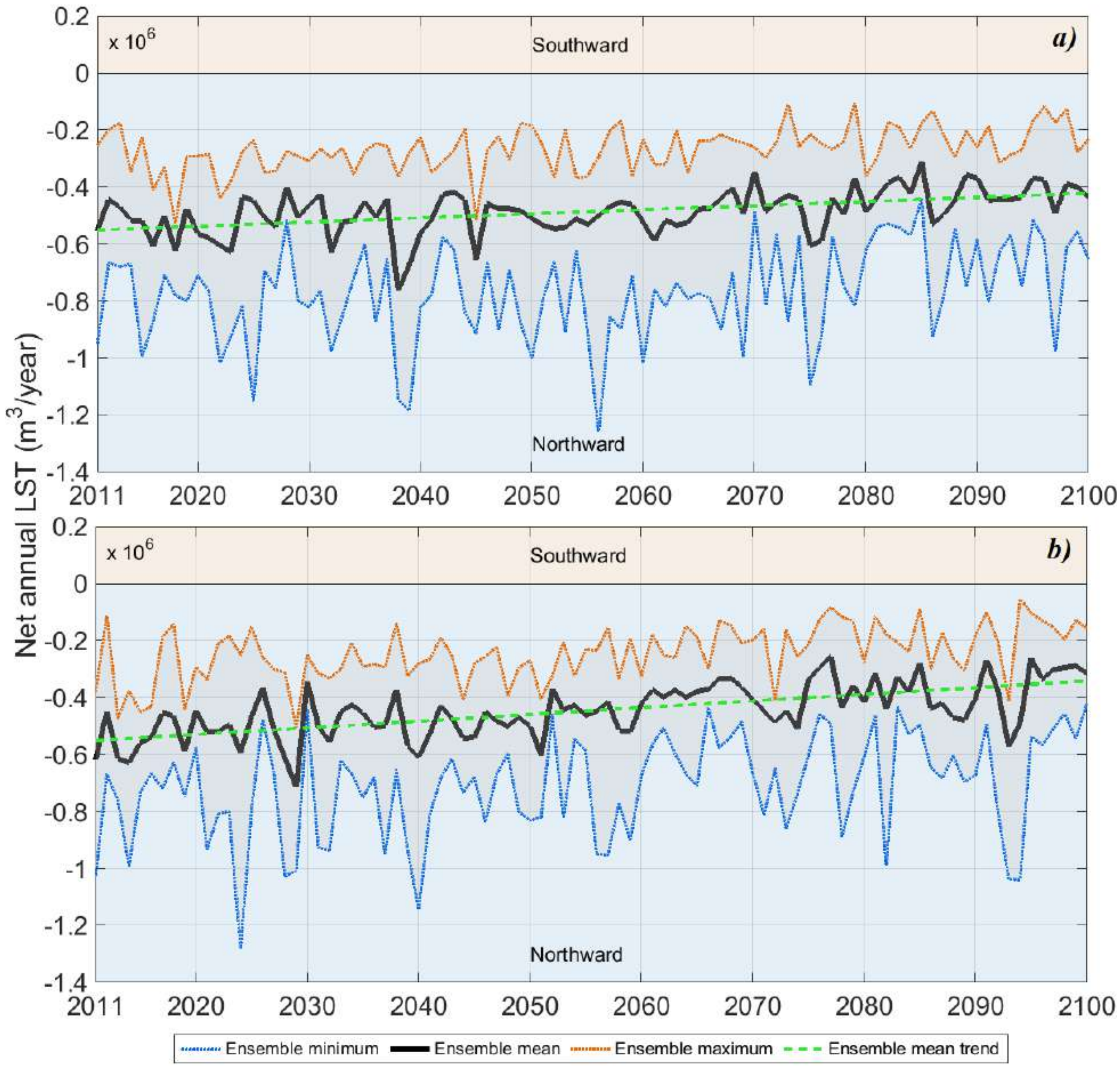

Figure 72 – LST yearly rates (m^3/year) at the Costa da Caparica key-location for the (a) RCP4.5 and (b) RCP8.5 scenarios.

The projected Costa da Caparica shorelines resulting from projected wave action are shown in Figure 73 to Figure 76. In the central and southern portions of the area, shorelines are projected to remain stable due to the existence of a long seawall extending from Praia de São João da Caparica onto Nova Praia, covering approximately 3 km. In the northern portion, however, from Praia da Cova do Vapor to Praia de São João da Caparica, extensive consistent retreats are projected to occur from wave action alone, ranging between 160 m and 220 m between ensemble members, for all future periods and scenarios. Such behavior, despite possibly amplified by the results of Figure 71, is compatible with the MWD projections for this area, indicating a slight northwards rotation (Table 11), allowing extensive erosion on the northernmost stretch of Praia de São João da Caparica, which is oriented to the SW. In fact, it was shown that while the SW (210-230º) component of the wave climate at this study location is projected to decrease, from 9.70% during the historical period, towards 9.16%, 8.80%, 8.63% and 8.28%, during 2041-2070 and 2071-2100, under RCP4.5 and RCP8.5, respectively, the W (250-270º) component is projected to increase, from 35.87% (historical), towards 36.15%, 36.45%, 36.43% and 36.84%, respectively (Table 11). These changes, along with the ones for the remaining sectors, might exacerbate the erosive processes in southward-facing beaches, such as in the northern portion of Praia de São João da Caparica.

Figure 73 – Projected shorelines at the Costa da Caparica key-location forced by the 6-member ensemble of wave climate projections in 2070 (snapshot) under the RCP4.5 scenario, excluding the effects of SLR (wave forcing only). The black dashed line represents the present (2018) shoreline.

Figure 74 – Same as in Figure 73 but for 2070 under the RCP8.5 scenario.

Figure 75 – Same as in Figure 73 but for 2100 under the RCP4.5 scenario.

Figure 76 – Same as in Figure 73 but for 2100 under the RCP8.5 scenario.

The final shoreline projections for the RCP4.5 and RCP8.5 scenarios, considering both the effects of the projected wave climate (ensemble mean shoreline) and SLR (mean projection), are shown in Figure 77 and Figure 78, respectively. Overall, shoreline retreat can be observed throughout the Costa da Caparica for all future periods and scenarios. Between them, differences are generally small, due to the long seawalls protecting Costa da Caparica urban areas facing the ocean.

In Figure 77, the mean projected SLR value from the 21-member ensemble at the closest grid-point (37ºN, 10ºW) considering the RCP4.5 scenario is used, at 0.50 m (0.67 m) in 2070 (2100). This leads to retreats (from the 2018 reference values) of up to 60 m (80 m) between Nova Praia and Praia da Saúde, 100 m (100 m) in Praia do Dragão Vermelho and Praia Nova (southern urban area of Costa da Caparica), 280 m (290 m) in Praia de São João da Caparica, on the northermost part of the study area, near Cova do Vapor. Conversely, at the southern portion of Praia de São João da Caparica, shoreline accretion is projected, up to 50 m (40 m) by 2070 (2100), north of the groin, indicating a local southward sediment transport. This is compatible with the MWD projections for this area, which indicate a slight northwards rotation (Figure 44 and

Table 14 – Same as in Table 11, but for the Costa da Caparica key-location.), allowing extensive erosion on the northernmost stretch of Praia de São João da Caparica, which is oriented to the SW. In fact, it was shown that while the SW (210-230º) component of the wave climate at this key-location is projected to decrease, from 9.70% during the historical period, towards 9.16%, 8.80%, 8.63% and 8.28%, during 2041-2070 and 2071-2100, under RCP4.5 and RCP8.5, respectively, the W (250-270º) component is projected to increase, from 35.87% (historical), towards 36.15%, 36.45%, 36.43% and 36.84%, respectively. These changes, along with the ones for the remaining sectors, might exacerbate the erosive processes in southward-facing beaches, such as in the northern portion of Praia de São João da Caparica.

At the beaches adjacent to the central and northern urban area of Costa da Caparica, shoreline projections for the RCP4.5 scenario depict a relatively stable evolution, blocked by the seawall, given that by 2018 the shoreline was already placed close to it, with almost no accommodation space left.

In Figure 78, the mean SLR projected under the RCP8.5 scenario is used, at 0.58 m (0.88 m) in 2070 (2100). Future projected shoreline retreats for Costa da Caparica under this scenario, considering no human intervention, are overall similar to the ones for the RCP4.5, mostly due to the configuration of the study area, namely regarding the existence of a long seawall which blocks further shoreline retreats. Highlight to the Praia de São João da Caparica, for which the shoreline retreats in its northernmost portion are projected to reach 300 m under RCP8.5 by 2100. Conversely, in the opposite end, accretions of up to 60 m (50 m) are projected, until 2070 (2100). Interestingly, at Praia da Cova do Vapor, the shoreline is projected to remain stable under this scenario, whereas under the RCP4.5, retreats of up to 170 m (190 m) are projected to occur, demonstrating increased sensitivity even to slight changes in the MWD.

Overall, Figure 77 and Figure 78 depict overall shoreline retreats for Costa da Caparica, blocked in most of its extension by lack of further accommodation space due to the existence of the seawall adjacent to the most urbanized area. Without human intervention, this protection measure might not be enough to sustain the effects of extreme wave events, given the projected disappearance of the neighboring beaches.

Figure 77 – Projected mean shorelines at the Costa da Caparica key-location forced by the 6-member ensemble of wave climate projections in (black) 2070 and (red) 2100 (snapshots) under the RCP4.5 scenario, including the effects of SLR (mean projection). The blue line represents the present (2018) shoreline.

Figure 78 – Same as in Figure 77 but for the RCP8.5 scenario.

4.4.5. Praia de Faro

The ShorelineS performance is representing shoreline evolution at the Praia de Faro key-location between 2008 and 2018 is showed in Figure 79, using the propagated-corrected-propagated ERA5 wave data, synchronized with observations, as forcing. At Praia de Faro, the behavior of the shoreline can be considered quite homogeneous, due to its naturally linear configuration, and the absence of hard human interventions (*e.g.*, groins, breakwaters, seawalls, etc.). For these reasons, Praia de Faro is the location with a better performance from the ShorelineS model, able to represent the evolution of the shoreline over 10 years in time, with differences consistently below 20 m when compared with the actual observed shoreline of 2018. Therefore, the ShorelineS performance is considered very good for the adopted parameterization, providing the necessary confidence in the model to reasonably project the natural evolution of the shoreline in this coastal stretch throughout the 21st century.

Figure 79 – Praia de Faro's observed shoreline (2018) versus modelled shoreline in 2018 from 2008 initial conditions, forced by the propagated-corrected-propagated ERA5 reanalysis.

The projected LST rates at Praia de Faro towards 2100 are shown in Figure 80. These projections assume mostly negative values (*i.e.*, northwards net transport, in this case, with a reduce northward component, in a slow northwesterly transport), with an ensemble mean of -0.083 x 10^6 m^3/year (-0.079 x 10^6 m^3/year) for the RCP4.5 (RCP8.5) scenario at the beginning of the 21st century (2011-2040). Despite reduced, in comparison to previous key-locations, ensemble mean LST rates are still projected to decrease for both scenarios, towards -0.078 x 10^6 m^3/year (-0.062 x 10^6 m^3/year) during 2041-2070 and -0.066 x 10^6 m^3/year (-0.053 x 10^6 m^3/year) during 2071-2100. Throughout the 21st century, the lower mean projected LST rates for the RCP8.5 are compatible with the local projected decrease in wave energy. From 2011 to 2100, a mean trend of -301 m^3/year (-504 m^3/year) is identified, for the RCP4.5 (RCP8.5) scenario (Table 17).

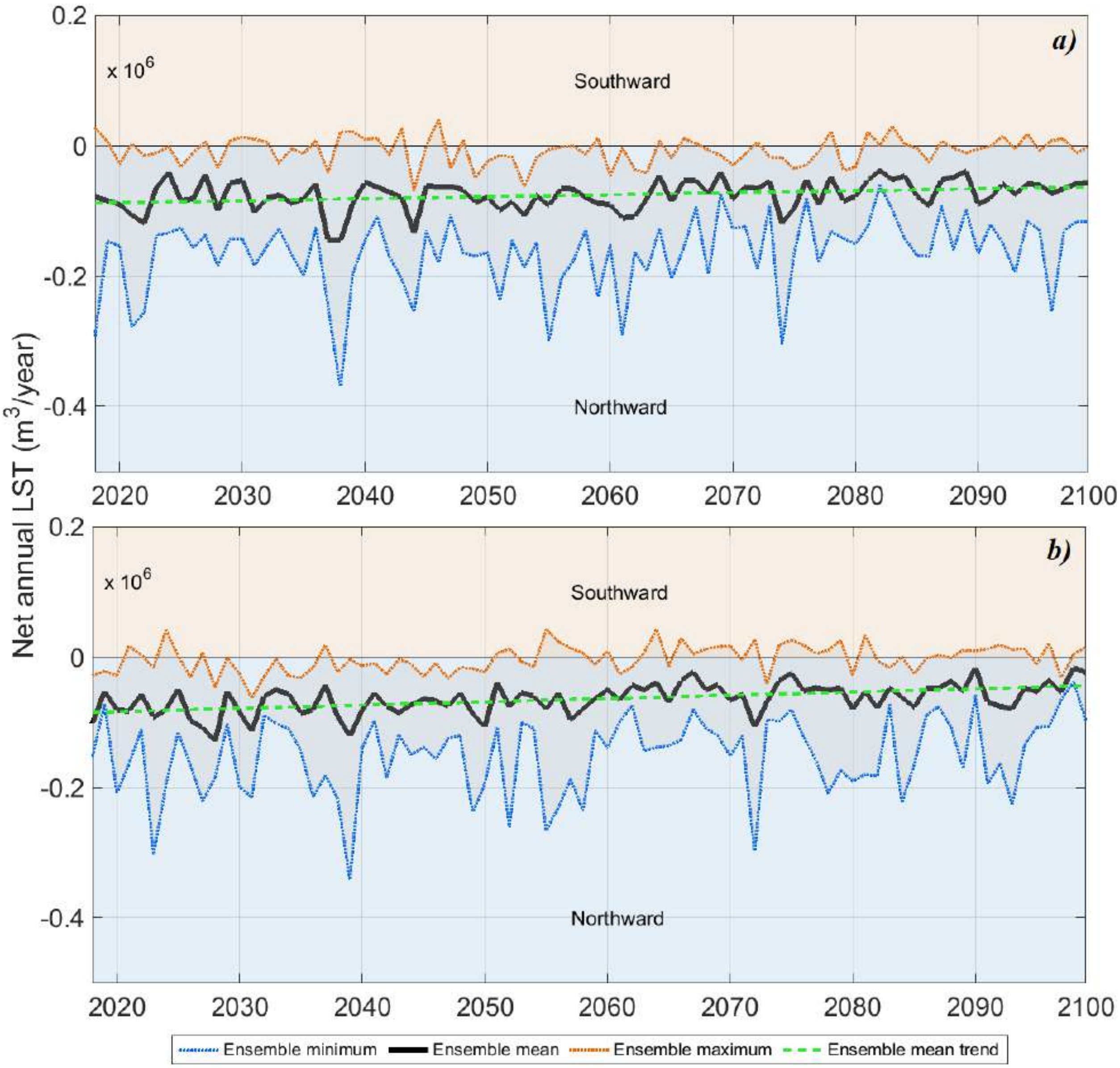

Figure 80 – LST yearly rates (m^3/year) at the Praia de Faro key-location for the (a) RCP4.5 and (b) RCP8.5 scenarios.

The projected Praia de Faro shorelines, from the 6-member ensemble of wave climate projections (excluding the additional effects of SLR), at the end of the 2041-2070 (2071-2100) time-slice, are shown in Figure 81 and Figure 82 (Figure 83 and Figure 84), for the RCP4.5 and RCP8.5, respectively. This area, composed of long sandy beaches, is projected to change almost uniformly with wave action. The expected retreats are greater where the accommodation space allows, *i.e.*, away from the most densely populated area, near the bridge that connects the island to the mainland. The erosion related to wave action alone is projected to be kept below 30 m by 2070 under RCP4.5, and range between 20 m and 60 m by 2100, under RCP8.5. Between ensemble members, uncertainty is low (generally below 20 m, slightly greater for the RCP8.5 projections, but overall, still the lowest between the five key-locations), given the homogeneous geomorphological structure of the area (same type, without natural adherent structures of hard-human interventions, and under the same orientation), and the dynamics of the regional wave climate, with less extreme events and less directional variability than in the other locations.

Figure 81 – Projected shorelines at the Praia de Faro key-location forced by the 6-member ensemble of wave climate projections in 2070 (snapshot) under the RCP4.5 scenario, excluding the effects of SLR (wave forcing only). The black dashed line represents the present (2018) shoreline.

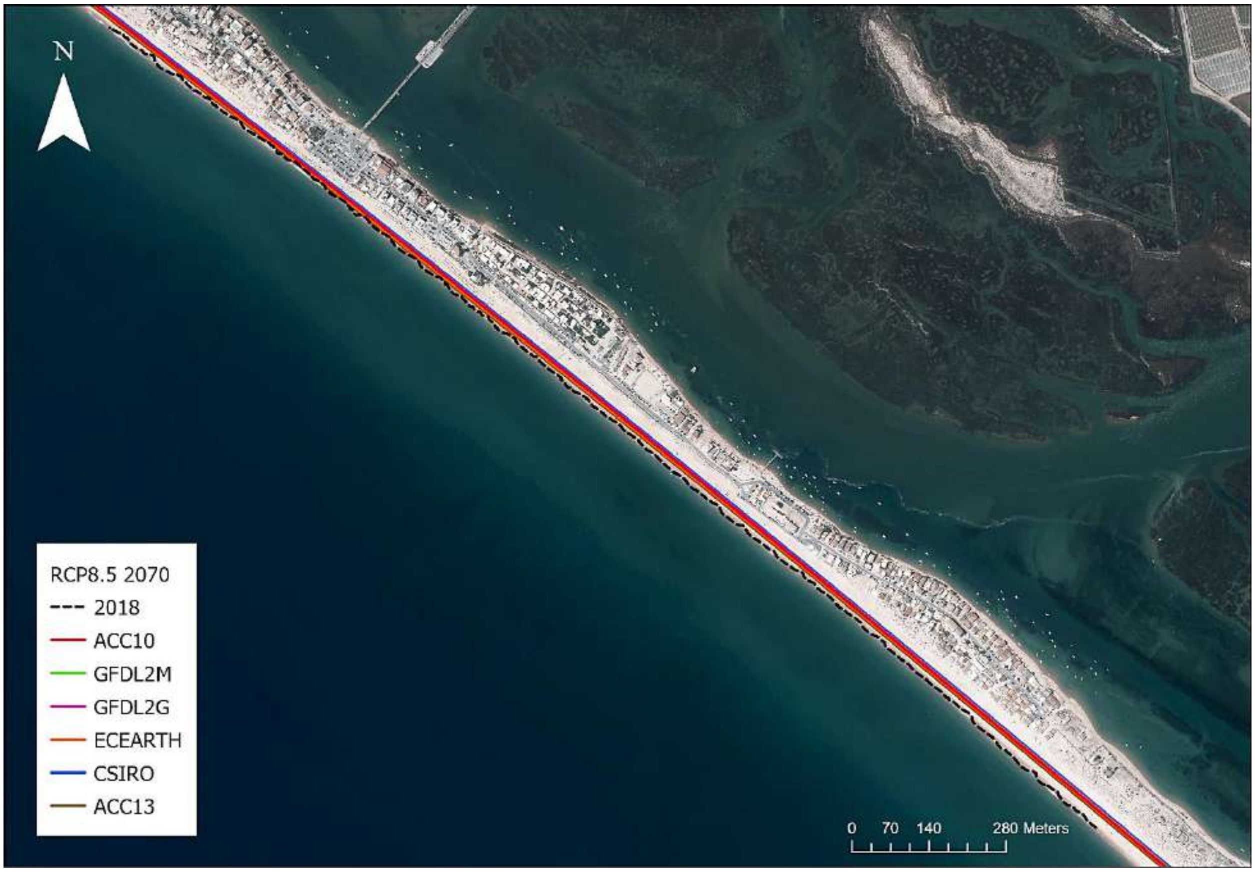

Figure 82 – Same as in Figure 81 but for 2070 under the RCP8.5 scenario.

Figure 83 – Same as in Figure 81 but for 2100 under the RCP4.5 scenario.

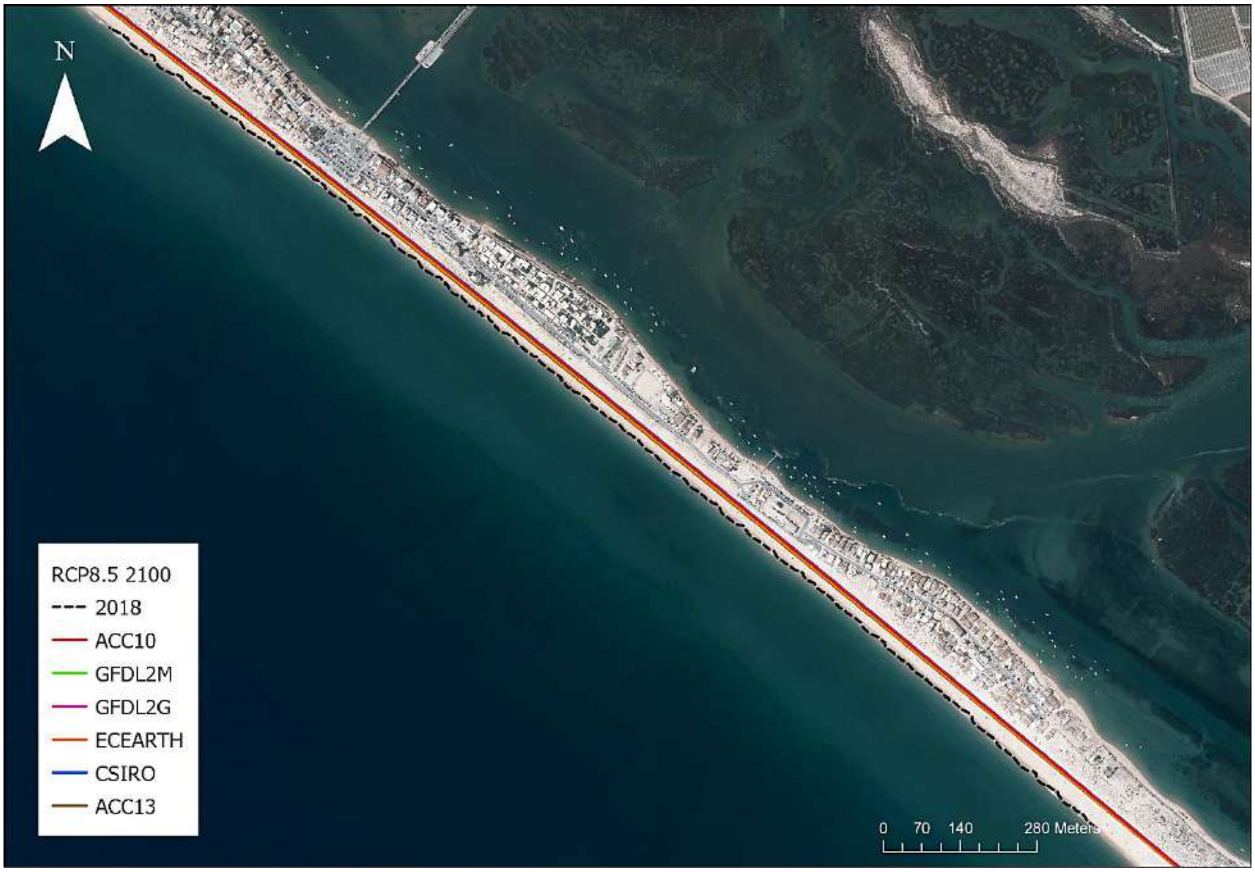

Figure 84 – Same as in Figure 81 but for 2100 under the RCP8.5 scenario.

At the Praia de Faro key-location, the final shoreline projections for the RCP4.5 and RCP8.5 scenarios, considering both the effects of the projected wave climate (ensemble mean shoreline) and SLR (mean projection), are shown in Figure 85 and Figure 86, respectively. Similarly to what was observed in Figure 81 to Figure 84, at this location, the long low sandy beaches without artificial structures allow a consistent retreat throughout the entire area, depending (almost exclusively) on the SLR values. Overall, shoreline retreats are visible at Praia de Faro, for all future periods and scenarios. Differences are related to the magnitude of the SLR and the effect of the application of Bruun's rule, with maximum retreats ranging between 0 m and 50 m for 2070 under RCP4.5, and 40 m and 120 m for 2100 under RCP8.5.

Figure 85 – Projected mean shorelines at the Praia de Faro key-location forced by the 6-member ensemble of wave climate projections in (black) 2070 and (red) 2100 (snapshots) under the RCP4.5 scenario, including the effects of SLR (mean projection). The blue line represents the present (2018) shoreline.

Figure 86 – Same as in Figure 85 but for the RCP8.5 scenario.

4.5. Dynamic modelling of future projected coastal flooding

4.5.1. Future projected DTMs

Consistent overall shoreline retreats were shown to be expected for all key-locations, mainly driven by SLR, whereas the shape of the shoreline was shown to be mostly affected by changes in the climatological wave characteristics, especially MWD, leading to northward beach rotations, especially in the northern and central western coastlines of Portugal Mainland. These new, high-resolution shoreline projections were then used to drive the PCR algorithm (the reader is referred to section 3.2.2) along the cross-shore profiles, allowing to modify the reference DTMs accounting for the projected changes in the shorelines.

Figure 87 shows, for each key-location (each row), the reference (2018) and future projected DTMs by 2070 and 2100, under the RCP4.5 and RCP8.5 scenarios. At Ofir, the reference DTMs shows a dune system spanning throughout most of the area (Figure 87a), offering better natural protection at Praia da

Bonança and Praia de Fao, given the higher topographic heights there, up to 18.23 m. The northern stretch shows less natural resilience, with most of the beachfront areas located below 10 m height. The combined effect of SLR and waves is projected to change the DTMs, mainly by moving the profiles landward, while reducing the natural strength of the dune system. In fact, by 2070 (2100), the topographic heights are projected to top at 14.90 m (15.62 m) and 14.89 m (14.64 m), under RCP4.5 and RCP8.5, respectively. SLR is also projected to change the profiles facing the Cávado River estuary, further weakening the northernmost portion of the domain.

At Costa Nova (Figure 87f to Figure 87j), the reference DTM shows a long and intact dune system spanning throughout the entire domain, although wider in the northern half. The urban areas of Costa Nova are shown to be protected by natural terrain elevations of up to 13.9 m. By 2070, both DTMs (RCP4.5 and RCP8.5) reflect the shoreline retreats previously found, especially south of the groins. Although no shoreline recovery is expected north of the groins, increases in the dune thickness are projected to occur. However, not only is the future (2070) maximum topographic height lower than the reference one (13.4 m and 13.1 m for both scenarios, respectively), but the overall dune system is projected to become sectioned, with the areas south of the groins showing almost no natural protection. By 2100, while the overall behavior is projected to be similar, the fragility of (also sectioned) dune system is exacerbated. The maximum topographic heights are expected to be reduced to 12.6 m for both scenarios.

Along the Cova Gala domain, the future projected DTMs (Figure 87l to Figure 87o) show similar behavioral characteristics when compared to the reference one (Figure 87k), as in Ofir and Costa Nova. The combined effects of SLR and wave action are projected to reduce the strength of the dune systems in the northermost and southernmost portions of the domain, by displacing them landwards while reducing their maximum topographic heights (by about 3 m). Especially for the northern dune cord, such an expected displacement might not be physically achievable, due to the proximity to the Figueira da Foz harbor infrastructure, locally increasing the vulnerability to future extreme events across all projected periods and scenarios.

At Costa da Caparica, the reference and future projected DTMs are shown in Figure 87p to Figure 87t. The existence of a seawall (of about 3 km) along the urban front required a slightly different approach to obtain the modified DTMs, given the rigidness of that portion of the domain, unsusceptible to natural changes in the future. Therefore, the future profiles between Praia de São João da Caparica and Praia da Saúde were considered the same as the reference ones, being the modifications applied only outside this range. In the northernmost part of the domain, between Praia da Cova do Vapor and Praia de São João da Caparica, the considerable coastal retreats previously identified are also represented here, by a complete disruption of the dune cord, increasing the exposure of inland areas to extreme events. There, the maximum topographic height is projected to reduce from approximately 10 m (reference; Figure 87p) to less than 6 m by 2100 under RCP8.5 (Figure 87t). A reduction in the natural resiliency of the southernmost dune system is also projected to occur, although less expressively than in the northern areas of the domain.

Finally, at Praia de Faro, the reference DTM shows a long and wide dune system, between the Atlantic Ocean and the Ria Formosa (Figure 87u). In the context of rising sea levels and constant wave action, while slight shoreline retreats are expected, no major changes in the future projected DTMs are identified, besides a slight but consistent reduction in its maximum vertical expression (below 0.3 m).

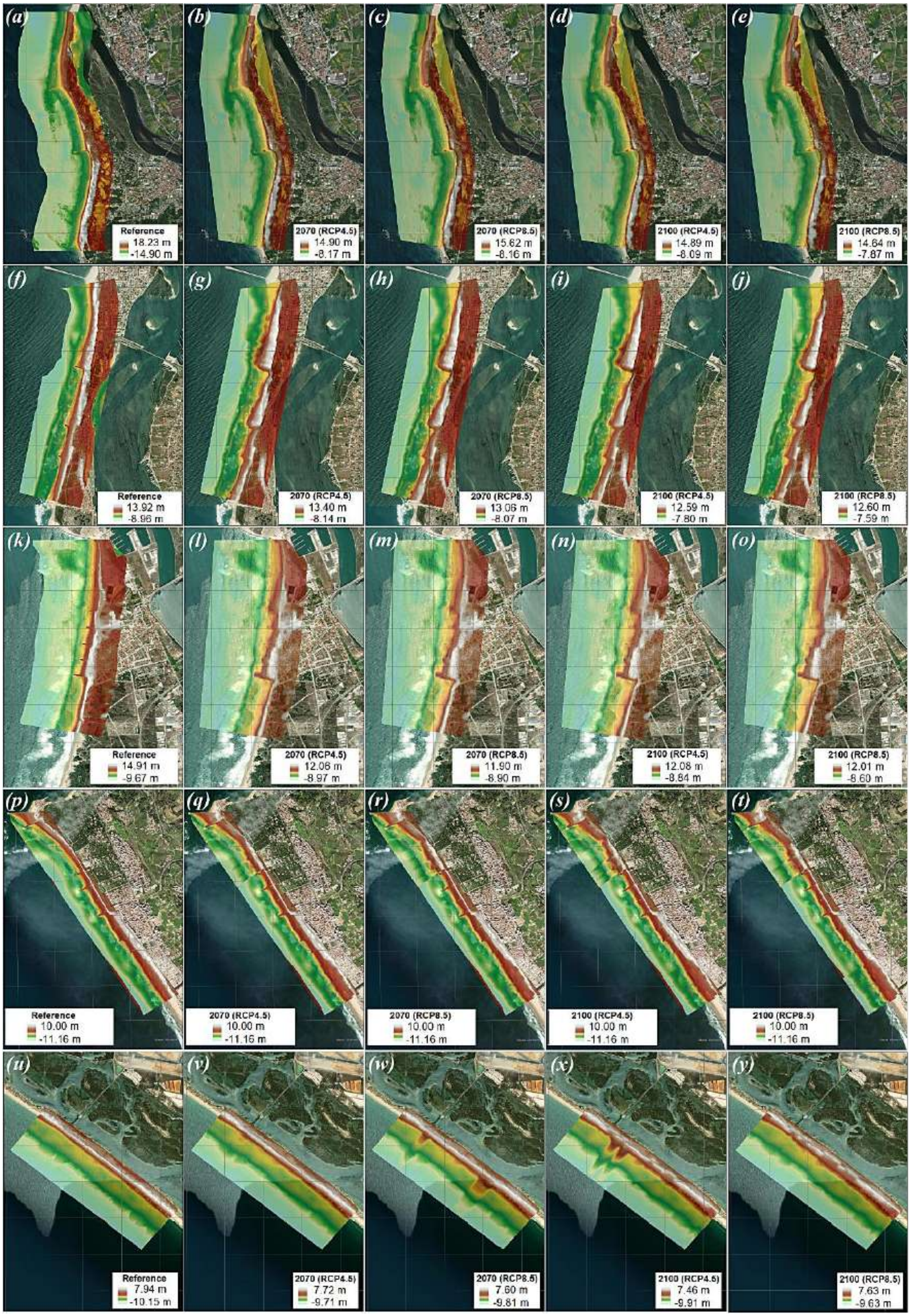

Figure 87 – (a,f,k,p,u) Reference and future projected DTMs across (a–e) Ofir, (f–j) Costa Nova, (k–o) Cova Gala, (p–t) Costa da Caparica and (u–y) Praia de Faro, by (b,g,l,q,v) 2070 under RCP4.5, (c,h,m,r,w) 2070 under RCP8.5, (d,i,n,s,x) 2100 under RCP4.5 and (e,j,o,t,y) 2100 under RCP8.5.

4.5.2. Selection of future projected extreme events

The last phase of the dynamic modelling across the five key-locations uses the XBeach model to project future coastal flooding conditions with high resolution (4 m cross-shore and 20 m alongshore), based on the DTMs produced using the shoreline projections in section 4.4. The forcing hydrodynamic conditions are composed of a TWL (accounting for SLR, tides and storm surge) and a sea state (H_S, T_p and MWD). To reduce computational costs, a single event (value for each parameter) was used to define the forcing conditions, instead of a time-series or a three-dimensional field. As previously, an ensemble approach is used here, for both the TWL and waves, focusing on extreme events, which pose greater coastal threats. Hence, three risk levels were selected for each of the parameters at each key-location, for each of the future time-slices and scenarios, representing the ensemble's uncertainty range. For the TWL, the 4-, 25- and 100-year return levels were computed, based on the mean SLR, tides and on the range of storm surge conditions provided by the future projections of the 6-member ensemble, through a combined CDF (the reader is referred to section 3.3.1). For the waves, an energy indicator was first computed, based on the formula for wave energy ($\mathrm{E} = (\rho g^2/64\pi)\, T_m\, {H_S}^2$; Holthuijsen, 2007), and for each of the 6 ensemble members, the future projected event better corresponding to the 99th percentile of E was selected. In this approach, the T_p was used instead of the T_m, being T_p the peak period corresponding to the most energetic wave component in the wave spectrum. Note that each of the three events for a given 99th percentile of E are not directly related to the extreme coastal flooding extent, considering that even a lower energy extreme wave event combined with a favorable MWD can lead to greater flooding than the most energetic wave events, if the incoming MWD is unfavorable (*i.e.*, not perpendicular to the shoreline). Therefore, the three wave energy levels are henceforth named as "WAVES1" to "WAVES3", depicting the ensemble uncertainty range, and associated projected probability of occurrence (being "WAVES2" the most likely projection, *i.e.*, the average of the 99th percentile of E). Given that the methodology at national scale is based on the mean SLR projections, here only the projected coastal flooding conditions based on the 25-year return level of the TWL are shown, as required to validate and evaluate the large-scale vulnerability assessment. The XBeach forcing parameters are described in Table 18 to Table 22.

4.5.3. Ofir

For the Ofir key-location, the following data was used to compute the respective TWL: tide model of Viana do Castelo tide gauge, to build the unbiased 30-year period CDF (1991-2020); unbiased SSL CDFs of the 6-member ensemble at the coast; and CDFs from the 21-member SLR ensemble, considering the closest grid-point (41ºN, 10ºW). The CDF of the SSL ensemble, based on the GEV distribution, required bias correction, in order to fit the historical storm surge GEV modelling of Leixões and Viana do Castelo tide gauge data. Additionally, to fit the final tide CDF to the observation's maximum tide GEV of Viana do Castelo, an amplitude factor of SSL and a MSL constant (related to the MSL in the year 2000, relative to the CASCAIS1938 national vertical datum) were applied. After the validation of the procedure with historical recorded tides, the respective projected combined CDFs were obtained for the 2041-2070 and 2071-2100 future periods under the RCP4.5 and RCP8.5 scenarios (Figure 88), from which the 4-, 25- and 100-year TWL return levels (here assumed as the minimum, mean and maximum ensemble values, for extreme events) were extracted.

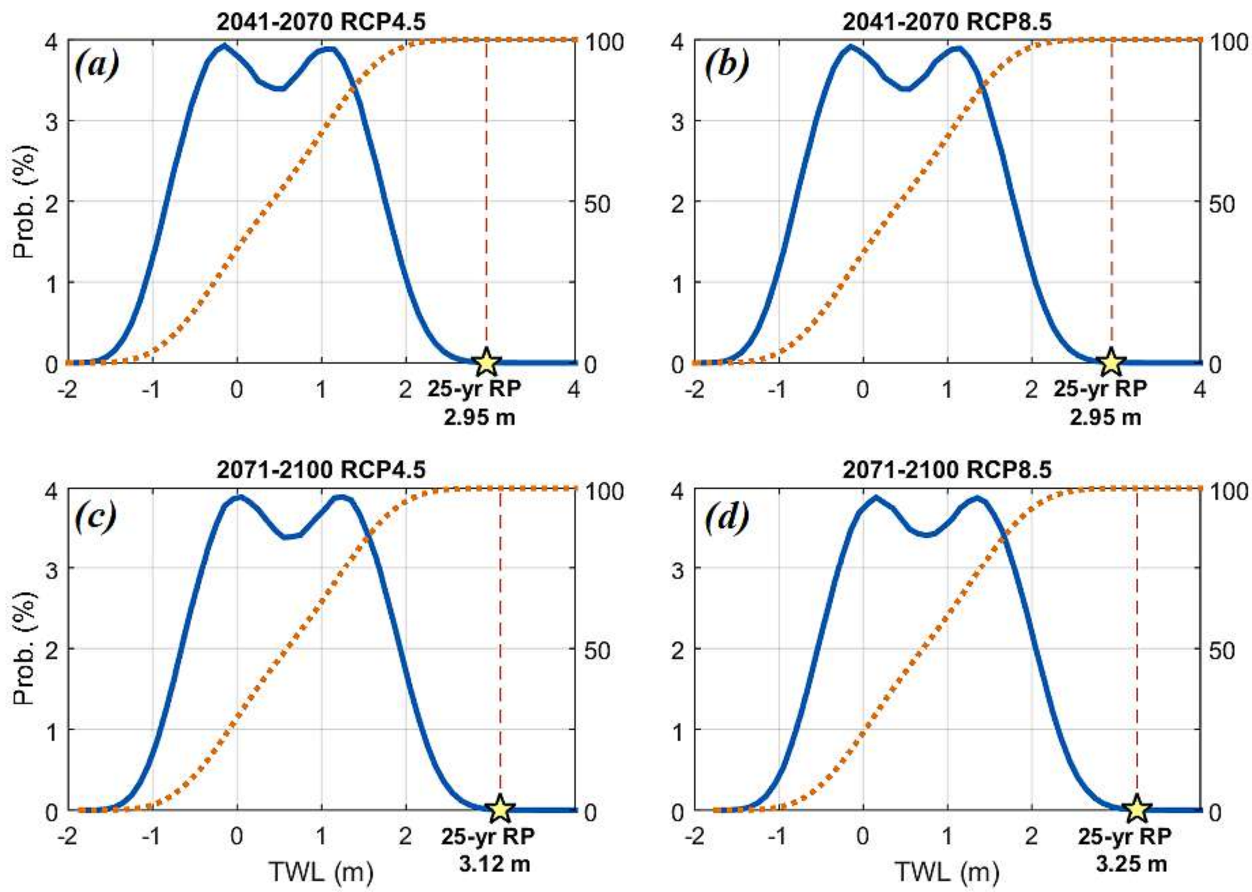

Figure 88 – Combined total tide PDF (blue line) for the Ofir key-location, using future projected SLR, tides and SSLs for the (left) RCP4.5 and (right) RCP8.5 scenarios, during (left) 2041-2070 and (right) 2071-2100, and respective CDF (orange line), with the reference to the 0.005% exceeding probability, corresponding to the combined 25-year return level.

The TWL and extreme wave conditions used to force the XBeach are described in Table 18, for each of the future projected time-slices and scenarios at Ofir. Overall, the projections indicate an increase in the TWL values towards the end of the 21st century for both scenarios, although more expressive for the RCP8.5 than for the RCP4.5. The ensemble 99th percentile range for projected wave energy conditions shows, for both scenarios, an increase in the amplitude of the associated H_S values, ranging from 3.69 m to

5.88 m for 2071-2100 under the RCP8.5 scenario, compatible with ever-higher extreme H_S values in the expected future. While the T_p associated to the 99% percentile energy is projected to slightly decrease, the MWD range for these extreme events is expected to become narrower towards the end of the 21st century, between 270º–283º (RCP4.5) and 281º–286º (RCP8.5). Such behavior is compatible with a projected decrease in the frequency of occurrence of north-westerly storm events.

Table 18 – Parameters used to force XBeach to produce future coastal flooding projections at the Ofir key-location.

Ofir			
2041-2070 (RCP4.5)			
	Min ensemble	**Mean ensemble**	**Max ensemble**
TWL (m)	2.60	2.95	3.25
$\mathbf{H_S}$ **(m)**	5.10	5.22	5.35
$\mathbf{T_p}$ **(s)**	13.19	14.87	17.83
MWD (º)	256.95	275.86	293.58
2041-2070 (RCP8.5)			
	Min ensemble	**Mean ensemble**	**Max ensemble**
TWL (m)	2.63	2.95	3.25
$\mathbf{H_S}$ **(m)**	4.76	5.16	5.57
$\mathbf{T_p}$ **(s)**	13.05	14.68	15.24
MWD (º)	276.56	283.33	290.58
2071-2100 (RCP4.5)			
	Min ensemble	**Mean ensemble**	**Max ensemble**
TWL (m)	2.78	3.12	3.45
$\mathbf{H_S}$ **(m)**	4.88	5.21	5.73
$\mathbf{T_p}$ **(s)**	13.17	14.23	14.92
MWD (º)	283.05	270.31	280.25
2071-2100 (RCP8.5)			
	Min ensemble	**Mean ensemble**	**Max ensemble**
TWL (m)	2.92	3.25	3.55
$\mathbf{H_S}$ **(m)**	3.69	5.05	5.88
$\mathbf{T_p}$ **(s)**	15.45	14.91	15.04
MWD (º)	286.17	280.88	283.25

Figure 89 shows the future projected coastal flooding extension under the RCP4.5 scenario by the end of the 2041-2070 time-slice at the Ofir key-location. It should be noted that, along this area, the coastal profile assumes different orientations, generally ranging from 250º to 280º). Therefore, the relevance of the incoming MWD on the coastal flooding results for each coastal section is enhanced, in comparison with the H_S and T_p values. For that reason, in Figure 89, the extension of flooding from the minimum TWL and wave energy conditions (incoming from 256º) exceeds the remaining mean and maximum ones (incoming from 276º and 294º, respectively). By 2070, under RCP4.5, the maximum flooding extent profiles are able to overtop the dune system at Ofir and produce flooding inland, along urbanized area, especially at Praia de Ofir and Praia da Bonança.

Figure 90 is similar to Figure 89, showing the range of projected coastal floodings by 2070, but under the RCP8.5 scenario. In this case, the three maximum extent profiles assume similar positioning. While the maximum ensemble values TWL, H_S and Tp values are greater than the minimum and mean counterparts, the MWD associated to each group promotes a balancing of the resulting flooding extents. Nevertheless, urbanized areas near Praia de Ofir and Praia da Bonança are consistently projected to be affected, up to 120 m inland from the reference (2018) shorelines.

Figure 91 is similar to Figure 89, although referring to the coastal flood projections by the end of the 2071-2100 time-slice. By the end of the 21st century, under the RCP4.5 scenario, flooding is consistently expected to reach locations further inland, in comparison with the results for 2070. In Figure 89, the most affected portion of the area corresponds to the northern half of Praia de Ofir, south of the first groin, where flooding is not only projected to reach habitational area facing the sea, but also areas facing the Cávado River estuary, approximately 200 m from the reference (2018) shorelines, under the mean and maximum ensemble conditions.

Figure 92 is similar to Figure 89, nevertheless corresponding to the coastal flooding projections by the end of the 2071-2100 time-slice and under the RCP8.5 scenario. Widespread coastal flooding is projected under extreme events in Figure 92, being all urbanized areas close to Praia de Ofir and Praia da Bonança at risk. In fact, consistent flooding of urbanized areas facing the ocean is projected for all TWL and extreme wave event levels, containing low and high-density habitational areas and commercial areas, such as stores, restaurants and a beach resort. Particularly at Praia de Ofir, considering the maximum ensemble projections, run-up lines reach the Cávado River estuary, approximately 250 m inland from the reference (2018) shorelines. Under these conditions, a water corridor would be created between the ocean and the estuary, isolating the northern portion of the Praia de Ofir into a temporary island, potentially resulting in a complete disruption of habitability conditions.

Overall, it should be noted that, particularly at the Ofir key-location, the increased dependence of the results on the main incoming direction of propagation implies that, if an idealized “maximum ensemble” event were to occur with a MWD range roughly between 240º and 260º, the maximum coastal flooding extent could potentially be greater. Nevertheless, such event is not depicted in the results of the 6-member propagated and bias corrected ensemble of wave climate projections and therefore was not considered.

Figure 89 – Future projected extreme coastal flooding at Ofir, considering a 25-year RP TWL value (ETWL) and three levels of 99th percentile nearshore wave energy conditions (WAVES1, WAVES2 and WAVES3 – ensemble uncertainty), over the projected DTM by 2070 under the RCP4.5 scenario. Shading represents the flooded area departing from the reference (2018) shoreline. Green, blue and red shadings refer to areas projected to be flooded under the WAVES1, WAVES2 and WAVES3 ensemble projections, respectively. Orange shading refers to areas projected to be consistently flooded under two or three extreme wave energy conditions simultaneously.

Figure 90 – Same as in Figure 89 but for the RCP8.5 scenario.

Figure 91 – Same as in Figure 89, but for 2100 under the RCP4.5 scenario.

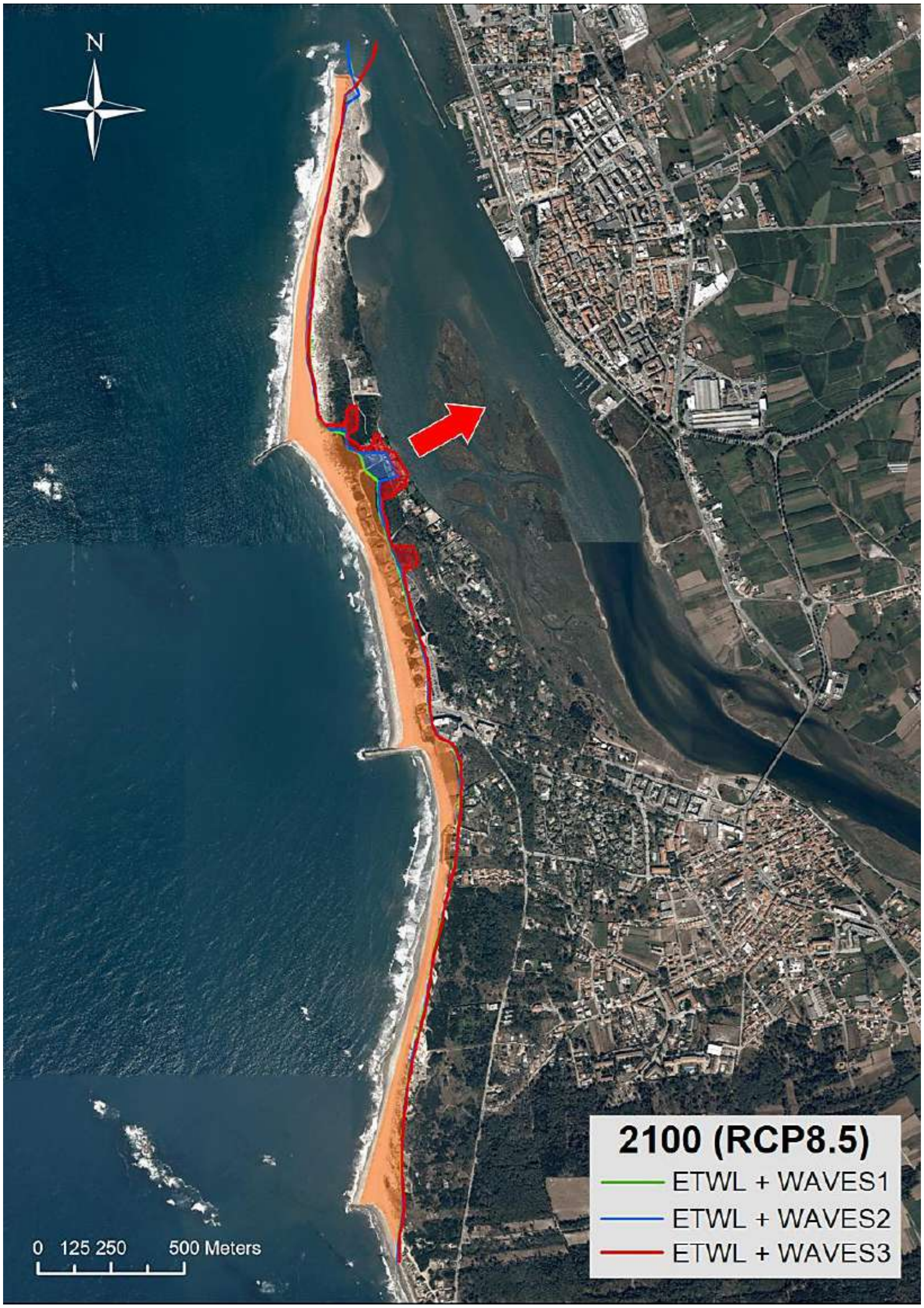

Figure 92 – Same as in Figure 91 but for the RCP8.5 scenario.

4.5.4. Costa Nova

To the Costa Nova key-location, the following data was used for the respective TWL: tide model of Aveiro tide gauge, to build the unbiased 30-year period CDF (1991-2020); unbiased SSL CDFs of the 6-member ensemble at the coast; and CDFs from the 21-member SLR ensemble, considering the closest grid-point (41ºN, 10ºW). The CDF of the SSL ensemble, based on the GEV distribution, required bias correction, in order to fit the historical storm surge GEV modelling of Aveiro tide gauge data. Additionally, to fit the final tide CDF to the observation's maximum tide GEV of Aveiro, an amplitude factor of SSL and a MSL constant (related to the MSL in the year 2000, relative to the CASCAIS1938 national vertical datum) were applied. After the validation of the procedure with historical recorded tides, the respective projected combined CDFs were obtained for the 2041-2070 and 2071-2100 future periods under the RCP4.5 and RCP8.5 scenarios (Figure 93), from which the 4-, 25- and 100-year TWL return levels (here assumed as the minimum, mean and maximum ensemble values of extreme events) were extracted.

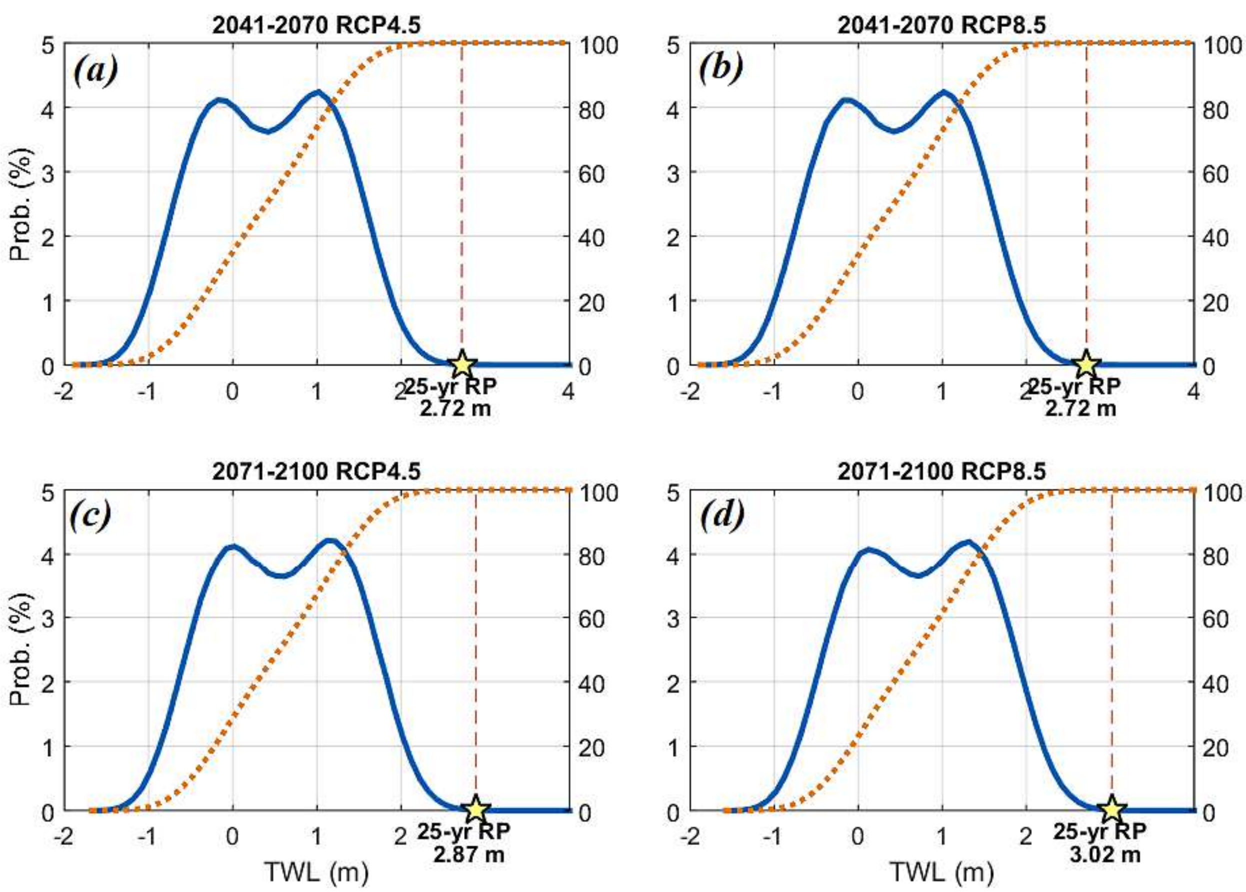

Figure 93 – Combined total tide PDF (blue line) for the Costa Nova key-location, using future projected SLR, tides and SSLs for the (left) RCP4.5 and (right) RCP8.5 scenarios, during (left) 2041-2070 and (right) 2071-2100, and respective CDF (orange line), with the reference to the 0.005% exceeding probability, corresponding to the combined 25-year return level.

The XBeach forcing conditions are described in Table 19, for each of the future projected time-slices and scenarios. Overall, the projections indicate an increase in the TWL values towards the end of the 21st century for both scenarios and a slight decrease in the 99th percentile H_S for the RCP4.5 scenario. Nevertheless, for this scenario, the extreme T_p values are projected to increase, up to 17.70 s. It is worth noticing that the maximum ensemble wave storm events show, for all instances, a greater southerly component than their minimum counterparts (although still incoming from W to WNW).

Table 19 – Same as in Table 18, but for the Costa Nova key-location.

Costa Nova			
2041-2070 (RCP4.5)			
	Min ensemble	**Mean ensemble**	**Max ensemble**
TWL (m)	2.41	2.72	3.02
H_S (m)	5.75	6.31	7.34
T_p (s)	13.11	13.48	16.07
MWD (º)	290.97	285.16	275.03
2041-2070 (RCP8.5)			
	Min ensemble	**Mean ensemble**	**Max ensemble**
TWL (m)	2.45	2.72	3.02
H_S (m)	6.07	6.06	7.49
T_p (s)	11.88	14.44	14.90
MWD (º)	293.84	285.49	284.08
2071-2100 (RCP4.5)			
	Min ensemble	**Mean ensemble**	**Max ensemble**
TWL (m)	2.54	2.87	3.12
H_S (m)	5.46	6.10	6.89
T_p (s)	13.52	13.87	17.70
MWD (º)	292	286.35	287.35
2071-2100 (RCP8.5)			
	Min ensemble	**Mean ensemble**	**Max ensemble**
TWL (m)	2.72	3.02	3.22
H_S (m)	6.09	6.30	7.39
T_p (s)	11.14	13.13	14.79
MWD (º)	276.79	280.97	265.16

The future projected coastal flooding conditions under the RCP4.5 scenario by the end of the 2041-2070 time-slice at the Costa Nova key-location are shown in Figure 94. The most vulnerable locations along the domain are those immediately South of the groins, where erosion was shown to be more severe (section 4.4.2). In fact, the maximum flooding extent profiles are similar to the future projected shoreline ones in Figure 61, despite a slight displacement further inland. In most of the locations, the extreme TWL and wave conditions by 2070 under the RCP4.5 scenario are not able to overtop of the dune system at Praia de Costa Nova – Norte and Praia da Barra. However, at Praia de Costa Nova – Sul, South of the third groin, overtopping and flooding of urban area is projected to occur considering the maximum ensemble wave energy conditions, affecting populated areas until Avenida da Bela Vista. Such projection is, nevertheless, associated to a low probability of occurrence.

Figure 95 is similar to Figure 94, depicting the projected coastal flooding extent by 2070, but under the RCP8.5 scenario. Interestingly, while the extreme run-up lines are generally positioned further inland than their RCP4.5 counterparts, due to higher SLR values, here no flooding of urban area is projected to occur. Such difference is related to lower 99th percentile wave energy for the ensemble members under the RCP8.5. In fact, while the maximum H_S is projected to increase, from 7.34 m to 7.49 m, T_p is projected to decrease from 16.07 s to 14.90 s.

Figure 96 is similar to Figure 94, representing nevertheless the expected coastal flooding by the end of the 2071-2100 time-slice. By 2100, under the RCP4.5 scenario, flooding is projected further inland, overtopping the dune system at several locations, namely at Praia de Costa Nova – Norte, south of the first groin, where the wave forcing conditions provided by the ensemble for the 99th percentile are consistent in showing run-up lines close to urban area, but also south of Praia da Barra and at Praia de Costa Nova – Sul. Especially in this last location, flooding is expected for both the mean and maximum ensemble conditions, corresponding to flooding of up to 23000 m^2 of urban area, almost reaching Avenida José Estevão, facing the opposite shore of Costa Nova and the inland waters of Ria de Aveiro.

By 2100 and under the RCP8.5 scenario, projections in Figure 97, similar to Figure 95, show the largest expected area of coastal flooding under 25-year return level TWL and extreme wave conditions. Across the entire domain, areas of future projected flooding are visible: at Praia de Costa Nova – Norte, the ensemble run-up lines range from 150 m to 350 m inland, corresponding to urban flooding from Avenida Fernandes Lavrador (ensemble minimum) up to Parque de Campismo da Barra (ensemble maximum). Further South, flooding is projected to reach populated areas West of Avenida José Estêvão, representing 46000 m^2 (ensemble minimum) to 66000 m^2 (ensemble maximum) of flooded area. At Praia de Costa Nova – Sul, urban flooding is also projected to occur for both the mean and maximum ensemble conditions, adding up to 6000 m^2 and 32000 m^2, respectively.

Figure 94 – Future projected extreme coastal flooding at Costa Nova, considering a 25-year RP TWL value (ETWL) and three levels of 99th percentile nearshore wave energy conditions (WAVES1, WAVES2 and WAVES3 – ensemble uncertainty), over the projected DTM by 2070 under the RCP4.5 scenario. Shading represents the flooded area departing from the reference (2018) shoreline. Green, blue and red shadings refer to areas projected to be flooded under the WAVES1, WAVES2 and WAVES3 ensemble projections, respectively. Orange shading refers to areas projected to be consistently flooded under two or three extreme wave energy conditions simultaneously.

Figure 95 – Same as in Figure 94, but for the RCP8.5 scenario.

Figure 96 – Same as in Figure 94, but for 2100 under the RCP4.5 scenario.

Figure 97 – Same as in Figure 96, but for the RCP8.5 scenario.

4.5.5. Cova Gala

For the Cova Gala key-location, the TWLs were obtained using: tide model of Figueira da Foz tide gauge, to build the unbiased 30-year period CDF (1991-2020); unbiased SSL CDFs of the 6-member ensemble at the coast; and CDFs from the 21-member SLR ensemble, considering the closest grid-point (39ºN, 10ºW). The CDF of the SSL ensemble, based on the GEV distribution, required bias correction, in order to fit the historical storm surge GEV modelling of Aveiro tide gauge data (due to the absence of Figueira da Foz historical data). Additionally, to fit the final tide CDF to the observation's maximum tide GEV of Figueira da Foz, an amplitude factor of SSL and a MSL constant (related to the MSL in the year 2000, relative to the CASCAIS1938 national vertical datum) were applied. After the validation of the procedure with historical recorded tides, the respective projected combined CDFs were obtained for the 2041-2070 and 2071-2100 future periods under the RCP4.5 and RCP8.5 scenarios (Figure 98), from which the 4-, 25- and 100-year TWL return levels (here assumed as the minimum, mean and maximum ensemble values of extreme events) were extracted.

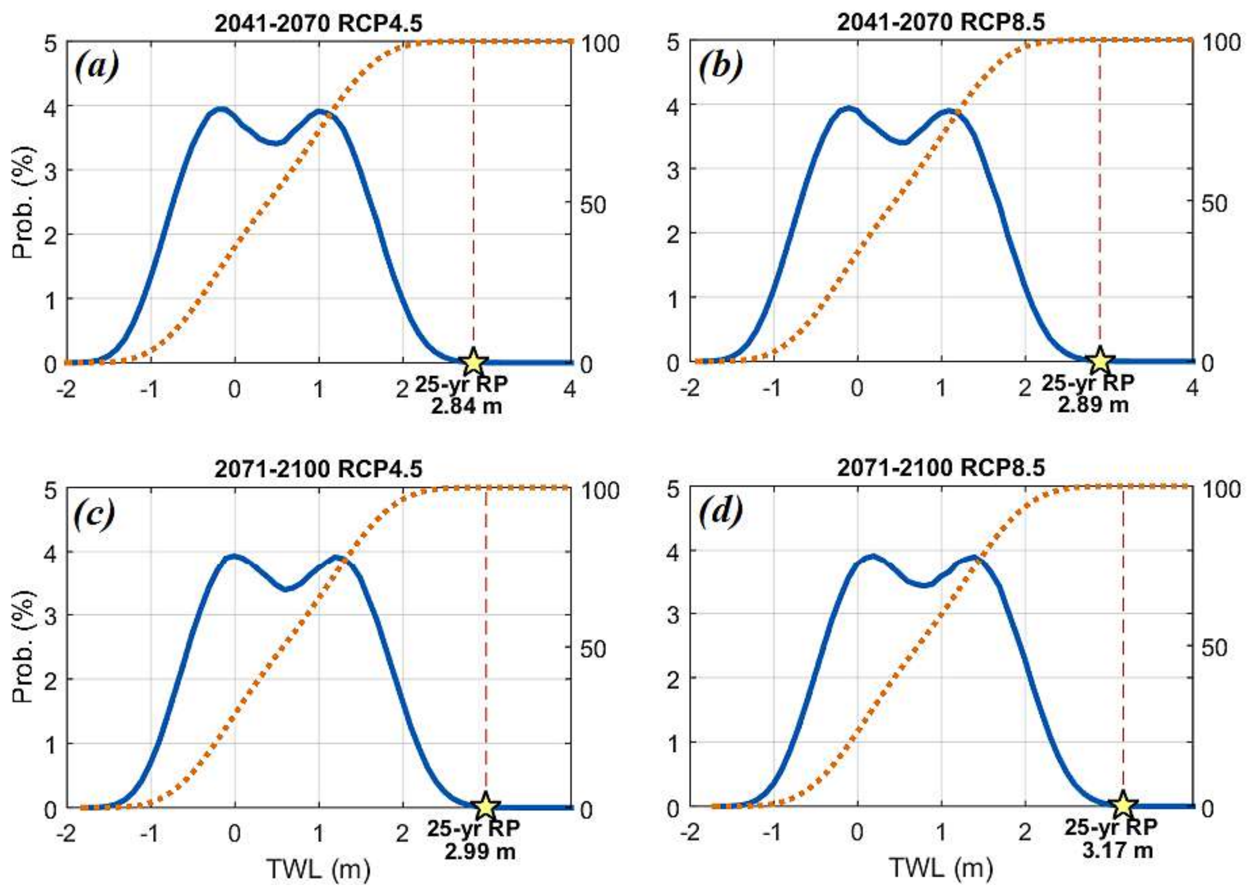

Figure 98 – Combined total tide PDF (blue line) for the Cova Gala key-location, using future projected SLR, tides and SSLs for the (left) RCP4.5 and (right) RCP8.5 scenarios, during (left) 2041-2070 and (right) 2071-2100, and respective CDF (orange line), with the reference to the 0.005% exceeding probability, corresponding to the combined 25-year return level.

The XBeach forcing conditions considering each of the future projected time-slices and scenarios are described in Table 21. Until the end of the 21st century, the TWL is projected to increase, mainly due to SLR, yet, the extreme wave energy conditions corresponding to the ensemble 99% percentile are projected to become slightly weaker, except for the maximum ensemble instance under the RCP4.5.

Table 20 – Same as in Table 18, but for the Cova Gala key-location.

Cova Gala			
2041-2070 (RCP4.5)			
	Min ensemble	**Mean ensemble**	**Max ensemble**
TWL (m)	2.55	2.84	3.09
H_S (m)	4.67	5.10	4.96
T_p (s)	12.17	12.49	14.27
MWD (º)	297.08	287.47	282.43
2041-2070 (RCP8.5)			
	Min ensemble	**Mean ensemble**	**Max ensemble**
TWL (m)	2.60	2.89	3.19
H_S (m)	4.67	4.94	5.24
T_p (s)	13.53	13.28	12.69
MWD (º)	297.50	289.17	290.08
2071-2100 (RCP4.5)			
	Min ensemble	**Mean ensemble**	**Max ensemble**
TWL (m)	2.73	2.99	3.29
H_S (m)	4.07	4.92	5.17
T_p (s)	14.96	12.98	13.14
MWD (º)	281.63	288.38	291.06
2071-2100 (RCP8.5)			
	Min ensemble	**Mean ensemble**	**Max ensemble**
TWL (m)	2.89	3.17	3.39
H_S (m)	4.44	4.86	5.08
T_p (s)	14.47	13.34	13.63
MWD (º)	290.92	294.69	296.93

Figure 99 depicts the future projected coastal flooding conditions under the RCP4.5 scenario by the end of the 2041-2070 time-slice at the Cova Gala key-location. Like in the previous areas, the most vulnerable locations along the domain are generally located South of the groins. It is worth mentioning that a groin is also located immediately North of the domain (although not visible), affecting its northernmost part. Additionally, due to the highly artificialized topographic elements in this area (as a part of Figueira da Foz harbour), results should be analyzed with caution. By 2070, under RCP4.5, results show no major coastal flooding occurrences in urban area, although the groins and most of the beach areas are consistently projected to become temporarily submerged. Communication routes closer to the beached are also projected to suffer from flooding under extreme conditions, especially in Praia do Cabedelo and Praia do Hospital.

Figure 100 is similar to Figure 99, but for the RCP8.5 scenario. In comparison with Figure 99, differences are marginal, although representing a consistent inland displacement of the maximum run-up lines. Despite the higher TWLs, extreme wave conditions are not able to overtop the main artificial and natural defense structures at Cova Gala.

Figure 101 is similar to Figure 99, considering, nevertheless, the coastal flooding extent by the end of the 2071-2100 time slice, under RCP4.5. By 2100, flooding is projected further inland, overtopping the dune system at several locations, namely at Praia do Cabedelo, Praia do Hospital, and partially at Praia de Cova Gala – Norte and Praia de Cova Gala – Sul. Although no urban area is projected to become directly affected by flooding, by the end of the 21st century under the RCP4.5 scenario, maximum run-up lines are projected to become meters away from habitational areas and further communication routes.

Finally, in Figure 102, similar to Figure 99 but for the 2071-2100 time-slice under RCP8.5, extreme coastal flooding projections point to strong physical impacts on structures near Praia do Hospital and Praia de Cova Gala – Norte, and partially at Praia de Cova Gala – Sul. Especially near Praia do Hospital, que parking lot which provides both access to the beach and to the hospital is projected to become temporarily flooded considering all TWL and 99% percentile ensemble conditions. Maximum run-up lines are projected to lay closer to urban areas than in the previous scenarios, partially affecting habitational buildings at the northern end of Praia de Cova Gala – Sul. It should be noted that a 99% percentile event can and will be exceeded at some point, since it does not correspond to a maximum extreme value, and therefore stronger wave events may occur, producing coastal flooding deeper inside urban area.

Figure 99 – Future projected extreme coastal flooding at Cova Gala, considering a 25-year RP TWL value (ETWL) and three levels of 99th percentile nearshore wave energy conditions (WAVES1, WAVES2 and WAVES3 – ensemble uncertainty), over the projected DTM by 2070 under the RCP4.5 scenario. Shading represents the flooded area departing from the reference (2018) shoreline. Green, blue and red shadings refer to areas projected to be flooded under the WAVES1, WAVES2 and WAVES3 ensemble projections, respectively. Orange shading refers to areas projected to be consistently flooded under two or three extreme wave energy conditions simultaneously.

Figure 100 – Same as in Figure 99, but for the RCP8.5 scenario.

Figure 101 – Same as in Figure 99, but for 2100 under the RCP4.5 scenario.

Figure 102 – Same as in Figure 101, but for the RCP8.5 scenario.

4.5.6. Costa da Caparica

For the Costa da Caparica key-location, the TWLs were obtained using: tide model of Cascais tide gauge, to build the unbiased 30-year period CDF (1991-2020); unbiased SSL CDFs of the 6-member ensemble at the coast; and CDFs from the 21-member SLR ensemble, considering the closest grid-point (37ºN, 10ºW). The CDF of the SSL ensemble, based on the GEV distribution, required bias correction, in order to fit the historical storm surge GEV modelling of Cascais tide gauge data. Additionally, to fit the final tide CDF to the observation's maximum tide GEV of Cascais, an amplitude factor of SSL and a MSL constant (related to the MSL in the year 2000, relative to the CASCAIS1938 national vertical datum) were applied. After the validation of the procedure with historical recorded tides, the respective projected combined CDFs were obtained for the 2041-2070 and 2071-2100 future periods under the RCP4.5 and RCP8.5 scenarios (Figure 103), from which the 4-, 25- and 100-year TWL return levels (here assumed as the minimum, mean and maximum ensemble values of extreme events) were extracted.

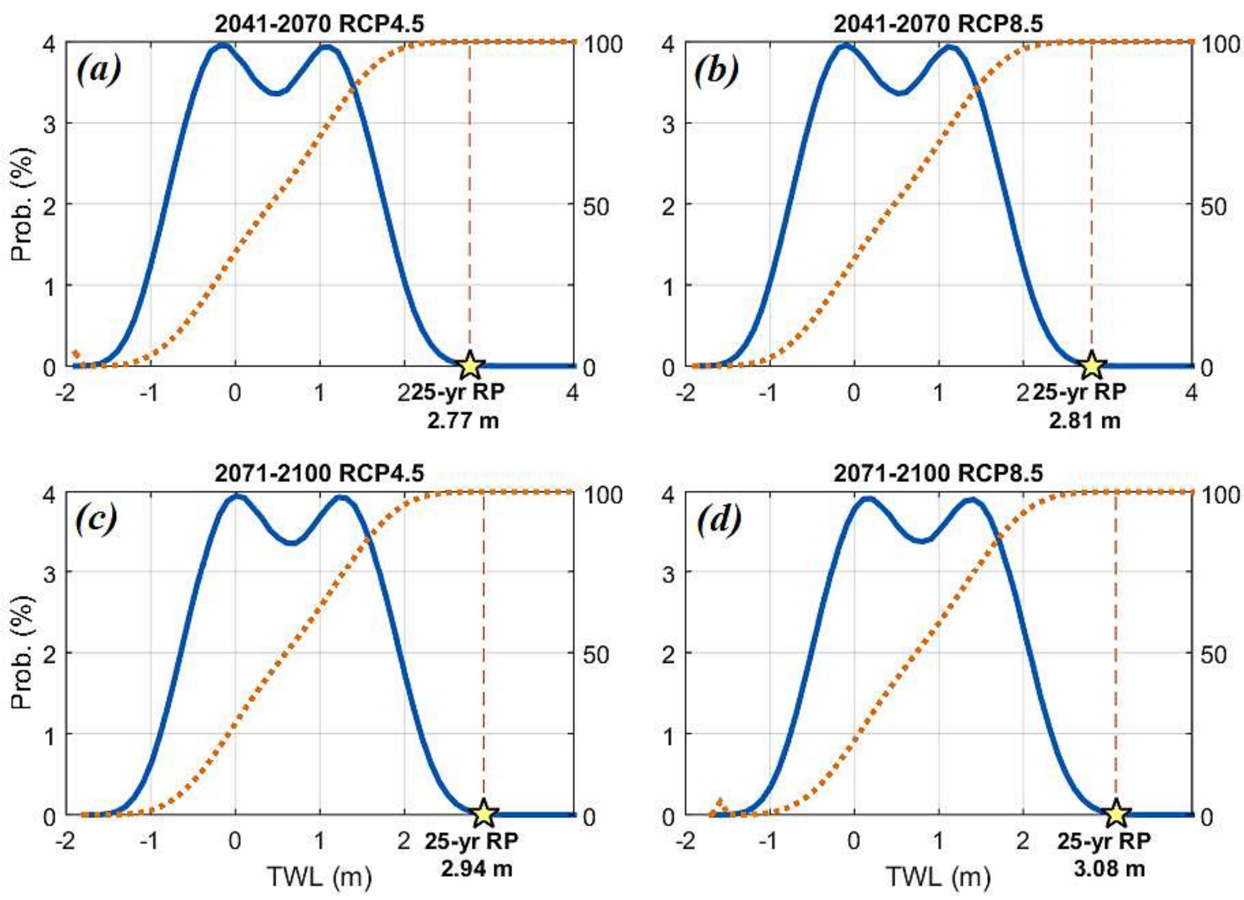

Figure 103 – Combined total tide PDF (blue line) for the Costa da Caparica key-location, using future projected SLR, tides and SSLs for the (left) RCP4.5 and (right) RCP8.5 scenarios, during (left) 2041-2070 and (right) 2071-2100, and respective CDF (orange line), with the reference to the 0.005% exceeding probability, corresponding to the combined 25-year return level.

The TWLs and extreme wave conditions used to force the XBeach are described in Table 21, for each of the future projected time-slices and scenarios at Costa da Caparica. Overall, similarly to the previous key-locations, the projections indicate an increase in the TWL values towards the end of the 21st century for both scenarios, mainly related to the SLR. The ensemble 99th percentile range for projected wave energy conditions shows, for both scenarios, a slight increase in the maximum associated H_S values, but a decrease in the minimum ones, compatible with a greater range of uncertainty towards the end of the 21st century regarding the extreme events. The T_p associated to the 99% percentile energy is projected to remain relatively stable, especially after 2070. Note that within the H_S and T_p values, the minimum and maximum instances do not always correspond to the minimum and maximum values of the parameters, since these values are ranked by total energy (E). Regarding the MWD, a slight but clear northward (counterclockwise) rotation trend is visible towards the end of the 21st century in both scenarios. Such behavior was already inferred from the projected LSTs along the area (Figure 72) and from the projected shoreline profiles in Praia de São João da Caparica (Figure 73 to Figure 78).

Table 21 – Same as in Table 18, but for the Costa da Caparica key-location.

Costa da Caparica			
2041-2070 (RCP4.5)			
	Min ensemble	**Mean ensemble**	**Max ensemble**
TWL (m)	2.53	2.77	2.91
H_S (m)	3.65	3.56	3.34
T_p (s)	10.95	13.53	16.72
MWD (º)	213.62	221.25	224.12
2041-2070 (RCP8.5)			
	Min ensemble	**Mean ensemble**	**Max ensemble**
TWL (m)	2.59	2.81	3.01
H_S (m)	3.19	3.50	3.62
T_p (s)	13.41	13.11	13.42
MWD (º)	229.62	223.64	224.39
2071-2100 (RCP4.5)			
	Min ensemble	**Mean ensemble**	**Max ensemble**
TWL (m)	2.71	2.94	3.11
H_S (m)	3.17	3.51	3.85
T_p (s)	13.77	13.37	12.31
MWD (º)	227.03	223.53	218.95
2071-2100 (RCP8.5)			
	Min ensemble	**Mean ensemble**	**Max ensemble**
TWL (m)	2.88	3.08	3.21
H_S (m)	3.06	3.46	3.70
T_p (s)	12.88	13.05	13.37
MWD (º)	229.09	224.35	229.36

Figure 104 depicts the future projected coastal flooding extension under the RCP4.5 scenario by the end of the 2041-2070 time-slice at the Costa da Caparica key-location. The coastal profile along this area assumes slightly different orientations, ranging from approximately 220º in the northernmost portion of the domain, at Praia de São João da Caparica, to 240º-245º in the remaining extension. Under this coastal setting and considering the existence of multiple artificial defence structures (groins) along the domain, extreme coastal flooding is expected to show increased dependency on the incoming MWD. For that reason, between Figure 105 and Figure 106, the extension of flooding projected at Praia do Inatel for the maximum 99th percentile ensemble wave energy instances (red lines) is greater by 2070 under RCP8.5, than by 2100 under RCP4.5, despite the higher TWL and more severe waves. The difference in MWD, from 224º (more perpendicular to the coast) to 219º (less perpendicular to the coast), respectively, is enough to produce greater flooding extension, despite the more moderate forcing conditions. By 2070 under RCP4.5 (Figure 104), the maximum flooding extent profiles are not able to overtop the long seawall protecting Costa da Caparica's urbanized ocean front. Nevertheless, local services at Praia de São João da Caparica (restaurants, bars, lounges, small warehouses and parking lots) are projected to be threatened by the landward expression of the run-up lines (under all ensemble conditions; up to 200 m) as soon as by 2070 under the moderate RCP4.5 scenario (Figure 104).

Figure 105 is similar to Figure 104, showing the projected extreme coastal flooding extensions by 2070, but under the RCP8.5 scenario. Considering RCP8.5 conditions, differences are visible at Praia da Cova do Vapor, in the uppermost part of the domain, where the three maximum extent profiles assume a similar positioning, further inland when compared to Figure 104. While run-up lines are similar at Praia de São João da Caparica, under the maximum 99th percentile ensemble wave energy conditions (and a more suitable MWD), flooding is projected to cover most of Praia do Inatel sandy area. Along the urbanized ocean front of Costa da Caparica, under the same maximum energy conditions, overtopping of the seawall is visible in Figure 105 at Praia do CDS, with flooding affecting local services (restaurants, bars), a portion of the Pedro Álvares Cabral street, and the "P1" parking lot.

Figure 106 is similar to Figure 104, but for the end of the 2071-2100 time-slice, under the RCP4.5 scenario. By the end of the 21st century, flooding is consistently expected to reach locations further inland, in comparison with the results for 2070. In Figure 106, the most affected portions of the area correspond to the northernmost and southernmost ones. At Praia de São João da Caparica, extreme coastal flooding is projected up to 250 m inland, threatening (besides the local services mentioned before) one communication route to Cova do Vapor. Under RCP4.5 forcing conditions, by 2100, no overtopping of the Costa da Caparica seawall is projected. Nevertheless, between Praia do Tarquínio-Paraíso and Nova Praia, maximum run-up lines are projected further inland, towards the base of the seawall.

Figure 107 is similar to Figure 104, corresponding nevertheless to the coastal flooding projections by the end of the 2071-2100 time-slice and under the RCP8.5 scenario. Widespread coastal flooding is projected under extreme events at Costa da Caparica, especially for the maximum 99th percentile wave action characteristics. At Praia de São João da Caparica, flooding is projected the threaten all current infrastructure, overtopping the already fragilized dune system at this location (Figure 87). Further South, at Praia do Inatel, maximum run-up lines are expected to reach the base of the seawall, except for the minimum ensemble energy instance, projected to be lower than for the remaining periods and scenarios (at 121 kW/m), associated to the 229º incoming MWD, which may have also contributed to smaller inundation extent, due to the protection offered from the groins South of the beach. Even within these expected conditions, Praia do Inatel shows, considering the current coastal configuration, enhanced resiliency to the impacts of climate change. While between Praia do Norte and Praia de Santo António the seawall is projected to withstand the considered future extreme events, along the urbanized ocean front of Costa da Caparica (Praia do CDS), mean and maximum energy run-up lines are expected further inland, directly affecting local services and urbanized area beyond the “P1” parking lot. Nevertheless, by the end of the 21st century under RCP8.5, the most threatened area (under all projected wave energy conditions) is located South of Praia do Tarquínio-Paraíso, where overtopping of the seawall is expected. Extreme coastal flooding is projected to threaten all local services in the first row of infrastructure (after the seawall), the General Humberto Delgado avenue, as well as the services along the second main row of infrastructure, which include high-density habitational areas. For the mean and maximum ensemble run-up lines, flooding projections extend up to Pero de Alenquer street. Note that, similarly to Costa Nova (Figure 97), flooding in densely urbanized areas may exceed the extension given by the XBeach model, given that buildings and streets are not considered in the projected DTMs, which may redirect the water flow further inland.

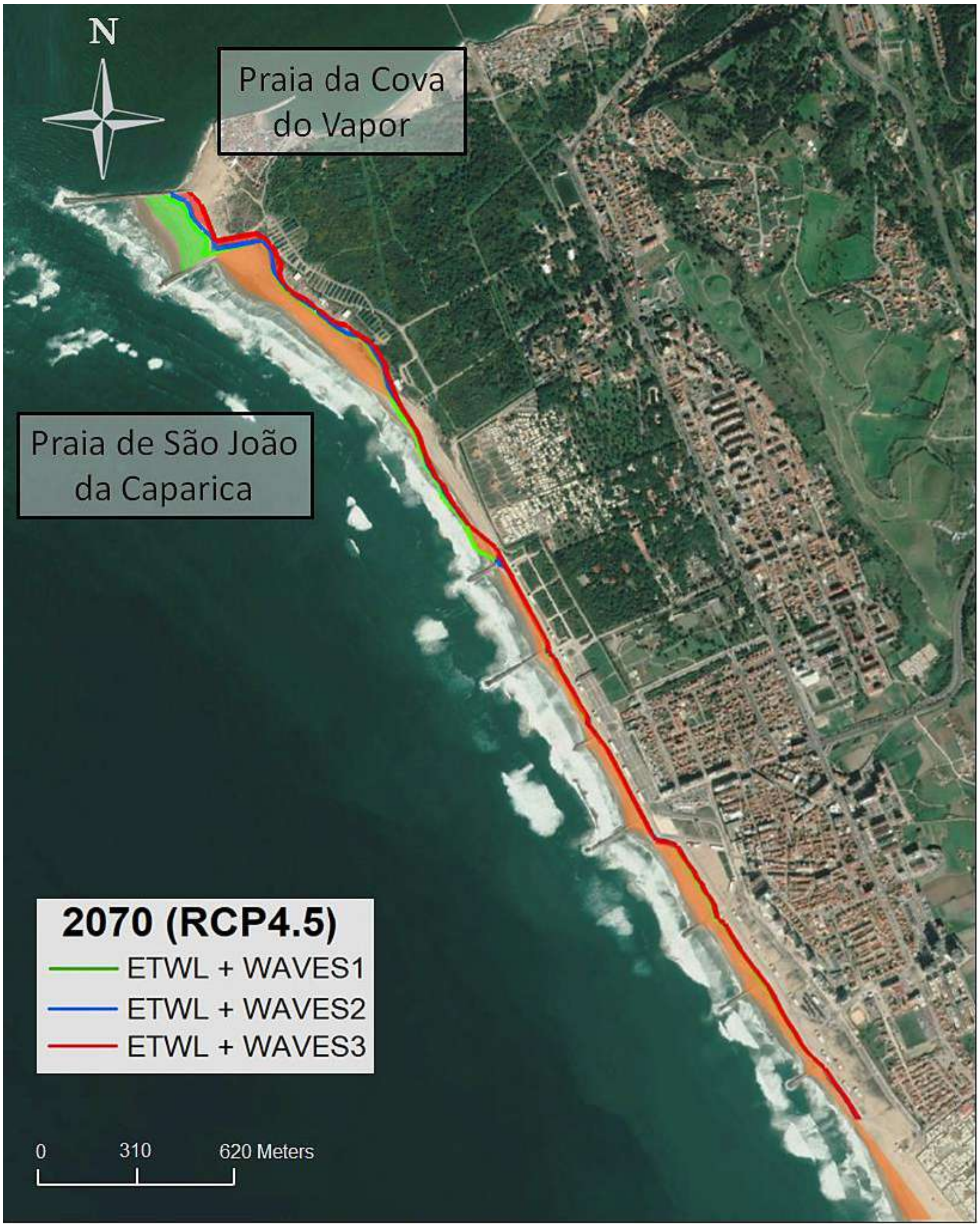

Figure 104 – Future projected extreme coastal flooding at Costa da Caparica, considering a 25-year RP TWL value (ETWL) and three levels of 99th percentile nearshore wave energy conditions (WAVES1, WAVES2 and WAVES3 – ensemble uncertainty), over the projected DTM by 2070 under the RCP4.5 scenario. Shading represents the flooded area departing from the reference (2018) shoreline. Green, blue and red shadings refer to areas projected to be flooded under the WAVES1, WAVES2 and WAVES3 ensemble projections, respectively. Orange shading refers to areas projected to be consistently flooded under two or three extreme wave energy conditions simultaneously.

Figure 105 – Same as in Figure 104, but for the RCP8.5 scenario.

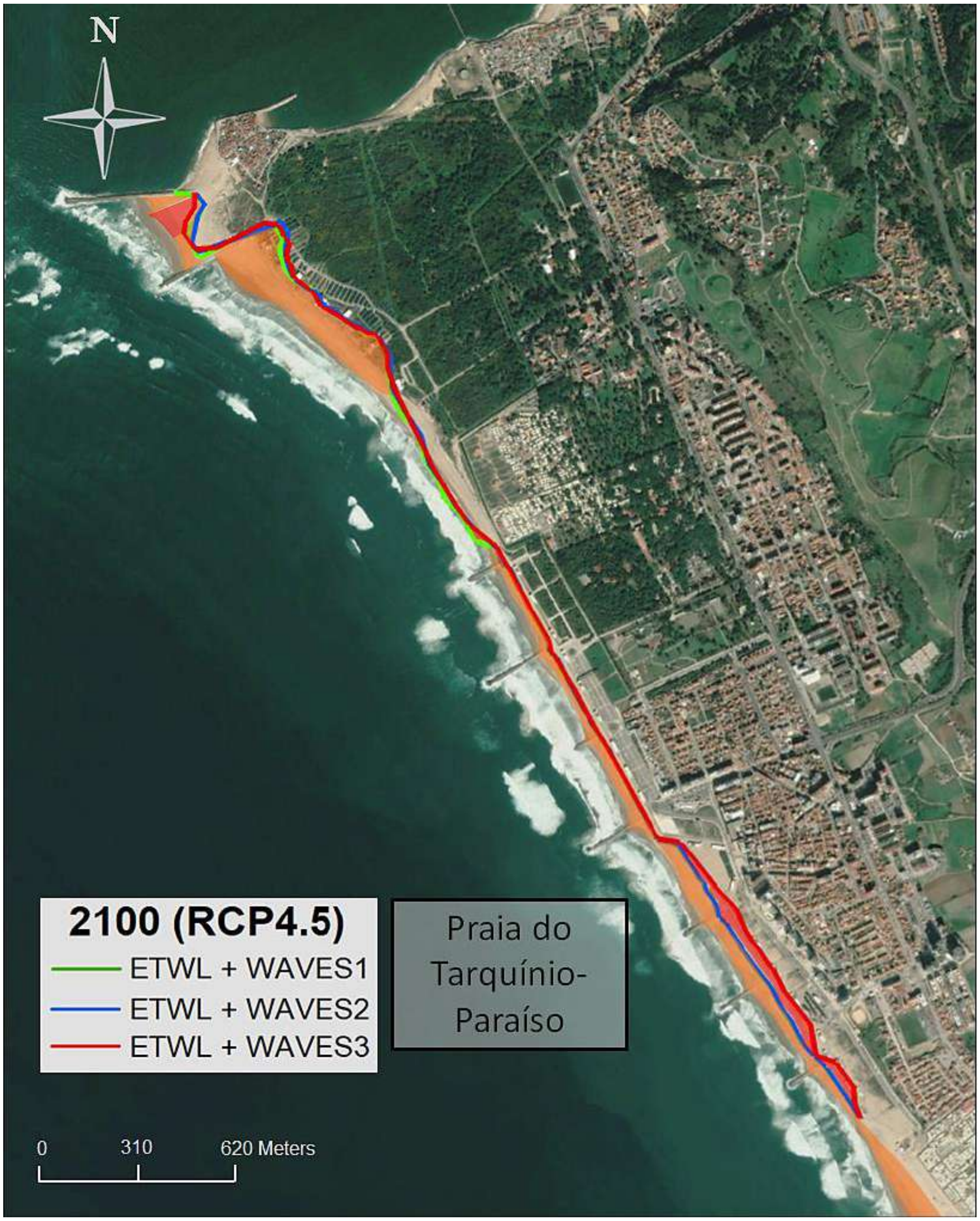

Figure 106 – Same as in Figure 104, but for 2100 under the RCP4.5 scenario.

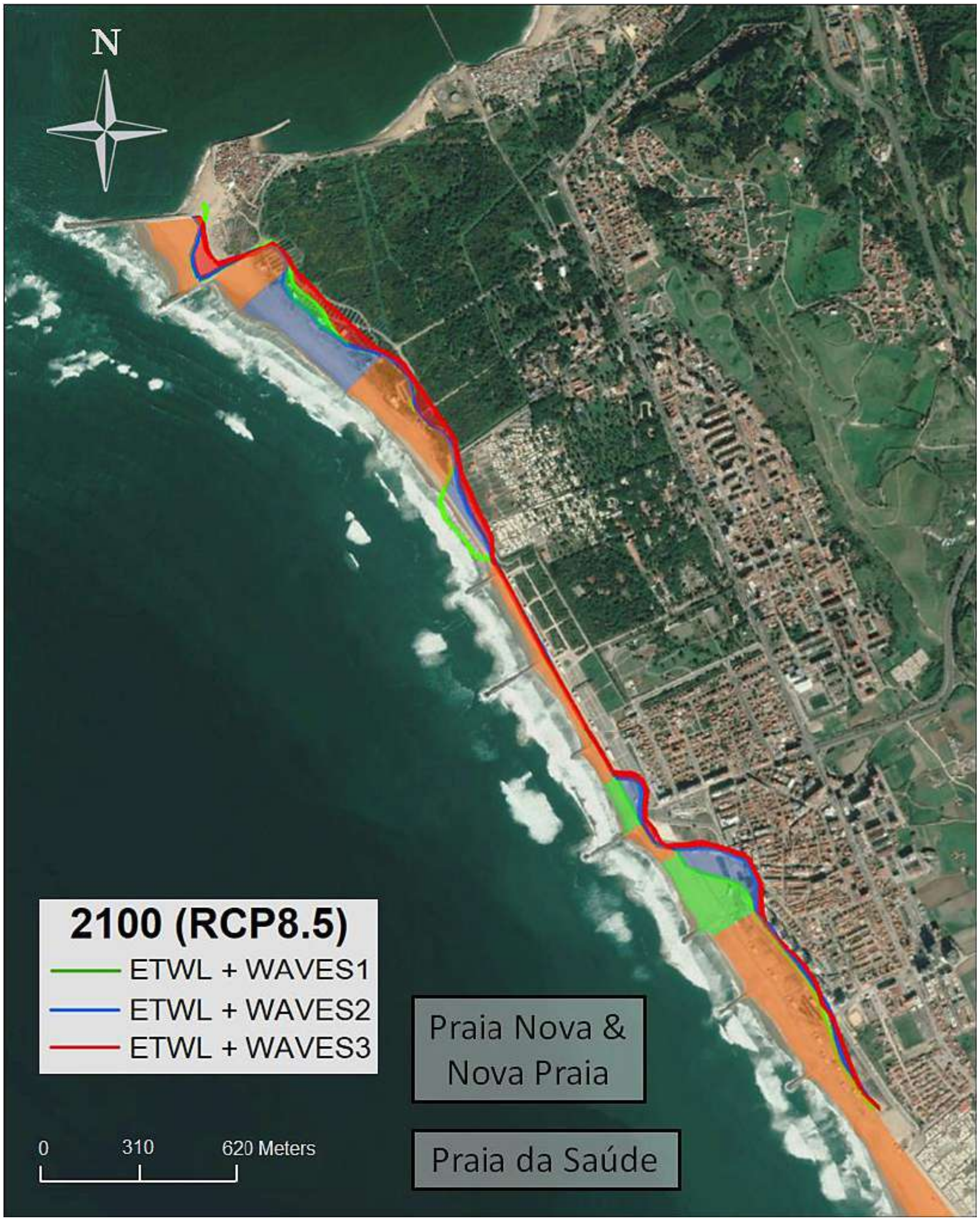

Figure 107 – Same as in Figure 106, but for the RCP8.5 scenario.

4.5.7. Praia de Faro

For the Praia de Faro key-location, the following data was used to compute the respective TWL: tide model of the Lagos tide gauge, to build the unbiased 30-year period CDF (1991-2020); unbiased SSL CDFs of the 6-member ensemble at the coast; and CDFs from the 21-member SLR ensemble, considering the closest grid-point (36ºN, 8ºW). The CDF of the SSL ensemble, based on the GEV distribution, required bias correction, in order to fit the historical storm surge GEV modelling of Lagos tide gauge data. Additionally, to fit the final tide CDF to the observation's maximum tide GEV of Lagos, an amplitude factor of SSL and a MSL constant (related to the MSL in the year 2000, relative to the CASCAIS1938 national vertical datum) were applied. After the validation of the procedure with historical recorded tides, the respective projected combined CDFs were obtained for the 2041-2070 and 2071-2100 future periods under the RCP4.5 and RCP8.5 scenarios (Figure 103), from which the 4-, 25- and 100-year TWL return levels (here assumed as the minimum, mean and maximum ensemble values of extreme events) were extracted.

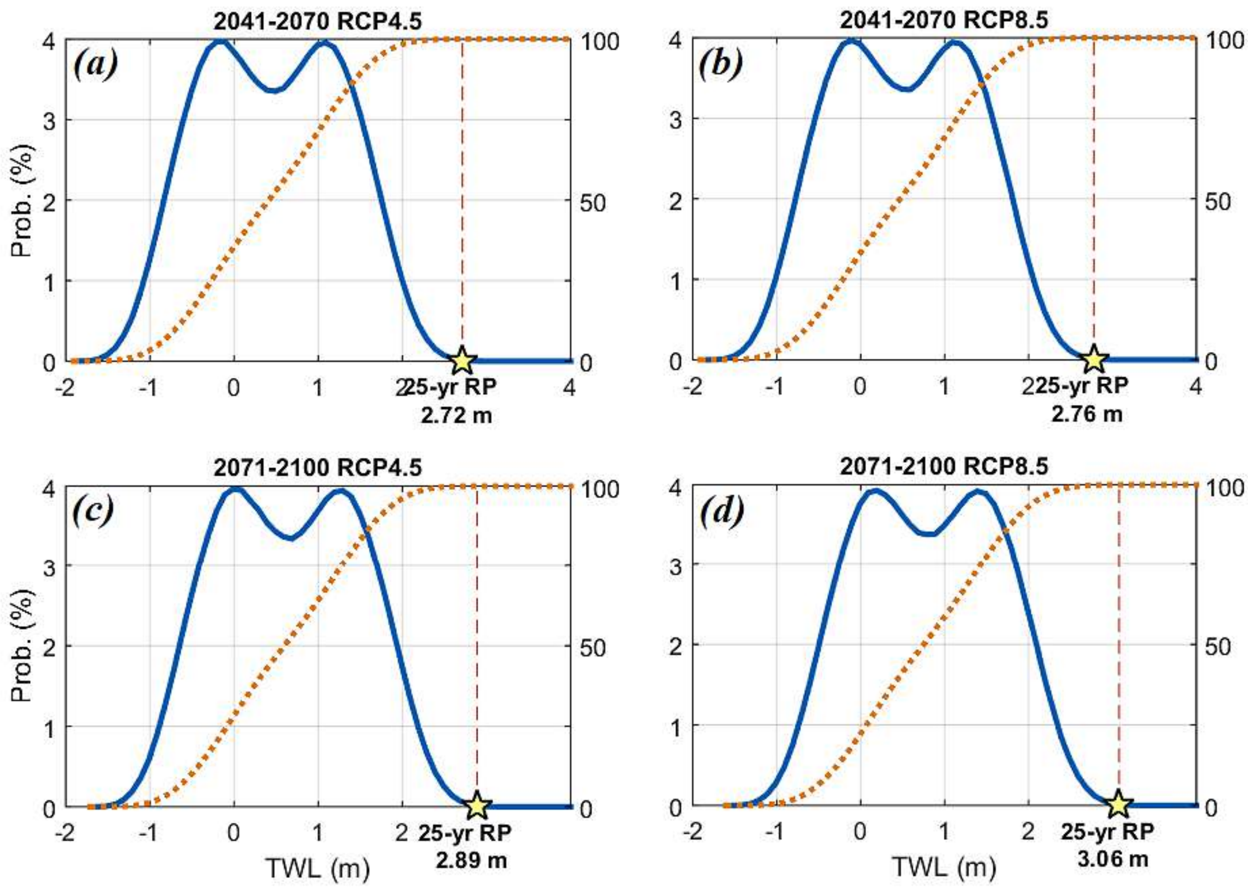

Figure 108 – Combined total tide PDF (blue line) for the Praia de Faro key-location, using future projected SLR, tides and SSLs for the (left) RCP4.5 and (right) RCP8.5 scenarios, during (left) 2041-2070 and (right) 2071-2100, and respective CDF (orange line), with the reference to the 0.005% exceeding probability, corresponding to the combined 25-year return level.

The TWLs and extreme wave conditions used to force the XBeach at Praia de Faro are described in Table 22, for each of the future projected time-slices and scenarios. Overall, not differently to the remaining key-locations, projections indicate an increase in the TWL values towards the end of the 21st century for both scenarios, which are mainly related to the SLR component. The ensemble 99th percentile energy shows a slight projected reduction between 2070 and 2100, for both scenarios, although more expressively for the RCP8.5, from 54.6 kW/m to 53.0 kW/m, respectively. This change is motivated by the H_S behavior, which is also projected to slightly decrease towards 2100, except for the maximum 99th percentile ensemble energy under RCP4.5. Nevertheless, this extreme event is projected to be accompanied by a relatively low T_p (8.86 s), leading to a decrease in the total energy when compared to the maximum 2070 one. Considering the incoming MWD, the results show relatively similar projections among the future periods and scenarios, except for the absence of southerly (178º) extreme events outside 2041-2070 under RCP4.5.

Table 22 – Same as in Table 18, but for the Praia de Faro key-location.

Praia de Faro			
2041-2070 (RCP4.5)			
	Min ensemble	**Mean ensemble**	**Max ensemble**
TWL (m)	2.50	2.72	2.89
H_S (m)	2.32	2.29	2.53
T_p (s)	8.11	10.74	9.95
MWD (º)	178.53	160.02	155.47
2041-2070 (RCP8.5)			
	Min ensemble	**Mean ensemble**	**Max ensemble**
TWL (m)	2.57	2.76	2.89
H_S (m)	1.55	2.11	2.15
T_p (s)	16.33	11.40	11.82
MWD (º)	162.21	158.06	157.96
2071-2100 (RCP4.5)			
	Min ensemble	**Mean ensemble**	**Max ensemble**
TWL (m)	2.69	2.89	2.99
H_S (m)	2.05	2.07	2.68
T_p (s)	9.67	12.77	8.86
MWD (º)	164.74	159.40	159.44
2071-2100 (RCP8.5)			
	Min ensemble	**Mean ensemble**	**Max ensemble**
TWL (m)	2.87	3.06	3.19
H_S (m)	1.90	1.94	1.76
T_p (s)	11.19	12.79	17.12
MWD (º)	164.30	158.51	157.47

Figure 109 shows the future projected coastal flooding extension by the end of the 2041-2070 time-slice under the RCP4.5 scenario at the Faro key-location. Here, the coastal profile is consistently oriented to the southwest (approximately 225º). Nevertheless, all the future projected extreme events are characterized by $MWDs$ ranging from 155º to 178º, and therefore, none of the events hits the coast perpendicularly. Therefore, for the extreme events considered, the impact of H_S and T_p (and overall TWL) dominates over MWD. By 2070, under RCP4.5, the maximum projected flooding extensions surpass the sandy beaches, reaching the beginning of the urbanized area, threatening the first row of communication routes (Nascente avenue).

Figure 110 is similar to Figure 109, but under the RCP8.5 scenario. In this case, the maximum extent of extreme coastal flooding is projected to consistently move landward (up to 120m from the reference shoreline), especially under the maximum 99th percentile ensemble energy conditions. Similarly to the RCP4.5 (Figure 109), ensemble uncertainty related to wave energy is generally well contained. Under this scenario, the first row of habitational infrastructure is already projected to be physically affected by flooding, for all ensemble projections.

Figure 111 is similar to Figure 109, although referring to the coastal flood projections by the end of the 2071-2100 time-slice, under the RCP4.5 scenario. By the end of the 21st century, flooding is consistently expected to reach locations further inland, in comparison with the results for 2070, well within urbanized areas. The main communication route within Praia de Faro (Nascente avenue) is projected to become inoperative, as extreme flooding is expected to cover most of its extension in the area. Nevertheless, flooding by 2100 under RCP4.5 is mainly restricted to the lowest areas of Praia de Faro, essentially compromising parking lots besides the first row of infrastructure.

Figure 112 is similar to Figure 109, nevertheless corresponding to the coastal flooding projections by the end of the 2071-2100 time-slice and under the RCP8.5 scenario. Widespread flooding is projected under extreme events for the RCP8.5, being the majority of the urbanized areas at risk in Praia de Faro. Especially for the maximum 99th percentile ensemble wave energy conditions, run-up lines are expected to reach the opposite shores of Praia de Faro, facing the Ria Formosa, approximately 140 m inland from the reference shorelines. Similarly to Ofir (Figure 92), under such a projection, water corridors would be established between the ocean and the Ria Formosa, creating a set of small, temporary islands, potentially leading to a complete disruption of habitability conditions.

Figure 109 – Future projected extreme coastal flooding at Praia de Faro, considering a 25-year RP TWL value (ETWL) and three levels of 99th percentile nearshore wave energy conditions (WAVES1, WAVES2 and WAVES3 – ensemble uncertainty), over the projected DTM by 2070 under the RCP4.5 scenario. Shading represents the flooded area departing from the reference (2018) shoreline. Green, blue and red shadings refer to areas projected to be flooded under the WAVES1, WAVES2 and WAVES3 ensemble projections, respectively. Orange shading refers to areas projected to be consistently flooded under two or three extreme wave energy conditions simultaneously.

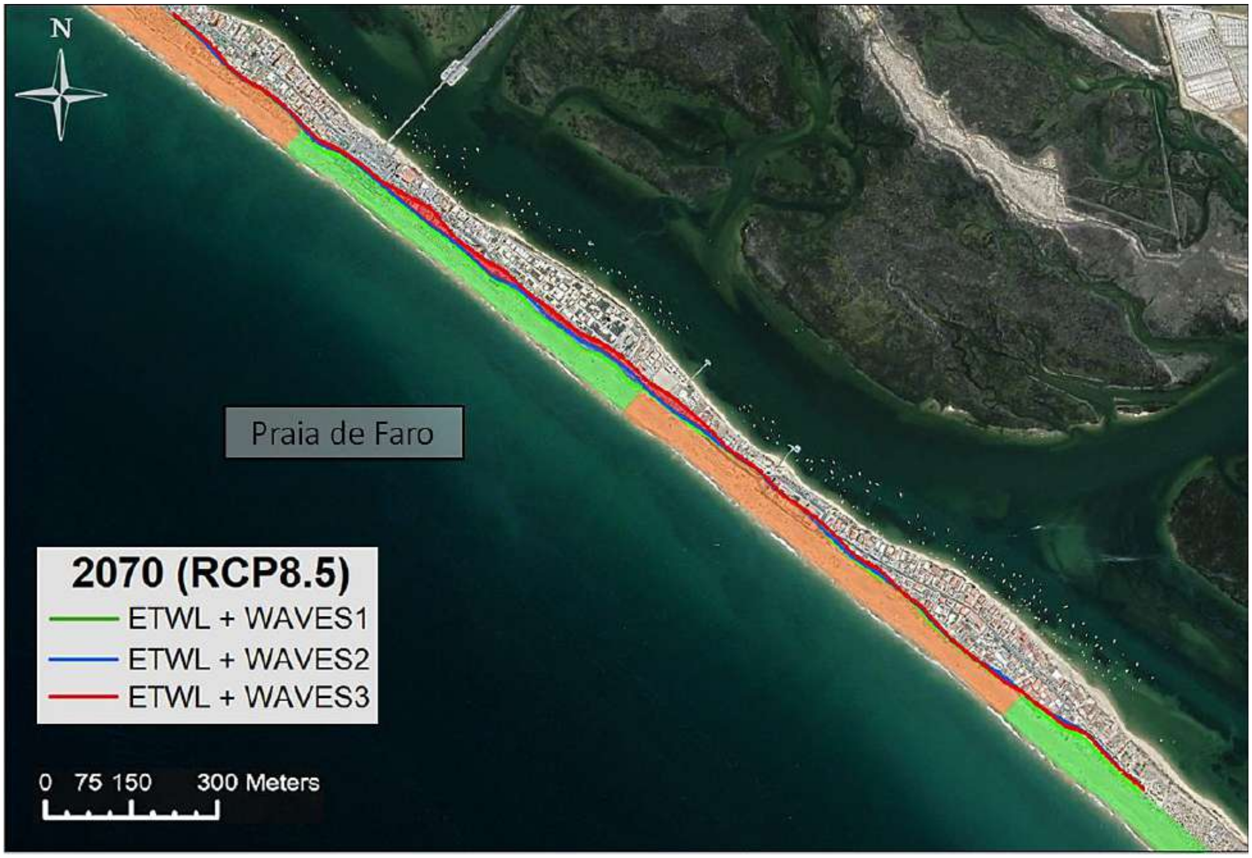

Figure 110 – Same as in Figure 109, but for the RCP8.5 scenario.

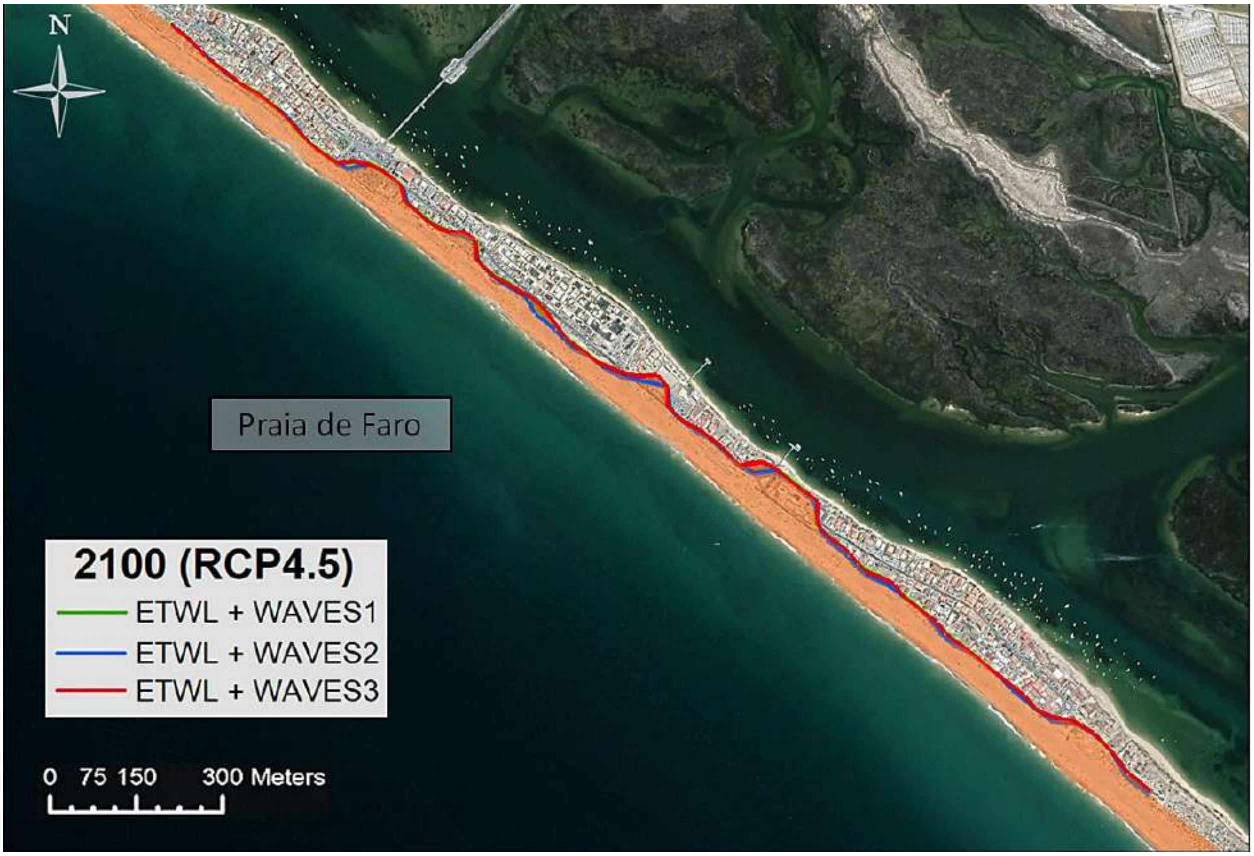

Figure 111 – Same as in Figure 109, but for 2100 under the RCP4.5 scenario.

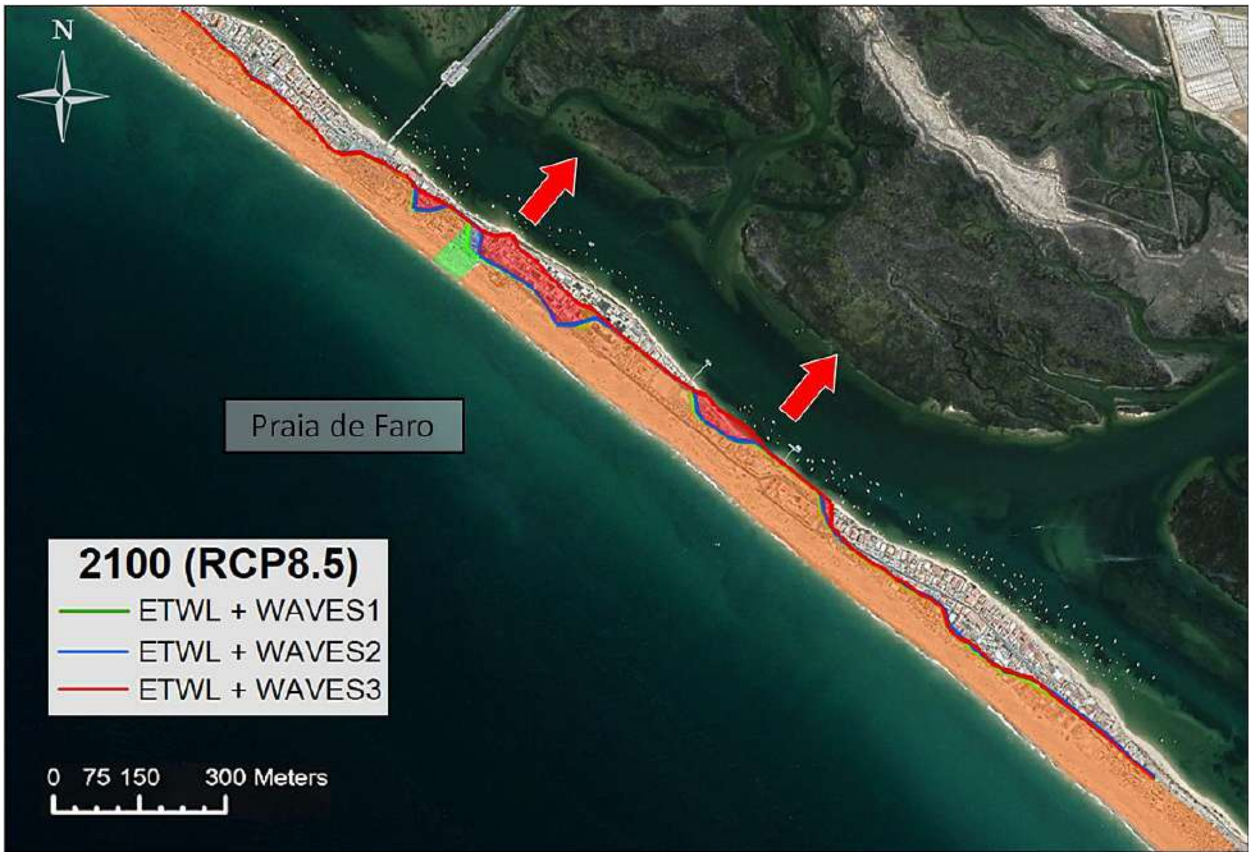

Figure 112 – Same as in Figure 111, but for the RCP8.5 scenario.

4.6. Cartography of Coastal Vulnerability

The cartography of coastal vulnerability was developed based on the approach detailed in section 3.3. The CVI is computed for the open coastal areas (facing the ocean), using the PCR method, in which the maximum overwash lines are estimated over the modified profiles of the sandy beach sections of the coast, and for the inland waters (estuaries and lagoons), based on the RP-associated values of TWL. Once the CVI estimated for both domain typologies, it is concatenated, and the total CVI is obtained. Note that the CVI presented in Figure 113 to Figure 175 is inversely related to the TWL RPs used and, consequently, their physical impacts. Therefore, areas with low CVI are in fact the ones projected to be vulnerable to the most extreme events (100-year RP of TWLs), which, due to their scarcer nature, are related to a lower CVI. On the other hand, areas with high CVI are the ones more vulnerable to the less extreme TWL events (4-year RP). The coastal areas under CVI classification (any level) are summarized in Table 23 to

Table 28, for each of the districts within each coastal section, considering both ocean-facing and inland stretches, for all future periods and scenarios. Note that the areas shown in these tables correspond to the projected areas under CVI classification in the future (maximum overwash lines for the referred RPs), departing from the 2018 shoreline, representing an effective difference between future and present climate conditions.

The coast was divided into six sections, Caminha-Espinho, Espinho-Figueira da Foz, Figueira da Foz-Peniche, Peniche-Setúbal, Tróia-Odeceixe, and Algarve. This division ensured a clearer presentation of the results, considering the specific conditions of each section, also allowing a connection with the key-locations where the hydro- morphodynamical validation and evaluation processes were initially conducted.

4.6.1. Section 1 – Caminha-Espinho

The first section, ranging from Caminha (Minho River mouth) to Espinho, encompasses a coastal stretch of about 115 km in length. It is dominated by low rocky beaches and cliffs, intersected, nevertheless, by low sandy beaches, often backed by dunar systems, such as Moledo, Duna do Caldeirão, Cabedelo, Castelo do Neiva, Esposende, Ofir and Bonança, Ramalha, Pedra Negra, Azurara, Ávore, Pedra do Corgo, Canide, Madalena and Aguda. Overall, considering the ocean-facing coastlines, it can be seen that even at the end of the first future period (2041-2070), under the moderate RCP4.5 scenario, some areas with infrastructure, including human housing are already projected to be under moderate to high vulnerability classification (Figure 113), namely in Esposende and along the Madalena-Valadares coastal stretch. Towards the end of the century, and under the RCP8.5 scenario, vulnerable areas attain greater extensions (Figure 114 to Figure 116). In fact, Table 23 shows that for the Viana do Castelo, Braga and Porto districts, the projected ocean-facing coastal areas under CVI classification tend to increase, from 0.78 km^2, 1.52 km^2

and 5.27 km^2 (2070 under RCP4.5) to 1.54 km^2, 1.91 km^2 and 6.19 km^2 (2100 under RCP8.5), respectively. For the coastlines facing inland waters (restricted to estuaries in this coastal section), projections are generally worse in terms of vulnerability, due to the extensive low-lying areas on both shores of the rivers, often used for agricultural, industrial, leisure or even habitational purposes. Despite considering just five estuaries, Table 23 shows that the areas under CVI for these locations range from 10.2 km^2, 1.41 km^2 and 0.69 km^2 (2070 under RCP4.5) to 11.1 km^2, 1.77 km^2, 0.92 km^2 (2100 under RCP8.5). Figure 117 to Figure 121 show a detailed CVI cartography for the Minho, Lima, Neiva, Cávado and Ave river estuaries and adjacent ocean-facing coastal stretches, respectively. Especially for the Lima (Figure 118), Cávado (Figure 120) and Ave (Figure 121) estuaries, their proximity to major urban centers (namely Viana do Castelo, Esposende and Vila do Conde) leads to high CVIs across deeply urbanized area, particularly in Esposende and Vila do Conde (*i.e.*, high flooding probability for 4-year TWL RP). In Viana do Castelo, on the northern shores of the Lima River, que CVIs are lower, nevertheless, most of its downtown is still projected to become flooded under a 100-year TWL RP in the future (especially by 2100 under RCP8.5, but also visible for the remaining future periods and scenarios).

Figure 113 – CVI for Section 1 – Caminha-Espinho, by 2070 under the RCP4.5 scenario.

Figure 114 – Same as in Figure 113, but for the RCP8.5 scenario.

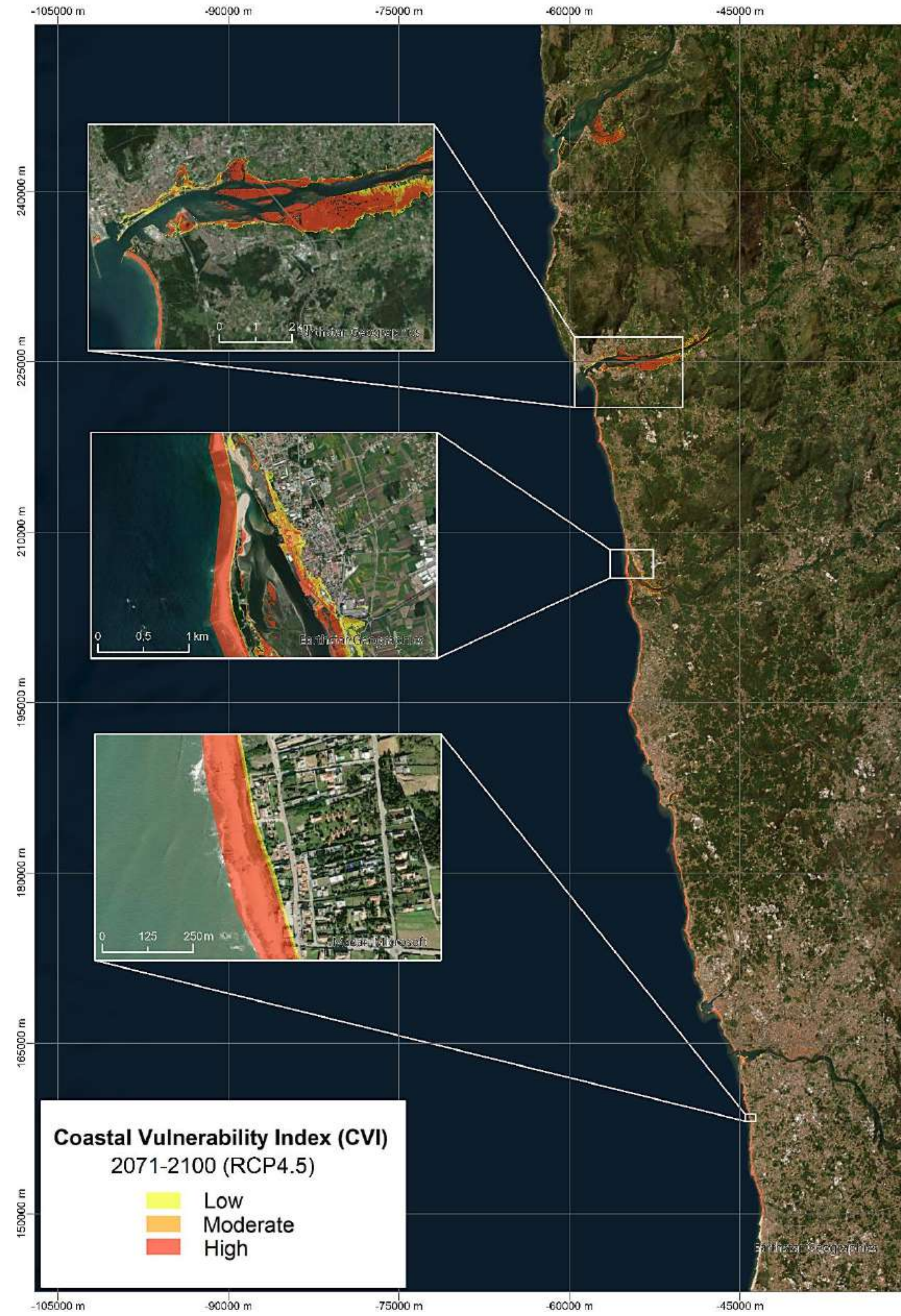

Figure 115 – Same as in Figure 113, but for 2100 under the RCP4.5 scenario.

Figure 116 – Same as in Figure 113, but for 2100 under the RCP8.5 scenario.

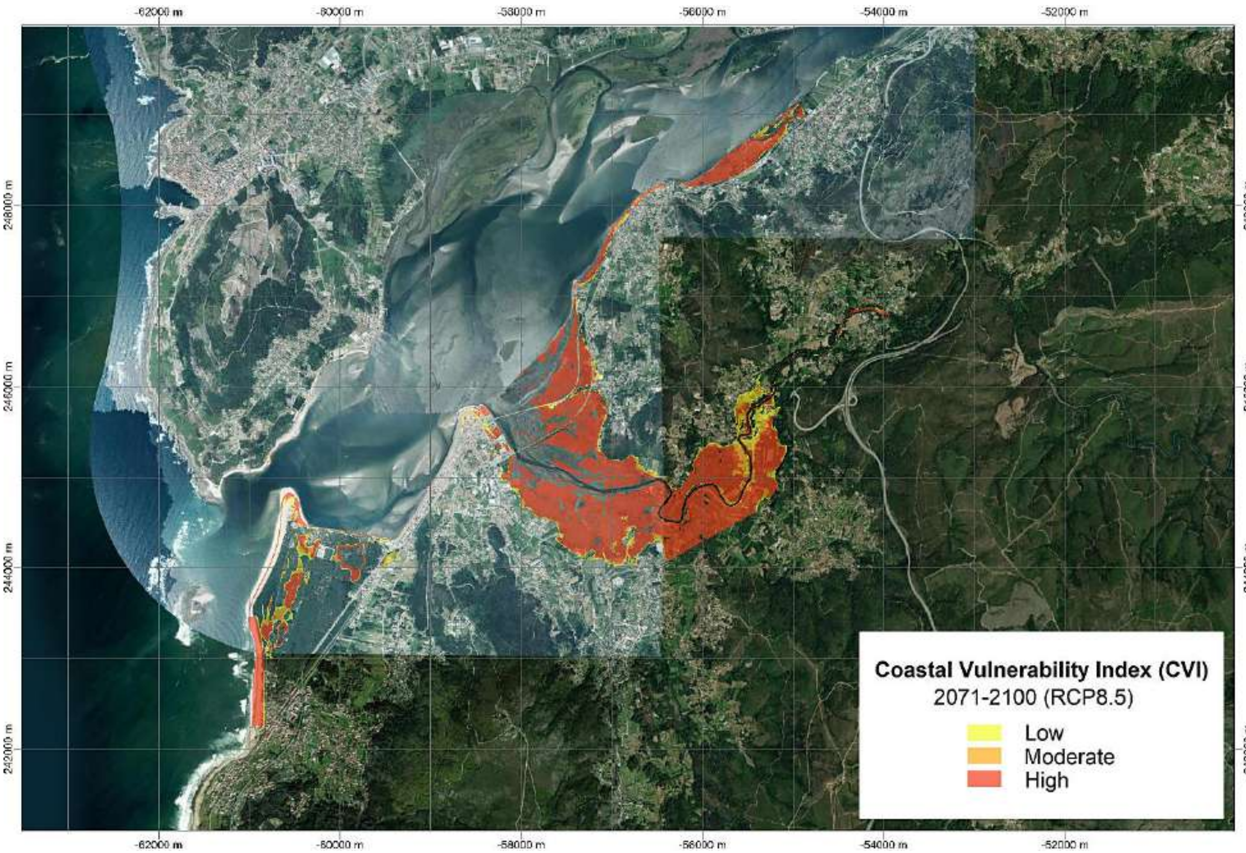

Figure 117 – CVI for Caminha (within Section 1 – Caminha-Espinho), by 2100 under the RCP8.5 scenario.

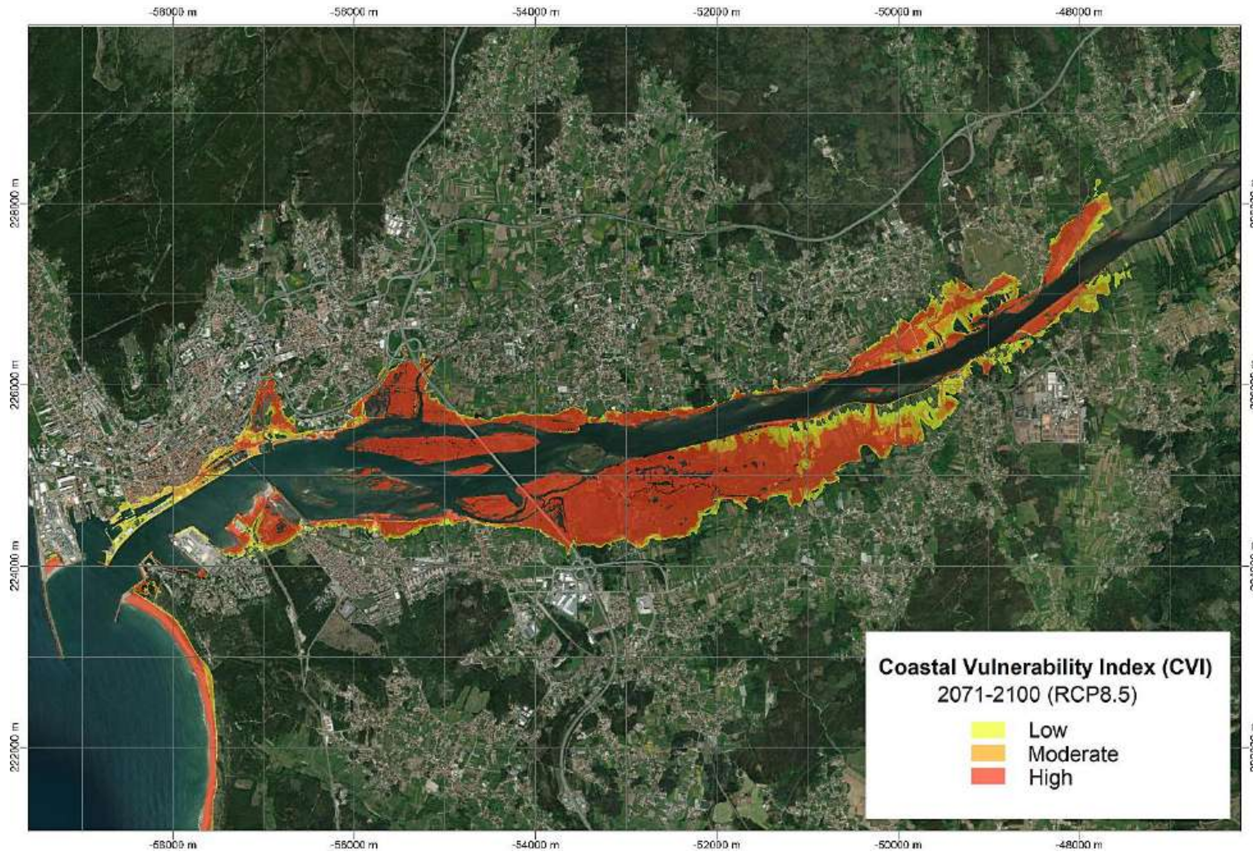

Figure 118 – Same as in Figure 117, but for Viana do Castelo (within Section 1 – Caminha-Espinho).

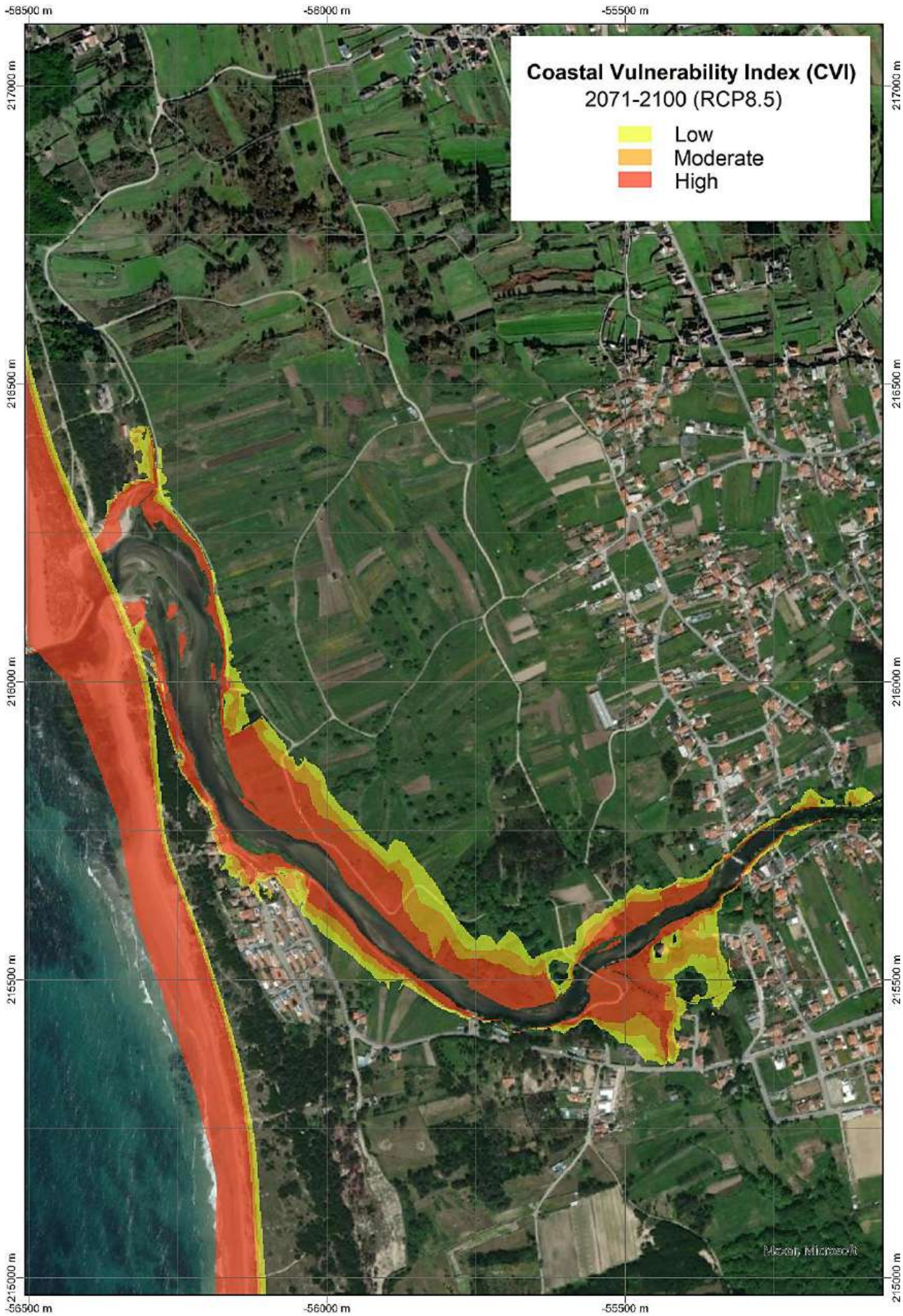

Figure 119 – Same as in Figure 117, but for the Neiva River mouth and Praia das Antas (within Section 1 – Caminha-Espinho).

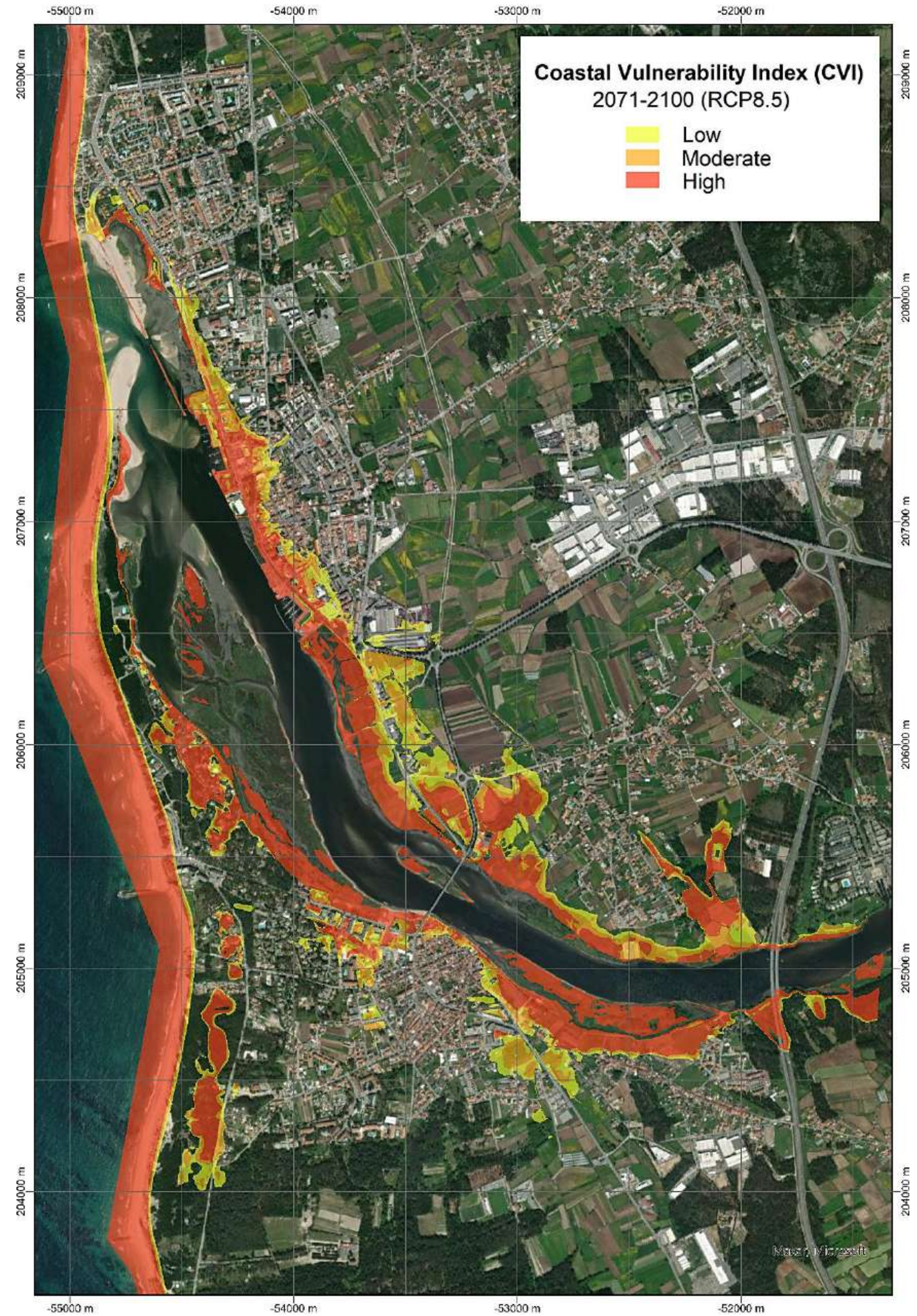

Figure 120 – Same as in Figure 117, but for Esposende and Ofir (within Section 1 – Caminha-Espinho).

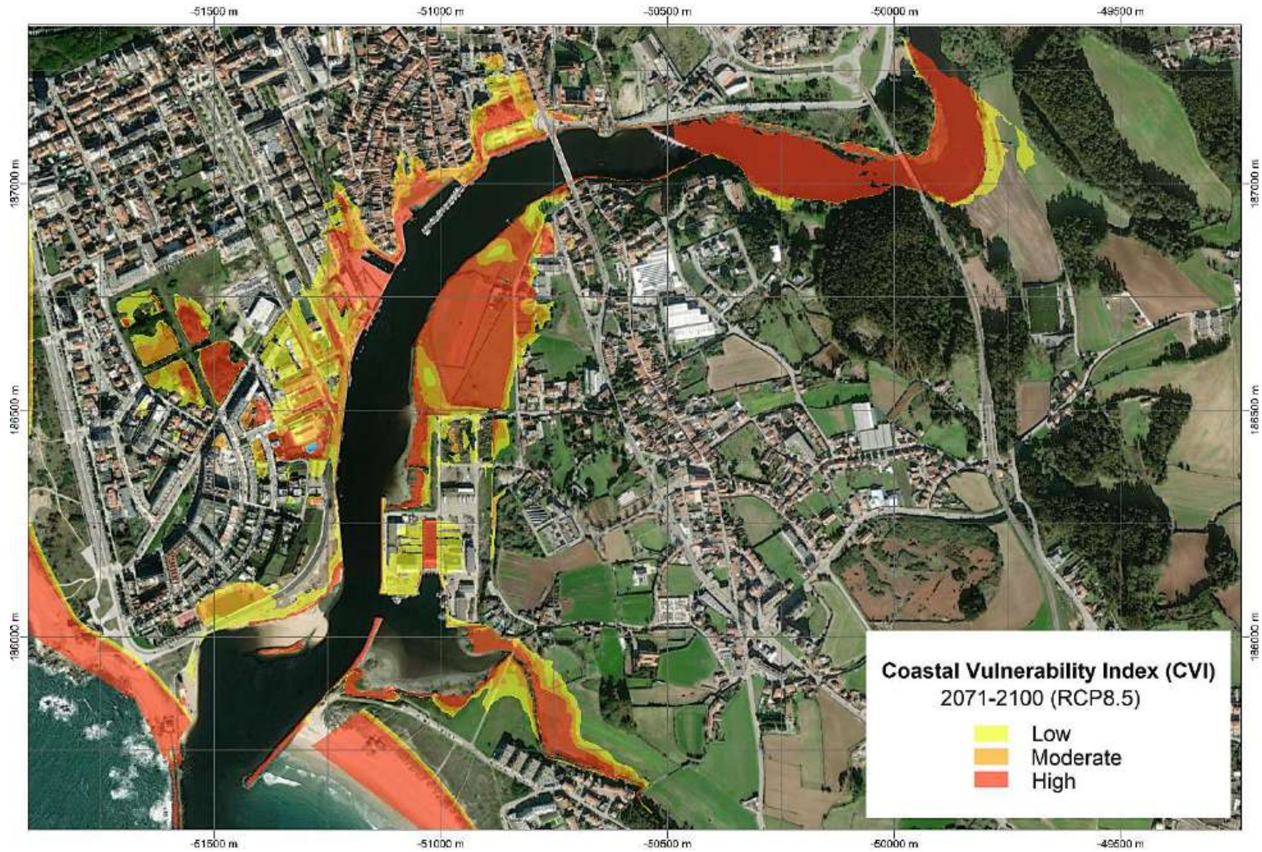

Figure 121 – Same as in Figure 117, but for Vila do Conde (within Section 1 – Caminha-Espinho).

Table 23 – Area (in km^2) of the coastal stretches under CVI classifications for each district within Section 1 – Caminha-Espinho, by 2070 (end of the 2041-2070 period) and 2100 (end of the 2070-2100 period), under both RCP4.5 and RCP8.5 scenarios.

Coastal areas under CVI classification for Section 1 – Caminha-Espinho			
2070 (RCP4.5)			
District	**Ocean-facing (km^2)**	**Inland (km^2)**	**Total (km^2)**
Viana do Castelo	0.78	10.2	10.9
Braga	1.52	1.41	2.93
Porto	5.27	0.69	5.96
2070 (RCP8.5)			
District	**Ocean-facing (km^2)**	**Inland (km^2)**	**Total (km^2)**
Viana do Castelo	1.14	9.67	10.8
Braga	1.60	1.41	3.01
Porto	4.87	0.69	5.56
2100 (RCP4.5)			
District	**Ocean-facing (km^2)**	**Inland (km^2)**	**Total (km^2)**
Viana do Castelo	1.37	10.6	12.0
Braga	1.83	1.65	3.48
Porto	5.74	0.84	6.57
2100 (RCP8.5)			
District	**Ocean-facing (km^2)**	**Inland (km^2)**	**Total (km^2)**
Viana do Castelo	1.54	11.1	12.6
Braga	1.91	1.77	3.69
Porto	6.19	0.92	7.11

4.6.2. Section 2 – Espinho-Figueira da Foz

The second section ranges from Espinho to Figueira da Foz (North of the Mondego River mouth), considering an almost straight coastal stretch of about 110 km in length, similarly to Section 1. This stretch, however, is mainly composed of long low sandy beaches, intersected by the largest Portuguese lagoon system, the Ria de Aveiro. The inland waters from Ria de Aveiro extend for more than 300 km^2, representing a unique, low-land landscape, and several natural and sociocultural resources. Its hydrodynamic regime is dominated by tides, and variations in the TWLs may pose a serious physical and socioeconomic threat. The ocean-facing coastal areas comprehend important sandy beaches and dunar systems, such as in Esmoriz, Maceda, Furadouro, Torreira, São Jacinto, Barra, Costa Nova, Vagueira, Areão, Mira, Tocha, Costinha and Quiaios.

Overall, considering the ocean-facing coastlines, it can be seen that even at the end of the first future period (2041-2070), under the moderate RCP4.5 scenario, some areas with infrastructure, including human housing are already projected to be under high vulnerability classification (Figure 122), including Espinho, Silvade and Esmoriz. Towards the end of the century, and under the RCP8.5 scenario, vulnerable areas attain greater extensions, especially across Ria de Aveiro (Figure 123 to Figure 125), and specifically at the urban areas of São Jacinto, Barra, Costa Nova, Gafanha da Nazaré (including the Aveiro harbor), and downtown Aveiro, for which high CVI classifications are shown in Figure 126, directly related to a high future projected frequency of flooding (associated to a 4-year RP of TWL along the shorelines of Ria de Aveiro inland waters). Note that specifically for downtown Aveiro, one of the most densely urbanized areas in this coastal section, high CVIs are present even for the moderate RCP4.5 scenario, in both future projected time periods.

Aveiro is one of the Portuguese districts with the largest future projected areas under CVI classification, totalizing 60.3 km^2 and 61.1 km^2, by 2100, under RCP4.5 and RCP8.5, respectively. From these values, 53.8 km^2 and 54.5 km^2 (89%) correspond to future projected flooding in locations adjacent to inland waters (from which the Ria de Aveiro ones are largely dominant). Table 24 also shows that for the Aveiro and Coimbra districts, the projected ocean-facing coastal areas under CVI classification tend to increase, from 5.75 km^2 and 4.19 km^2 (2070 under RCP4.5) to 6.53 km^2 and 7.55 km^2 (2100 under RCP8.5), respectively. These, although smaller than the ones related to the inland waters, still represent a major projected change in the coastal vulnerability and flooding extension, in comparison with the historical values.

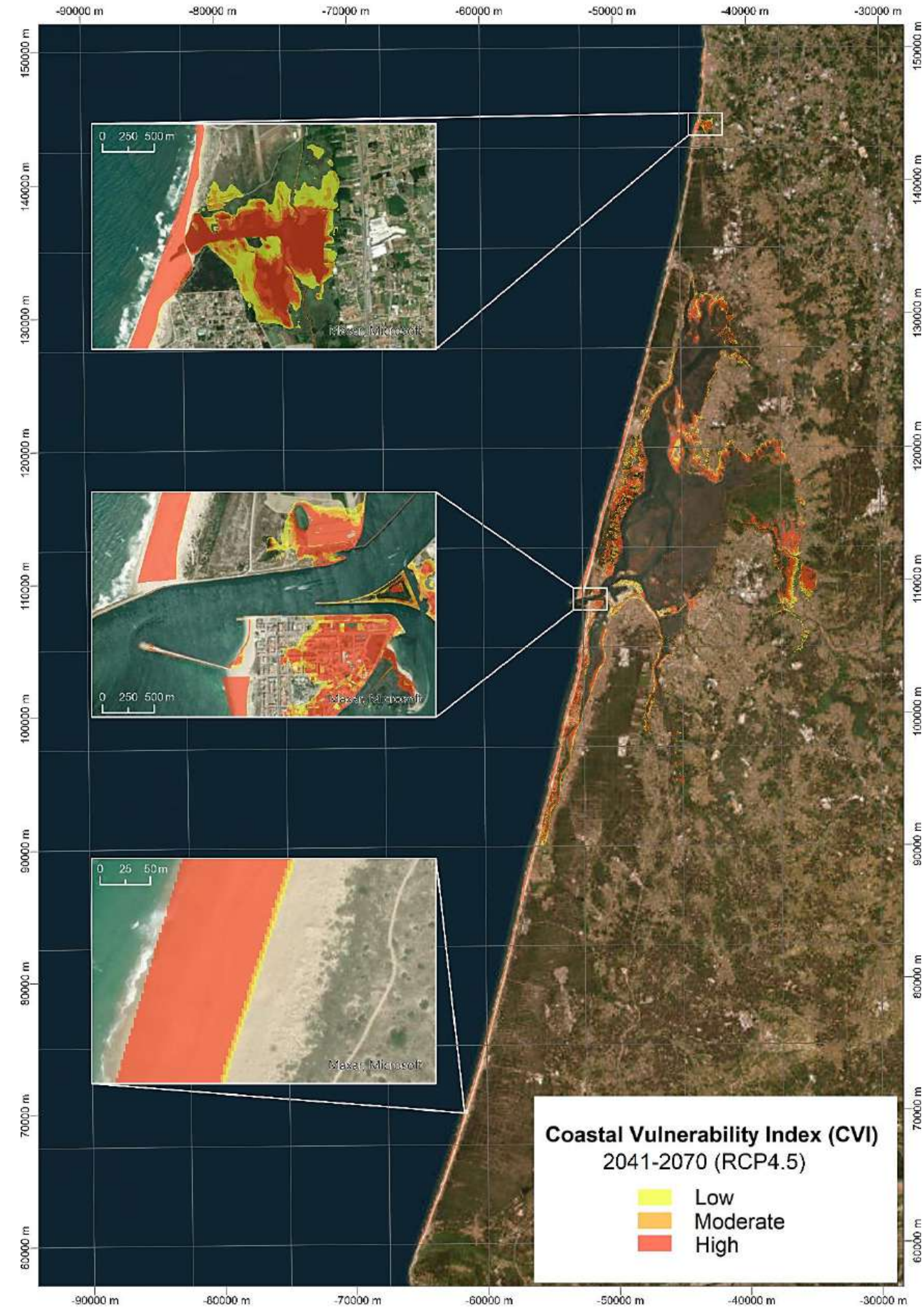

Figure 122 – CVI for Section 2 – Espinho-Figueira da Foz, by 2070 under the RCP4.5 scenario.

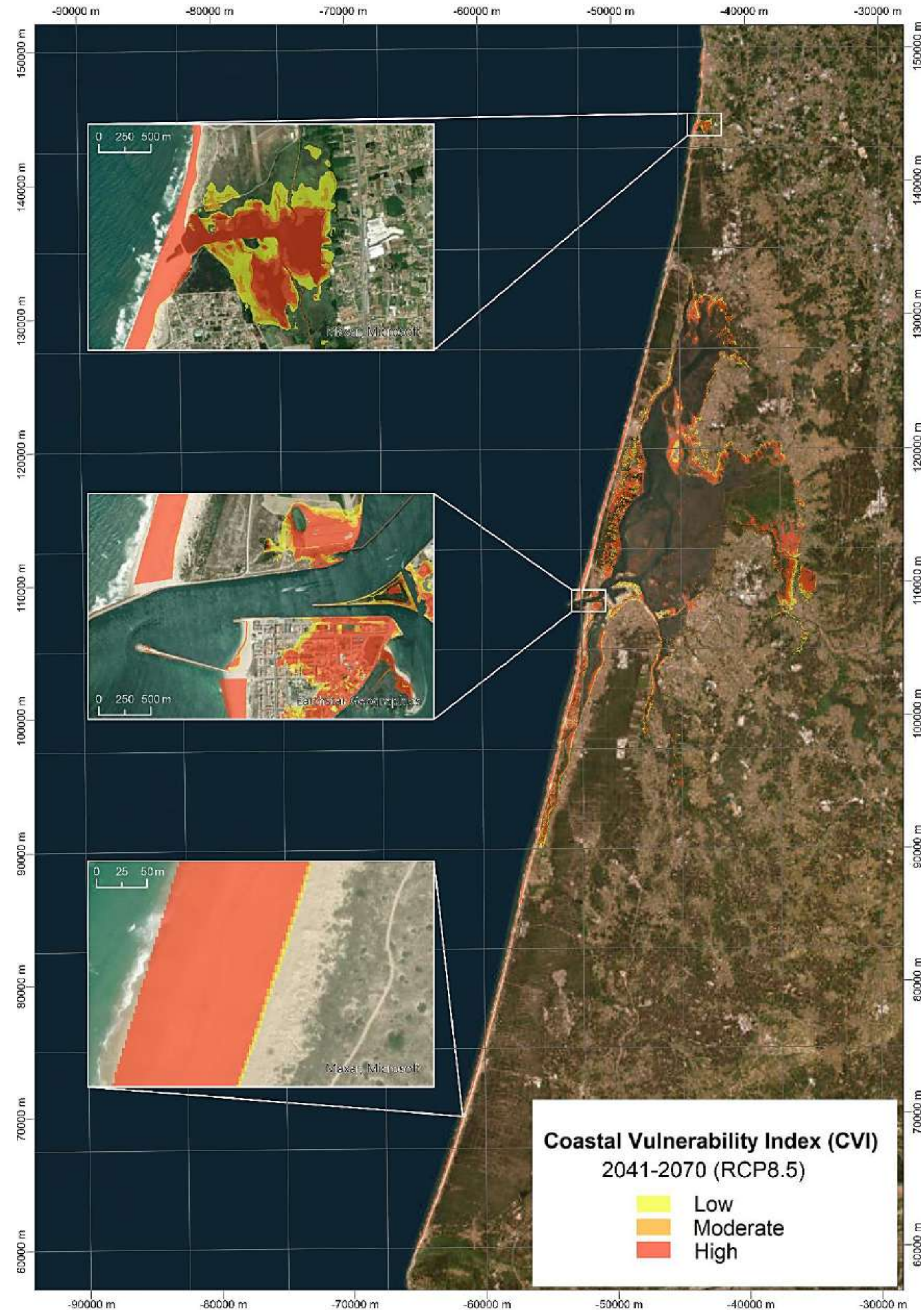

Figure 123 – Same as in Figure 122, but for the RCP8.5 scenario.

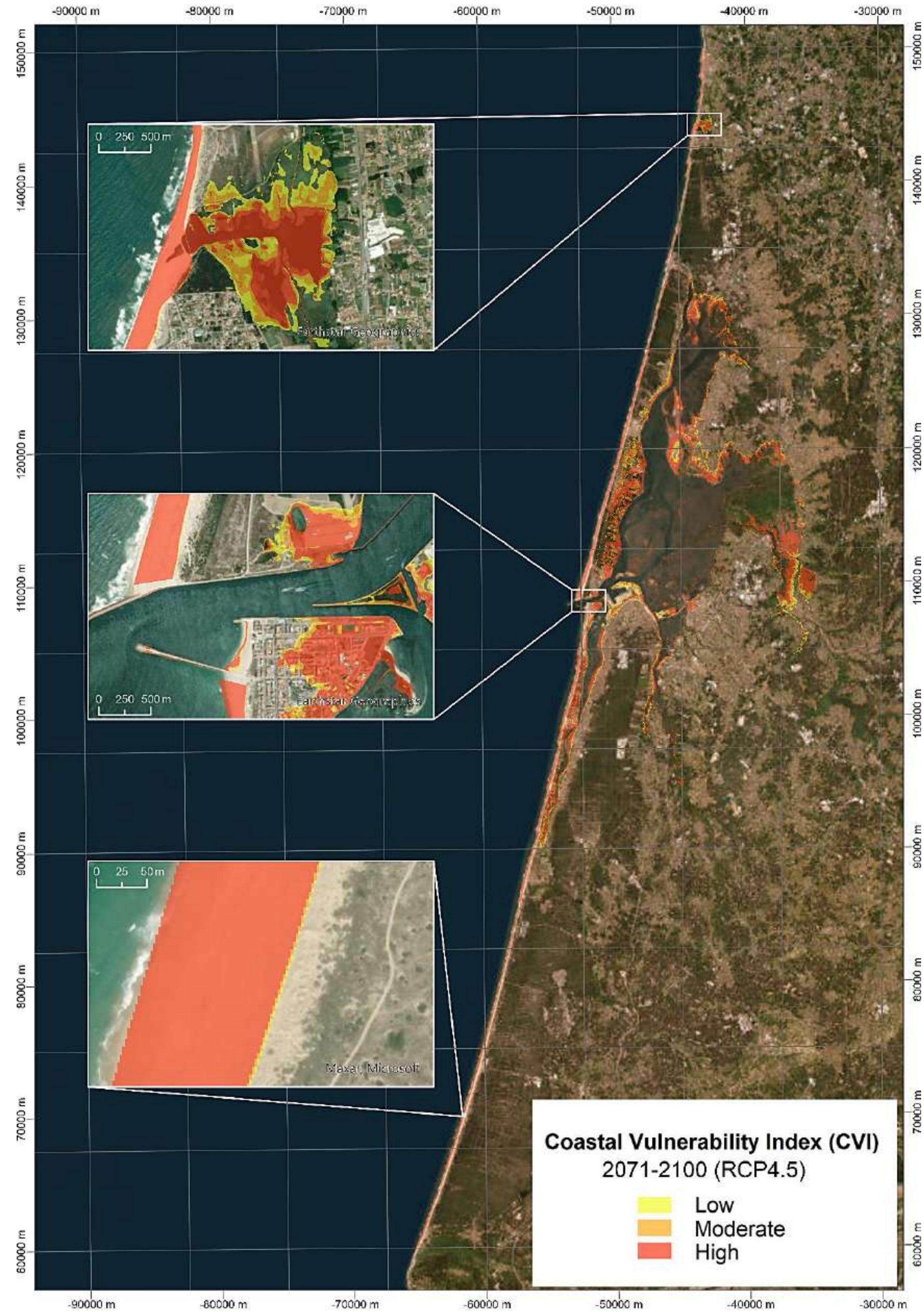

Figure 124 – Same as in Figure 122, but for 2100 under the RCP4.5 scenario.

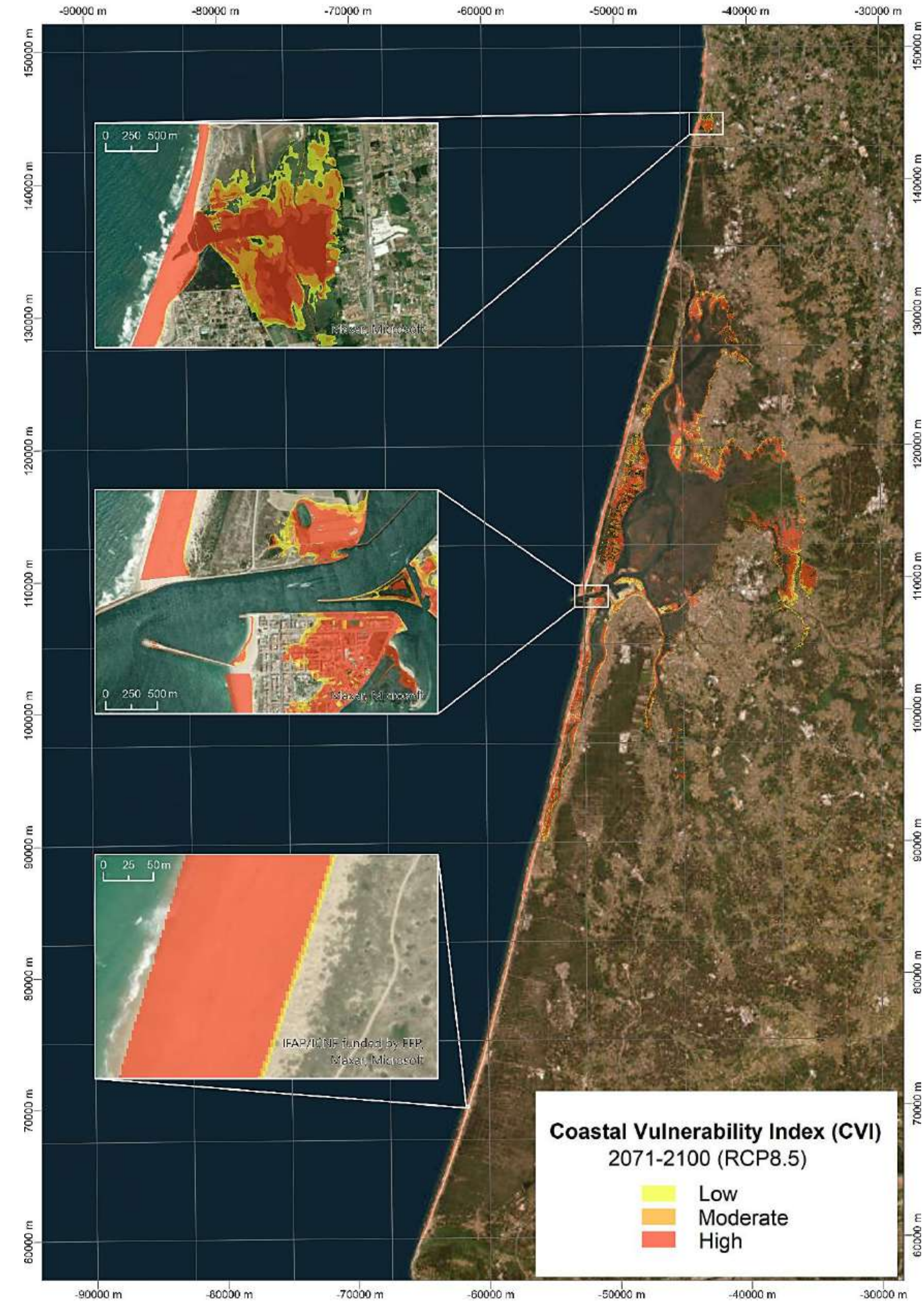

Figure 125 – Same as in Figure 122, but for 2100 under the RCP8.5 scenario.

Figure 126 – CVI for Aveiro / São Jacinto / Barra / Costa Nova (within Section 2 – Espinho-Figueira da Foz), by 2100 under the RCP8.5 scenario.

Table 24 – Same as in Table 23, but for Section 2 – Espinho-Figueira da Foz.

Coastal areas under CVI classification for Section 2 – Espinho-Figueira da Foz			
2070 (RCP4.5)			
District	**Ocean-facing (km^2)**	**Inland (km^2)**	**Total (km^2)**
Aveiro	5.75	50.6	56.3
Coimbra	4.19	4.88	9.07
2070 (RCP8.5)			
District	**Ocean-facing (km^2)**	**Inland (km^2)**	**Total (km^2)**
Aveiro	5.51	50.2	55.7
Coimbra	6.88	5.11	12.0
2100 (RCP4.5)			
District	**Ocean-facing (km^2)**	**Inland (km^2)**	**Total (km^2)**
Aveiro	6.59	53.8	60.3
Coimbra	7.17	5.42	12.6
2100 (RCP8.5)			
District	**Ocean-facing (km^2)**	**Inland (km^2)**	**Total (km^2)**
Aveiro	6.53	54.5	61.1
Coimbra	7.55	5.77	13.3

4.6.3. Section 3 – Figueira da Foz-Peniche

The third section ranges from Figueira da Foz (South of the Mondego River mouth) to Peniche, considering an almost straight coastal stretch of about 130 km in length. This section, generally facing WNW from Figueira da Foz to Nazaré, and NW from Nazaré to Peniche (and even N at some areas of the Peniche and Baleal peninsulas) comprises mainly low sandy beaches, intersected by rocky cliffs (especially in the southern half of the section), the Mondego River mouth (and estuary) and the Óbidos coastal lagoon. Other interesting features are also present, such as the São Martinho do Porto bay, and the Peniche and Baleal peninsulas. The ocean-facing coastal areas comprehend important sandy beaches and dunar systems, such as in Cova Gala, Lavos, Leirosa, Osso da Baleia, Pedrógão, Samouco, Pedras Negras, Areeira, São Gião, Salgado, São Martinho do Porto, Foz do Arelho and Baleal.

Overall, in this section, the ocean-facing coastlines under CVI dominate over the ones facing inland waters (Table 26). Nevertheless, some of the low-laying areas in the Mondego estuary and Óbidos lagoon present high CVIs even at the end of the 2041-2070 period under RCP4.5 (Figure 127), a projection compatible with increasingly risky conditions in urbanized or industrial areas, such as the Figueira da Foz harbor. A worsening of vulnerability conditions is projected, towards the end of the 21st century, for both scenarios, especially the RCP8.5, for which many ocean-facing coastal stretches present high CVIs very close to, or even within urban area. Examples are the Vieira de Leiria beachfront (Figure 130, for which moderate to high CVIs are already projected for the first row of urban infrastructure at the end of the first future period – 2070 – under RCP4.5), Nazaré harbor (Figure 131), São Martinho do Porto (Figure 132) and the lowest urbanized portions of northern Baleal and Peniche (Figure 130).

Table 25 demonstrates that, within the Leiria district, the ocean-facing coastal areas under CVI classifications are projected to increase, from 6.23 km^2 (2070 under RCP4.5) to 6.50 km^2 (2100 under RCP8.5). For the coastlines facing inland waters, the areas are also projected to increase, from 3.78 km^2 to 4.75 km^2, respectively, maintaining, nevertheless, lower values than for the ocean-facing ones.

Figure 127 – CVI for Section 3 – Figueira da Foz-Peniche, by 2070 under the RCP4.5 scenario.

Figure 128 – Same as in Figure 127, but for the RCP8.5 scenario.

Figure 129 – Same as in Figure 127, but for 2100 under the RCP4.5 scenario.

Figure 130 – Same as in Figure 127, but for 2100 under the RCP8.5 scenario.

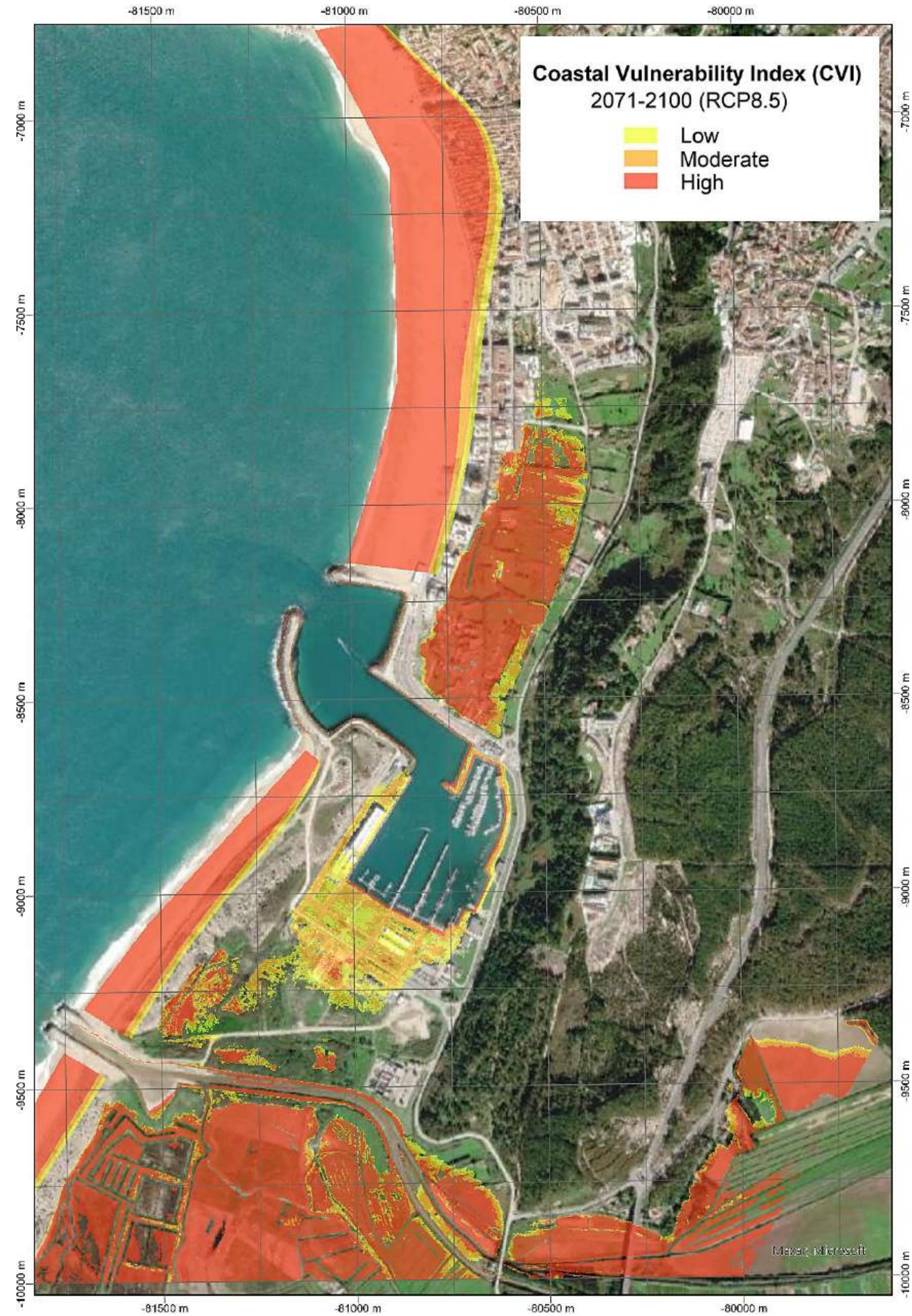

Figure 131 – CVI for Nazaré (within Section 3 – Figueira da Foz-Peniche), by 2100 under the RCP8.5 scenario.

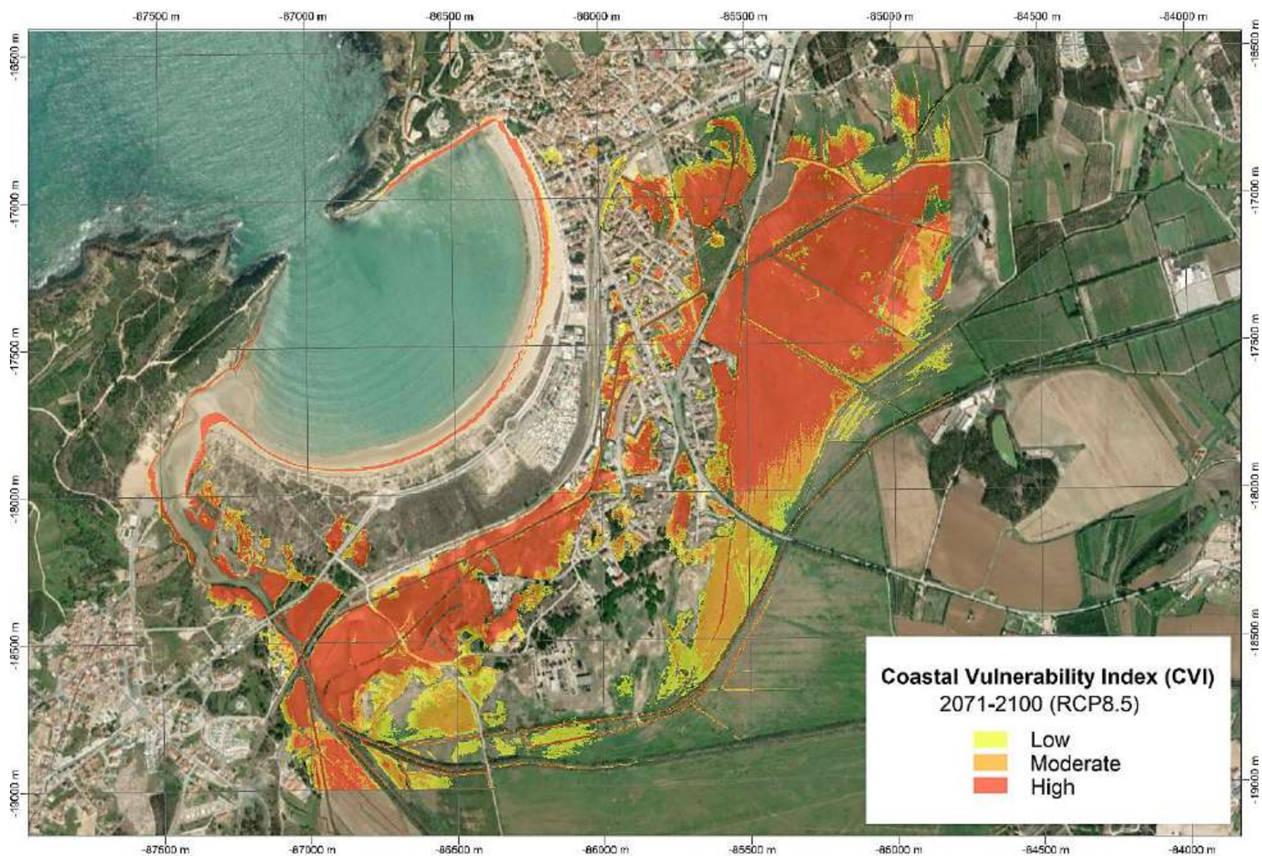

Figure 132 – Same as in Figure 131, but for São Martinho do Porto (within Section 3 – Figueira da Foz-Peniche).

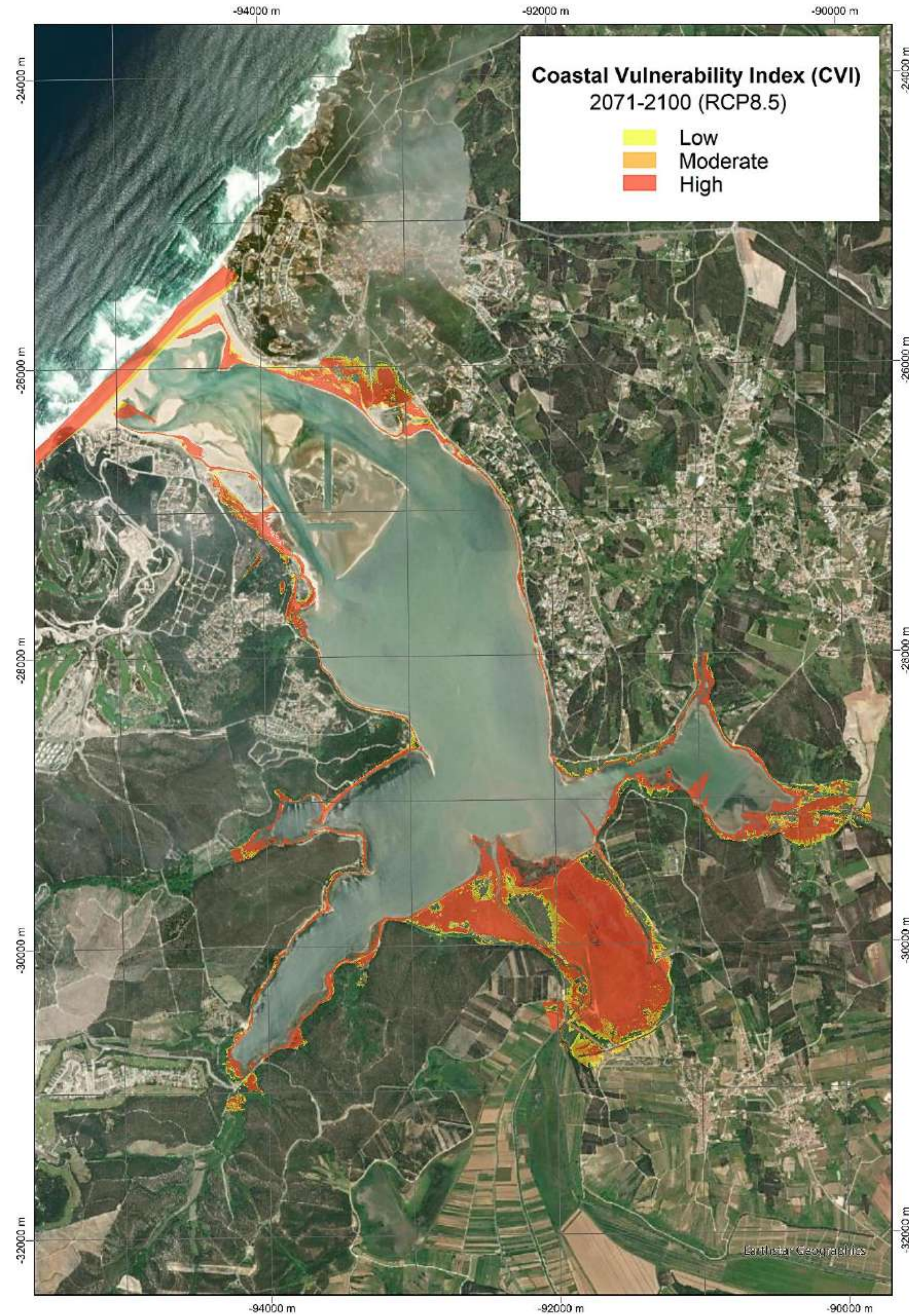

Figure 133 – Same as in Figure 131, but for Óbidos (within Section 3 – Figueira da Foz-Peniche).

Table 25 – Same as in Table 23, but for Section 3 – Figueira da Foz-Peniche.

Coastal areas under CVI classification for Section 3 – Figueira da Foz-Peniche			
2070 (RCP4.5)			
District	**Ocean-facing (km^2)**	**Inland (km^2)**	**Total (km^2)**
Leiria	6.23	3.78	10.0
2070 (RCP8.5)			
District	**Ocean-facing (km^2)**	**Inland (km^2)**	**Total (km^2)**
Leiria	5.71	4.12	9.83
2100 (RCP4.5)			
District	**Ocean-facing (km^2)**	**Inland (km^2)**	**Total (km^2)**
Leiria	6.07	4.44	10.5
2100 (RCP8.5)			
District	**Ocean-facing (km^2)**	**Inland (km^2)**	**Total (km^2)**
Leiria	6.50	4.75	11.3

4.6.4. Section 4 – Peniche-Setúbal

The fourth section ranges from Peniche to Setúbal (North of the Sado River mouth), considering a coastal stretch of about 190 km in length. This section comprises a multitude of coastal typologies, from sandy beaches intersected by rocky cliffs (mainly from Peniche to Cascais), to urban beaches (between Cascais and Lisbon, but also in Costa da Caparica) and the large Tagus River estuary. The ocean-facing coastlines are mostly oriented to the W and S. The Portuguese capital, Lisbon, is located within this section, as well as other smaller-scale interesting features, such as the Grande, Alcabrichel, Sizandro, Lizandro, Jamor (largely artificialized), Trancão and Sorraia River mouths, and the Albufeira coastal lagoon. Important sandy beaches include Supertubos, Areia Branca, Zimbral, Valmitão, Conchas, Santa Rita, Mirante, Santa Cruz, Azul / Foz do Sizandro, Foz do Lizandro, Vigia, Magoito, Grande, Guincho, Carcavelos, Costa da Caparica (several ones), Fonte da Telha, Meco and Sesimbra / Califórnia. At Guincho and Costa da Caparica (Cova do Vapor and São João), these sandy beaches are backed by dunar systems.

Overall, between Peniche and Setúbal, the coastlines facing inland waters show increased vulnerability to climate change, in comparison to the ocean-facing ones, mostly due to the low-lying areas surrounding the Tagus River estuary. These are the ones contributing most to the total area under CVI within Section 4 (Table 26). There, high CVIs dominate over moderate and low ones, even at the end of the 2041-2070 period, under RCP4.5 (Figure 135). By 2100, a worsening of the vulnerability conditions is expected to occur, especially under RCP8.5 and throughout the inland waters' coastlines, more sensitive to SLR. Most of the areas surrounding the Tagus River estuary are depicted as under high CVIs (Figure 141), with relevant population centers and infrastructure projected to be affected, such as Vila Franca de Xira, Alhandra, Alverca, Cacilhas, Seixal, Barreiro, Lavradio, Baixa da Banheira, Moita, Montijo, Alcochete, among others. All the lowest topographic areas of the capital city of Lisbon are also depicted as under moderate to high CVIs by 2100, especially for the RCP8.5 projections. Locally, within Lisbon, the areas of Marvila, Cais do Sodré, Alcântara, Belém and Cruz Quebrada are the ones projected to be more extensively threatened (Figure 145). Considering the ocean-facing coastlines, at Costa da Caparica, CVIs are projected to be moderate to high for all future periods and scenarios, especially between Cova do Vapor and São João da Caparica. By 2100 (RCP8.5), most urbanized areas north of the A38 / Av. 1º de Maio routes and west of the fossil cliff are projected to be under high CVIs (Figure 145).

Table 26 shows to total areas under CVI classification for each district within Section 4, considering the ocean-facing and inland waters' coastlines, as well as their joint values. Lisbon is the Portuguese district with the largest future projected areas under CVI classification, totalizing 218 km^2 and 221 km^2, by 2100, under RCP4.5 and RCP8.5, respectively. It should be noted that, from these values, 217 km^2 and 220 km^2 (~99%) correspond to future projected flooding in locations adjacent to inland waters (from which the Tagus River estuary ones are largely dominant). For the ocean-facing coastlines within this section, although the areas projected as under CVI classifications are shown to be quite smaller than for the inland waters, projected increases are also visible in Table 26 towards the end of the 21st century for both scenarios, peaking at 3.48 km^2 (RCP4.5) and 3.33 km^2 (RCP8.5) by 2100. The largest horizontal CVI extension projected under RCP4.5 is motivated by the higher expected 99th percentile wave energy for this scenario (Table 21).

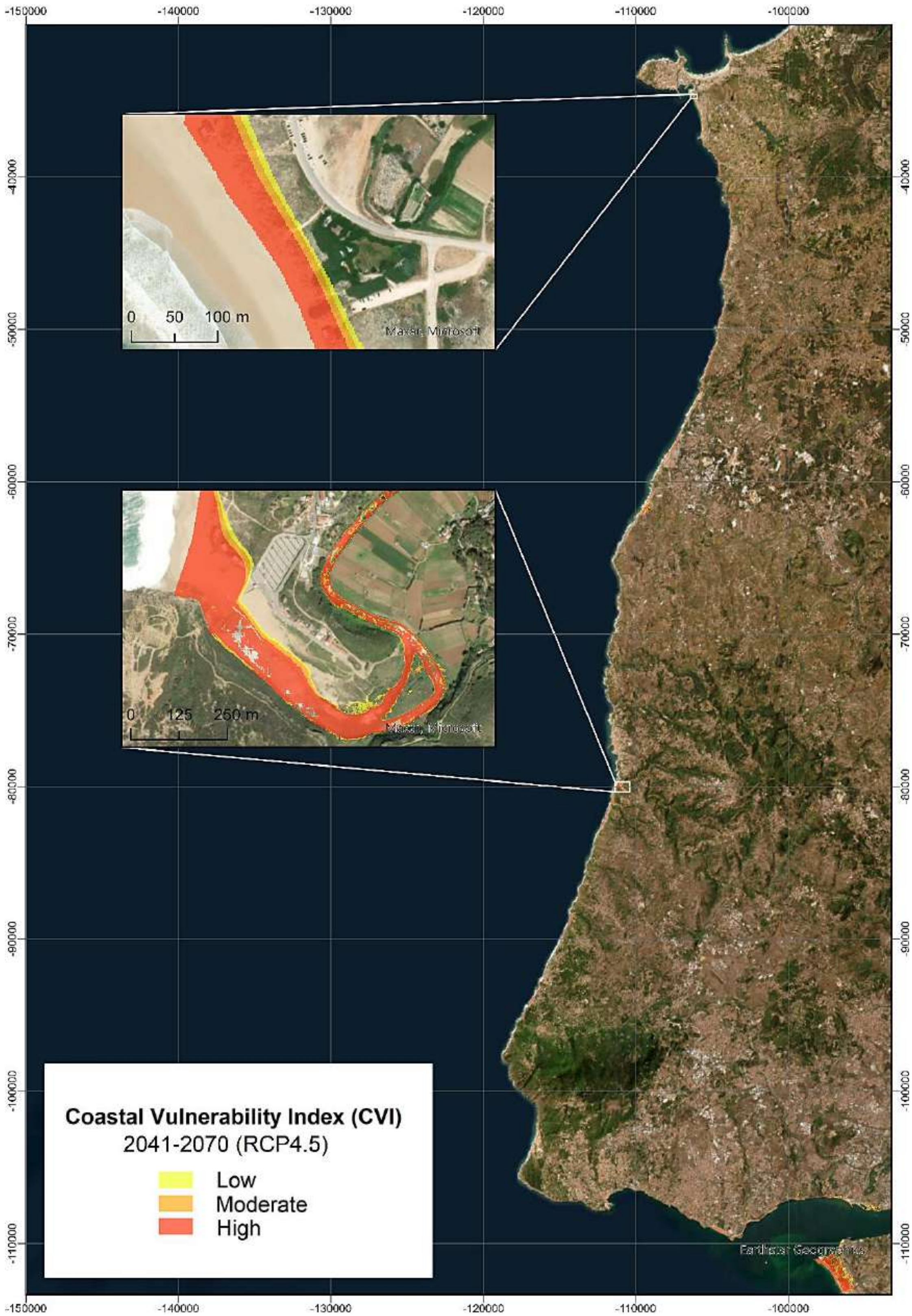

Figure 134 – CVI for Section 4 (part I) – Peniche-Setúbal, by 2070 under the RCP4.5 scenario.

Figure 135 – CVI for Section 4 (part II) – Peniche-Setúbal, by 2070 under the RCP4.5 scenario.

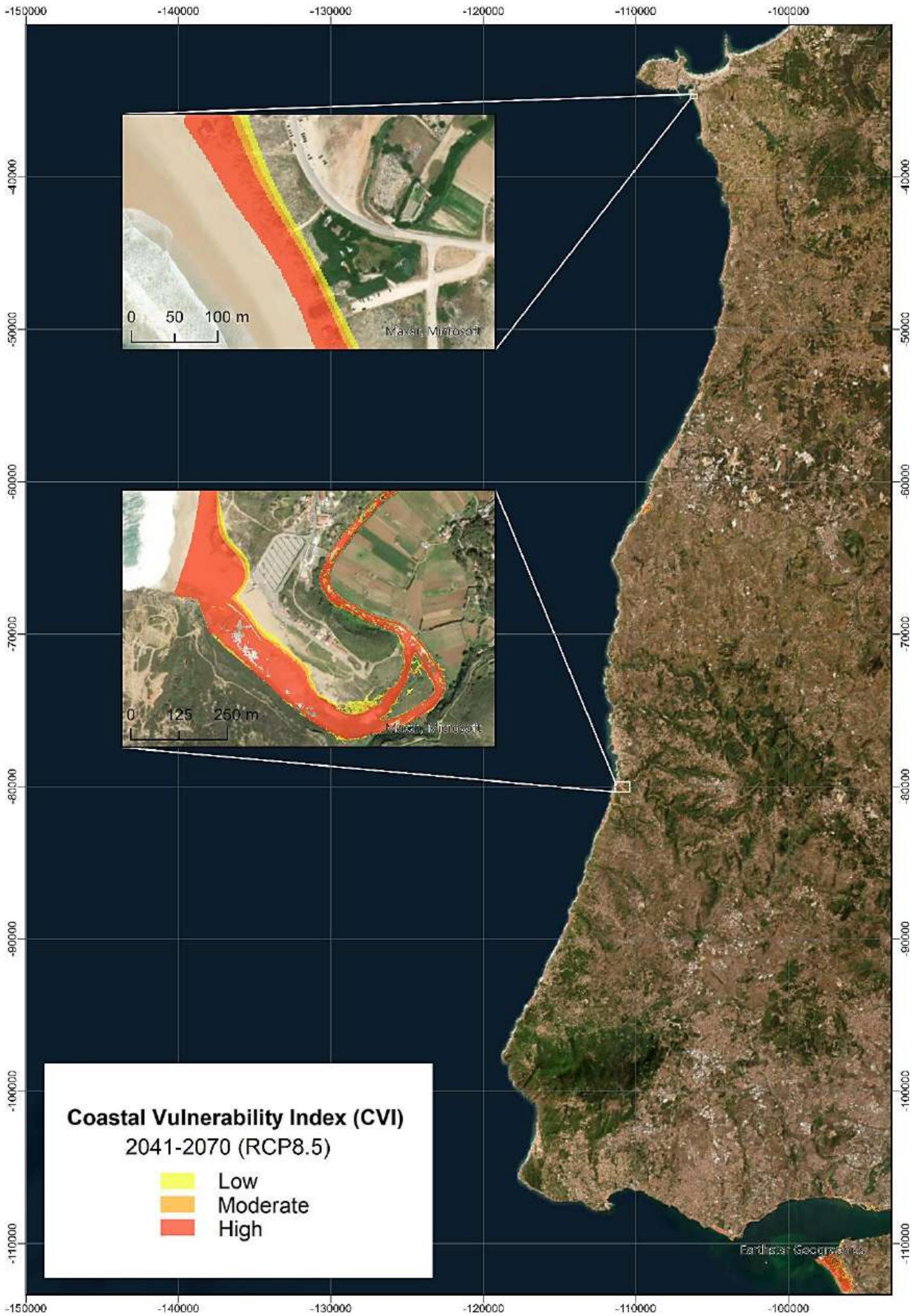

Figure 136 – Same as in Figure 134, but under the RCP8.5 scenario.

Figure 137 – Same as in Figure 135, but under the RCP8.5 scenario.

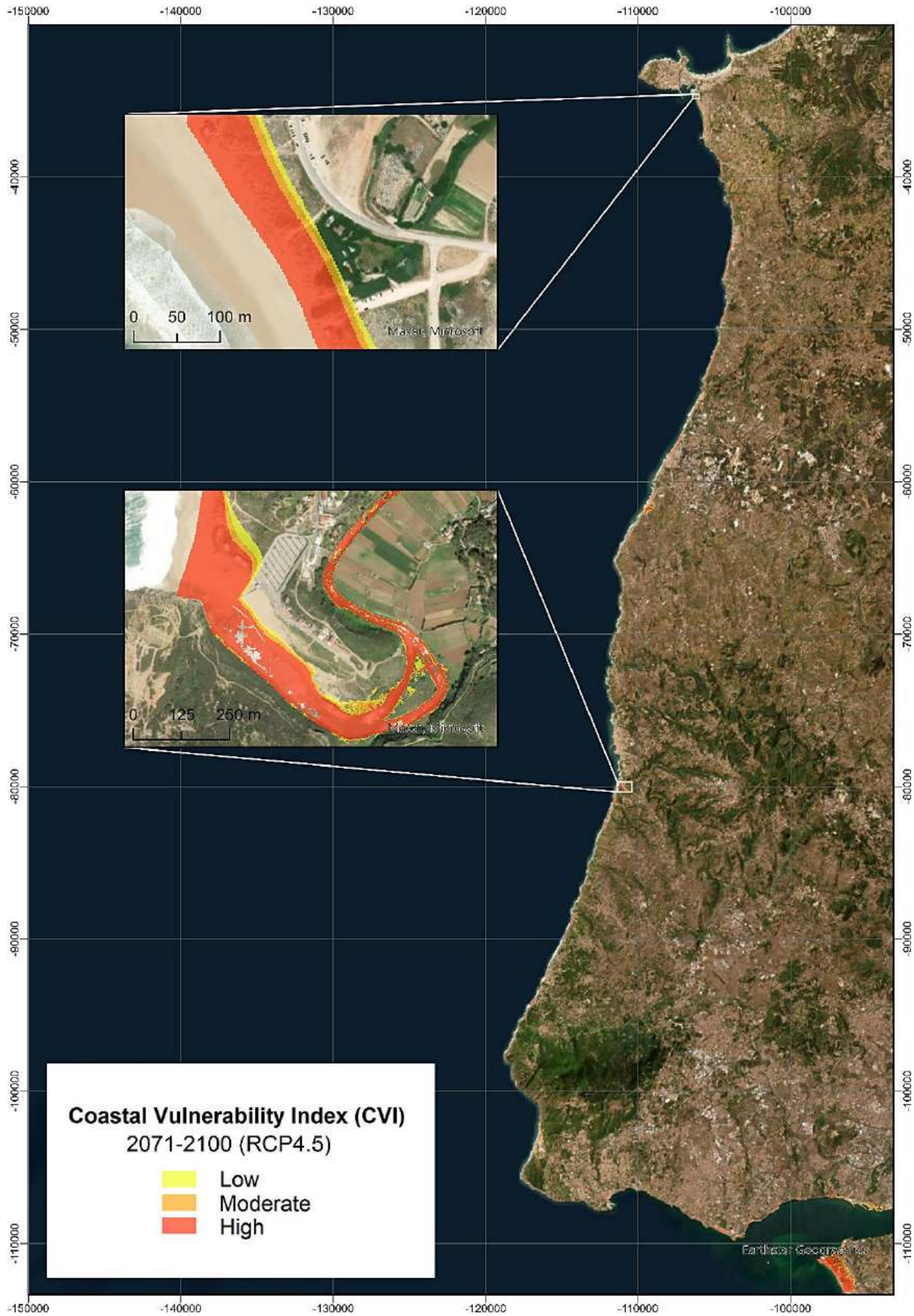

Figure 138 – Same as in Figure 134, but for 2100 under the RCP4.5 scenario.

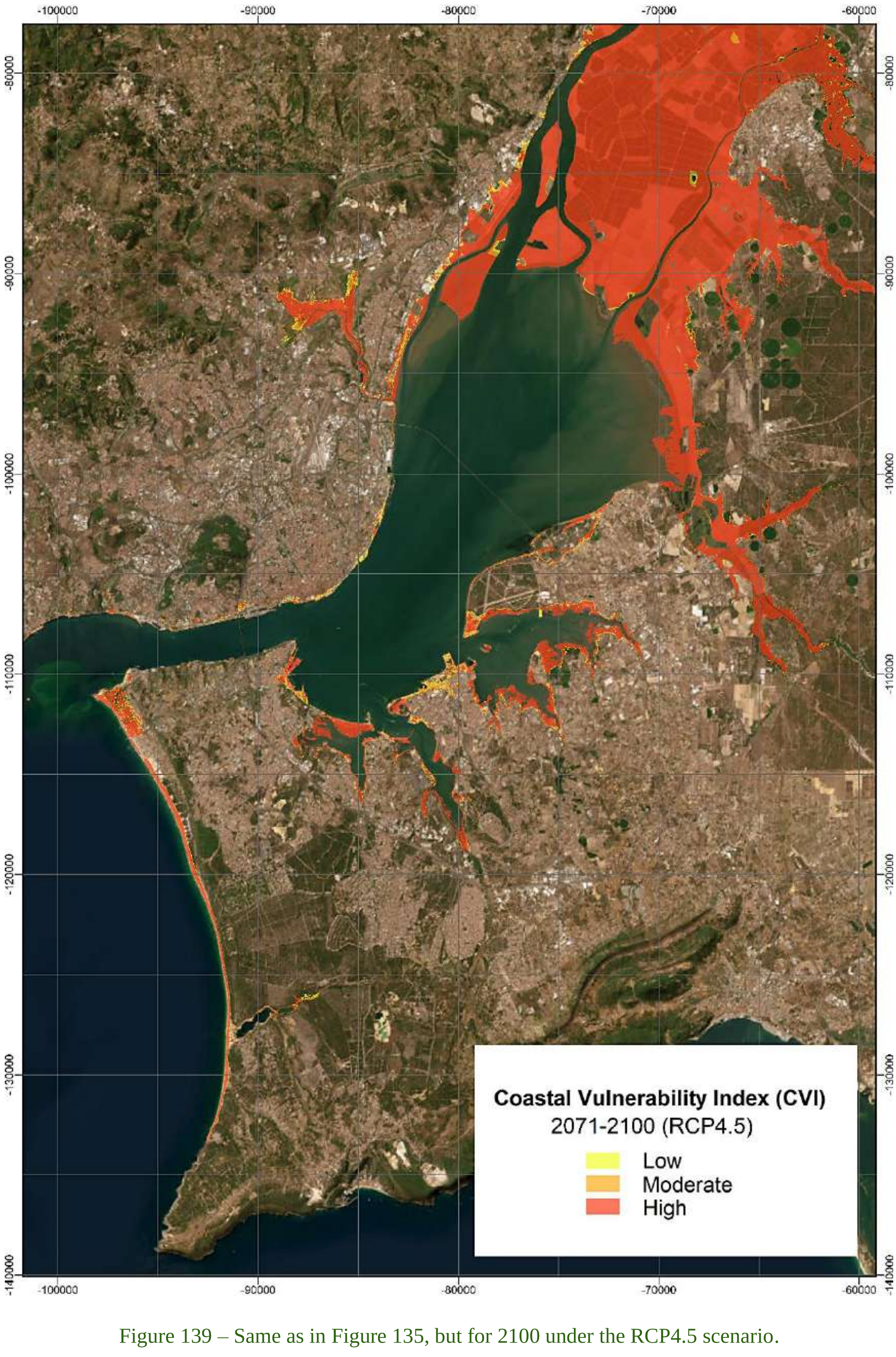

Figure 139 – Same as in Figure 135, but for 2100 under the RCP4.5 scenario.

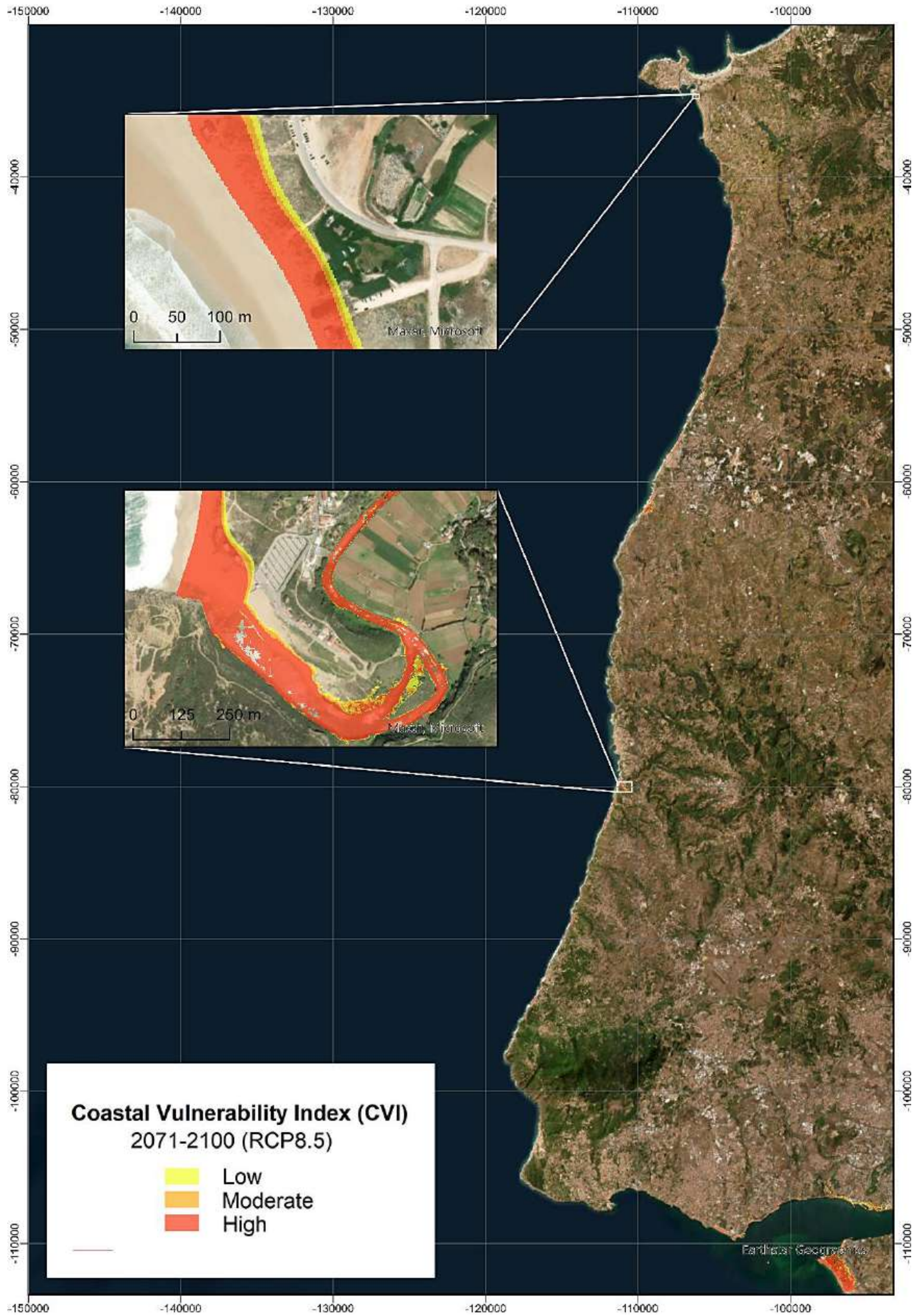

Figure 140 – Same as in Figure 134, but for 2100 under the RCP8.5 scenario.

Figure 141 – Same as in Figure 135, but for 2100 under the RCP8.5 scenario.

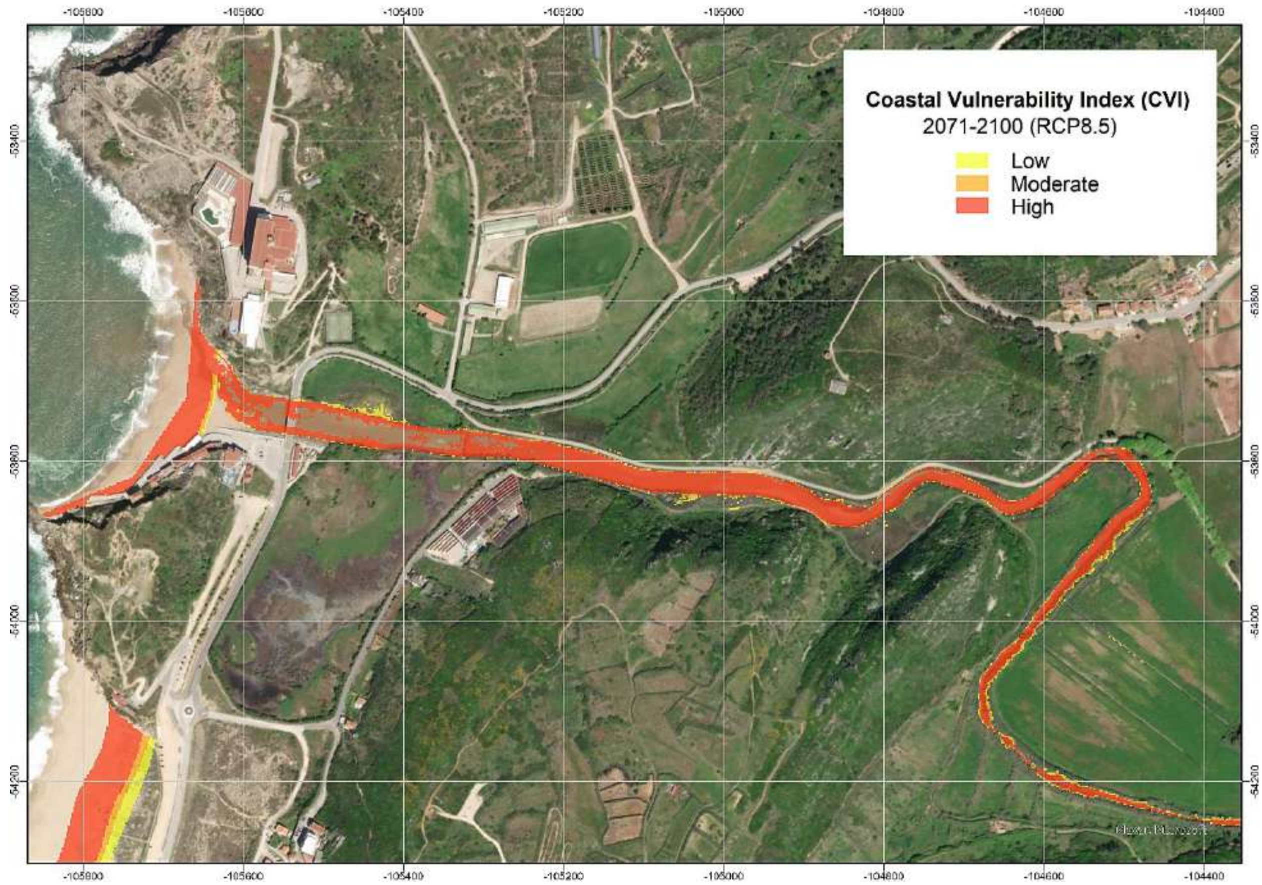

Figure 142 – CVI for Porto Novo (within section 4 – Peniche-Setúbal), for 2100 under the RCP8.5 scenario.

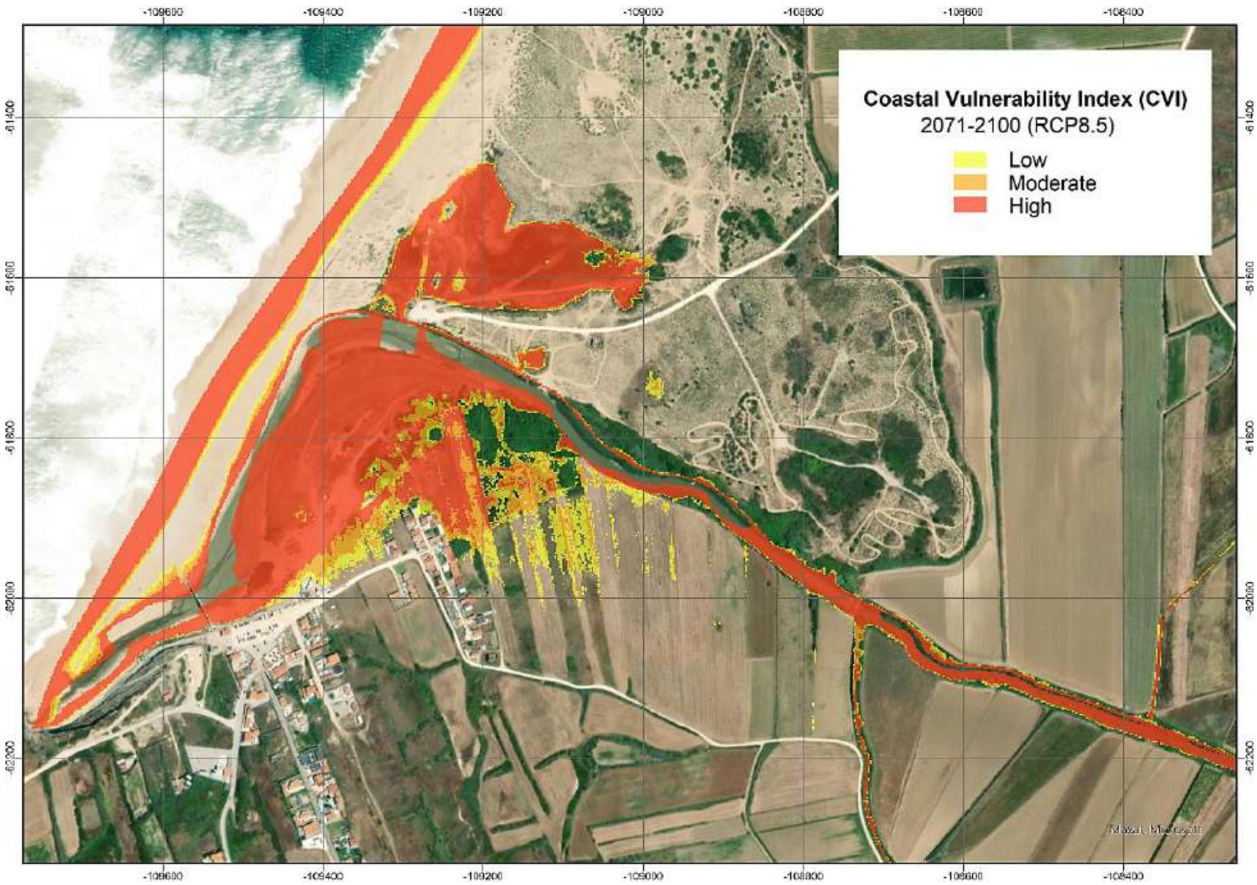

Figure 143 – Same as in Figure 141, but for Sizandro River mouth and Praia Azul (within section 4 – Peniche-Setúbal).

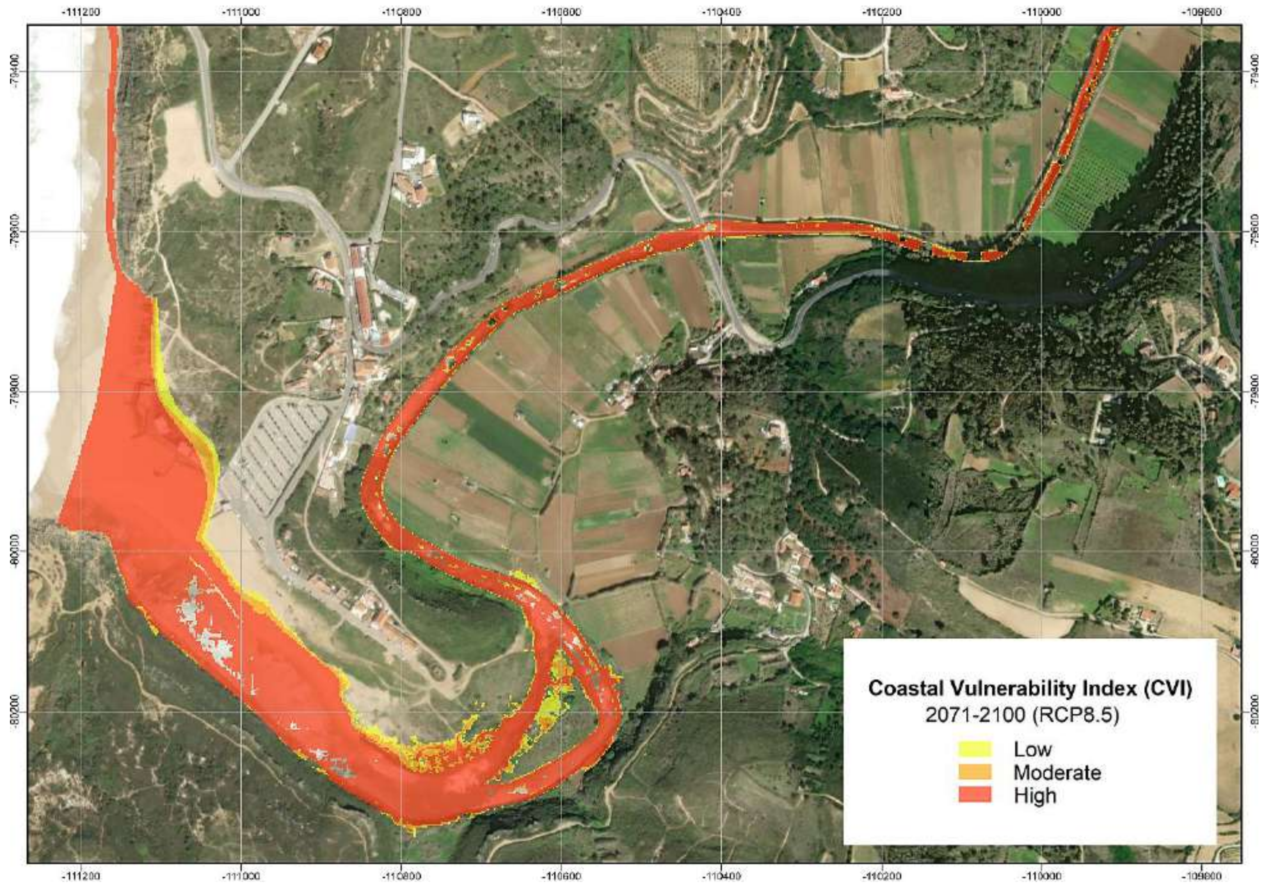

Figure 144 – Same as in Figure 141, but for Lizandro River mouth (within section 4 – Peniche-Setúbal).

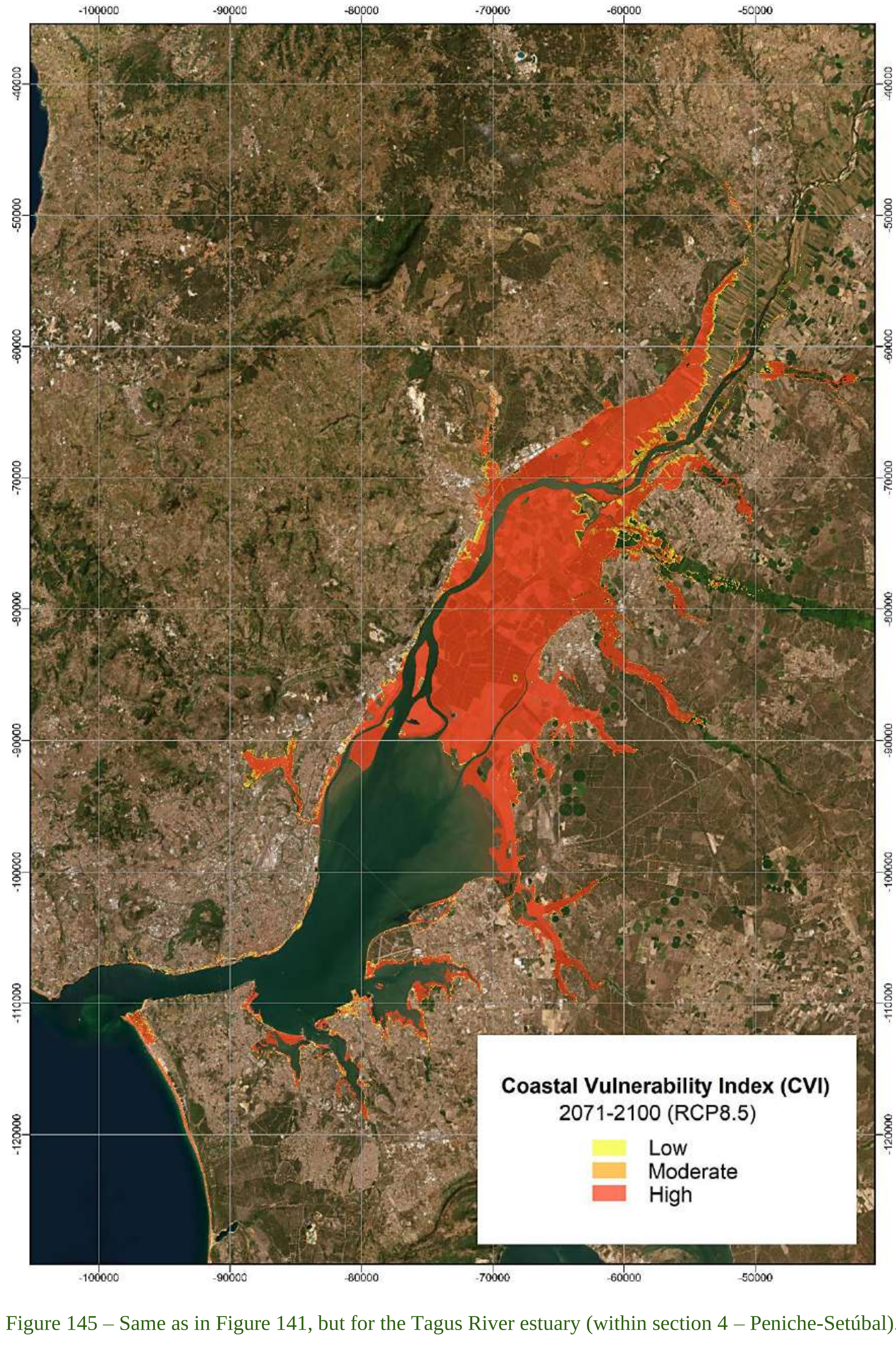

Figure 145 – Same as in Figure 141, but for the Tagus River estuary (within section 4 – Peniche-Setúbal).

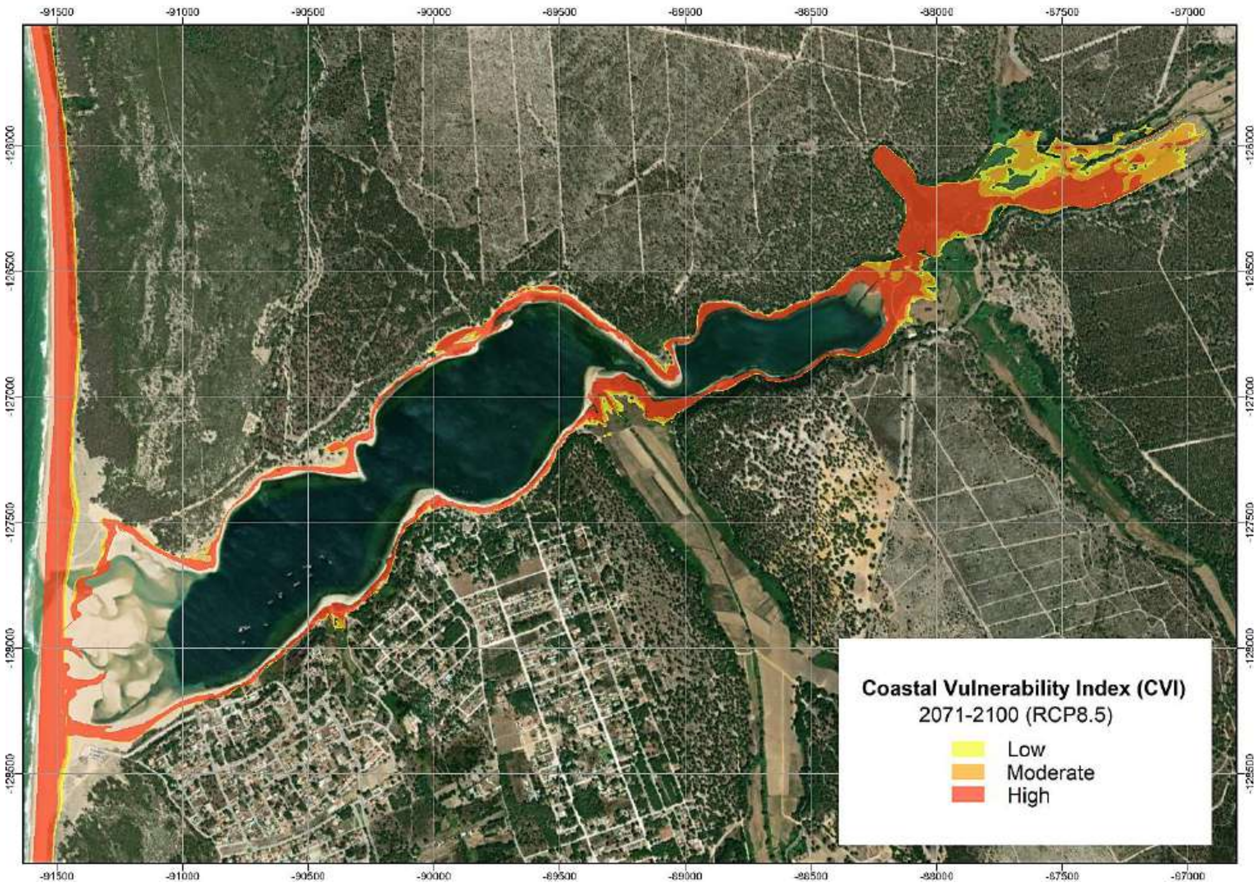

Figure 146 – Same as in Figure 141, but for Albufeira lagoon (within section 4 – Peniche-Setúbal).

Table 26 – Same as in Table 23, but for Section 4 – Peniche-Setúbal.

Coastal areas under CVI classification for Section 4 – Peniche-Setúbal			
2070 (RCP4.5)			
District	**Ocean-facing (km²)**	**Inland (km²)**	**Total (km²)**
Santarém	0.00	121	121
Lisboa	1.02	213	214
Setúbal	2.46	30.7	33.1
2070 (RCP8.5)			
District	**Ocean-facing (km²)**	**Inland (km²)**	**Total (km²)**
Santarém	0.00	122	122
Lisboa	0.99	213	214
Setúbal	2.37	29.8	32.2
2100 (RCP4.5)			
District	**Ocean-facing (km²)**	**Inland (km²)**	**Total (km²)**
Santarém	0.00	126	126
Lisboa	1.03	217	218
Setúbal	2.73	31.2	33.9
2100 (RCP8.5)			
District	**Ocean-facing (km²)**	**Inland (km²)**	**Total (km²)**
Santarém	0.00	131	131
Lisboa	0.97	220	221
Setúbal	2.36	32.6	34.9

4.6.5. Section 5 – Troia-Odeceixe

The fifth section ranges from Troia (South of the Sado River mouth) to Odeceixe, considering a quite diverse coastal stretch of about 140 km in length, and mostly facing W. It includes the Sado River estuary in its northernmost portion, the Troia peninsula, with extensive low-lying sandy beaches often backed by dune systems down to Sines, transitioning into rocky cliffs and generally small beaches, where fine sediments are limited. Relevant sandy beaches include Troia-Mar, Costa da Galé, Torre, Comporta, Carvalhal, Galé, Melides, Areão and São Torpes. Several lagoon systems are present within Section 5, especially between Troia and Sines (*e.g.*, Melides, Santo André, Sancha).

Overall, similarly to Section 4, it can be seen, from Figure 147 to Figure 158, that the areas projected to become most vulnerable in the future correspond to the inland waters' coastlines, namely within the Sado River estuary and the Melides and Santo André lagoon systems. Although high CVIs are projected along the long sandy Troia-Sines coastal stretch, the total area expected to become highly vulnerable in the future is almost one order of magnitude less than for the inland waters (Table 27). In fact, at the Sado River estuary, several populational centers are expected to be affected by the projected increase in the TWLs, driven, in these locations, mainly by SLR. While low-to-moderate CVIs are projected for downtown Setúbal and Setúbal harbor by 2070 under RCP4.5 (Figure 147), high CVIs can be expected by 2100 under RCP8.5 (Figure 156), exposing communities and valuable infrastructure to the rising waters. Other peripheric villages within the Sado River estuary are also projected to be affected from as soon as 2070 under RCP4.5, namely Marateca, Monte Novo, Alcácer do Sal, Moitinha and Carrascal. Along the ocean-facing coastline, although no major populational centers under CVI classification are identified, some small settlements such as near Praia da Raposa are expected to be highly vulnerable to the changes in the coastal TWLs, even considering the 4-year RP by 2070 under RCP4.5 (Figure 147). Finally, for the Sines harbor, vulnerability is also high.

Table 27 shows, as expected, the largest areas under CVI to be adjacent to inland waters in Section 5. While the total ocean-facing area varies between 7.99 km^2 (2070 under RCP4.5) to 10.6 km^2 (2100 under RCP4.5), for the inland waters, these values ascend to 40.7 km^2 (2070 under RCP4.5) and 44.8 km^2 (2100 under RCP8.5). Note that similarly to Section 4, the areas under CVI for the ocean-facing (inland waters) coastlines are larger under RCP4.5 (RCP8.5). Such behavior is due to the contribution of waves along the ocean-facing coastal areas, for which the 99^{th} percentile energy is projected to be lower under RCP8.5. For inland waters, the TWL is driven almost exclusively by SLR, projected to increase steadily, especially under RCP8.5. The areas under CVI associated to inland waters range between 80.6% (2100 under RCP4.5) and 83.6% (2070 under RCP4.5) of the global value.

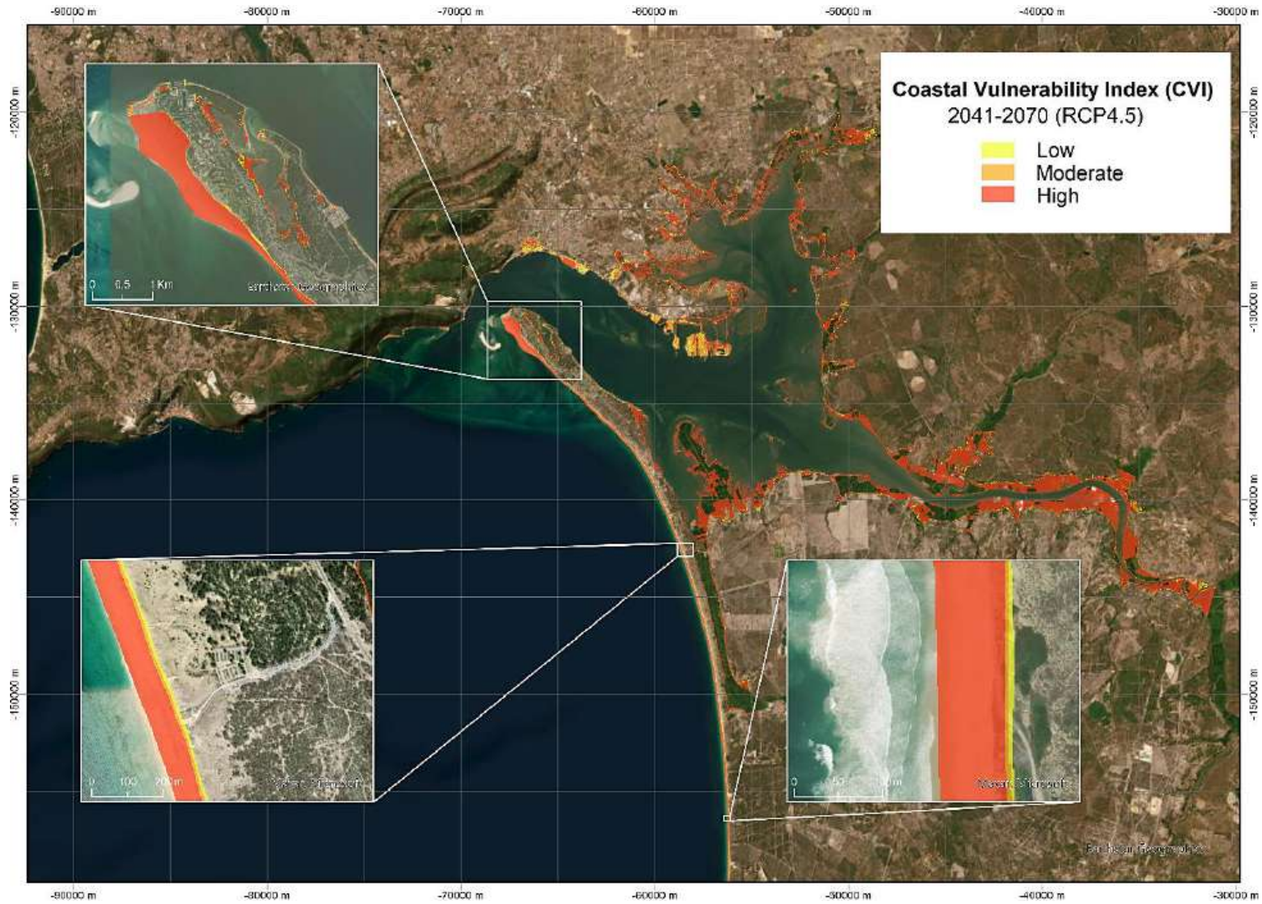

Figure 147 – CVI for Section 5 (part I) – Troia-Odeceixe, by 2070 under the RCP4.5 scenario.

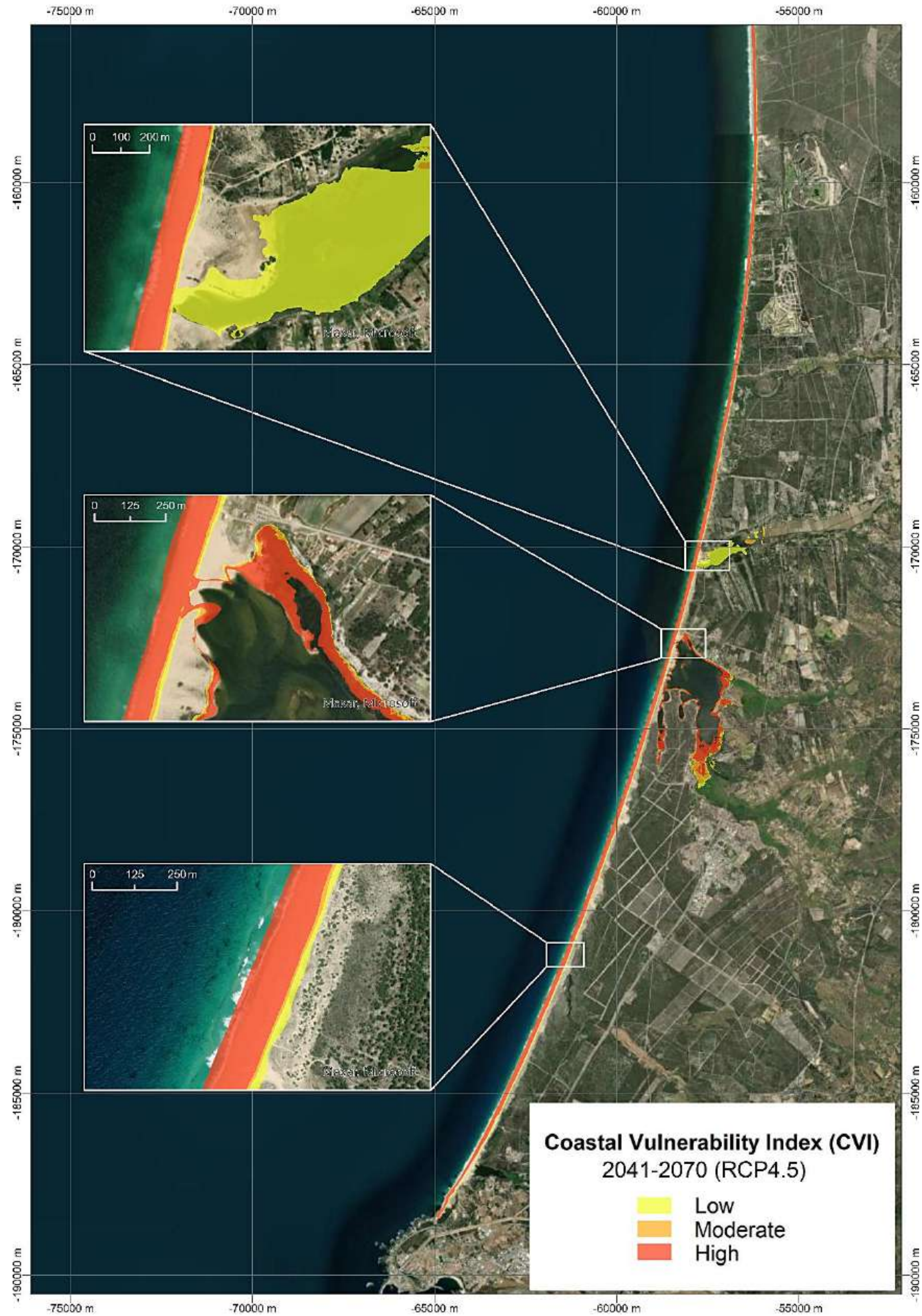

Figure 148 – CVI for Section 5 (part II) – Troia-Odeceixe, by 2070 under the RCP4.5 scenario.

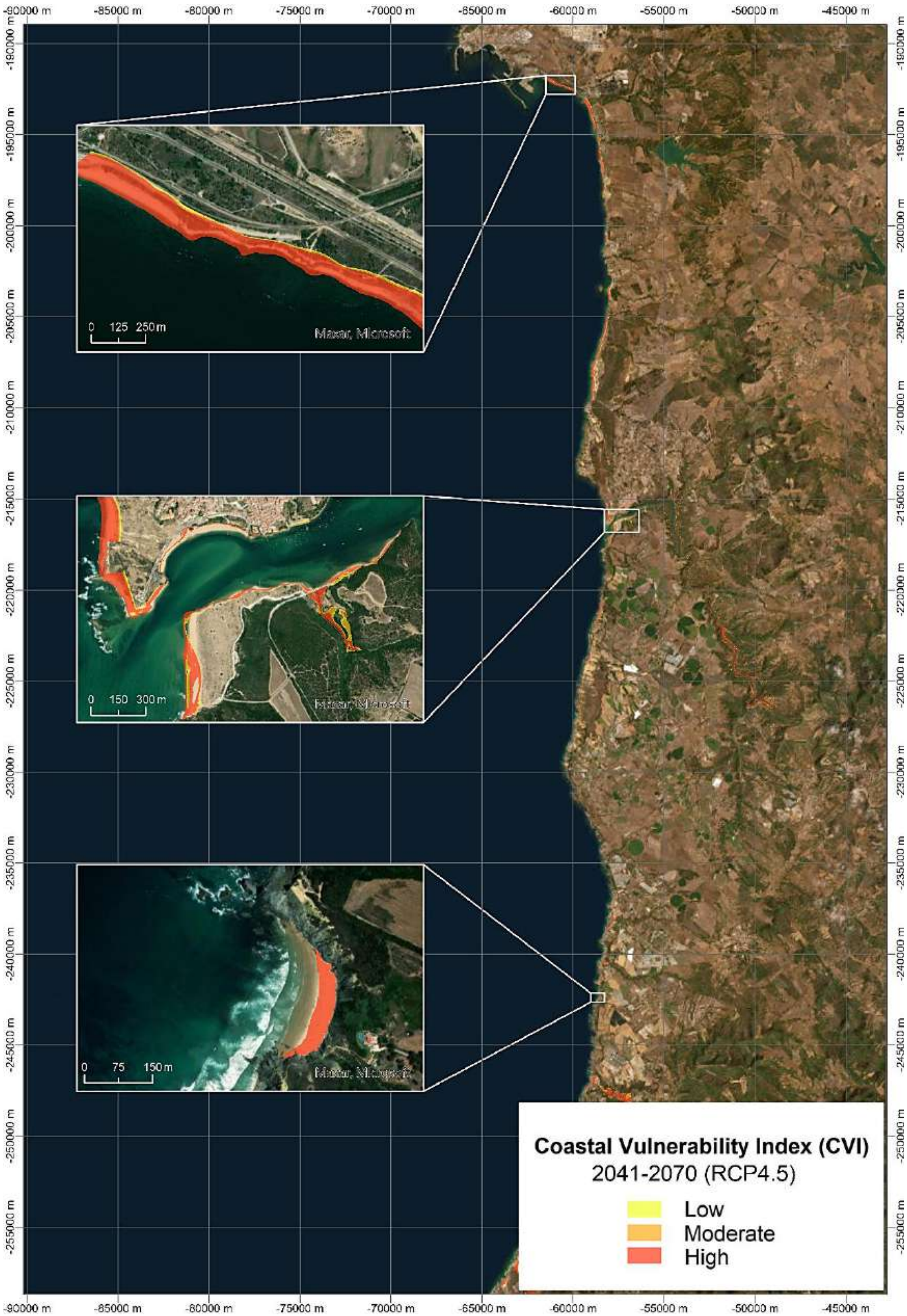

Figure 149 – CVI for Section 5 (part III) – Troia-Odeceixe, by 2070 under the RCP4.5 scenario.

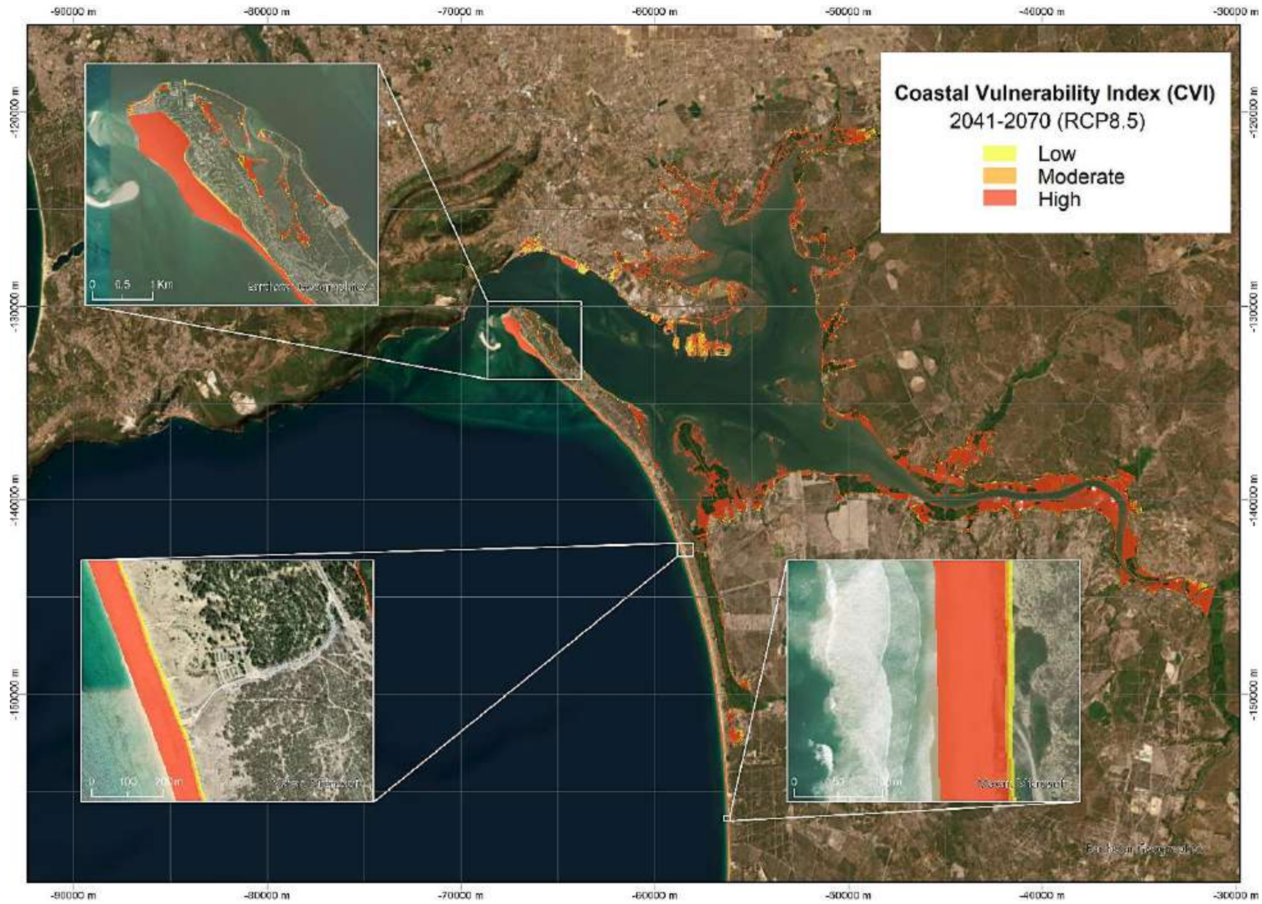

Figure 150 – Same as in Figure 147, but under the RCP8.5 scenario.

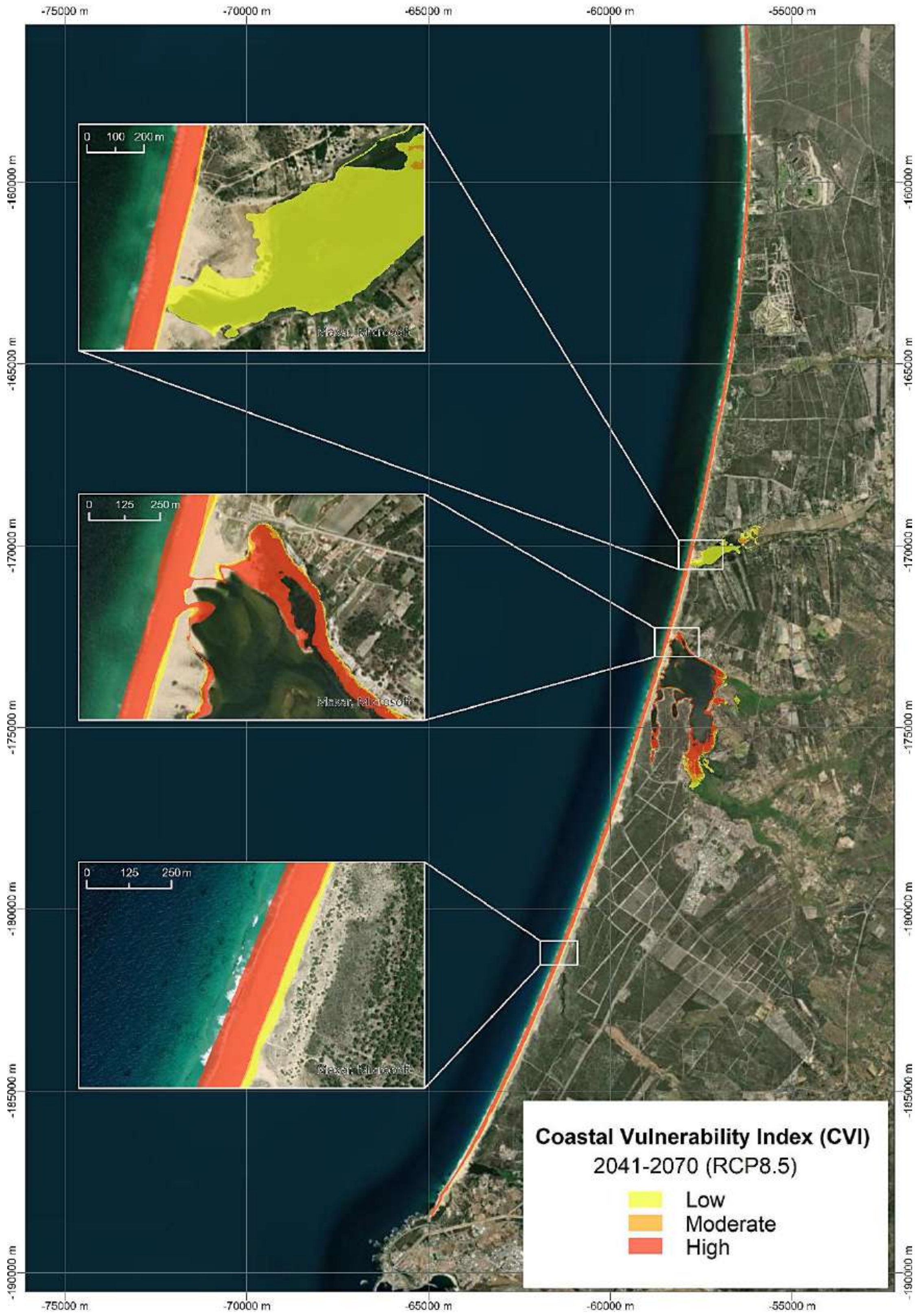

Figure 151 – Same as in Figure 148, but under the RCP8.5 scenario.

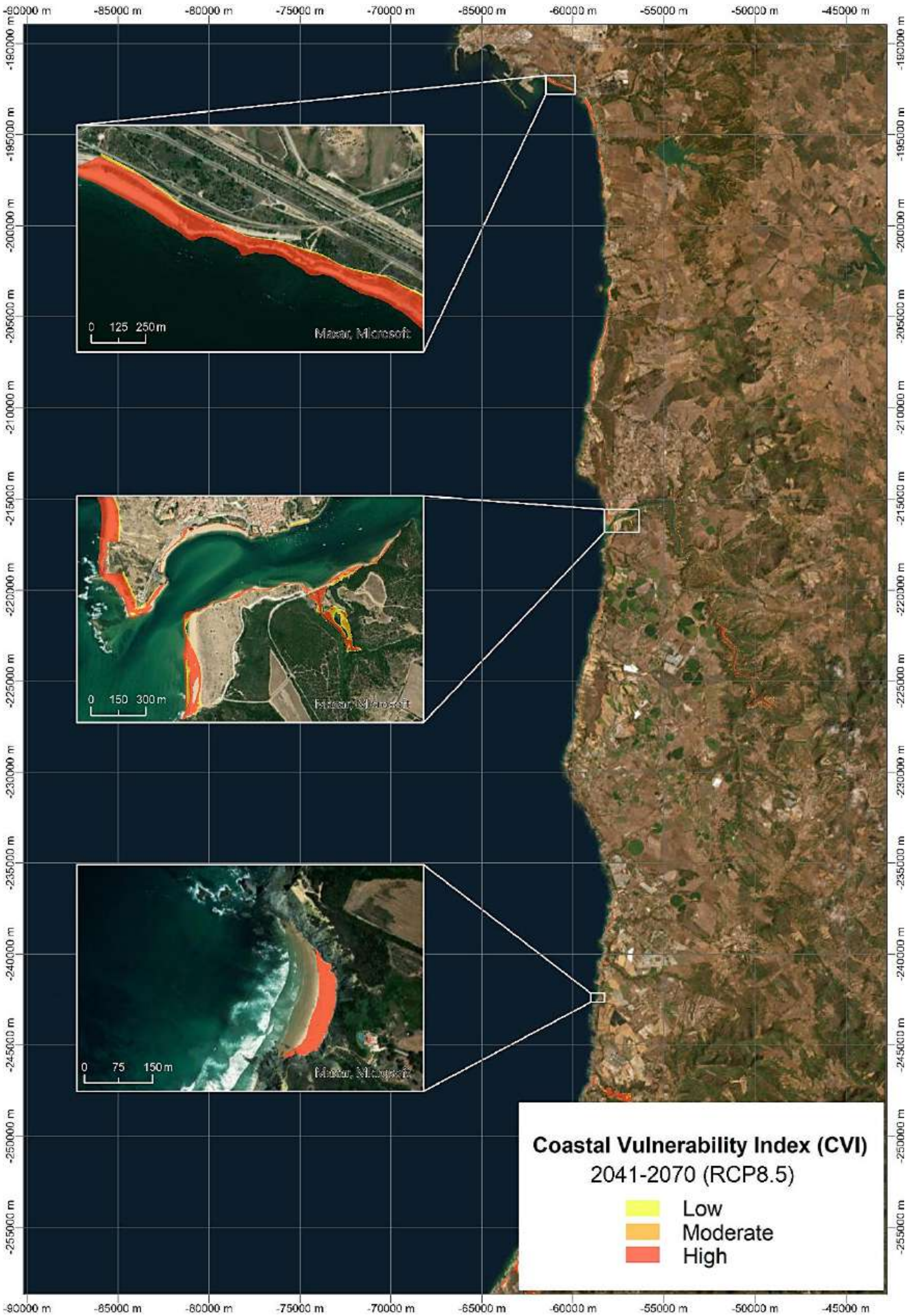

Figure 152 – Same as in Figure 149, but under the RCP8.5 scenario.

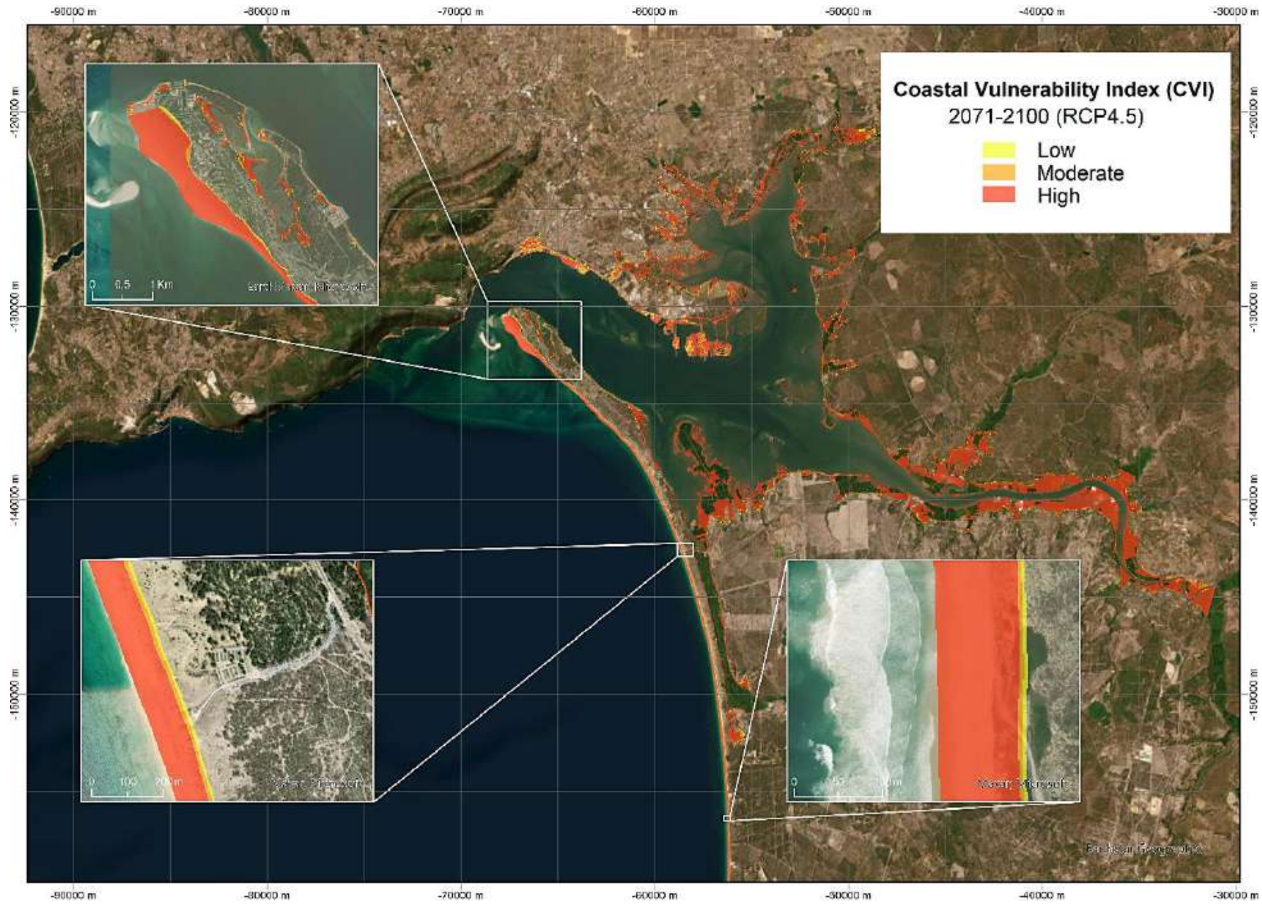

Figure 153 – Same as in Figure 147, but for 2100 under the RCP4.5 scenario.

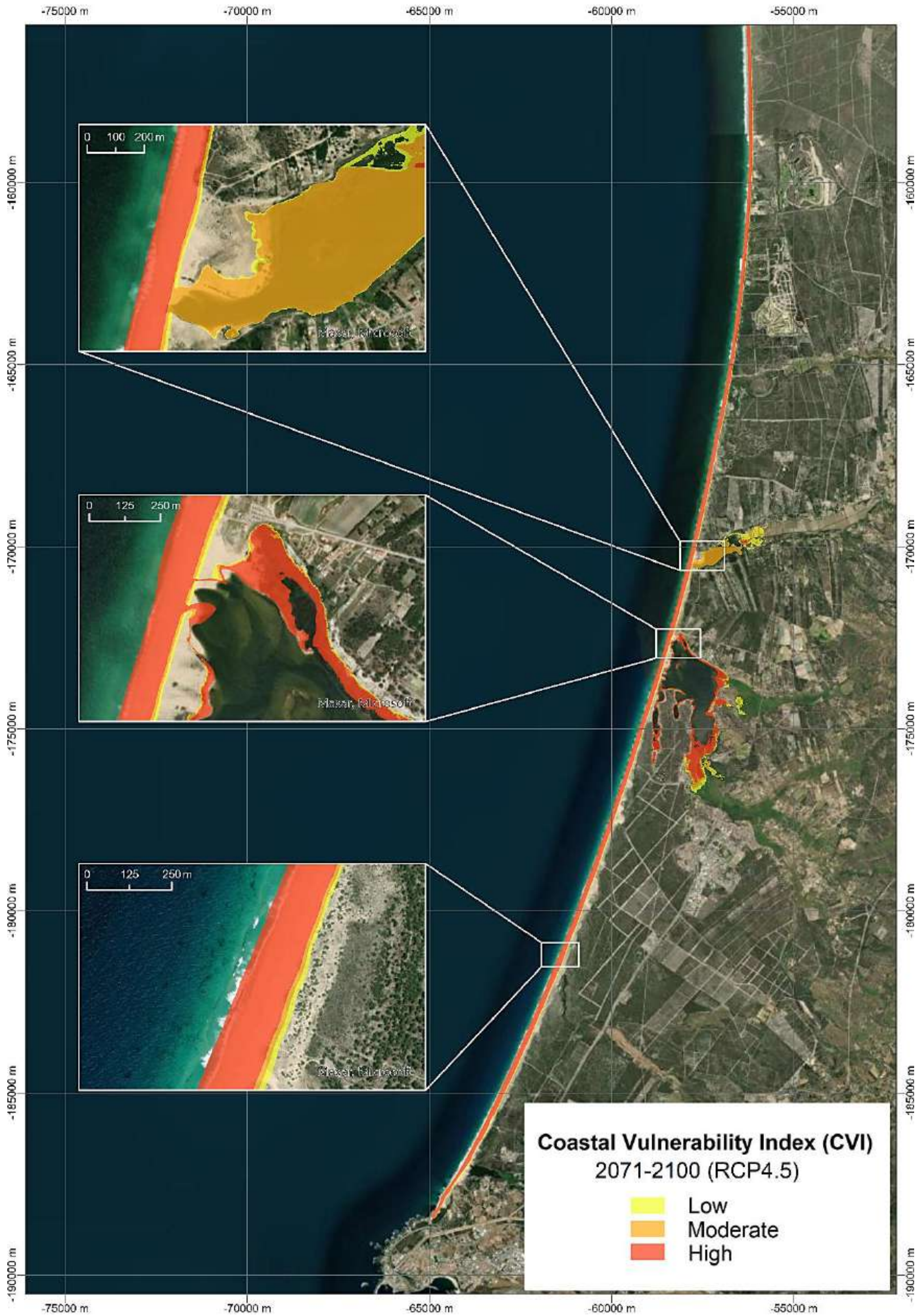

Figure 154 – Same as in Figure 148, but for 2100 under the RCP4.5 scenario.

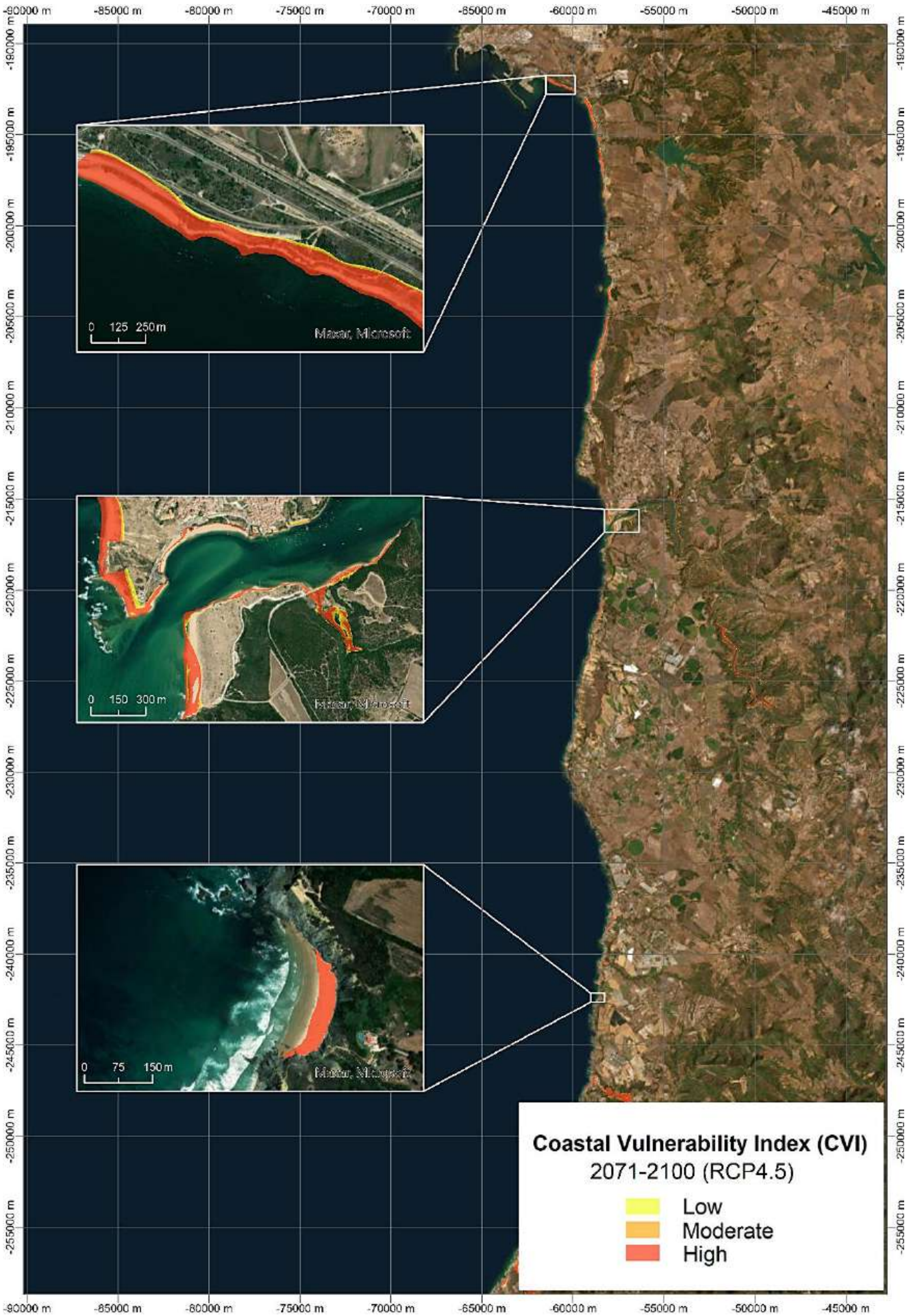

Figure 155 – Same as in Figure 149, but for 2100 under the RCP4.5 scenario.

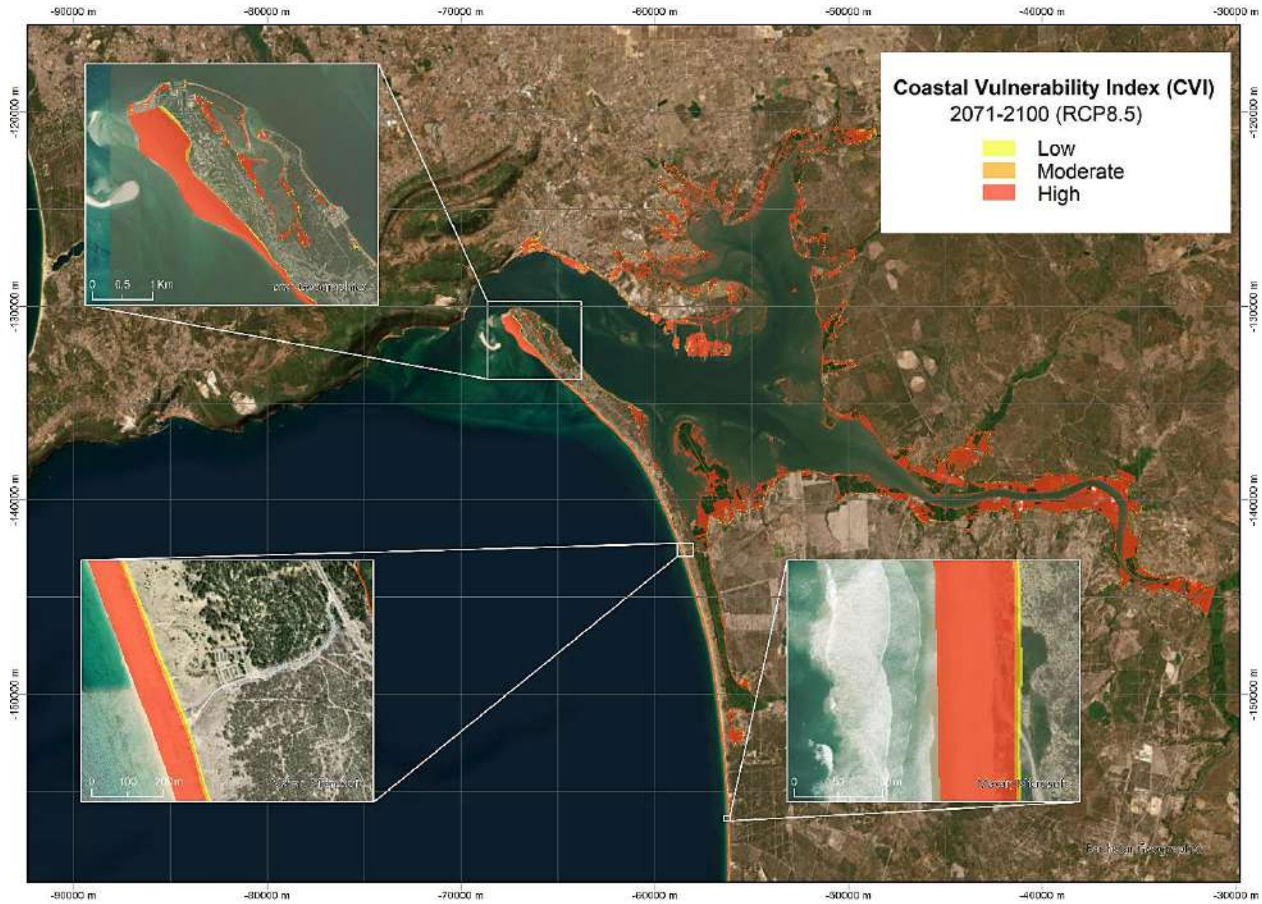

Figure 156 – Same as in Figure 147, but for 2100 under the RCP8.5 scenario.

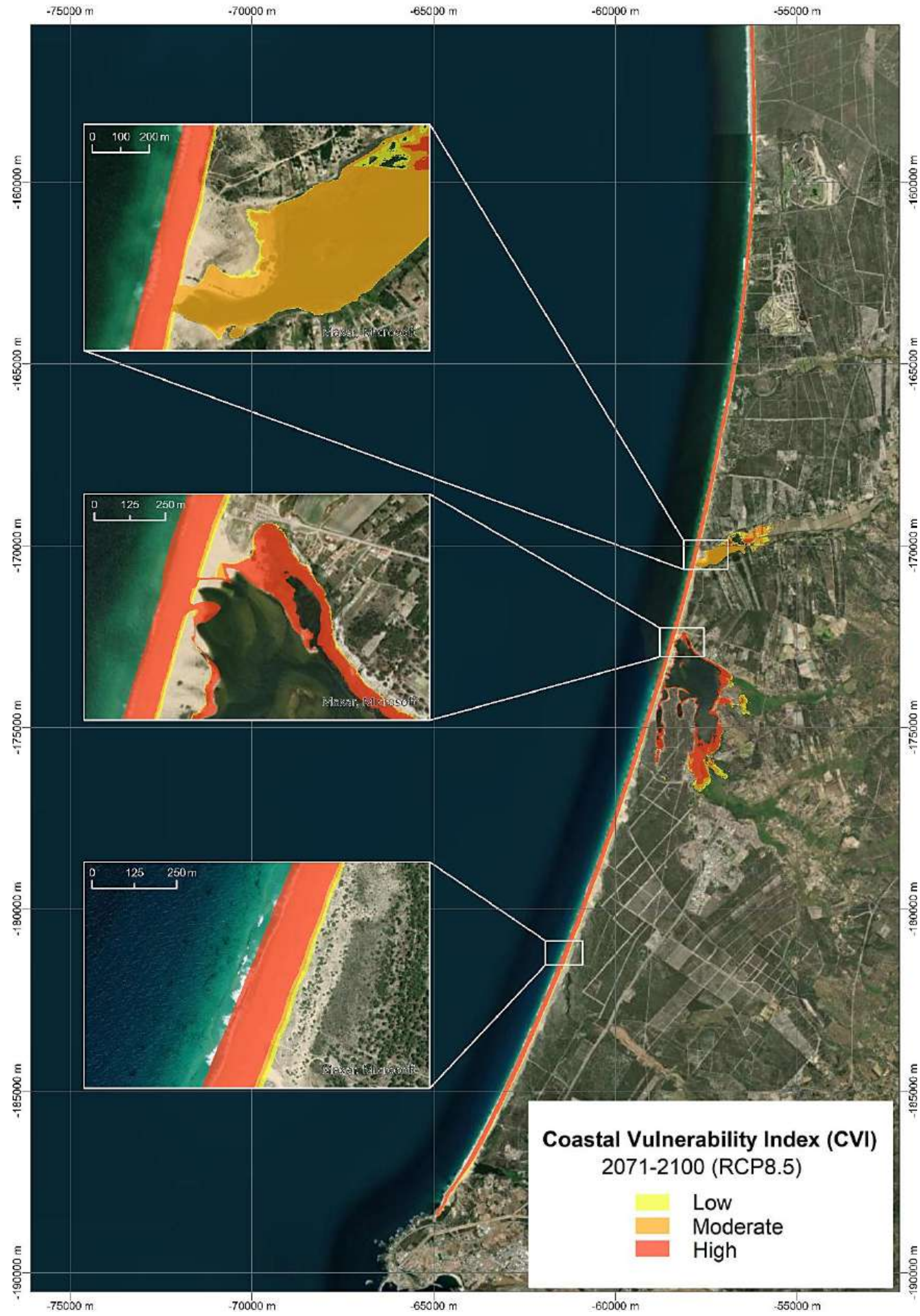

Figure 157 – Same as in Figure 148, but for 2100 under the RCP8.5 scenario.

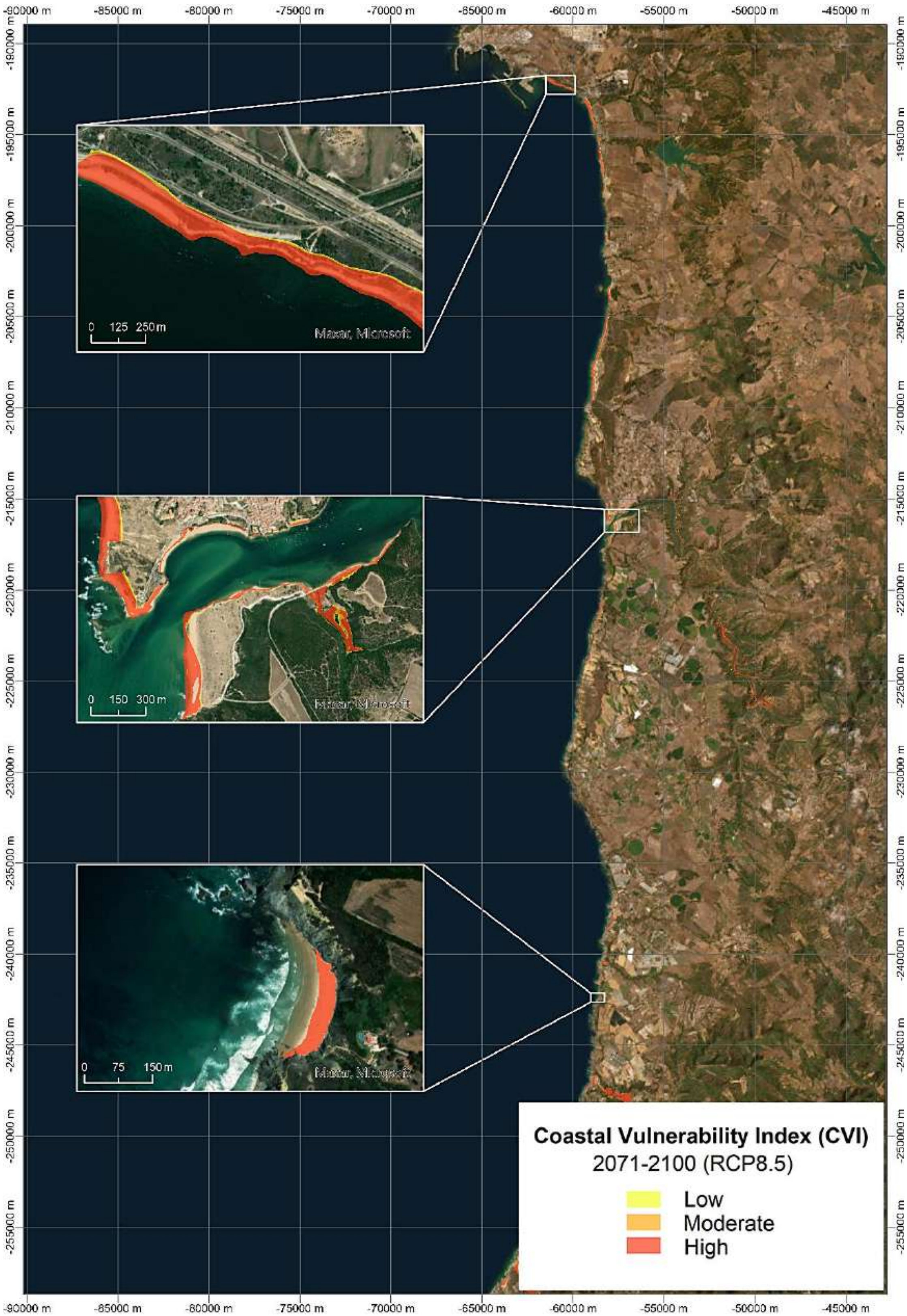

Figure 158 – Same as in Figure 149, but for 2100 under the RCP8.5 scenario.

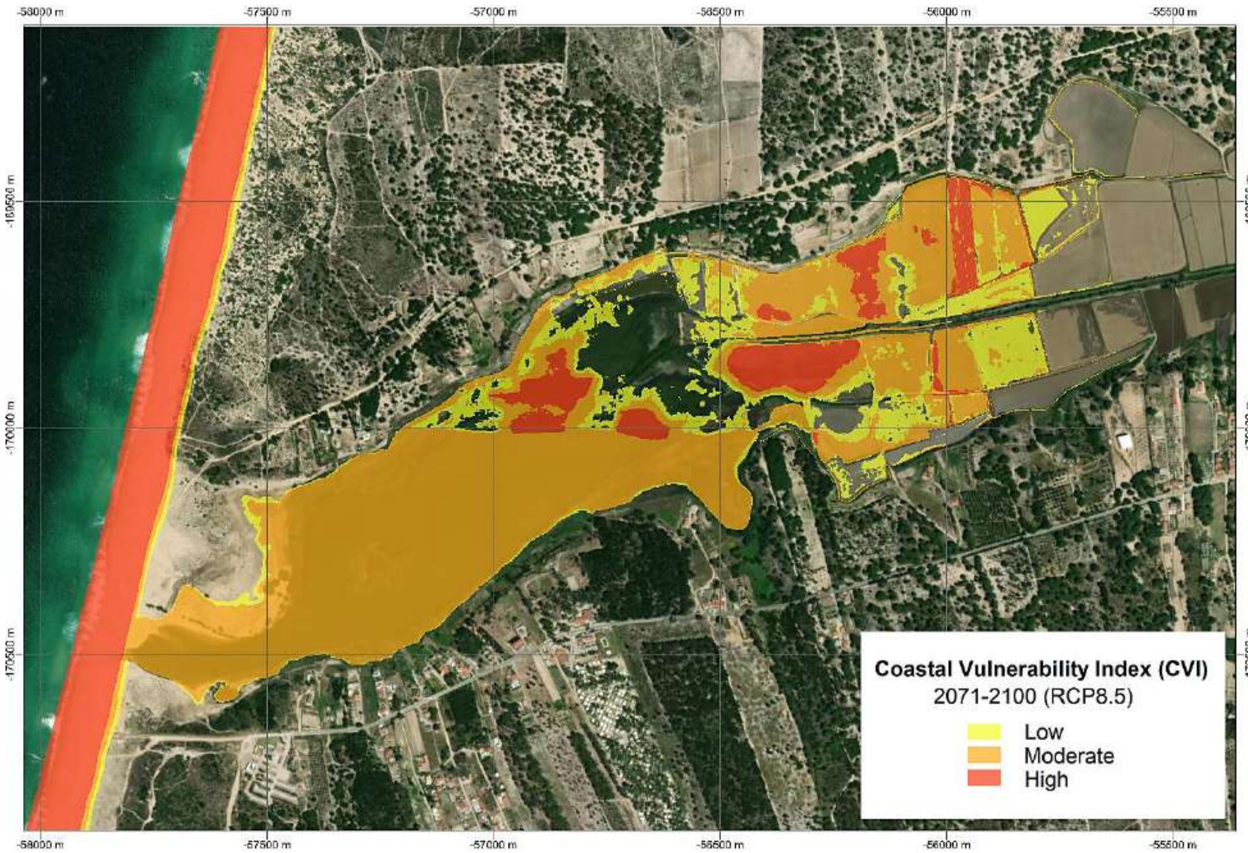

Figure 159 – CVI for Melides lagoon (within section 5 – Troia-Odeceixe), for 2100 under the RCP8.5 scenario.

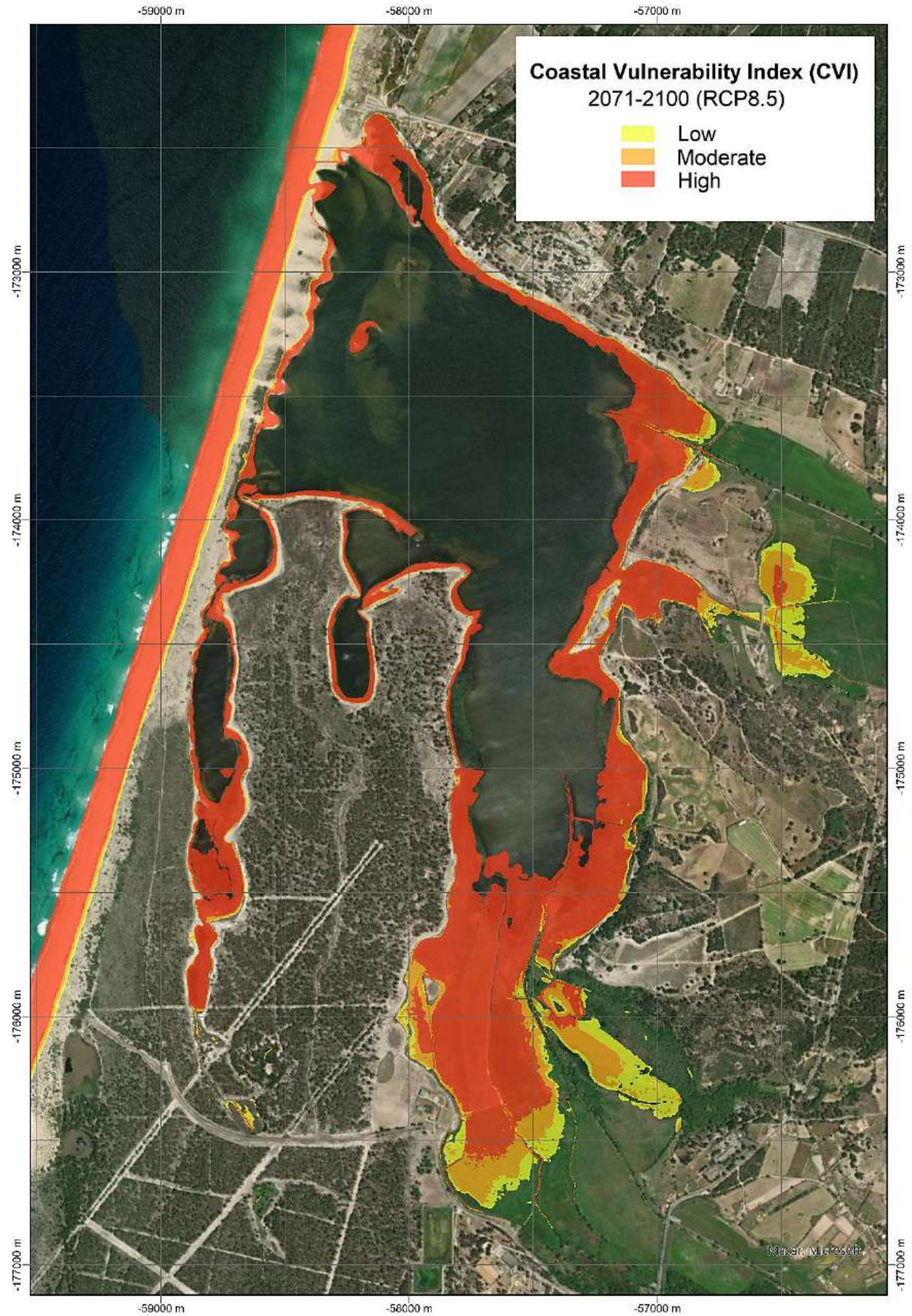

Figure 160 – Same as in Figure 159, but for Santo André lagoon (within section 5 – Troia-Odeceixe).

Figure 161 – Same as in Figure 159, but for Vila Nova de Milfontes (within section 5 – Troia-Odeceixe).

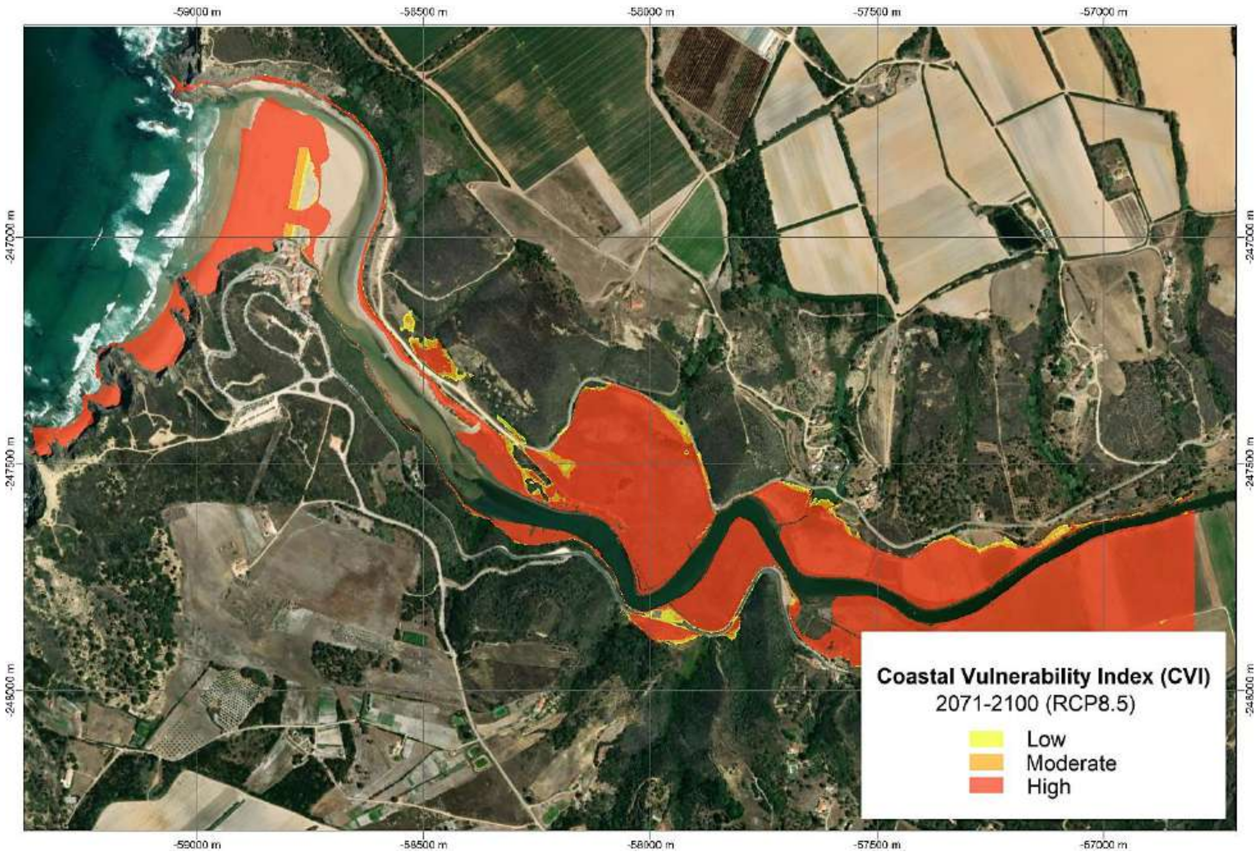

Figure 162 – Same as in Figure 159, but for Odeceixe (within section 5 – Troia-Odeceixe).

Table 27 – Same as in Table 23, but for Section 5 – Troia-Odeceixe.

Coastal areas under CVI classification for Section 5 – Tróia-Odeceixe			
2070 (RCP4.5)			
District	**Ocean-facing (km²)**	**Inland (km²)**	**Total (km²)**
Setúbal	7.58	39.6	47.2
Beja	0.411	1.09	1.52
2070 (RCP8.5)			
District	**Ocean-facing (km²)**	**Inland (km²)**	**Total (km²)**
Setúbal	8.02	41.4	49.5
Beja	0.847	1.14	1.99
2100 (RCP4.5)			
District	**Ocean-facing (km²)**	**Inland (km²)**	**Total (km²)**
Setúbal	9.63	42.5	52.1
Beja	0.921	1.17	2.15
2100 (RCP8.5)			
District	**Ocean-facing (km²)**	**Inland (km²)**	**Total (km²)**
Setúbal	9.00	43.6	52.6
Beja	0.861	1.20	2.07

4.6.6. Section 6 – Algarve

The sixth section ranges from Odeceixe to Vila Real de Santo António (Algarve region), considering a quite diverse coastal stretch of about 230 km in length. This section also shows quite diverse coastal morphologies, from the rocky cliffs and small embedded beaches of southwestern Portugal (along the "Sudoeste Alentejano e Costa Vicentina" natural park and the "Barlavento" region of the Algarve), to the long, low-lying sandy beaches of the "Sotavento" region of the Algarve, featuring estuaries (*e.g.*, Arade and Guadiana rivers) and a large lagoon system, the Ria Formosa. The inland waters from Ria Formosa extend for approximately 180 km^2, representing a unique landscape with multiple ecosystems and natural resources, despite local communities and socioeconomic activities. Within the Ria Formosa, low-lying sandy islands exist, namely Praia de Faro (Island), Deserta, Farol, Culatra and Armona. The ocean-facing coastal areas comprehend important sandy beaches such as Amoreira, Arrifana, Bordeira, Amado, Cordoama and Ponta Ruiva within the W-NW-facing coastlines, and Martinhal, Andorinha, Salema, Luz, Alvor, Torralta, Rocha, Salgados, Grande (de Pêra), Galé, Alemães, Oura, Santa Eulália, Falésia, Quarteira, Trafal, Ancão, Praia de Faro, Barreta, Farol, Culatra, Armona, Fuseta, Tavira, Cabanas, Cacela, Manta Rota, Altura, Monte Gordo and Santo António along the Algarve coastlines facing S.

Overall, although some local areas of the Costa Vicentina are projected to become highly vulnerable to the effects of climate change on TWLs and wave action even by the end of the first future time-slice (2041-2070) under the moderate RCP4.5 scenario (Figure 163, Figure 171 and Figure 172), the largest areas of high CVIs are located within the south-facing coastlines of the Algarve region (especially at the estuaries and the Ria Formosa; Figure 164, Figure 166, Figure 168 and Figure 170). There, communities and infrastructures also show greater exposure to changes in mean and extreme sea levels. By 2100, considering the RCP8.5 scenario, Figure 173 shows high CVIs projected within several urbanized areas in the cities of Lagos and Portimão, as well as in the village of Alvor. In central Algarve, along the Ria Formosa, Figure 174 shows moderate-to-high CVIs, expected across the entirety of the Praia de Faro, Deserta, Farol, Culatra and Armona islands. Further inland, the lowest areas of Faro (including the historical center), Olhão, Fuseta, Tavira and Conceição are also projected to exhibit high vulnerability, given the projected TWLs. Note that high CVIs are expected inside the perimeter of Faro International Airport (Gago Coutinho Airport) even by 2070 under RCP4.5 (covering a progressively larger area towards the end of the 21st century under the RCP8.5). Finally, at the Guadiana River estuary (Figure 175), moderate-to-high (high) CVIs are projected in the majority of its extension by 2070 under RCP4.5 (2100 under RCP8.5), covering most of the "Reserva Natural do Sapal de Castro Marim" and almost half of the Vila Real de Santo

António urban area, compromising its population and infrastructure. High CVIs are also expected along the N125 route from Vila Real de Santo António to Monte Gordo, covering part of its urban area as well.

Table 28 shows the largest areas under CVI along the inland waters of Section 6. Within the Algarve region (Faro district), the total ocean-facing areas under CVI range between 6.46 km^2 (by 2070 under RCP4.5) and 12.5 km^2 (by 2100 under RCP8.5), whereas for the inland waters these values ascend to 36.2 km^2 (2070 under RCP4.5) and 40.8 km^2 (2100 under RCP8.5), representing, between scenarios, from 76.4% to 84.8% of the global value.

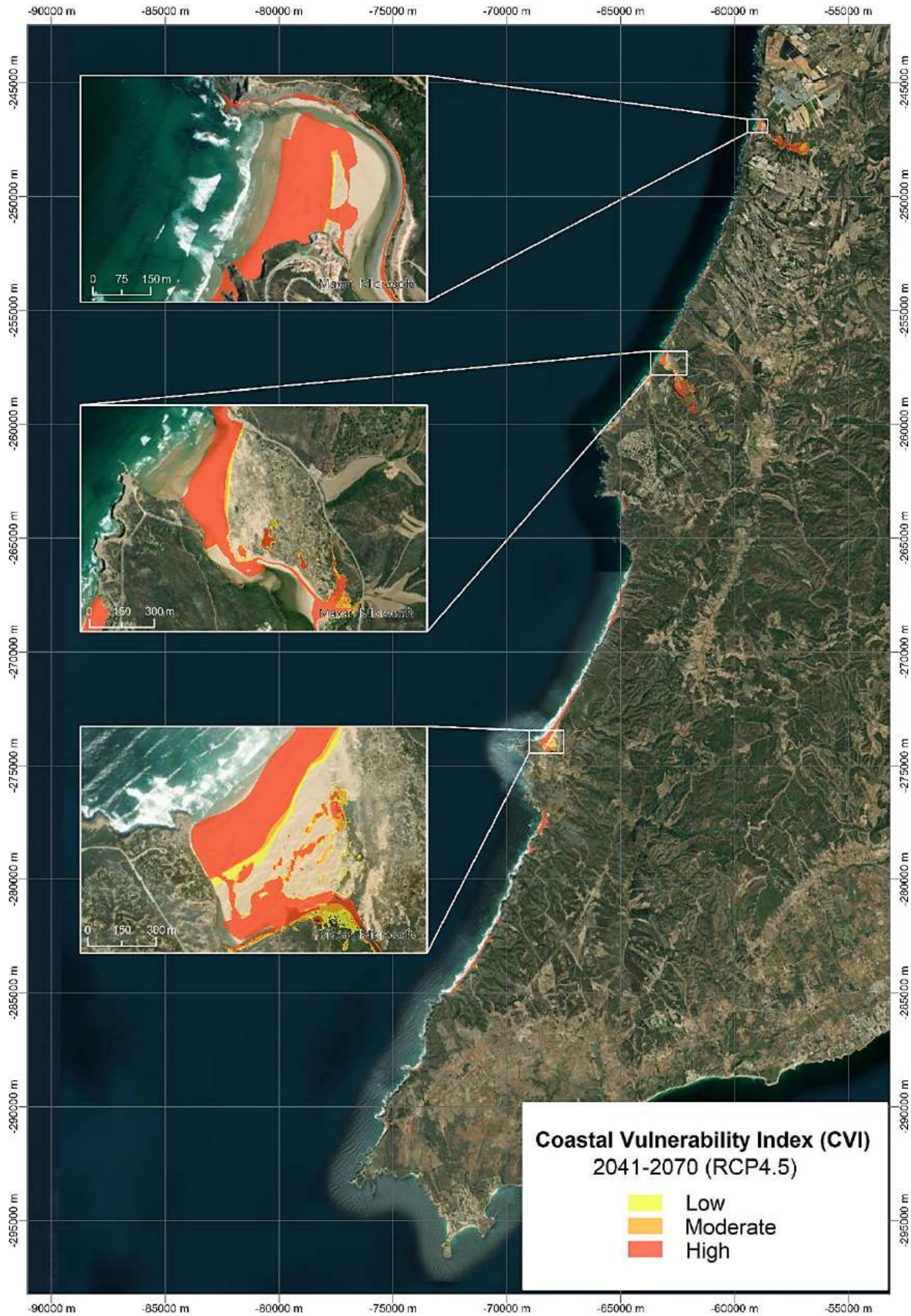

Figure 163 – CVI for Section 6 (part I) – Algarve, by 2070 under the RCP4.5 scenario.

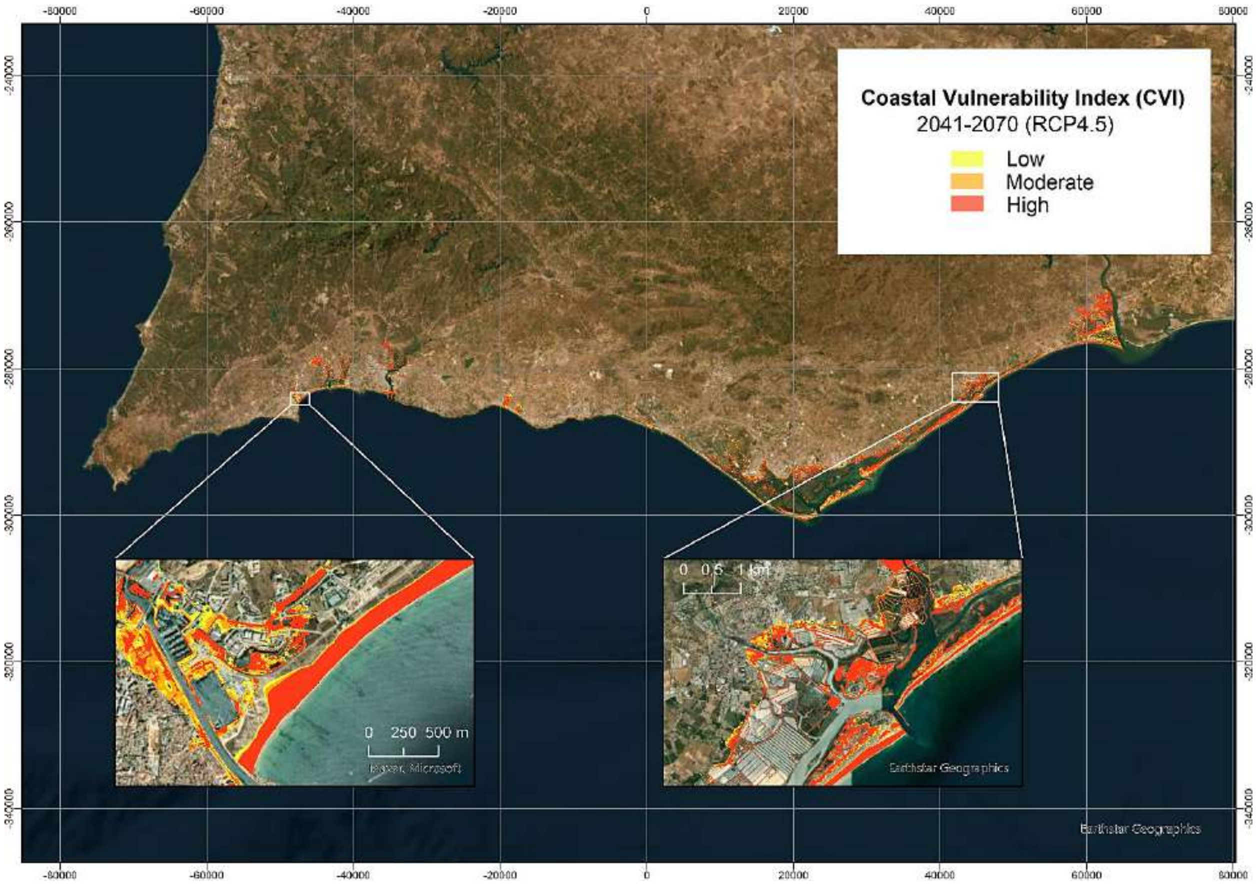

Figure 164 – CVI for Section 6 (part II) – Algarve, by 2070 under the RCP4.5 scenario.

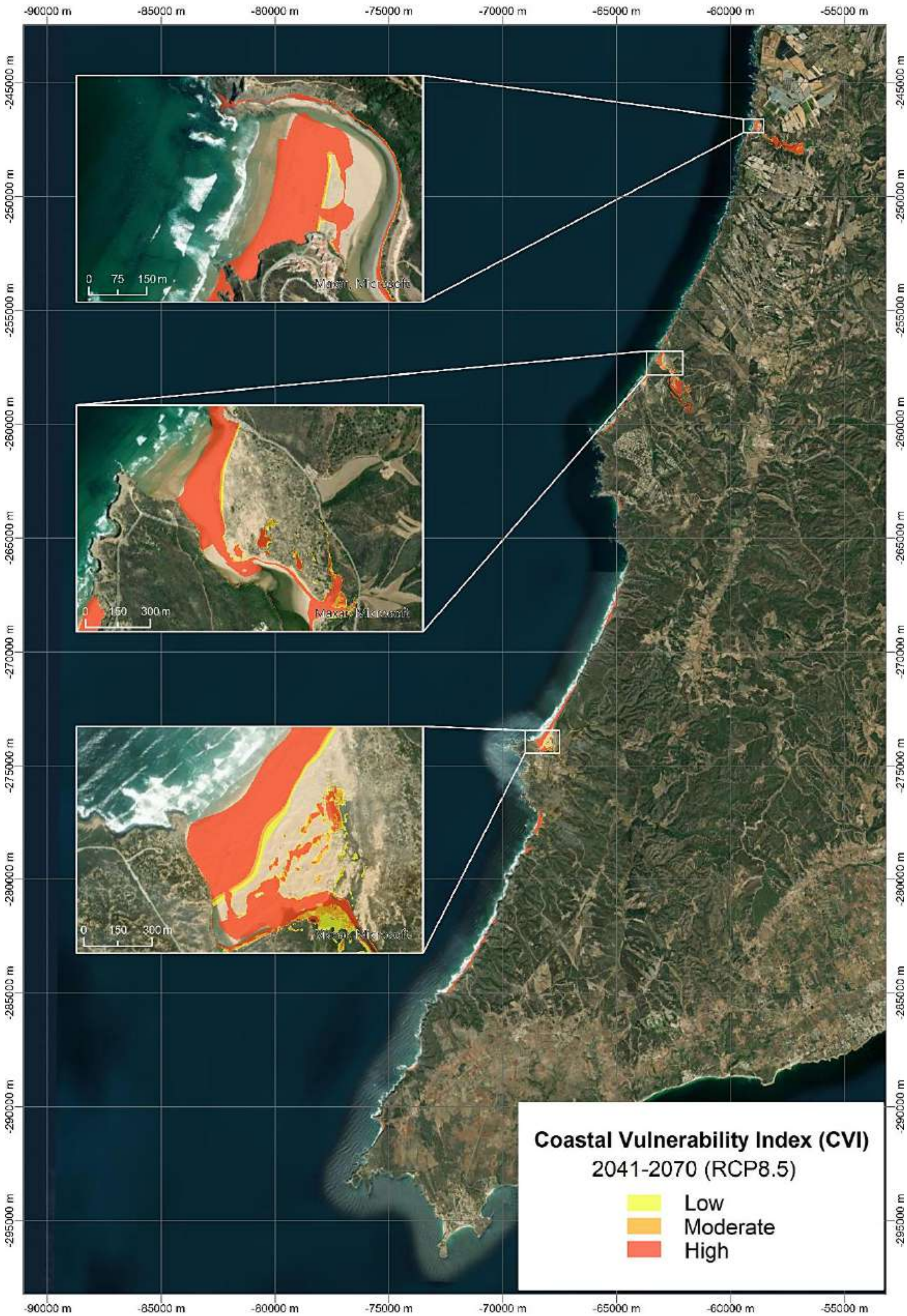

Figure 165 – Same as in Figure 163, but under the RCP8.5 scenario.

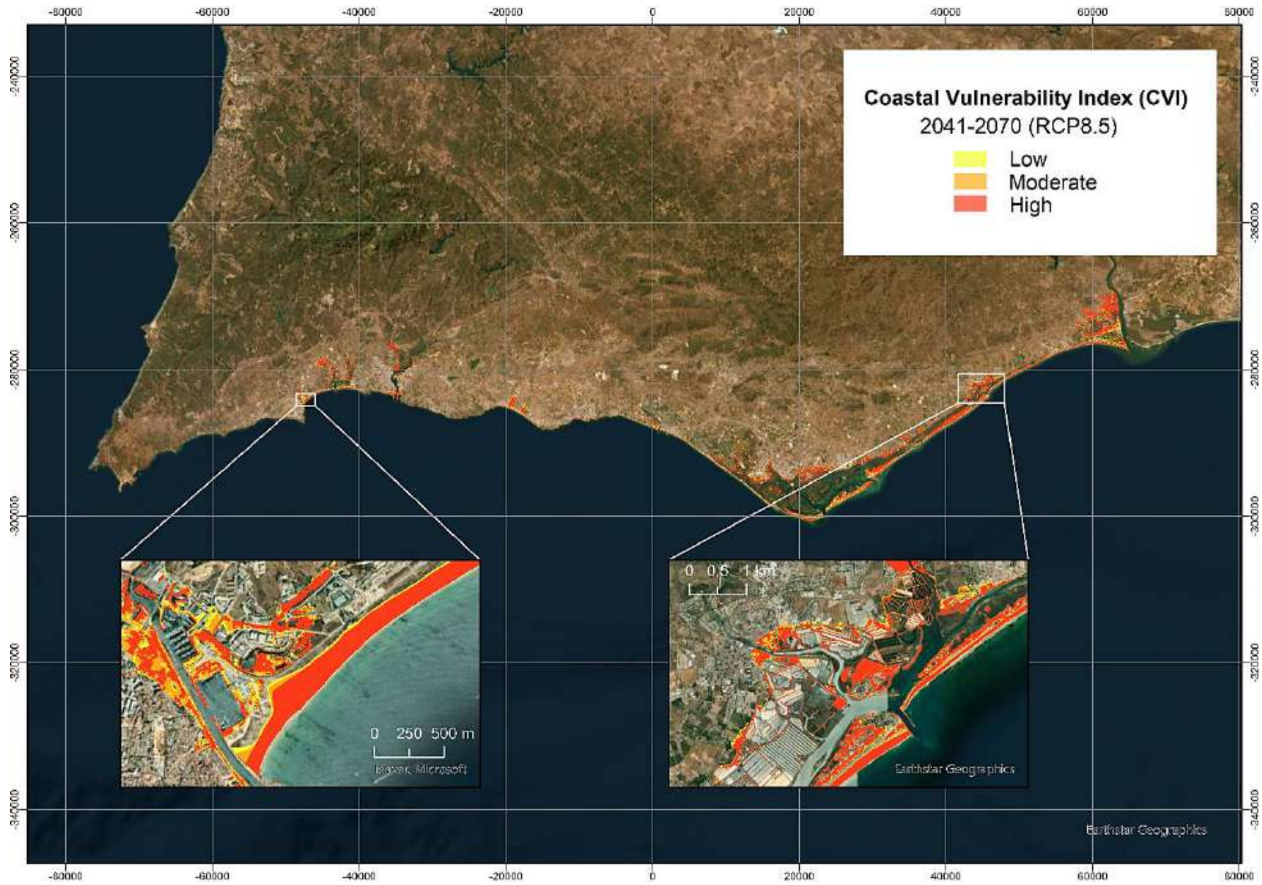

Figure 166 – Same as in Figure 164, but under the RCP8.5 scenario.

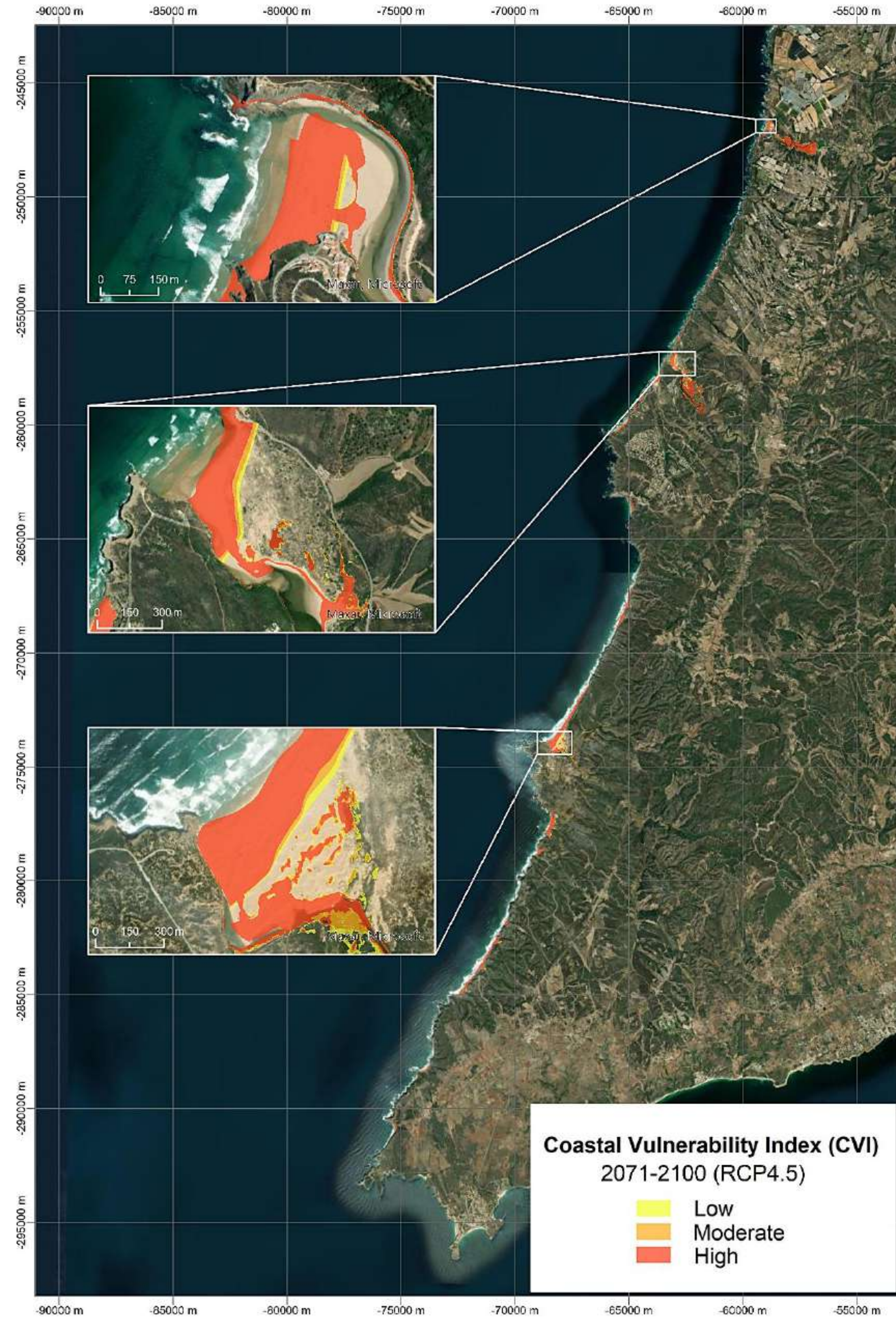

Figure 167 – Same as in Figure 163, but for 2100 under the RCP4.5 scenario.

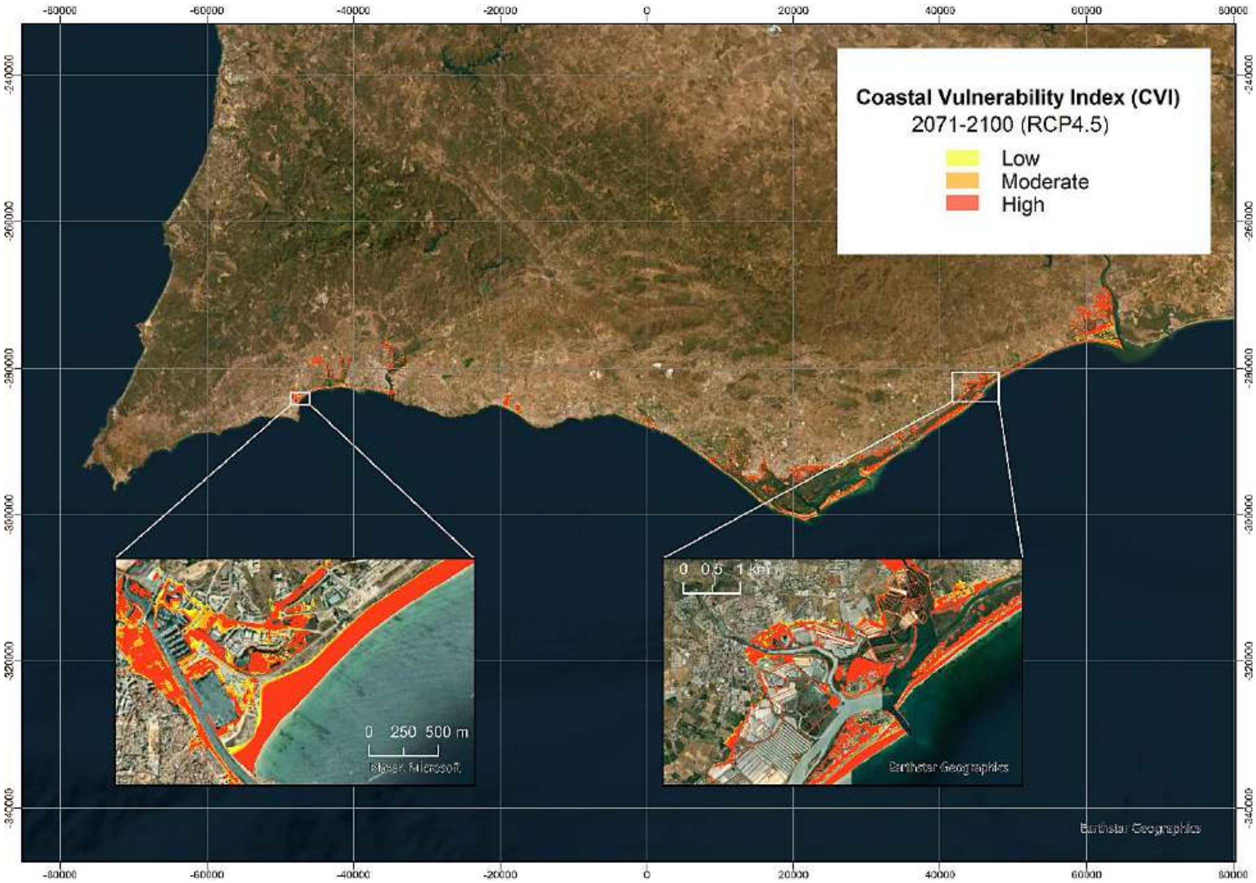

Figure 168 – Same as in Figure 164, but for 2100 under the RCP4.5 scenario.

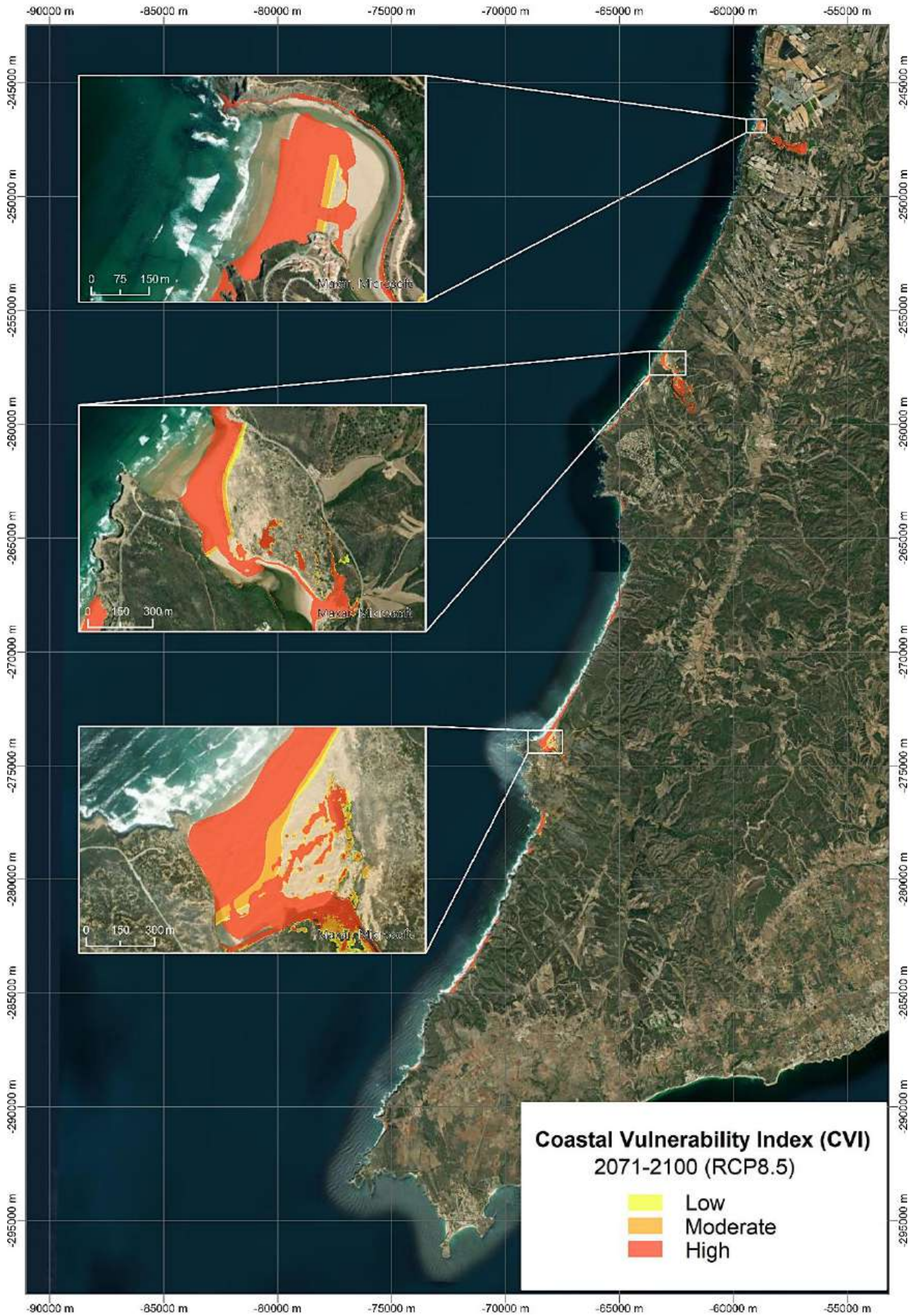

Figure 169 – Same as in Figure 163, but for 2100 under the RCP8.5 scenario.

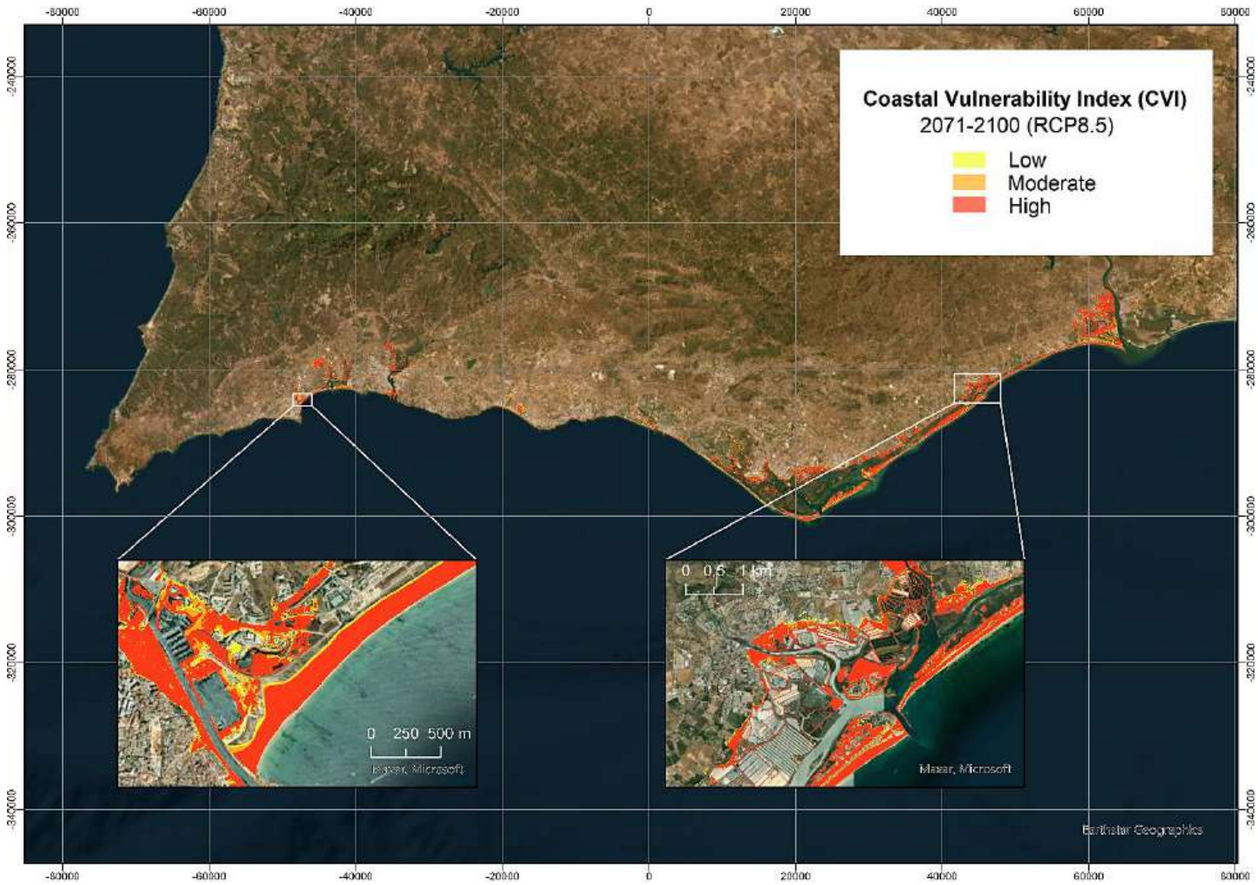

Figure 170 – Same as in Figure 164, but for 2100 under the RCP8.5 scenario.

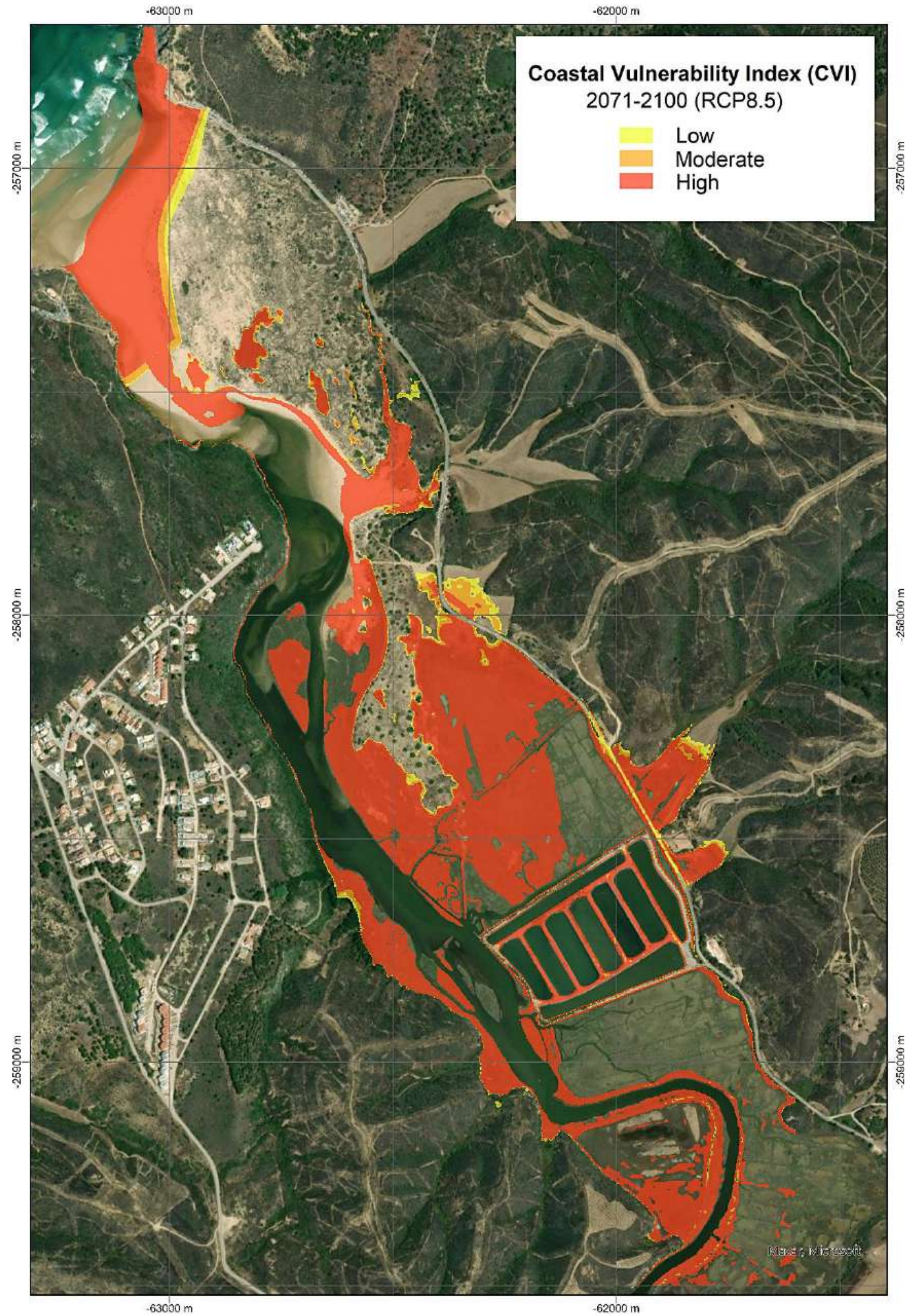

Figure 171 – CVI for Praia da Amoreira (within section 6 – Algarve), for 2100 under the RCP8.5 scenario.

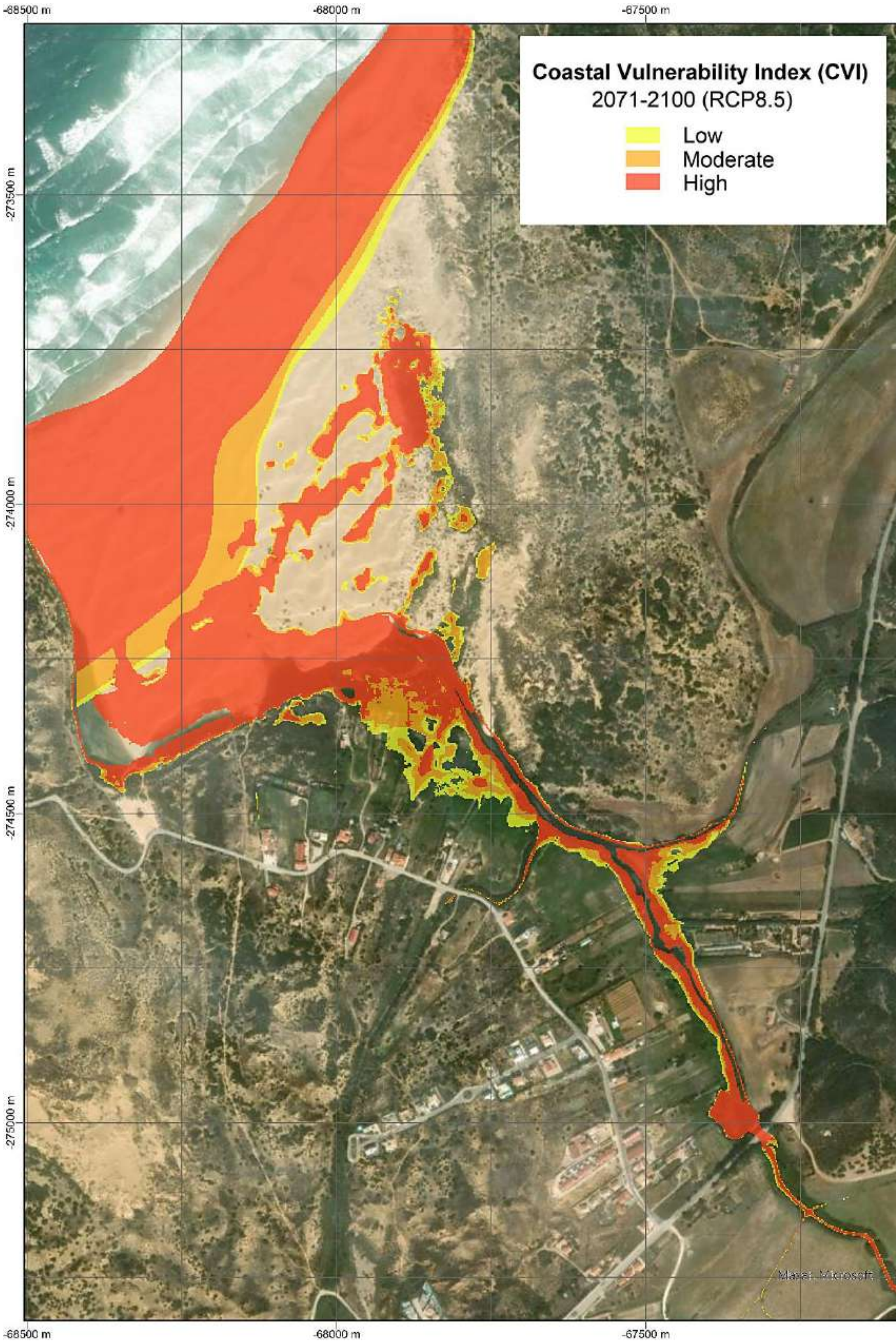

Figure 172 – Same as in Figure 171, but for Praia da Bordeira (within section 6 – Algarve).

Figure 173 – Same as in Figure 171, but for Lagos-Portimão coastal stretch (within section 6 – Algarve).

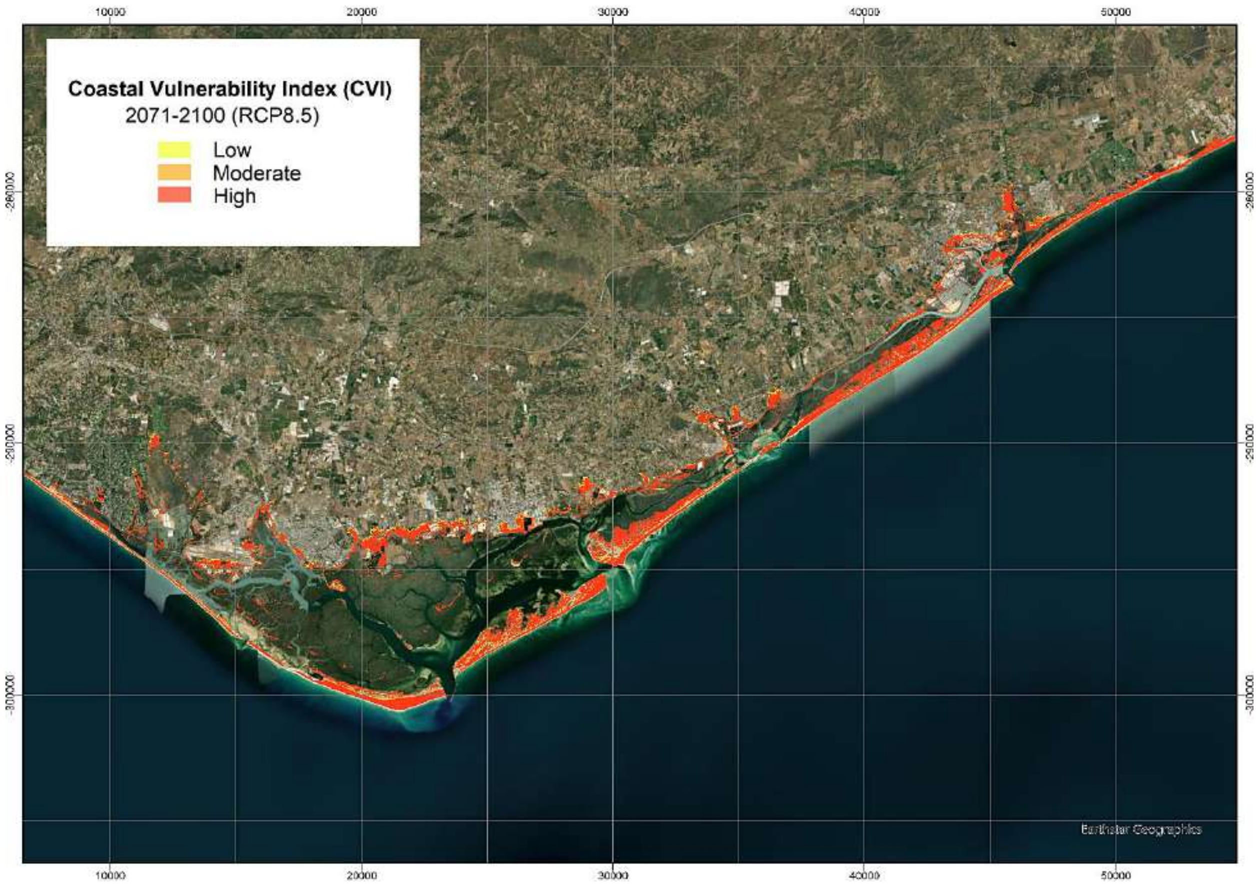

Figure 174 – Same as in Figure 171, but for Ria Formosa (within section 6 – Algarve).

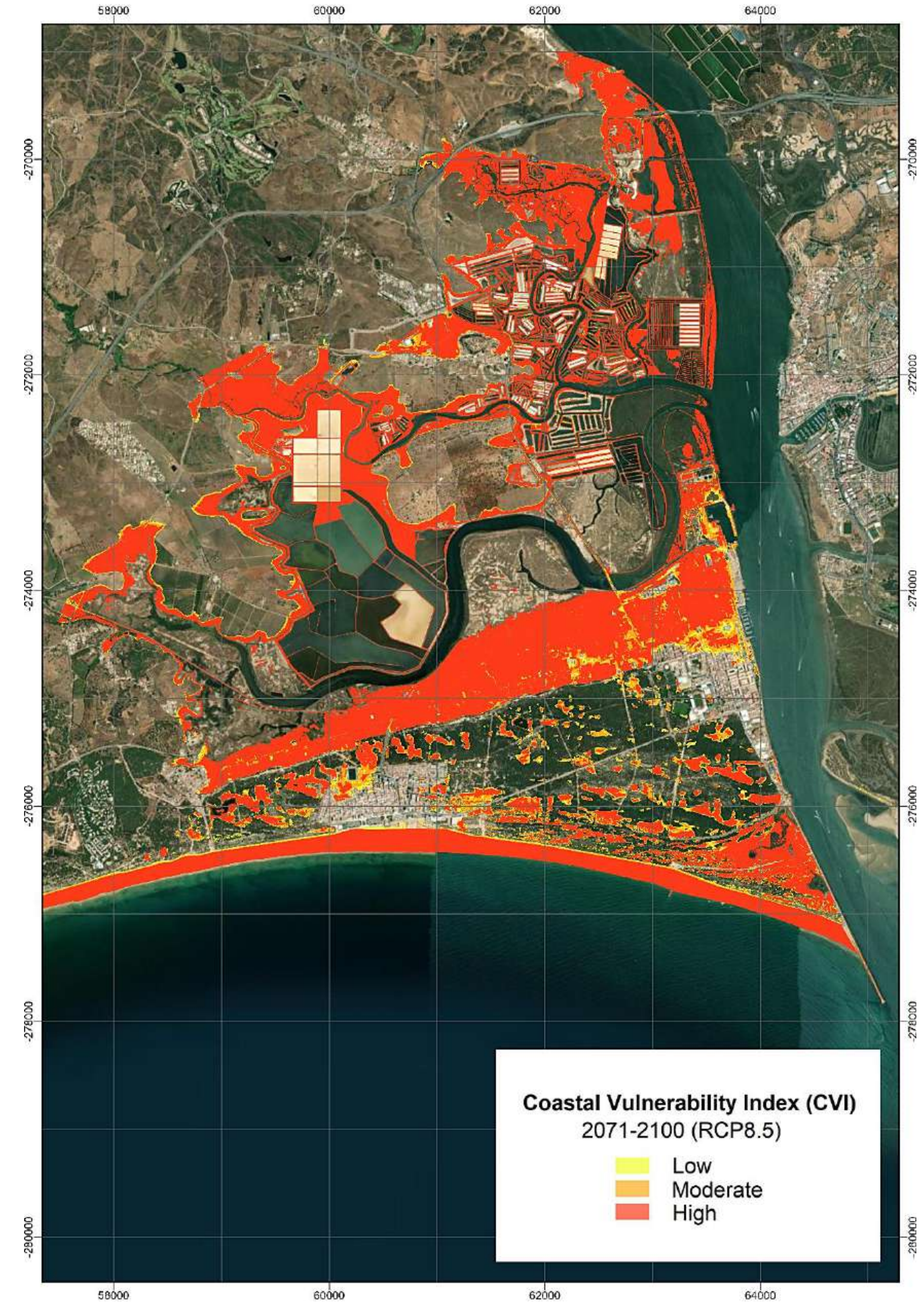

Figure 175 – Same as in Figure 171, but for the Guadiana River estuary (within section 6 – Algarve).

Table 28 – Same as in Table 23, but for Section 6 – Algarve.

Coastal areas under CVI classification for Section 6 – Algarve			
2070 (RCP4.5)			
District	**Ocean-facing (km^2)**	**Inland (km^2)**	**Total (km^2)**
Faro	6.46	36.2	42.7
2070 (RCP8.5)			
District	**Ocean-facing (km^2)**	**Inland (km^2)**	**Total (km^2)**
Faro	11.2	36.3	47.5
2100 (RCP4.5)			
District	**Ocean-facing (km^2)**	**Inland (km^2)**	**Total (km^2)**
Faro	11.6	38.3	49.9
2100 (RCP8.5)			
District	**Ocean-facing (km^2)**	**Inland (km^2)**	**Total (km^2)**
Faro	12.5	40.8	53.3

4.6.7. Mainland Portugal

In the last six sub-sections, the cartography of coastal vulnerability (characterized by the CVI) was shown, for each of the six coastal sections of Mainland Portugal. This division allowed a clearer depiction of the projected CVIs and associated physical impacts, in a local-to-regional view, which was shown to vary considerably depending on the analyzed section due to the highly diversified nature of the Portuguese coastline. While the areas under CVI classification were presented for each district within the analyzed sections, an integration of the results previously reported on all Mainland Portugal districts is required. Therefore, the areas under CVI are shown in Figure 176 to Figure 179, and Table 29 to Table 35, across all coastal districts from Mainland Portugal, divided similarly to Table 23 to Table 28, in ocean-facing and inland coastal areas, and finally, the total projected area under CVI. Furthermore, the details of the areas under CVI are explored through Table 30 to Table 36, by a thorough description of the areas under each CVI classification level, along each Portuguese coastal municipality, totalizing 66 administrative regions.

The projected areas under CVI in the future vary considerably between districts. The largest total threatened area is projected to be in the Lisbon district, for all future periods and scenarios, ranging between 214 km^2 (2070 under RCP4.5; Table 29) and 221 km^2 (2100 under RCP8.5; Table 35). Such large areas are intrinsically connected to the Tagus River estuary, surrounded by low-lying terrain and a dynamic intertidal behavior. Conversely, Beja is the district with the smallest total projected area under CVI, ranging between 1.52 km^2 (Table 29) and 2.15 km^2 (Table 34), due to its generally rocky coastal configuration, with cliffs and small embedded beaches.

When considering the total threatened area, at a national scale, the projected values for the ocean-facing coastlines ascend to 41.7 km^2, 49.7 km^2, 54.7 km^2 and 55.9 km^2, for 2070 under RCP4.5 and RCP8.5, and 2100 under RCP4.5 and RCP8.5, respectively. These threatened areas are projected to amount to 3.09, 3.68, 4.05 and 4.14 times the observed area that has been lost between 1958 and 2021, corresponding to 13.5 km^2 (updated from Pinto *et al.*, 2016). Note, nevertheless, that these areas are related to future projected 99th percentile wave characteristics under a 100-year TWL, relative to the 2011 reference shoreline. Regarding inland waters, the overall threatened area at a national scale is expected to ascend to 514 km^2 (548 km^2) by 2070 under RCP4.5 (2100 under RCP8.5). The global value, including both ocean-facing and inland coastlines under CVI is projected to reach up to 604 km^2 by 2100 under the RCP8.5 scenario.

Table 29 – Area (in km^2) of the coastal stretches under CVI classifications for each of the Mainland Portugal districts for 2070 (end of the 2041-2070 period) under the RCP4.5 scenario.

Coastal areas under CVI classification in Mainland Portugal			
2070 (RCP4.5)			
District	**Ocean-facing (km^2)**	**Inland (km^2)**	**Total (km^2)**
Viana do Castelo	0.78	10.2	10.9
Braga	1.52	1.41	2.93
Porto	5.27	0.69	5.96
Aveiro	5.75	50.6	56.3
Coimbra	4.19	4.88	9.07
Leiria	6.23	3.78	10.0
Santarém	0.00	121	121
Lisboa	1.02	213	214
Setúbal	10.0	70.3	80.3
Beja	0.411	1.09	1.52
Faro	6.46	36.2	42.7
Portugal	41.7	514	555

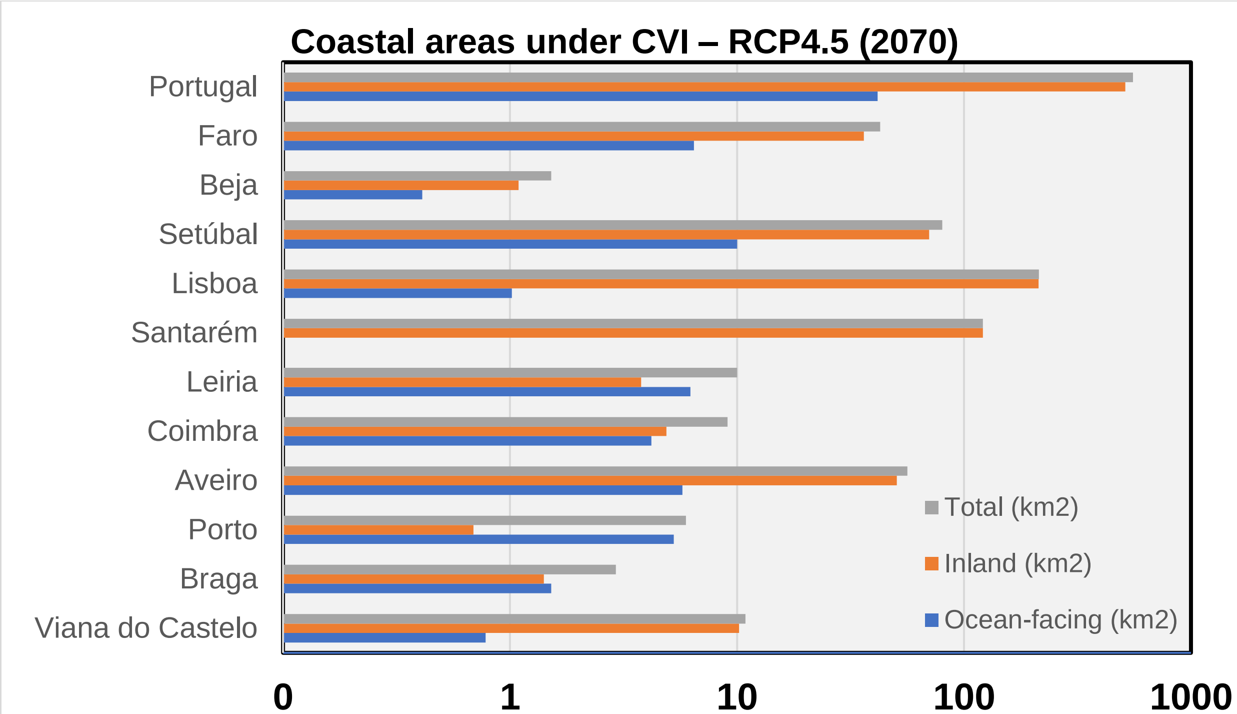

Figure 176 – Areas (in km^2) of the coastal stretches under CVI classifications for each of the Mainland Portugal districts for 2070 (end of the 2041-2070 period) under the RCP4.5 scenario.

Table 30 – Area (in km^2) of the coastal stretches under each CVI classification level, for each of the Mainland Portugal municipalities, by 2070 (end of the 2041-2070 period) under the RCP4.5 scenario.

2070 RCP4.5						
Municipality	**CVI**	**Total area (km^2)**	**Ocean-facing coastlines (km^2)**	**Inland waters (km^2)**	**All coastlines (km^2)**	**Normalized area (%)**
Caminha	3	3.702	0.219	2.542	2.761	74.56
	2		0.009	0.583	0.592	90.54
	1		0.009	0.342	0.350	100.00
Viana do Castelo	3	7.234	0.530	4.250	4.780	66.07
	2		0.000	1.354	1.354	84.79
	1		0.010	1.090	1.100	100.00
Esposende	3	2.934	1.410	0.669	2.079	70.85
	2		0.061	0.405	0.465	86.72
	1		0.048	0.341	0.390	100.00
Póvoa de Varzim	3	1.252	1.109	0.009	1.118	89.26
	2		0.048	0.024	0.071	94.96
	1		0.046	0.017	0.063	100.00
Vila do Conde	3	1.545	1.098	0.187	1.285	83.17
	2		0.039	0.082	0.121	91.02
	1		0.035	0.103	0.139	100.00
Matosinhos	3	1.175	1.048	0.032	1.080	91.92
	2		0.039	0.012	0.051	96.29
	1		0.034	0.010	0.044	100.00
Porto	3	0.109	0.073	0.019	0.091	84.11

	2		0.003	0.005	0.008	91.35
	1		0.003	0.007	0.009	100.00
Vila Nova de Gaia	3	1.878	1.546	0.097	1.643	87.48
	2		0.080	0.036	0.116	93.67
	1		0.069	0.050	0.119	100.00
Espinho	3	0.827	0.414	0.201	0.614	74.31
	2		0.009	0.064	0.072	83.08
	1		0.012	0.128	0.140	100.00
Ovar	3	5.253	0.870	2.723	3.594	68.42
	2		0.032	0.857	0.890	85.36
	1		0.034	0.735	0.769	100.00
Murtosa	3	15.844	1.485	7.788	9.272	58.52
	2		0.031	3.423	3.454	80.32
	1		0.032	3.086	3.118	100.00
Estarreja	3	3.726	0.000	2.349	2.349	63.04
	2		0.000	0.738	0.738	82.85
	1		0.000	0.639	0.639	100.00
Aveiro	3	11.163	1.115	5.892	7.007	62.77
	2		0.018	2.090	2.109	81.66
	1		0.041	2.006	2.047	100.00
Albergaria-a-Velha	3	6.990	0.000	5.113	5.113	73.15
	2		0.000	1.118	1.118	89.14
	1		0.000	0.759	0.759	100.00
Ílhavo	3	7.454	0.751	3.405	4.156	55.75
	2		0.015	1.469	1.484	75.66
	1		0.014	1.800	1.814	100.00
Vagos	3	5.086	0.845	2.718	3.563	70.06
	2		0.015	0.798	0.813	86.04
	1		0.020	0.690	0.710	100.00
Mira	3	3.020	1.180	0.865	2.044	67.69
	2		0.043	0.424	0.467	83.13
	1		0.039	0.470	0.509	100.00
Cantanhede	3	0.628	0.586	0.000	0.586	93.43
	2		0.019	0.000	0.019	96.46
	1		0.022	0.000	0.022	100.00
Figueira da Foz	3	5.418	2.148	2.030	4.178	77.12
	2		0.071	0.632	0.703	90.09
	1		0.079	0.457	0.536	99.99
Pombal	3	1.059	0.983	0.000	0.983	92.80
	2		0.039	0.000	0.039	96.52
	1		0.037	0.000	0.037	100.00
Leiria	3	1.102	1.023	0.000	1.023	92.92
	2		0.039	0.000	0.039	96.47
	1		0.039	0.000	0.039	100.00
Marinha Grande	3	1.699	1.462	0.056	1.518	89.38
	2		0.066	0.031	0.097	95.06
	1		0.060	0.024	0.084	100.00
Alcobaça	3	1.518	0.332	0.398	0.730	48.10
	2		0.015	0.460	0.475	79.41
	1		0.012	0.301	0.312	100.00
Nazaré	3	1.983	1.142	0.455	1.597	80.54
	2		0.077	0.152	0.229	92.09
	1		0.068	0.089	0.157	100.00
Caldas da Rainha	3	0.476	0.082	0.135	0.217	45.51
	2		0.000	0.154	0.154	77.90
	1		0.004	0.102	0.105	100.00
Óbidos	3	1.553	0.119	0.870	0.989	63.68
	2		0.007	0.356	0.363	87.02
	1		0.006	0.196	0.202	100.00

Peniche	3	0.613	0.531	0.000	0.531	86.62
	2		0.042	0.000	0.042	93.47
	1		0.040	0.000	0.040	100.00
Lourinhã	3	0.266	0.250	0.000	0.250	94.14
	2		0.011	0.000	0.011	98.16
	1		0.005	0.000	0.005	100.00
Torres Vedras	3	0.488	0.270	0.118	0.388	79.44
	2		0.000	0.064	0.064	92.62
	1		0.000	0.036	0.036	100.00
Mafra	3	0.208	0.093	0.077	0.169	81.19
	2		0.000	0.023	0.023	92.12
	1		0.000	0.016	0.016	100.00
Sintra	3	0.229	0.206	0.000	0.206	89.69
	2		0.013	0.000	0.013	95.45
	1		0.010	0.000	0.010	100.00
Cascais	3	0.164	0.145	0.000	0.145	88.42
	2		0.011	0.000	0.011	94.99
	1		0.008	0.000	0.008	100.00
Oeiras	3	0.283	0.000	0.169	0.169	59.91
	2		0.000	0.049	0.049	77.08
	1		0.000	0.065	0.065	100.00
Lisboa	3	1.052	0.000	0.349	0.349	33.15
	2		0.000	0.225	0.225	54.50
	1		0.000	0.479	0.479	100.00
Loures	3	6.603	0.000	4.585	4.585	69.43
	2		0.000	1.004	1.004	84.64
	1		0.000	1.014	1.014	100.00
Vila Franca de Xira	3	152.123	0.000	143.747	143.747	94.49
	2		0.000	5.498	5.498	98.11
	1		0.000	2.879	2.879	100.00
Alenquer	3	4.635	0.000	3.896	3.896	84.05
	2		0.000	0.419	0.419	93.08
	1		0.000	0.321	0.321	100.00
Azambuja	3	48.372	0.000	41.711	41.711	86.23
	2		0.000	3.611	3.611	93.69
	1		0.000	3.051	3.051	100.00
Cartaxo	3	18.936	0.000	13.932	13.932	73.57
	2		0.000	2.615	2.615	87.38
	1		0.000	2.390	2.390	100.00
Santarém	3	0.675	0.000	0.267	0.267	39.56
	2		0.000	0.193	0.193	68.13
	1		0.000	0.215	0.215	100.00
Alpiarça	3	0.001	0.000	0.000	0.000	0.00
	2		0.000	0.000	0.000	4.94
	1		0.000	0.001	0.001	100.00
Almeirim	3	0.433	0.000	0.259	0.259	59.72
	2		0.000	0.070	0.070	75.97
	1		0.000	0.104	0.104	100.00
Salvaterra de Magos	3	13.377	0.000	9.283	9.283	69.40
	2		0.000	2.307	2.307	86.64
	1		0.000	1.787	1.787	100.00
Coruche	3	0.029	0.000	0.004	0.004	14.84
	2		0.000	0.009	0.009	44.37
	1		0.000	0.016	0.016	100.00
Benavente	3	87.764	0.000	77.160	77.160	87.92
	2		0.000	5.646	5.646	94.35
	1		0.000	4.958	4.958	100.00
Alcochete	3	12.846	0.000	11.775	11.775	91.67
	2		0.000	0.583	0.583	96.21

	1		0.000	0.487	0.487	100.00
Montijo	3	3.792	0.000	2.458	2.458	64.83
	2		0.000	0.811	0.811	86.21
	1		0.000	0.523	0.523	100.00
Moita	3	4.379	0.000	3.406	3.406	77.78
	2		0.000	0.526	0.526	89.80
	1		0.000	0.447	0.447	100.00
Barreiro	3	2.684	0.000	1.269	1.269	47.28
	2		0.000	0.476	0.476	65.01
	1		0.000	0.939	0.939	100.00
Seixal	3	3.561	0.000	2.829	2.829	79.45
	2		0.000	0.379	0.379	90.08
	1		0.000	0.353	0.353	100.00
Almada	3	4.459	1.338	1.255	2.593	58.16
	2		0.169	1.000	1.170	84.39
	1		0.083	0.613	0.696	100.00
Sesimbra	3	1.440	0.874	0.261	1.135	78.85
	2		0.000	0.166	0.166	90.34
	1		0.000	0.139	0.139	100.00
Setúbal	3	8.855	0.080	5.405	5.485	61.94
	2		0.005	2.336	2.341	88.38
	1		0.001	1.028	1.029	100.00
Palmela	3	2.736	0.000	2.278	2.278	83.26
	2		0.000	0.278	0.278	93.38
	1		0.000	0.181	0.181	100.00
Alcácer do Sal	3	25.314	0.000	23.347	23.347	92.23
	2		0.000	1.375	1.375	97.66
	1		0.000	0.592	0.592	100.00
Grândola	3	6.225	4.123	0.908	5.030	80.80
	2		0.289	0.143	0.431	87.73
	1		0.298	0.466	0.764	100.00
Santiago do Cacém	3	2.224	0.782	0.885	1.667	74.96
	2		0.075	0.270	0.345	90.48
	1		0.078	0.134	0.212	100.00
Sines	3	1.849	1.552	0.000	1.552	83.92
	2		0.110	0.000	0.110	89.89
	1		0.187	0.000	0.187	100.00
Odemira	3	1.520	0.372	0.962	1.335	87.81
	2		0.019	0.099	0.118	95.56
	1		0.020	0.048	0.067	100.00
Aljezur	3	1.792	0.837	0.694	1.532	85.50
	2		0.022	0.151	0.172	95.11
	1		0.034	0.054	0.088	100.00
Vila do Bispo	3	0.513	0.485	0.000	0.485	94.54
	2		0.015	0.000	0.015	97.47
	1		0.013	0.000	0.013	100.00
Lagos	3	2.222	0.285	1.229	1.514	68.15
	2		0.030	0.371	0.401	86.20
	1		0.034	0.273	0.307	100.00
Portimão	3	2.272	0.158	1.598	1.755	77.27
	2		0.029	0.262	0.291	90.09
	1		0.025	0.200	0.225	100.00
Lagoa	3	0.595	0.079	0.407	0.486	81.66
	2		0.001	0.058	0.059	91.63
	1		0.000	0.049	0.050	100.00
Silves	3	1.606	0.117	0.915	1.032	64.27
	2		0.026	0.328	0.353	86.28
	1		0.020	0.201	0.220	100.00
Albufeira	3	0.659	0.365	0.082	0.447	67.87

	2		0.071	0.046	0.117	85.63
	1		0.047	0.047	0.095	100.00
Loulé	3	2.120	0.304	1.195	1.499	70.72
	2		0.138	0.205	0.344	86.93
	1		0.104	0.174	0.277	100.00
Faro	3	7.108	0.694	4.384	5.078	71.43
	2		0.093	1.038	1.131	87.34
	1		0.140	0.761	0.900	100.00
Olhão	3	5.913	0.278	3.879	4.157	70.29
	2		0.049	0.933	0.982	86.90
	1		0.049	0.726	0.775	100.00
Tavira	3	7.290	0.839	5.068	5.907	81.03
	2		0.071	0.766	0.837	92.50
	1		0.071	0.476	0.547	100.00
Vila Real de Santo António	3	5.349	0.588	2.922	3.510	65.63
	2		0.050	0.944	0.993	84.21
	1		0.062	0.783	0.845	100.00
Castro Marim	3	5.265	0.194	4.390	4.583	87.05
	2		0.018	0.386	0.404	94.73
	1		0.022	0.256	0.278	100.00

Table 31 – Same as in Table 29, but for the RCP8.5 scenario.

Coastal areas under CVI classification in Mainland Portugal			
2070 (RCP8.5)			
District	**Ocean-facing (km^2)**	**Inland (km^2)**	**Total (km^2)**
Viana do Castelo	1.14	9.67	10.8
Braga	1.60	1.41	3.01
Porto	4.87	0.69	5.56
Aveiro	5.51	50.2	55.7
Coimbra	6.88	5.11	12.0
Leiria	5.71	4.12	9.83
Santarém	0.00	122	122
Lisboa	0.99	213	214
Setúbal	10.4	71.3	81.7
Beja	0.847	1.14	1.99
Faro	11.2	36.3	47.5
Portugal	49.7	516	565

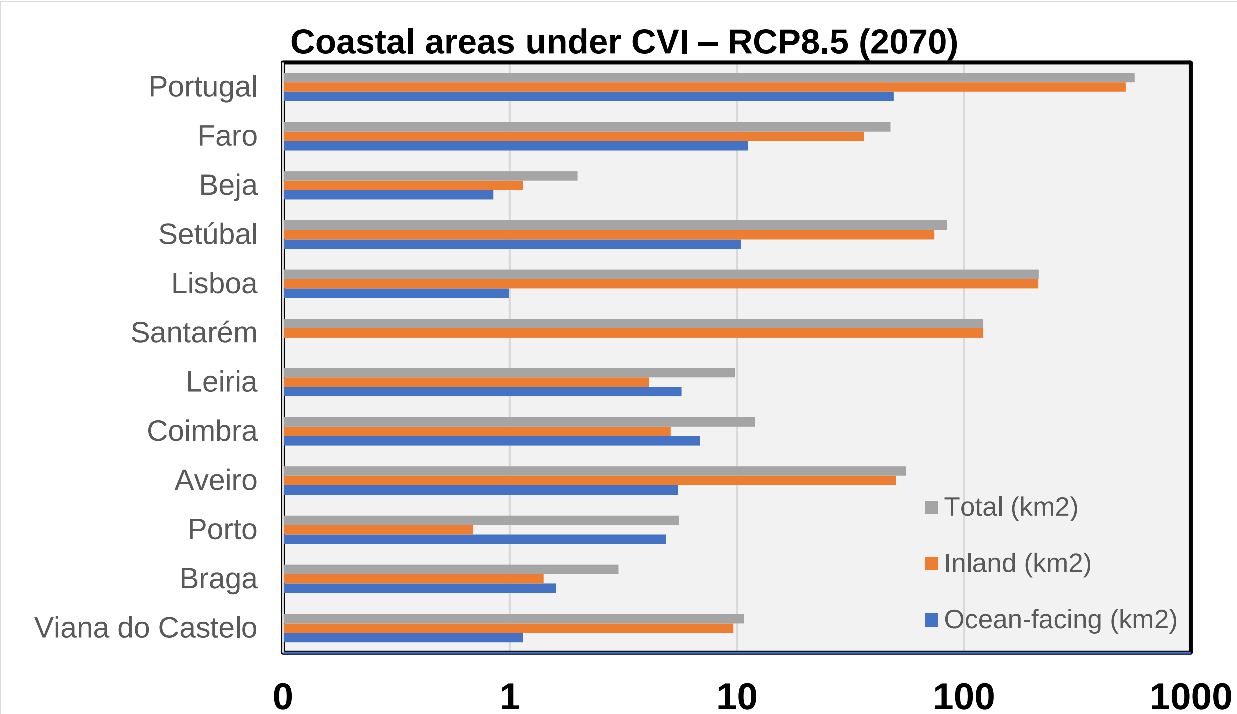

Figure 177 – Same as in Figure 176, but for the RCP8.5 scenario.

Table 32 – Same as in Table 30, but for the RCP8.5 scenario.

2070 RCP8.5						
Municipality	**CVI**	**Total area (km^2)**	**Ocean-facing coastlines (km^2)**	**Inland waters (km^2)**	**All coastlines (km^2)**	**Normalized area (%)**
Caminha	3	3.699	0.219	2.598	2.816	76.13
	2		0.007	0.527	0.534	90.57
	1		0.007	0.342	0.349	100.00
Viana do Castelo	3	7.114	0.842	3.938	4.780	67.19
	2		0.031	1.211	1.243	84.66
	1		0.035	1.057	1.092	100.00
Esposende	3	3.011	1.516	0.697	2.213	73.49
	2		0.042	0.376	0.418	87.36
	1		0.039	0.341	0.381	100.00
Póvoa de Varzim	3	1.166	1.049	0.010	1.058	90.76
	2		0.033	0.023	0.056	95.53
	1		0.035	0.017	0.052	100.00
Vila do Conde	3	1.438	1.008	0.193	1.201	83.47
	2		0.030	0.076	0.106	90.87
	1		0.028	0.103	0.131	100.00
Matosinhos	3	1.224	1.109	0.032	1.141	93.29
	2		0.033	0.012	0.045	96.96
	1		0.027	0.010	0.037	100.00
Porto	3	0.085	0.050	0.019	0.069	80.53
	2		0.002	0.005	0.007	88.57
	1		0.003	0.007	0.010	100.00

Vila Nova de Gaia	3	1.647	1.337	0.098	1.435	87.13
	2		0.055	0.036	0.091	92.68
	1		0.071	0.050	0.121	100.00
Espinho	3	1.010	0.596	0.207	0.804	79.60
	2		0.007	0.057	0.064	85.98
	1		0.014	0.127	0.142	100.00
Ovar	3	5.277	0.905	2.831	3.736	70.81
	2		0.020	0.750	0.771	85.41
	1		0.032	0.737	0.770	100.00
Murtosa	3	14.394	0.055	8.272	8.328	57.86
	2		0.018	2.939	2.957	78.40
	1		0.024	3.086	3.110	100.00
Estarreja	3	3.731	0.000	2.441	2.441	65.42
	2		0.000	0.650	0.650	82.84
	1		0.000	0.640	0.640	100.00
Aveiro	3	12.735	2.701	6.224	8.925	70.08
	2		0.021	1.759	1.780	84.06
	1		0.024	2.006	2.030	100.00
Albergaria-a-Velha	3	6.989	0.000	5.290	5.290	75.68
	2		0.000	0.940	0.940	89.14
	1		0.000	0.759	0.759	100.00
Ílhavo	3	7.498	0.788	3.592	4.381	58.43
	2		0.014	1.281	1.296	75.71
	1		0.021	1.800	1.821	100.00
Vagos	3	5.092	0.862	2.830	3.691	72.49
	2		0.010	0.687	0.697	86.18
	1		0.014	0.690	0.704	100.00
Mira	3	3.064	1.245	0.921	2.166	70.70
	2		0.032	0.368	0.400	83.75
	1		0.028	0.470	0.498	100.00
Cantanhede	3	0.808	0.772	0.000	0.772	95.54
	2		0.014	0.000	0.014	97.30
	1		0.022	0.000	0.022	100.00
Figueira da Foz	3	8.112	4.590	2.235	6.824	84.12
	2		0.082	0.482	0.564	91.08
	1		0.093	0.630	0.724	100.00
Pombal	3	0.364	0.283	0.000	0.283	77.65
	2		0.044	0.000	0.044	89.62
	1		0.038	0.000	0.038	100.00
Leiria	3	0.575	0.480	0.000	0.480	83.47
	2		0.046	0.000	0.046	91.51
	1		0.049	0.000	0.049	100.00
Marinha Grande	3	1.883	1.583	0.067	1.650	87.66
	2		0.088	0.022	0.110	93.51
	1		0.084	0.038	0.122	100.00
Alcobaça	3	2.643	1.335	0.552	1.887	71.41
	2		0.015	0.342	0.357	84.91
	1		0.014	0.385	0.399	100.00
Nazaré	3	1.526	0.611	0.511	1.122	73.52
	2		0.084	0.106	0.190	85.97
	1		0.077	0.137	0.214	100.00
Caldas da Rainha	3	0.467	0.005	0.213	0.218	46.70
	2		0.000	0.120	0.120	72.51
	1		0.001	0.127	0.128	100.00
Óbidos	3	1.706	0.174	0.999	1.173	68.79
	2		0.019	0.253	0.273	84.76
	1		0.010	0.249	0.260	100.00
Peniche	3	0.667	0.595	0.000	0.595	89.25
	2		0.035	0.000	0.035	94.52

	1		0.037	0.000	0.037	100.04
Lourinhã	3	0.287	0.270	0.000	0.270	93.90
	2		0.012	0.000	0.012	97.97
	1		0.006	0.000	0.006	100.00
Torres Vedras	3	0.310	0.149	0.128	0.277	89.46
	2		0.000	0.018	0.018	95.33
	1		0.000	0.014	0.014	100.00
Mafra	3	0.108	0.016	0.080	0.096	88.69
	2		0.000	0.007	0.007	94.92
	1		0.000	0.006	0.006	100.00
Sintra	3	0.337	0.318	0.000	0.318	94.37
	2		0.011	0.000	0.011	97.78
	1		0.007	0.000	0.007	100.00
Cascais	3	0.193	0.178	0.000	0.178	92.29
	2		0.008	0.000	0.008	96.56
	1		0.007	0.000	0.007	100.00
Oeiras	3	0.363	0.000	0.254	0.254	69.82
	2		0.000	0.060	0.060	86.40
	1		0.000	0.049	0.049	100.00
Lisboa	3	0.955	0.000	0.329	0.329	34.48
	2		0.000	0.259	0.259	61.62
	1		0.000	0.367	0.367	100.00
Loures	3	6.014	0.000	4.392	4.392	73.03
	2		0.000	0.904	0.904	88.07
	1		0.000	0.717	0.717	100.00
Vila Franca de Xira	3	152.820	0.000	146.811	146.811	96.07
	2		0.000	3.917	3.917	98.63
	1		0.000	2.092	2.092	100.00
Alenquer	3	4.638	0.000	4.005	4.005	86.36
	2		0.000	0.419	0.419	95.39
	1		0.000	0.214	0.214	100.00
Azambuja	3	48.378	0.000	42.890	42.890	88.66
	2		0.000	3.201	3.201	95.27
	1		0.000	2.288	2.288	100.00
Cartaxo	3	18.941	0.000	14.642	14.642	77.30
	2		0.000	2.617	2.617	91.12
	1		0.000	1.683	1.683	100.00
Santarém	3	0.676	0.000	0.309	0.309	45.63
	2		0.000	0.205	0.205	75.99
	1		0.000	0.162	0.162	100.00
Alpiarça	3	0.001	0.000	0.000	0.000	0.00
	2		0.000	0.000	0.000	28.05
	1		0.000	0.001	0.001	100.00
Almeirim	3	0.426	0.000	0.269	0.269	63.16
	2		0.000	0.075	0.075	80.80
	1		0.000	0.082	0.082	100.00
Salvaterra de Magos	3	13.376	0.000	9.896	9.896	73.98
	2		0.000	2.192	2.192	90.37
	1		0.000	1.288	1.288	100.00
Coruche	3	0.029	0.000	0.006	0.006	21.02
	2		0.000	0.011	0.011	59.55
	1		0.000	0.012	0.012	100.00
Benavente	3	88.446	0.000	79.222	79.222	89.57
	2		0.000	5.894	5.894	96.23
	1		0.000	3.331	3.331	100.00
Alcochete	3	12.170	0.000	11.253	11.253	92.47
	2		0.000	0.577	0.577	97.21
	1		0.000	0.340	0.340	100.00
Montijo	3	3.777	0.000	2.654	2.654	70.26

	2		0.000	0.770	0.770	90.66
	1		0.000	0.353	0.353	100.00
Moita	3	4.438	0.000	3.614	3.614	81.43
	2		0.000	0.506	0.506	92.84
	1		0.000	0.318	0.318	100.00
Barreiro	3	2.657	0.000	1.326	1.326	49.91
	2		0.000	0.638	0.638	73.94
	1		0.000	0.692	0.692	100.00
Seixal	3	3.532	0.000	2.900	2.900	82.12
	2		0.000	0.383	0.383	92.97
	1		0.000	0.248	0.248	100.00
Almada	3	4.650	1.558	1.496	3.054	65.67
	2		0.137	0.975	1.111	89.57
	1		0.086	0.399	0.485	100.00
Sesimbra	3	0.981	0.593	0.281	0.873	89.03
	2		0.000	0.056	0.056	94.77
	1		0.000	0.052	0.052	100.05
Setúbal	3	9.314	0.051	6.005	6.055	65.01
	2		0.006	2.043	2.049	87.01
	1		0.005	1.205	1.209	100.00
Palmela	3	2.859	0.000	2.348	2.348	82.13
	2		0.000	0.265	0.265	91.39
	1		0.000	0.246	0.246	100.00
Alcácer do Sal	3	25.654	0.000	23.779	23.779	92.69
	2		0.000	1.157	1.157	97.20
	1		0.000	0.719	0.719	100.00
Grândola	3	7.336	4.572	1.404	5.977	81.47
	2		0.242	0.225	0.466	87.83
	1		0.263	0.630	0.893	100.00
Santiago do Cacém	3	3.122	1.547	0.958	2.504	80.21
	2		0.082	0.239	0.322	90.51
	1		0.073	0.223	0.296	100.00
Sines	3	1.184	0.929	0.000	0.929	78.43
	2		0.090	0.000	0.090	86.02
	1		0.166	0.000	0.166	100.00
Odemira	3	1.989	0.808	0.988	1.796	90.32
	2		0.020	0.087	0.108	95.73
	1		0.019	0.066	0.085	100.00
Aljezur	3	2.036	1.061	0.739	1.800	88.41
	2		0.019	0.117	0.136	95.11
	1		0.028	0.071	0.100	100.00
Vila do Bispo	3	0.616	0.594	0.000	0.594	96.39
	2		0.010	0.000	0.010	97.99
	1		0.012	0.000	0.012	99.92
Lagos	3	2.586	0.624	1.346	1.970	76.15
	2		0.045	0.321	0.366	90.30
	1		0.045	0.206	0.251	100.00
Portimão	3	2.728	0.570	1.685	2.255	82.67
	2		0.050	0.223	0.273	92.67
	1		0.047	0.153	0.200	100.00
Lagoa	3	0.624	0.109	0.424	0.533	85.46
	2		0.000	0.051	0.052	93.75
	1		0.000	0.039	0.039	100.00
Silves	3	1.651	0.155	1.027	1.182	71.62
	2		0.024	0.267	0.291	89.24
	1		0.028	0.149	0.178	100.00
Albufeira	3	0.829	0.544	0.091	0.635	76.58
	2		0.064	0.047	0.110	89.89
	1		0.046	0.037	0.084	100.00

Loulé	3	2.235	0.390	1.264	1.654	74.03
	2		0.152	0.175	0.326	88.64
	1		0.116	0.138	0.254	100.00
Faro	3	8.789	2.101	4.738	6.839	77.82
	2		0.243	0.884	1.127	90.65
	1		0.249	0.573	0.822	100.00
Olhão	3	7.160	1.534	4.168	5.702	79.64
	2		0.038	0.825	0.863	91.69
	1		0.044	0.552	0.595	100.00
Tavira	3	6.718	0.254	5.345	5.599	83.35
	2		0.083	0.620	0.702	93.80
	1		0.065	0.351	0.416	100.00
Vila Real de Santo António	3	5.285	0.452	3.211	3.664	69.31
	2		0.086	0.848	0.934	86.98
	1		0.098	0.590	0.688	100.00
Castro Marim	3	6.242	1.152	4.525	5.677	90.95
	2		0.029	0.314	0.343	96.44
	1		0.028	0.194	0.222	100.00

Table 33 – Same as in Table 29, but for 2100 under the RCP4.5 scenario.

Coastal areas under CVI classification in Mainland Portugal			
2100 (RCP4.5)			
District	**Ocean-facing (km^2)**	**Inland (km^2)**	**Total (km^2)**
Viana do Castelo	1.37	10.6	12.0
Braga	1.83	1.65	3.48
Porto	5.74	0.84	6.57
Aveiro	6.59	53.8	60.3
Coimbra	7.17	5.42	12.6
Leiria	6.07	4.44	10.5
Santarém	0.00	126	126
Lisboa	1.03	217	218
Setúbal	12.4	73.7	86.0
Beja	0.921	1.17	2.15
Faro	11.6	38.3	49.9
Portugal	54.7	532	587

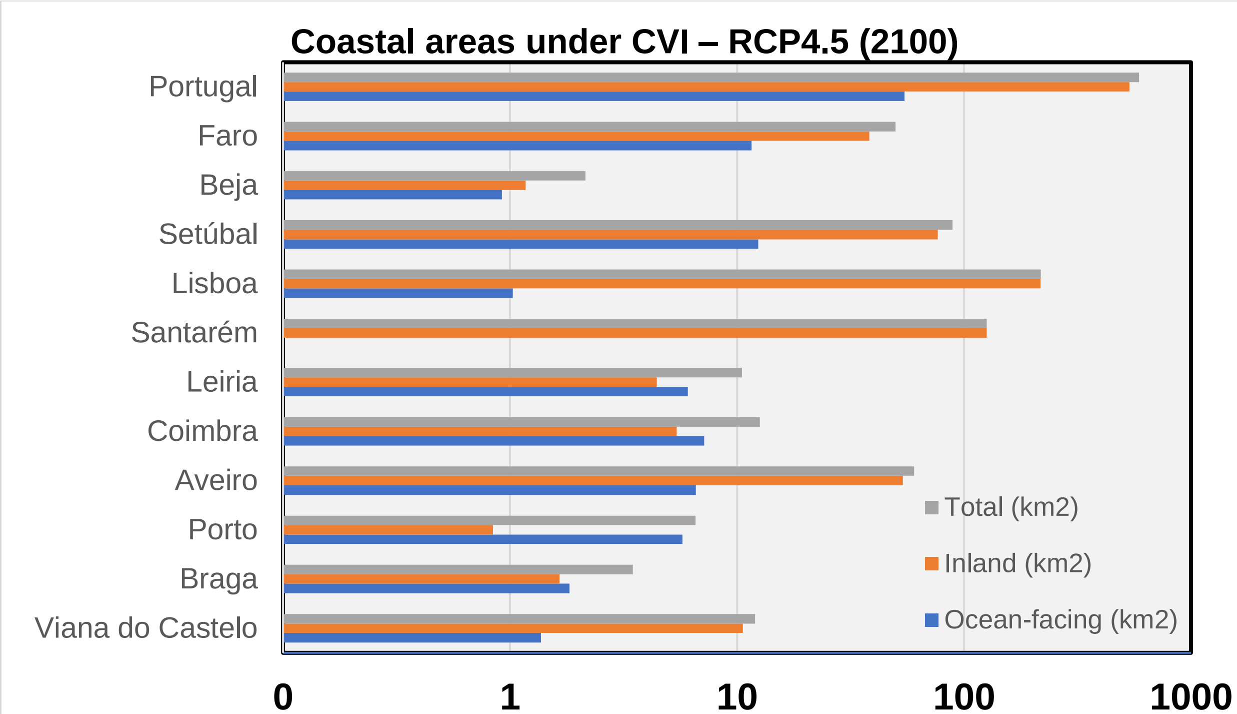

Figure 178 – Same as in Figure 176, but for 2100 under the RCP4.5 scenario.

Table 34 – Same as in Table 30, but for 2100 under the RCP4.5 scenario.

2100 RCP4.5						
Municipality	**CVI**	**Total area (km^2)**	**Ocean-facing coastlines (km^2)**	**Inland waters (km^2)**	**All coastlines (km^2)**	**Normalized area (%)**
Caminha	3	3.951	0.253	2.854	3.107	78.64
	2		0.010	0.467	0.478	90.73
	1		0.011	0.355	0.366	100.00
Viana do Castelo	3	8.048	0.982	4.468	5.449	67.72
	2		0.058	1.253	1.311	84.01
	1		0.059	1.228	1.287	100.00
Esposende	3	3.478	1.702	0.851	2.553	73.42
	2		0.063	0.397	0.460	86.66
	1		0.064	0.400	0.464	100.00
Póvoa de Varzim	3	1.397	1.228	0.015	1.243	88.99
	2		0.053	0.028	0.081	94.80
	1		0.053	0.020	0.073	100.00
Vila do Conde	3	1.680	1.144	0.224	1.368	81.46
	2		0.041	0.101	0.142	89.90
	1		0.038	0.131	0.170	100.00
Matosinhos	3	1.389	1.244	0.037	1.281	92.25
	2		0.043	0.013	0.056	96.26
	1		0.042	0.010	0.052	100.00
Porto	3	0.106	0.063	0.020	0.083	78.25
	2		0.004	0.007	0.011	88.37
	1		0.004	0.009	0.012	100.00
	3	2.002	1.589	0.107	1.696	84.74

Vila Nova de Gaia	2		0.097	0.058	0.155	92.48
	1		0.096	0.055	0.151	100.00
Espinho	3	1.114	0.644	0.222	0.866	77.74
	2		0.017	0.107	0.124	88.91
	1		0.011	0.113	0.124	100.00
Ovar	3	5.577	0.971	3.084	4.056	72.73
	2		0.036	0.892	0.928	89.37
	1		0.024	0.569	0.593	100.00
Murtosa	3	15.440	0.093	9.278	9.371	60.70
	2		0.030	3.493	3.523	83.52
	1		0.025	2.520	2.545	100.00
Estarreja	3	3.933	0.000	2.661	2.661	67.65
	2		0.000	0.813	0.813	88.31
	1		0.000	0.460	0.460	100.00
Aveiro	3	13.503	2.863	6.822	9.684	71.72
	2		0.029	2.138	2.167	87.77
	1		0.032	1.620	1.652	100.00
Albergaria-a-Velha	3	7.186	0.000	5.651	5.651	78.64
	2		0.000	0.991	0.991	92.43
	1		0.000	0.544	0.544	100.00
Ílhavo	3	8.245	0.834	4.032	4.867	59.02
	2		0.022	1.657	1.678	79.38
	1		0.017	1.683	1.701	100.00
Vagos	3	5.344	0.902	3.063	3.965	74.19
	2		0.020	0.799	0.819	89.52
	1		0.015	0.545	0.560	100.00
Mira	3	3.224	1.276	1.034	2.310	71.64
	2		0.042	0.495	0.537	88.30
	1		0.035	0.342	0.377	100.00
Cantanhede	3	0.875	0.821	0.000	0.821	93.83
	2		0.034	0.000	0.034	97.71
	1		0.020	0.000	0.020	100.00
Figueira da Foz	3	8.491	4.769	2.346	7.115	83.80
	2		0.089	0.370	0.459	89.20
	1		0.083	0.834	0.917	100.00
Pombal	3	0.407	0.309	0.000	0.309	76.03
	2		0.046	0.000	0.046	87.40
	1		0.051	0.000	0.051	100.00
Leiria	3	0.613	0.519	0.000	0.519	84.66
	2		0.050	0.000	0.050	92.87
	1		0.044	0.000	0.044	100.00
Marinha Grande	3	1.979	1.676	0.072	1.748	88.34
	2		0.084	0.017	0.101	93.47
	1		0.075	0.054	0.129	100.00
Alcobaça	3	2.837	1.398	0.632	2.029	71.55
	2		0.016	0.263	0.279	81.37
	1		0.013	0.515	0.529	100.00
Nazaré	3	1.664	0.694	0.538	1.231	74.00
	2		0.083	0.080	0.163	83.78
	1		0.075	0.195	0.270	100.00
Caldas da Rainha	3	0.522	0.002	0.239	0.241	46.11
	2		0.010	0.094	0.104	66.10
	1		0.011	0.166	0.177	100.00
Óbidos	3	1.768	0.184	1.062	1.245	70.44
	2		0.003	0.190	0.193	81.39
	1		0.003	0.326	0.329	100.00
Peniche	3	0.725	0.631	0.000	0.631	87.09
	2		0.047	0.000	0.047	93.51
	1		0.047	0.000	0.047	99.99

Lourinhã	3	0.292	0.277	0.000	0.277	95.04
	2		0.006	0.000	0.006	97.21
	1		0.008	0.000	0.008	100.00
Torres Vedras	3	0.333	0.150	0.150	0.301	90.39
	2		0.000	0.021	0.021	96.64
	1		0.000	0.011	0.011	100.00
Mafra	3	0.127	0.023	0.089	0.111	87.31
	2		0.000	0.008	0.008	93.48
	1		0.000	0.008	0.008	100.00
Sintra	3	0.350	0.333	0.000	0.333	95.17
	2		0.010	0.000	0.010	97.94
	1		0.007	0.000	0.007	100.00
Cascais	3	0.218	0.195	0.000	0.195	89.21
	2		0.012	0.000	0.012	94.74
	1		0.011	0.000	0.011	100.00
Oeiras	3	0.391	0.000	0.273	0.273	69.84
	2		0.000	0.068	0.068	87.31
	1		0.000	0.050	0.050	100.00
Lisboa	3	1.234	0.000	0.415	0.415	33.59
	2		0.000	0.404	0.404	66.35
	1		0.000	0.415	0.415	100.00
Loures	3	6.407	0.000	4.825	4.825	75.31
	2		0.000	0.976	0.976	90.56
	1		0.000	0.605	0.605	100.00
Vila Franca de Xira	3	154.054	0.000	148.893	148.893	96.65
	2		0.000	3.273	3.273	98.77
	1		0.000	1.889	1.889	100.00
Alenquer	3	4.754	0.000	4.211	4.211	88.58
	2		0.000	0.362	0.362	96.20
	1		0.000	0.181	0.181	100.00
Azambuja	3	49.604	0.000	44.522	44.522	89.75
	2		0.000	3.098	3.098	96.00
	1		0.000	1.985	1.985	100.00
Cartaxo	3	19.982	0.000	15.840	15.840	79.27
	2		0.000	2.563	2.563	92.10
	1		0.000	1.579	1.579	100.00
Santarém	3	0.763	0.000	0.398	0.398	52.19
	2		0.000	0.222	0.222	81.32
	1		0.000	0.143	0.143	100.00
Alpiarça	3	0.003	0.000	0.000	0.000	0.00
	2		0.000	0.001	0.001	26.21
	1		0.000	0.002	0.002	100.00
Almeirim	3	0.502	0.000	0.319	0.319	63.54
	2		0.000	0.101	0.101	83.58
	1		0.000	0.082	0.082	100.00
Salvaterra de Magos	3	14.085	0.000	10.992	10.992	78.04
	2		0.000	2.001	2.001	92.24
	1		0.000	1.093	1.093	100.00
Coruche	3	0.050	0.000	0.010	0.010	20.12
	2		0.000	0.016	0.016	51.80
	1		0.000	0.024	0.024	100.00
Benavente	3	90.423	0.000	81.670	81.670	90.32
	2		0.000	5.813	5.813	96.75
	1		0.000	2.939	2.939	100.00
Alcochete	3	12.386	0.000	11.550	11.550	93.25
	2		0.000	0.541	0.541	97.62
	1		0.000	0.295	0.295	100.00
Montijo	3	3.989	0.000	3.039	3.039	76.18
	2		0.000	0.642	0.642	92.27

	1		0.000	0.308	0.308	100.00
Moita	3	4.630	0.000	3.860	3.860	83.37
	2		0.000	0.486	0.486	93.86
	1		0.000	0.284	0.284	100.00
Barreiro	3	2.973	0.000	1.519	1.519	51.11
	2		0.000	0.934	0.934	82.53
	1		0.000	0.519	0.519	100.00
Seixal	3	3.657	0.000	3.073	3.073	84.05
	2		0.000	0.386	0.386	94.60
	1		0.000	0.197	0.197	100.00
Almada	3	5.100	1.852	1.989	3.841	75.31
	2		0.098	0.779	0.877	92.51
	1		0.092	0.290	0.382	100.00
Sesimbra	3	1.156	0.692	0.326	1.018	88.02
	2		0.000	0.075	0.075	94.49
	1		0.000	0.064	0.064	100.03
Setúbal	3	9.665	0.062	7.252	7.314	75.68
	2		0.003	1.710	1.713	93.40
	1		0.001	0.637	0.638	100.00
Palmela	3	2.949	0.000	2.489	2.489	84.42
	2		0.000	0.296	0.296	94.45
	1		0.000	0.164	0.164	100.00
Alcácer do Sal	3	25.940	0.000	24.444	24.444	94.23
	2		0.000	1.019	1.019	98.16
	1		0.000	0.478	0.478	100.00
Grândola	3	8.538	5.376	1.521	6.898	80.79
	2		0.382	0.616	0.998	92.47
	1		0.327	0.316	0.643	100.00
Santiago do Cacém	3	3.552	1.815	1.097	2.912	81.99
	2		0.086	0.240	0.325	91.16
	1		0.077	0.237	0.314	100.00
Sines	3	1.501	1.187	0.000	1.187	79.03
	2		0.161	0.000	0.161	89.75
	1		0.154	0.000	0.154	100.00
Odemira	3	2.095	0.868	1.038	1.906	91.01
	2		0.027	0.080	0.108	96.15
	1		0.026	0.055	0.081	100.00
Aljezur	3	2.149	1.115	0.810	1.925	89.59
	2		0.039	0.091	0.130	95.64
	1		0.034	0.059	0.094	100.00
Vila do Bispo	3	0.625	0.604	0.000	0.604	96.70
	2		0.010	0.000	0.010	98.31
	1		0.011	0.000	0.011	99.99
Lagos	3	2.722	0.649	1.550	2.199	80.79
	2		0.033	0.323	0.356	93.88
	1		0.028	0.138	0.167	100.00
Portimão	3	2.869	0.628	1.824	2.452	85.48
	2		0.028	0.236	0.264	94.67
	1		0.038	0.115	0.153	100.00
Lagoa	3	0.666	0.103	0.470	0.573	86.00
	2		0.000	0.059	0.059	94.82
	1		0.000	0.034	0.034	100.00
Silves	3	1.761	0.178	1.204	1.383	78.51
	2		0.017	0.239	0.256	93.06
	1		0.018	0.104	0.122	100.00
Albufeira	3	0.879	0.613	0.123	0.736	83.67
	2		0.030	0.054	0.084	93.19
	1		0.024	0.036	0.060	100.00
Loulé	3	2.376	0.562	1.379	1.941	81.69

	2		0.069	0.204	0.273	93.16
	1		0.061	0.102	0.162	100.00
Faro	3	9.355	2.501	5.328	7.829	83.68
	2		0.135	0.890	1.025	94.64
	1		0.112	0.389	0.501	100.00
Olhão	3	7.568	1.703	4.588	6.291	83.12
	2		0.050	0.831	0.881	94.77
	1		0.039	0.357	0.396	100.00
Tavira	3	6.928	0.239	5.781	6.020	86.89
	2		0.059	0.564	0.623	95.89
	1		0.051	0.234	0.285	100.00
Vila Real de Santo António	3	5.641	0.477	3.749	4.225	74.90
	2		0.057	0.924	0.981	92.29
	1		0.055	0.380	0.435	100.00
Castro Marim	3	6.398	1.202	4.730	5.932	92.72
	2		0.017	0.303	0.321	97.73
	1		0.014	0.131	0.145	100.00

Table 35 – Same as in Table 29, but for 2100 under the RCP8.5 scenario.

Coastal areas under CVI classification in Mainland Portugal			
2100 (RCP8.5)			
District	**Ocean-facing (km^2)**	**Inland (km^2)**	**Total (km^2)**
Viana do Castelo	1.54	11.1	12.6
Braga	1.91	1.77	3.69
Porto	6.19	0.92	7.11
Aveiro	6.53	54.5	61.1
Coimbra	7.55	5.77	13.3
Leiria	6.50	4.75	11.3
Santarém	0.00	131	131
Lisboa	0.97	220	221
Setúbal	11.4	76.2	87.5
Beja	0.861	1.20	2.07
Faro	12.5	40.8	53.3
Portugal	55.9	548	604

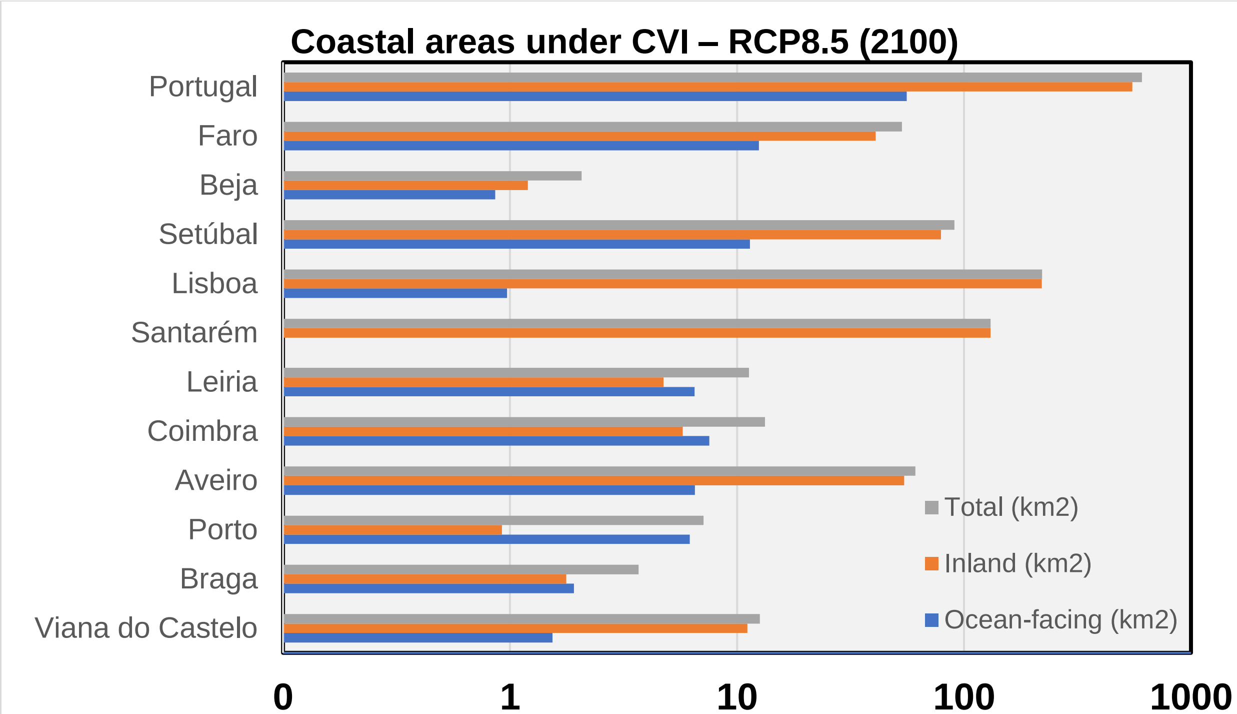

Figure 179 – Same as in Figure 176, but for 2100 under the RCP8.5 scenario.

Table 36 – Same as in Table 30, but for 2100 under the RCP8.5 scenario.

2100 RCP8.5						
Municipality	**CVI**	**Total area (km^2)**	**Ocean-facing coastlines (km^2)**	**Inland waters (km^2)**	**All coastlines (km^2)**	**Normalized area (%)**
Caminha	3	4.068	0.264	3.076	3.340	82.08
	2		0.013	0.391	0.404	92.01
	1		0.014	0.311	0.325	100.00
Viana do Castelo	3	8.562	1.060	5.025	6.085	71.07
	2		0.099	1.174	1.273	85.93
	1		0.086	1.119	1.204	100.00
Esposende	3	3.685	1.748	1.028	2.776	75.34
	2		0.082	0.377	0.459	87.79
	1		0.081	0.369	0.450	100.00
Póvoa de Varzim	3	1.488	1.278	0.029	1.307	87.88
	2		0.068	0.020	0.088	93.81
	1		0.068	0.025	0.092	100.00
Vila do Conde	3	1.797	1.185	0.261	1.446	80.47
	2		0.050	0.112	0.162	89.47
	1		0.053	0.136	0.189	100.00
Matosinhos	3	1.452	1.276	0.043	1.319	90.87
	2		0.056	0.011	0.067	95.45
	1		0.058	0.008	0.066	100.00
Porto	3	0.109	0.059	0.023	0.083	76.02
	2		0.004	0.007	0.011	86.08
	1		0.006	0.009	0.015	100.00

Vila Nova de Gaia	3	2.262	1.723	0.133	1.855	82.04
	2		0.155	0.051	0.206	91.13
	1		0.146	0.055	0.201	100.00
Espinho	3	1.217	0.680	0.265	0.945	77.62
	2		0.017	0.128	0.144	89.47
	1		0.015	0.113	0.128	100.00
Ovar	3	5.787	0.693	3.577	4.269	73.78
	2		0.207	0.737	0.943	90.08
	1		0.125	0.449	0.574	100.00
Murtosa	3	15.527	0.000	9.448	9.448	60.85
	2		0.446	3.086	3.531	83.59
	1		0.565	1.982	2.548	100.00
Estarreja	3	3.929	0.000	2.658	2.658	67.66
	2		0.000	0.812	0.812	88.33
	1		0.000	0.458	0.458	100.00
Aveiro	3	13.653	1.852	7.982	9.834	72.03
	2		0.167	2.006	2.173	87.94
	1		0.502	1.144	1.647	100.00
Albergaria-a-Velha	3	7.183	0.000	5.650	5.650	78.66
	2		0.000	0.990	0.990	92.44
	1		0.000	0.543	0.543	100.00
Ílhavo	3	8.330	0.076	4.873	4.949	59.41
	2		0.000	1.681	1.681	79.59
	1		0.350	1.350	1.701	100.00
Vagos	3	5.446	0.544	3.516	4.060	74.56
	2		0.133	0.690	0.823	89.67
	1		0.159	0.404	0.563	100.00
Mira	3	3.417	1.194	1.288	2.483	72.66
	2		0.083	0.470	0.554	88.87
	1		0.151	0.230	0.380	100.00
Cantanhede	3	0.910	0.863	0.000	0.863	94.78
	2		0.026	0.000	0.026	97.63
	1		0.022	0.000	0.022	100.00
Figueira da Foz	3	8.990	4.857	2.772	7.630	84.87
	2		0.177	0.575	0.752	93.23
	1		0.179	0.429	0.608	100.00
Pombal	3	0.532	0.299	0.000	0.299	56.20
	2		0.096	0.000	0.096	74.18
	1		0.137	0.000	0.137	100.00
Leiria	3	0.708	0.523	0.000	0.523	73.79
	2		0.091	0.000	0.091	86.63
	1		0.095	0.000	0.095	100.00
Marinha Grande	3	2.043	1.647	0.092	1.739	85.11
	2		0.126	0.036	0.162	93.02
	1		0.113	0.029	0.143	100.00
Alcobaça	3	2.972	1.380	0.932	2.312	77.79
	2		0.025	0.348	0.373	90.33
	1		0.015	0.272	0.287	100.00
Nazaré	3	1.797	0.706	0.628	1.334	74.22
	2		0.127	0.127	0.253	88.32
	1		0.109	0.101	0.210	100.00
Caldas da Rainha	3	0.565	0.007	0.347	0.354	62.78
	2		0.002	0.114	0.116	83.31
	1		0.017	0.077	0.094	100.00
Óbidos	3	1.871	0.190	1.278	1.468	78.47
	2		0.033	0.223	0.256	92.16
	1		0.000	0.147	0.147	100.00
Peniche	3	0.762	0.642	0.000	0.642	84.26
	2		0.056	0.000	0.056	91.66

	1		0.063	0.000	0.063	99.99
Lourinhã	3	0.295	0.283	0.000	0.283	95.90
	2		0.008	0.000	0.008	98.53
	1		0.004	0.000	0.004	100.00
Torres Vedras	3	0.315	0.121	0.177	0.297	94.23
	2		0.000	0.008	0.008	96.61
	1		0.000	0.011	0.011	100.00
Mafra	3	0.120	0.008	0.100	0.108	90.15
	2		0.000	0.007	0.007	95.65
	1		0.000	0.005	0.005	100.00
Sintra	3	0.343	0.320	0.000	0.320	93.18
	2		0.016	0.000	0.016	97.79
	1		0.008	0.000	0.008	100.00
Cascais	3	0.198	0.183	0.000	0.183	92.21
	2		0.008	0.000	0.008	96.11
	1		0.008	0.000	0.008	100.00
Oeiras	3	0.441	0.000	0.318	0.318	72.04
	2		0.000	0.077	0.077	89.42
	1		0.000	0.047	0.047	100.00
Lisboa	3	1.647	0.000	0.620	0.620	37.65
	2		0.000	0.627	0.627	75.70
	1		0.000	0.400	0.400	100.00
Loures	3	6.866	0.000	5.383	5.383	78.41
	2		0.000	1.032	1.032	93.44
	1		0.000	0.450	0.450	100.00
Vila Franca de Xira	3	155.620	0.000	150.961	150.961	97.01
	2		0.000	3.109	3.109	99.00
	1		0.000	1.550	1.550	100.00
Alenquer	3	4.933	0.000	4.451	4.451	90.24
	2		0.000	0.310	0.310	96.52
	1		0.000	0.172	0.172	100.00
Azambuja	3	50.588	0.000	46.315	46.315	91.55
	2		0.000	3.294	3.294	98.06
	1		0.000	0.979	0.979	100.00
Cartaxo	3	21.270	0.000	17.439	17.439	81.99
	2		0.000	2.554	2.554	94.00
	1		0.000	1.277	1.277	100.00
Santarém	3	0.899	0.000	0.532	0.532	59.15
	2		0.000	0.236	0.236	85.41
	1		0.000	0.131	0.131	100.00
Alpiarça	3	0.004	0.000	0.000	0.000	6.70
	2		0.000	0.002	0.002	60.95
	1		0.000	0.002	0.002	100.00
Almeirim	3	0.586	0.000	0.356	0.356	60.71
	2		0.000	0.129	0.129	82.69
	1		0.000	0.101	0.101	100.00
Salvaterra de Magos	3	14.879	0.000	12.240	12.240	82.27
	2		0.000	1.842	1.842	94.64
	1		0.000	0.797	0.797	100.00
Coruche	3	0.074	0.000	0.018	0.018	23.65
	2		0.000	0.032	0.032	67.05
	1		0.000	0.024	0.024	100.00
Benavente	3	92.762	0.000	85.523	85.523	92.20
	2		0.000	4.898	4.898	97.48
	1		0.000	2.342	2.342	100.00
Alcochete	3	12.605	0.000	11.882	11.882	94.27
	2		0.000	0.493	0.493	98.18
	1		0.000	0.229	0.229	100.00
Montijo	3	4.216	0.000	3.467	3.467	82.22

	2		0.000	0.518	0.518	94.50
	1		0.000	0.232	0.232	100.00
Moita	3	4.864	0.000	4.163	4.163	85.60
	2		0.000	0.470	0.470	95.27
	1		0.000	0.230	0.230	100.00
Barreiro	3	3.280	0.000	2.040	2.040	62.20
	2		0.000	0.935	0.935	90.72
	1		0.000	0.304	0.304	100.00
Seixal	3	3.804	0.000	3.316	3.316	87.17
	2		0.000	0.346	0.346	96.28
	1		0.000	0.142	0.142	100.00
Almada	3	5.124	1.672	2.528	4.200	81.97
	2		0.122	0.531	0.653	94.71
	1		0.062	0.209	0.271	100.00
Sesimbra	3	1.050	0.509	0.426	0.934	89.00
	2		0.000	0.060	0.060	94.73
	1		0.000	0.055	0.055	99.98
Setúbal	3	10.007	0.060	8.557	8.617	86.11
	2		0.000	0.939	0.939	95.49
	1		0.000	0.451	0.451	100.00
Palmela	3	3.057	0.000	2.711	2.711	88.70
	2		0.000	0.224	0.224	96.03
	1		0.000	0.121	0.121	100.00
Alcácer do Sal	3	26.233	0.000	25.249	25.249	96.25
	2		0.000	0.619	0.619	98.61
	1		0.000	0.365	0.365	100.00
Grândola	3	8.284	5.078	1.717	6.795	82.03
	2		0.309	0.686	0.995	94.04
	1		0.266	0.228	0.494	100.00
Santiago do Cacém	3	3.632	1.775	1.264	3.039	83.68
	2		0.072	0.261	0.332	92.83
	1		0.066	0.195	0.260	100.00
Sines	3	1.371	1.082	0.000	1.082	78.96
	2		0.146	0.000	0.146	89.59
	1		0.143	0.000	0.143	100.00
Odemira	3	2.065	0.818	1.099	1.918	92.86
	2		0.024	0.065	0.089	97.18
	1		0.019	0.039	0.058	100.00
Aljezur	3	2.200	1.118	0.879	1.998	90.80
	2		0.059	0.070	0.129	96.66
	1		0.026	0.047	0.073	100.00
Vila do Bispo	3	0.631	0.611	0.000	0.611	96.86
	2		0.011	0.000	0.011	98.55
	1		0.009	0.000	0.009	99.99
Lagos	3	3.004	0.676	1.842	2.518	83.84
	2		0.039	0.257	0.296	93.70
	1		0.039	0.150	0.189	100.00
Portimão	3	3.119	0.658	2.037	2.694	86.38
	2		0.039	0.211	0.250	94.40
	1		0.047	0.128	0.175	100.00
Lagoa	3	0.740	0.119	0.508	0.628	84.81
	2		0.000	0.064	0.064	93.47
	1		0.000	0.048	0.048	100.00
Silves	3	1.018	0.195	0.502	0.697	68.48
	2		0.018	0.185	0.202	88.33
	1		0.016	0.103	0.119	100.00
Albufeira	3	1.010	0.654	0.161	0.815	80.73
	2		0.033	0.070	0.104	90.99
	1		0.026	0.065	0.091	100.00

Loulé	3	2.617	0.650	1.499	2.149	82.12
	2		0.090	0.184	0.274	92.59
	1		0.079	0.115	0.194	100.00
Faro	3	10.158	2.930	5.846	8.775	86.39
	2		0.157	0.694	0.851	94.76
	1		0.105	0.427	0.532	100.00
Olhão	3	8.306	1.673	5.500	7.173	86.37
	2		0.030	0.665	0.695	94.74
	1		0.040	0.397	0.437	100.00
Tavira	3	7.292	0.192	6.336	6.529	89.54
	2		0.053	0.425	0.478	96.09
	1		0.036	0.250	0.285	100.00
Vila Real de Santo António	3	7.277	1.444	4.606	6.050	83.13
	2		0.063	0.700	0.763	93.62
	1		0.056	0.408	0.464	100.00
Castro Marim	3	5.911	0.469	5.007	5.477	92.65
	2		0.026	0.244	0.270	97.22
	1		0.018	0.146	0.164	100.00

5. Conclusions

This report is the result of a joint effort by Instituto Dom Luiz and APA through the National Roadmap for Adaptation XXI (RNA2100) project. It provides the most accurate, up-to-date, and coherent coastal vulnerability assessment for Mainland Portugal, to support the assessment of climate change impacts and decisions regarding adaptation and mitigation along the Portuguese coastal areas. The results presented in this report comprehend a central piece for an overview reflection on the impacts of climate change, and its translation into economic costs, adaptation and impact mitigation strategies and storylines.

From a climatic point of view, Mainland Portugal is located in the transition zone between the arid to semiarid subtropical climates of northern Africa, and the humid, temperate climate of northern Europe, a region commonly considered as climate change "hotspot". According to the Fifth Assessment Report of the Intergovernmental Panel on Climate Change, the observed and projected rates of climate change along the Mediterranean basin exceed the global trends for most variables. These include the ones relevant for the evolution of the coastal areas, as projections indicate considerable changes on the mean sea levels (through SLR), on storm surges, and wave climate parameters (Storlazzi *et al.*, 2018; Camelo *et al.*, 2020; Senechal *et al.*, 2011; Lemos *et al.*, 2021a).

The Portuguese coastal areas include some of the most vulnerable regions to climate change, comprising important populational centres and economically relevant hubs. The portion of Portuguese population living in coastal areas has rapidly increased in the last decades, as results from the CENSOS2021 show unprecedented human pressure along the coastlines. The continued rising sea levels along Portuguese coastlines, associated with the present scenario of coastal sedimentary imbalance, could result in unprecedented coastal flooding, in case no additional coastal protection and risk-reduction or adaptation measures are implemented (Duarte Santos *et al.*, 2017).

In the context of an increasing need for accurate physical and socioeconomic coastal vulnerability assessments, and incorporated in the RNA2100 project, this study proposed an innovative methodology to deal with the multivariate challenges of an accurate coastal vulnerability assessment for Portugal, considering the effects of SLR, tides, storm surge and waves along the coastal areas, focusing on an accurate depiction of future shoreline evolution and extreme coastal flooding, through high-resolution hydro- and morpho-dynamic modelling. Ensemble-based projections were used to drive a collection of dynamic models, providing baseline results for a complete, national-scale coastal vulnerability assessment, based on a composed coastal vulnerability index. Our results established the grounds for translating physical impacts into social and economic ones, as well as adaptation and impact mitigation measures.

This study provided the first consistent, ensemble-based assessment of future costal vulnerability for Portugal, from a large set of CMIP5 data. A 6-member ensemble of storm surge and wave climate projections, propagated nearshore to account for the effects of local bathymetry and bias corrected using an innovative and streamlined methodology based on a synergic combination of reanalysis and observational data, was used, along with a 21-member ensemble of SLR projections. High-resolution vulnerability projections, through a composed CVI, were generated for the Portuguese coastal areas, considering two future periods (2041-2070 and 2071-2100) and scenarios (RCP4.5 and RCP8.5). The empirical modelling frame to generate the CVI projections was based on the high-resolution dynamical modelling results along the five key-locations (Ofir, Costa Nova, Cova Gala, Costa da Caparica and Praia de Faro).

Regarding wave climate, nearshore H_S and MWD projections, as represented by the coastal propagated-corrected ensemble at each of the five key-locations, were summarized in Table 11. Overall, low northerly (high westerly) waves were shown to be projected to become more frequent (scarcer) in the future. Such behavior is consistent with the enhanced projected decreases in the mean H_S values along the eastern North Atlantic described by Lemos *et al.* (2021a) and others (*e.g.* Dobrynin *et al.*, 2015; Pérez *et al.*, 2015; Gallagher *et al.*, 2016; Aarnes *et al.*, 2017; Camus *et al.*, 2017; Casas-Prat *et al.*, 2018; Webb *et al.*, 2018; Morim *et al.*, 2018, 2019; Lemos *et al.*, 2019; 2020a). At Ofir and Costa Nova, the frequency increases of northerly waves ranged from 1.08% to 4.22% at Ofir, and 1.45% to 2.97% at Costa Nova, considering the 2041-2070 RCP4.5 and 2071-2100 RCP8.5 future projected periods (Table 4). At Cova Gala, projections also showed an increase in frequency for MWDs within 190º-290º (SSW-WNW, especially for the RCP4.5 2071-2100 future period, at 2.15%), in addition to the slight increase for the 310º-350º (NW-N) interval. In Costa da Caparica, directional frequency projected increases also revealed a bimodal behavior across 130º-210º (SE-SW) and northwards of 250º (WSW). The projected frequency decreases between 210º and 250º ranged from -1.75% (2041-2070 RCP4.5) to -3.72% (2071-2100 RCP8.5). Finally, at Praia de Faro, a decrease in the frequency of occurrence of MWDs southwards of 250º (WSW) has been found, except for the 130º-150º range (SE-SSE). Northwards of 250º, projected increases between 1.53% (2041-2070 RCP4.5) and 2.80% (2071-2100 RCP8.5) were shown to occur. It should be noted, nevertheless, that across Costa da Caparica and Praia de Faro, the ensemble slightly underestimated the southwesterly components while overestimating the westerly ones, even after the propagation-correction procedure (Table 8 and Table 9).

The ability of the ShorelineS model to accurately depict shoreline evolution at each key-location was assessed by reproducing the observed shoreline by the year 2018 from 2008 initial conditions (two moments where observations were available) using the propagated-corrected-propagated ERA5 reanalysis data. Overall, the performance assessment revealed a good agreement with observations, with mean biases and

MAEs ranging between -3.90 m and 11.8 m, and 5.70 and 31.9 m, respectively, and a generally better (poorer) representation at Praia de Faro (Costa da Caparica).

Future ensemble mean shoreline projections were shown in Figure 53, Figure 54, Figure 61, Figure 62, Figure 69, Figure 70, Figure 77, Figure 78, Figure 85 and Figure 86 for the five selected key-locations, considering the joint effects of SLR and wave action towards 2100. Future projected shorelines considering wave action alone from the 6-member ensemble were also shown between Figure 49 and Figure 84. Such an ensemble approach provided a useful tool to better quantify the uncertainty associated with the multi-model dynamic forcing and evaluate the robustness of the final mean shorelines (as well as the future extreme coastal flooding projections).

Overall, two main conclusions can be drawn from the shoreline projections: 1) future nearshore wave action, projected to become more northerly and less energetic, is projected to lead to northward beach rotations especially along the northern and central Portuguese coastal stretches (Ofir, Costa Nova and Cova Gala), promoting areas of "virtual accretion"; 2) the projected SLR effectively suppresses most of these accretion zones, leading to consistent projected shoreline retreats throughout all key-locations. These were shown to locally reach 100 m (120 m) by 2100 under RCP4.5 (RCP8.5) at Ofir, 200 m (210 m) at Costa Nova, 140 m (150 m) at Cova Gala, 290 m (300 m) along Costa da Caparica and 65 m (80 m) in Praia de Faro. Considering the mean behavior across the entire domain of each key-location, the average areawide projected shoreline retreats and ensemble inter-member uncertainties are depicted in Table 6, together with the overall projected lost area between the reference (2018) and future mean projected shorelines. While all mean retreats can be considered robust (exceeding the ensemble inter-member uncertainty range), Costa Nova showed the greatest uncertainty range between ensemble members. For the 2041-2070 future period, mean areawide retreats range between 26.6 m and 60.7 m (30.1 m and 53.7 m) under RCP4.5 (RCP8.5), whereas for 2071-2100 these range between 44.4 m and 84.2 m (43.7 m and 81.6 m). Mean retreats are often greater for the RCP4.5 scenario, mainly due to increased beach rotation projected under RCP8.5, with the addition of "virtual accretion" areas, immediately north of groins or other fixed structures that, although offset by SLR, contribute to reduced mean shoreline retreats overall. In addition to the projected changes in the nearshore waves' MWD, enhanced projected decreases in mean wave energy under RCP8.5 (Table 11, Figure 41 to Figure 45) were shown to result in lower LST rates than under RCP4.5 at Cova Gala, Costa da Caparica and Praia de Faro (Table 17). Such results indicate that a future climate trajectory under higher-emission scenarios could potentially alleviate the local need for beach nourishment interventions, especially along the central and southern Portuguese coastal areas. Absolute LST rates are, nevertheless, projected decrease along all key-locations, independently of the scenario, between -0.04% and -6.33%.

Finally, the projected lost areas between the reference (2018) and future mean shorelines range between 0.088 km^2 and 0.184 km^2 (0.118 km^2 and 0.197 km^2) by 2100, under RCP4.5 (RCP8.5), the smallest (greatest) losses expected to take place at Praia de Faro and Costa Nova (Cova Gala and Costa Nova). Throughout all key-locations (approximately 14 kilometers of coastline), the cumulative amount of the projected threatened area from 2018 to 2100 is 0.786 km^2, a relevant amount when comparted to the historical nationwide lost area, of 13.5 km^2 in 63 years (1958-2021), over 980 km of coastline (Pinto *et al.*, 2016).

Table 37 – Mean projected shoreline retreat (m) and mean ensemble inter-member uncertainty (m), and lost area from the reference shoreline (2018; km^2) along each key-location, considering the 6-member ensemble of shoreline projections driven by projected wave action and SLR. Projected values are extracted at the last year of each time-slice (2070 and 2100). Robust projected shoreline retreats (greater than the inter-member uncertainty) are underlined.

Mean shoreline retreat (mean ensemble uncertainty; m)				
	2070 (RCP4.5)	**2070 (RCP8.5)**	**2100 (RCP4.5)**	**2100 (RCP8.5)**
Ofir	<u>39.5</u> (13.6)	<u>30.7</u> (15.9)	<u>51.9</u> (22.0)	<u>56.2</u> (19.2)
Costa Nova	<u>60.7</u> (31.8)	<u>50.2</u> (37.5)	<u>84.2</u> (32.2)	<u>81.6</u> (44.5)
Cova Gala	<u>48.4</u> (23.7)	<u>53.7</u> (21.5)	<u>67.8</u> (17.5)	<u>77.0</u> (19.9)
Costa da Caparica	<u>42.9</u> (25.7)	<u>30.1</u> (27.5)	<u>54.9</u> (19.6)	<u>43.7</u> (25.8)
Praia de Faro	<u>26.6</u> (13.3)	<u>35.7</u> (12.7)	<u>44.4</u> (13.8)	<u>62.7</u> (11.1)
Lost area (km^2)				
	2070 (RCP4.5)	**2070 (RCP8.5)**	**2100 (RCP4.5)**	**2100 (RCP8.5)**
Ofir	0.092	0.089	0.157	0.188
Costa Nova	0.105	0.104	0.184	0.197
Cova Gala	0.071	0.081	0.103	0.118
Costa da Caparica	0.142	0.120	0.175	0.164
Praia de Faro	0.052	0.071	0.088	0.119
Total	**0.462**	**0.465**	**0.597**	**0.786**

Regarding the future DTMs, the PCR algorithm was shown to be able to reproduce the shoreline retreats obtained with the ShorelineS model along the cross-shore profiles at each key-location. These profiles were then used to build the 3-dimensional topographic model of the area (Figure 87). Overall, the projected DTMs reveal future fragilities to be enhanced considering SLR and wave action. Not only are the maximum topographic heights projected to reduce throughout all key-locations, but the dune systems, especially in the western Portuguese coast, are also projected to suffer from local sectioning of even complete erosion of the dunes. By 2070 (2100), the natural protection of the shoreline along each key-location is projected to be reduced, on average, by 13.3% (12.3%) under the RCP4.5 scenario, and by 10.5% (12.5%) under RCP8.5.

The future projected extreme coastal flooding, as depicted by 25-year TWL return values associated to three levels of 99th percentile wave energy conditions, was shown in Figure 89 to Figure 112. At Ofir, extreme coastal flooding was shown to be greater by 2100 under RCP8.5, creating conditions for the establishment of a water connection between the ocean and the Cávaro River estuary (Figure 92). Nevertheless, a more perpendicular incident MWD under extreme conditions by 2070 under RCP4.5 (Table 18) resulted in greater inundation extension during this period (0.214 km^2) than in the analogous one (under RCP8.5).

At Costa Nova, extreme coastal flooding was shown to be projected within urbanized area for all future periods and scenarios. Despite worse conditions by 2100 under RCP8.5 (Figure 97), local extreme flooding in the heart of the village may be expected by 2070 under RCP4.5 (Figure 94). The total flooding extents projected for the entire domain were shown to range between 0.137 km^2 and 0.401 km^2 (Table 38).

At Cova Gala, the current seawall, protecting most of the urbanized oceanfront, was shown to be enough to sustain the future projected extreme events depicted here. Nevertheless, outside its range, extreme coastal flooding run-up lines are expected to reach the Figueira da Foz harbor infrastructure, even by 2070 under RCP4.5 (Figure 99). By 2100, the surroundings of the local hospital and the southernmost urbanized areas of Cova Gala were shown as projected to be threatened under the extreme wave energy conditions considered, especially under RCP8.5 (Figure 102), for which a maximum flooding extension of 0.158 km^2 was found (Table 38).

South of Lisbon, in Caparica, future projections revealed two critical areas, threatened by the future expected extreme coastal flooding. Whereas by 2070 the mostly affected area was shown to correspond to the northern portion of the domain, at Praia de São João da Caparica (impacting uniquely local services infrastructure), by 2100, flooding was shown to extend to the densely urbanized areas of Costa da Caparica's oceanfront, overtopping the seawall (especially under RCP8.5; Figure 107) and threatening habitational hubs, besides services and communication routes. The total flooding extent projections for the entire domain vary between 0.165 km^2 and 0.493 km^2 (Table 38).

Finally, across Praia de Faro, local infrastructures were shown to be progressively threatened by the projected changes in water levels towards 2100, especially under the high-end RCP8.5 scenario (Figure 112). In case no additional measures are taken to mitigate the local impacts of the extreme events considered, permanent habitability conditions along most of the urbanized areas within Praia de Faro may become extensively disrupted. Despite the lower overall coastal flooding extensions found for this area, physical impacts were shown to be the greatest between all key-locations, potentially leading to temporary sectioning of the area into small islands between the Atlantic Ocean and the Ria Formosa under extreme events.

Overall, while extreme wave energy was shown to be projected to slightly decrease along the Portuguese coastlines (Lemos *et al.*, 2023b – Part I), synchronized action with increased TWLs (resulting essentially from SLR, but also from the joint occurrence of high spring tides or storm surge conditions) in the context of weaker natural protection structures (e.g. fragilized dune systems), may lead to unprecedented coastal flooding in the future, as summarized in Table 38. Throughout the five key-locations (approximately 14 kilometers of coastline), the future projected threatened area, expected to become flooded under extreme TWL and wave conditions, is projected to ascend a maximum of 0.657 km^2 (0.738 km^2) by 2070 under RCP4.5 (RCP8.5), and 0.873 km^2 (1.47 km^2) by 2100 under RCP4.5 (RCP8.5).

These results should be interpreted as a baseline projection, maintaining the current coastal defense structures with no additional coastal protection and risk-reduction measures implemented. Future Portuguese adaptation and mitigation measures should rely on "worst-case scenario" information to base their strategies and expect continuous changes well beyond the end of the 21st century (Lyon *et al.*, 2022), anticipating additional levels of protection to be implemented in the future. The combination of coastal retreat with high-frequency flooding could result in loss coastal ecosystems and fertile soil for agriculture given the potential landward intrusion of saltwater, besides the imminent risks for human life.

Table 38 – Projected threatened area by extreme coastal flooding at Ofir, Costa Nova, Cova Gala, Costa da Caparica, Praia de Faro and throughout all five key-locations, from the reference (2018; Lemos *et al.*, 2023b – Part I) shorelines, for each future period and scenario. "ETWL" stands for "extreme TWL", corresponding to the 25-year RP levels, and "minE" to "maxE" refer to the three ensemble energy (E) 99th percentile levels (lower-threshold, ensemble mean and higher-threshold).

Flooded area from reference (2018) shoreline – Ofir (km^2)				
	2041-2070 (RCP4.5)	**2041-2070 (RCP8.5)**	**2071-2100 (RCP4.5)**	**2071-2100 (RCP8.5)**
ETWL + minE	0.214	0.158	0.190	0.233
ETWL + meanE	0.103	0.159	0.193	0.240
ETWL + maxE	0.103	0.158	0.194	0.253
Flooded area from reference (2018) shoreline – Costa Nova (km^2)				
	2041-2070 (RCP4.5)	**2041-2070 (RCP8.5)**	**2071-2100 (RCP4.5)**	**2071-2100 (RCP8.5)**
ETWL + minE	0.137	0.161	0.196	0.291
ETWL + meanE	0.147	0.162	0.200	0.344
ETWL + maxE	0.147	0.169	0.227	0.401
Flooded area from reference (2018) shoreline – Cova Gala (km^2)				
	2041-2070 (RCP4.5)	**2041-2070 (RCP8.5)**	**2071-2100 (RCP4.5)**	**2071-2100 (RCP8.5)**
ETWL + minE	0.086	0.108	0.111	0.158
ETWL + meanE	0.087	0.096	0.130	0.156
ETWL + maxE	0.088	0.098	0.111	0.142
Flooded area from reference (2018) shoreline – Caparica (km^2)				
	2041-2070 (RCP4.5)	**2041-2070 (RCP8.5)**	**2071-2100 (RCP4.5)**	**2071-2100 (RCP8.5)**

ETWL + minE	0.165	0.192	0.208	0.414
ETWL + meanE	0.168	0.192	0.208	0.440
ETWL + maxE	0.174	0.201	0.229	0.493
Flooded area from reference (2018) shoreline – Praia de Faro (km^2)				
	2041-2070 (RCP4.5)	**2041-2070 (RCP8.5)**	**2071-2100 (RCP4.5)**	**2071-2100 (RCP8.5)**
ETWL + minE	0.055	0.108	0.110	0.166
ETWL + meanE	0.056	0.109	0.110	0.167
ETWL + maxE	0.057	0.112	0.112	0.179
Flooded area from reference (2018) shoreline – All key-locations (km^2)				
	2041-2070 (RCP4.5)	**2041-2070 (RCP8.5)**	**2071-2100 (RCP4.5)**	**2071-2100 (RCP8.5)**
ETWL + minE	0.657	0.727	0.816	1.26
ETWL + meanE	0.561	0.717	0.841	1.35
ETWL + maxE	0.570	0.738	0.873	1.47

The results from the dynamical modelling at the five key-locations based on multi-model, multi-process and multi-scenario approaches, played a crucial role designing the complete climate change impact assessment for the Portuguese coastal areas. In fact, the national-scale vulnerability assessment was based on the combination of different types of information, including the geomorphological characteristics, socioeconomic data related to population, infrastructures, communication routes and real estate property value, GCM/RCM-driven wave climate and TWL projections. Regarding the coastline retreat and wave-related run-up lines, the parametric modelling at national scale was directly calibrated using the results obtained for the five selected key-locations. Upon calibration, the parametric model was deemed fit to characterize coastal retreat, flooding and the overall vulnerability along the entire Portuguese coastline. The final results, presented in section 4.6, between Figure 113 and Figure 175, relied on a composed CVI. This index was computed for the ocean-facing coastlines using the PCR method (section 3.2.2), and for the inland waters based on the RP-associated values of TWL. It should be noted that areas with low CVI are, in fact, the ones projected to be vulnerable to the most extreme events (100-year RP of TWLs), which, due to their scarcer nature, are related to a lower CVI. On the other hand, areas with high CVI are the ones more vulnerable to less extreme (more frequent) TWL events (4-year RP).

National CVI cartography was divided into six coastal sections along Mainland Portugal, allowing a comprehensive assessment of the most vulnerable areas through a clearer, high-resolution depiction of the projected CVIs and associated physical impacts, shown to vary considerably depending on the analyzed section due to the highly diversified nature of the Portuguese coastline. From a local-to-regional point of view, along the Portuguese coastline, the municipality projected to exhibit the greatest vulnerable area, under the three CVI levels, was shown to be Grândola (Vila Franca de Xira) for the ocean-facing (inland waters) coastlines, for all future periods and scenarios. Within these municipalities, the projected areas under CVI were shown to vary between 4.71 km^2 (2070 under RCP8.5) and 6.09 km^2 (2100 under RCP4.5) at Grândola (ocean-facing coastlines), and 152 km^2 (2070 under RCP4.5) and 156 km^2 (2100 under RCP8.5) at Vila Franca de Xira (inland waters coastlines). Considering an approach by districts, the largest area projected under CVI in the future was shown to be in Lisbon district, for all future periods and scenarios, ranging between 214 km^2 (2070 under RCP4.5; Table 29) and 221 km^2 (2100 under RCP8.5; Table 35), related to the large Tagus River estuary, surrounded by low-lying terrain and a dynamic intertidal behavior. Conversely, Beja was shown to be the district with the smallest total projected area under CVI, ranging between 1.52 km^2 (Table 29) and 2.15 km^2 (Table 34), due to its generally rocky coastal configuration, with cliffs and small embedded beaches.

Finally, when considering the total threatened area for all types of coastlines along Mainland Portugal, the projected values for the ocean-facing coastlines were shown to ascend to 41.7 km^2 (2070 under RCP4.5), 49.7 km^2 (2070 under RCP8.5), 54.7 km^2 (2100 under RCP4.5) and 55.9 km^2 (2100 under RCP8.5). These areas, related to episodically flooded territory under extreme coastal events, are projected to amount to 3.09, 3.68, 4.05 and 4.14 times the area observed to have been lost between 1958 and 2021 (13.5 km^2). However, when considering inland waters, an additional value between 514 km^2 and 548 km^2 (2070 under RCP4.5 and 2100 under RCP8.5, respectively) must be considered. Therefore, for all types of coastlines along Mainland Portugal, the future area under CVI is projected to ascend to 604 km^2 by 2100, under the RCP8.5 scenario.

6. References

Aarnes, O. J., Reistad, M., Breivik, Ø., Bitner-Gregersen, E., Magnusson, A. K., Natvig, B., Vanem, E. (2017). Projected changes in significant wave height toward the end of the 21st century: Northeast Atlantic. *J. Geophys. Res. Oceans*, 122, 3394–3403.

Antunes, C. (2007). Previsão de Marés dos Portos Principais de Portugal. *FCUL Webpage*, http://webpages.fc.ul.pt/~cmantunes/hidrografia/hidro_mares.html.

Antunes, C. (2014). Eventos Extremos e a variação do Nível do mar. Actas das 3.as Jornadas de Engenharia Hidrográfica, 33–36. https://www.hidrografico.pt/jornada/4.

Antunes, C., Rocha, C., Catita, C. (2019). Coastal Flood Assessment due to Sea Level Rise and Extreme Storm Events: A Case Study of the Atlantic Coast of Portugal's Mainland. *Geosciences*, 9, 5:239. DOI: https://doi.org/10.3390/geosciences9050239

Ardhuin, F., *et al.* (2010). Semiempirical dissipation source functions for ocean waves. Part I: Definition, calibration, and validation, *J. Phys. Oceanogr.*, 40(9), 1917– 1941, doi:10.1175/2010jpo4324.1.

Athanasiou, P., van Dongeren, A., Giardino, A. *et al.* (2020). Uncertainties in projections of sandy beach erosion due to sea level rise: an analysis at the European scale. Sci Rep 10, 11895. DOI: https://doi.org/10.1038/s41598-020-68576-0.

Atkinson, A. L., Baldock, T. L., Birrien, F., Callaghan, D. P., Nielsen, P., Beuzen, T., Turner, I. L., Blenkinsopp, C. E., Ranasinghe, R. (2018). Laboratory investigation of the Bruun Rule and beach response to sea level rise. Coast. Eng., 136, 183-202. DOI: 10.1016/j.coastaleng.2018.03.003.

Bernardes, C., Fernández, S., Santos, F., Baptista, P., Silva, P.A., Abreu, T., Coelho, C., Lima, M., Carvalho, R. (2020). Estudo de Viabilidade da Transposição Aluvionar das Barras de Aveiro e da Figueira da Foz. *Relatório Intercalar 1. In Tarefa 1. Análise da Evolução Histórica da Embocadura da Laguna de Aveiro*. Universidade de Aveiro/Agência Portuguesa do Ambiente. Portugal. 59pp.

Bidlot, J., Janssen P., Abdalla, S. (2007). A revised formulation of ocean wave dissipation and its model impact. *Rep. ECMWF*, Reading, U. K..

Booij, N., Ris, R. C., and Holthuijsen, L.H. (1999). A third-generation wave model for coastal regains: 1. Model description and validation, *J. Geophys. Res.*, 104 (C4), 7649 – 7666. DOI: 10.1029/98JC02622.

Bruun, P. (1962). Sea-level rise as cause of shore erosion. American Society of Civil Engineering Proceedings. Journal of Waterways and Harbours Division 88, 117–130.

Bruun, P. (1988). The Bruun rule of erosion by sea-level rise: A discussion on large-scale two-and three-dimensional usages. Journal of Coastal Research 4, 627–648.

Cabral, J. (1995). Neotectónica em Portugal Continental (Vol. 31). Ministério da Indústria e Energia, Secretaria de Estado da Indústria, Instituto Geológico e Mineiro.

Camelo, J., Mayo, T. L., Gutmann, E. D. (2020). Projected Climate Change Impacts on Hurricane Storm Surge Inundation in the Coastal United States. *Frontiers in Built Environment*, 6, 207pp. DOI: https://doi.org/10.3389/fbuil.2020.588049.

Camus, P., Losada, I, J., Izaguirre, C., Espejo, A., Menéndez, M., Pérez, J. (2017). Statistical wave climate projections for coastal impact assessments. *Earth's Future*, 5, 918-933, doi:10.1002/2017EF000609.

Casas-Prat, M., Wang, X. L., Swart, N. (2018). CMIP5-based global wave climate projections including the entire Arctic Ocean. *Ocean Modelling*, 123, 66-85.

Church, J. A. *et al.* in *Climate Change 2013*: The Physical Science Basis (eds Stocker, T. F. *et al.*) 1140–1141 (IPCC, Cambridge Univ. Press, 2013).

Church, J.A., White, N.J. (2011). Sea-Level Rise from the Late 19th to the Early 21st Century. Surv. Geophys., 32, 585–602. doi:10.1007/s10712-011-9119-1.

Dee, D. P., *et al.* (2011). The ERA-Interim reanalysis: configuration and performance of the data assimilation system. *Quarterly Journal of the Royal Meteorological Society*, 137, 1830-1841.

Dobrynin, M., Murawski, J., Baehr, J., Ilyina, T. (2015). Detection and Attribution of Climate Change Signal in Ocean Wind Waves. *Journal of Climate*, 28, 4, 1578-1591.

Domingues, R. T., Neves de Jesus, S., Ferreira, O. (2021). Place attachment, risk perception, and preparedness in a population exposed to coastal hazards: A case study in Praia de Faro Beach, southern Portugal, *International Journal of Disaster Risk Reduction*, 60, 2021, 102288. DOI: https://doi.org/10.1016/j.ijdrr.2021.102288.

Duarte Santos, F., Lopes, A. M., Moniz, G. Ramos, L., Taborda, R. (2014). Gestão da Zona Costeira: o desfaio da mudança. Relatório do Grupo de Trabalho do Litoral, 154 p.

Duarte Santos, F., Mota Lopes, A., Moniz, G., Ramos, L., Taborda, R. (2017). Grupo de Trabalho do Litoral: Gestão da Zona Costeira: O desafo da mudança. Filipe Duarte Santos, Gil Penha-Lopes e António Mota Lopes (Eds). Lisboa (ISBN: 978-989-99962-1-2).

ECMWF. (2016). IFS Documentation CY41R2. https://www.ecmwf.int/node/16651.

EEA. (2006). The changing faces of Europe's coastal areas. *European Environment Agency*, Copenhagen.

EUROSION. (2003). Trends in Coastal Erosion in Europe. *Final Report of the Project 'Coastal erosion - Evaluation of the need for action'*. Leiden, The Netherlands: Directorate General Environment, European Commission.

Fan, Y., Held, I. M., Lin, S.-J., Wang, X. L. (2013). Ocean warming effect on surface gravity wave climate change for the end of the 21st century. *Journal of Climate*, 26, 6046-6066.

Fernández-Fernández, S., Baptista, P., Bernardes, C., Silva, P., Fontán-Bouzas, A., López-Olmedilla, L., Ferreira, C. (2019). Variação da linha de costa em praias arenosas: Aveiro (Portugal). Livro de resumos do IX Congresso sobre Planeamento e Gestão das Zonas Costeiras dos Países de Expressão Portuguesa, Lisboa (Portugal).

Ferreira, A. M., Coelho, C., Narra, P. (2020). Coastal erosion risk assessment to discuss mitigation strategies: Barra-Vagueira, Portugal. Natural Hazards, 105, 1069–1107. DOI: https://doi.org/10.1007/s11069-020-04349-2.

Figueiredo, P. M., Cabral, J., & Rockwell, T. K. (2014). Recognition of Pleistocene marine terraces in the southwest of Portugal (Iberian Peninsula): Evidences of regional Quaternary uplift. Annals of Geophysics, 56(6), 5. https://doi.org/10.4401/ag-6276.

Gesch, D.B. (2009). Analysis of Lidar Elevation Data for Improved Identification and Delineation of Lands Vulnerable to Sea Level Rise. J. Coast. Res. 2009, 49–58. doi: 10.2112/SI53-006.1.

Gornitz, V. in *Encyclopedia of Coastal Science*: Natural Hazards (eds Scwartz, M.) 678–684 (Springer, Dordrecht, The Netherlands, 2005). DOI: 10.1007/1-4020-3880-1_221.

Groot, R. *et al.* (2012). Global estimates of the value of ecosystems and their services in monetary units. Ecosystem Services, 1, 1, 50-61.

Günther, H., Hasselmann, S., Janssen, P. A. E. M. (1992). The WAM model Cycle 4. *Report No. 4*, Hamburg.

Hay, C.C., Morrow, E., Kopp, R.E., Mitrovica, J.X. (2015). Probabilistic reanalysis of twentieth-century sea-level rise. Nature, 517, 481–484. doi:10.1038/nature14093.

Hemer, M. A., Fan, Y., Mori, N., Semedo, A., Wang, X. (2013). Projected changes in wave climate from a multi-model ensemble. *Nature Climate Change*, 3, 471-476, DOI: 10.1038/NCLIMATE1791.

Hemer, M. A., Katzfey, J., Trenham, C. E. (2013a). Global dynamical projections of surface ocean wave climate for a future high greenhouse gas emission scenario. *Ocean Modelling*, 70, 221-245.

Hersbach, H., Bell, B., Berrisford, P., Hirahara, S., Horányi, A., Muñoz-Sabater, J., Nicolas, J., Peubey, C., Radu, R., Schepers, D., Simmons, A., Soci, C., Abdalla, S., Abellan, X., Balsamo, G., Bechtold, P., Biavati, G., Bidlot, J., Bonavita, M., Chiara, G., Dahlgren, P., Dee, D., Diamantakis, M., Dragani, R., Flemming, J., Forbes, R., Fuentes, M., Geer, A., Haimberger, L., Healy, S., Hogan, R., Hólm, E., Janisková, M., Keeley, S., Laloyaux, P., Lopez, P., Lupu, C., Radnoti, G., de Rosnay, P., Rozum, I., Vamborg, F., Villaume, S., Thépaut, J. (2020). The ERA5 global reanalysis. *Quarterly Journal of the Royal Meteorological Society*, 2020, 1-51.

Holthuijsen, L. H. (2007). Waves in oceanic and coastal waters. Cambridge, 387pp.

IHRH (2003) – Case 3: Costa da Caparica: Artificial sand nourishment with groyne field maintenance. EUrosion Project – Review of experiences of coastal erosion control and management. Vol. II. Report. pp – 43-60.

IPCC, 2022: Climate Change 2022: Impacts, Adaptation, and Vulnerability. Contribution of Working Group II to the Sixth Assessment Report of the Intergovernmental Panel on Climate Change [H.-O. Pörtner, D.C. Roberts, M. Tignor, E.S. Poloczanska, K. Mintenbeck, A. Alegría, M. Craig, S. Langsdorf, S. Löschke, V. Möller, A. Okem, B. Rama (eds.)]. Cambridge University Press. Cambridge University Press, Cambridge, UK and New York, NY, USA, 3056 pp., doi:10.1017/9781009325844.

IPCC. (2014). Climate Change 2014: Synthesis Report. Contribution of Working Groups I, II and III to the Fifth Assessment Report of the Intergovernmental Panel on Climate Change. IPCC, Geneva, Switzerland.

Jacob, D., *et al.* (2014). EURO-CORDEX: new high-resolution climate change projections for European impact research. *Regional Environmental Change*, 14, 563–578.

Jacob, D., *et al.* (2020). Regional climate downscaling over Europe: perspectives from the EURO-CORDEX community. *Regional Environmental Change*, 20, 51.

Johnson, G.C., Chambers, D.P. (2013). Ocean bottom pressure seasonal cycles and decadal trends from GRACE Release-05: Ocean circulation implications. J. Geophys. Res., 118, 228–240. doi:10.1002/jgrc.20307.

Komen, G. J., Cavalieri, L., Doneland, M., Hasselmann, S., Janssen, P. A. E. M. (1994). Dynamics and modeling of ocean waves. Cambridge: Cambridge University Press.

Kopp, R. E., Kemp, A. C., Bittermann, K., Horton, B. P., Donnelly, J. P., Gehrels, W. R., Hay, C. C., Mitrovica, J. X., Morrow, E. D., and Rahmstorf, S. (2016). Temperature-driven global sea-level variability in the Common Era. *Proceedings of the National Academy of Sciences*, 113 (11):E1434.

Leatherman, S. P., Zhang, K., Douglas, B. C. (2000). Sea Level Rise Shown to Drive Coastal Erosion. EOS, 81, 6, 55-57.

Lemos, G., Menendez, M., Semedo, A., Camus, P., Hemer, M., Dobrynin, M., Miranda, P. (2020a). On the need of bias correction methods for wave climate projections. *Global and Planetary Change*, 186, 103109.

Lemos, G., Semedo, A., Dobrynin, M., Behrens, A., Staneva, J., Bidlot, J.-R., Miranda, P. (2019). Mid-twenty-first century global wave climate projections: Results from a dynamic CMIP5 based ensemble. *Global and Planetary Change*, 172, 69-87.

Lemos, G., Semedo, A., Dobrynin, M., Menendez, M., Miranda, P. (2020b). Bias-Corrected CMIP5-Derived Single-Forcing Future Wind-Wave Climate Projections toward the End of the Twenty-First Century. *Journal of Applied Meteorology and Climatology*, 59, 9, 1393–1414. http://dx.doi.org/10.1175/jamc-d-19-0297.1.

Lemos, G., Semedo, A., Hemer, M., Menendez, M., Miranda, P. M. A.. (2021b). Remote climate change propagation across the oceans – the directional swell signature. *Environmental Research Letters*. DOI: https://doi.org/10.1088/1748-9326/ac046b.

Lemos, G., Semedo, A., Menendez, M., Miranda, P. M. A., Hemer, M. (2021). On the decreases in North Atlantic significant wave heights from climate projections. *Climate Dynamics*. DOI: https://doi.org/10.1007/s00382-021-05807-8.

Leuliette, E. W., Scharroo, R. (2010). Integrating Jason-2 into a multiple-altimeter climate data record. Mar. Geol., 33(sup 1), 504–517. doi:10.1080/01490419.2010.487795.

Luijendijk, A., Hagenaars, G., Ranasinghe, R. *et al.* (2018). The State of the World’s Beaches. Sci Rep 8, 6641. DOI: https://doi.org/10.1038/s41598-018-24630-6.

Lyon, C., Saupe, E., Smith, C., Hill, D., Beckerman, A., Stringer, L., Marchant, R., McKay, J., Burke, A., O’Higgins, P., Dunhill, A., Allen, B., Riel-Salvatore, J., Aze, T. (2022). Climate change research and action must look beyond 2100. *Global Change Biology*, 28, 349-361.

Mangor, K., Drønen, N. K., Kærgaard, K. H., Kristensen, S.E. (2017). Shoreline management guidelines, *DHI Water and Environment*. DHI, Hørsholm, Denmark. ISBN: 978-87-90634-04-9.

Maraun, D., Shepherd, T. G., Widmann, M., Zappa, G., Walton, D., Gutiérrez, J. M., Hagemann, S., Richter, I., Soares, P. M., Hall, A., Mearns, L.O. (2017). Towards process-informed bias correction of climate change simulations. Nature Climate Change, 7(11), 764-773.

Maraun, D., Huth, R., Gutiérrez, J. M., Martín, D. S., Dubrovsky, M., Fischer, A., Hertig, E., Soares, P. M. M., Bartholy, J., Pongrácz, R., Widmann, M. (2019). The VALUE perfect predictor experiment: evaluation of temporal variability. International Journal of Climatology, 39(9), 3786-3818.

Marcy, D., Brooks, W., Draganov, K., Hadley, B., Haynes, C., Herold, N., McCombs, J., Pendleton, M., Schmid, K., Sutherland, M., *et al.* (2011). New Mapping Tool and Techniques for Visualizing Sea Level Rise and Coastal Flooding Impacts. In Proceedings of the 2011 Solutions to Coastal Disasters Conference, Anchorage, AK, USA, 26–29 June 2011; pp. 474–490. doi:10.1061/41185(417)42.

McGranahan, G., Balk, D., Anderson, B. (2007). The rising tide: assessing the risks of climate change and human settlements in low elevation coastal zones. *Environment and Urbanization*, 19 (1), 17–37. doi:10.1177/0956247807076960.

Mentaschi, L., Vousdoukas, M. I., Voukouvalas, E., Dosio, A., Feyen, L. (2017). Global changes of extreme coastal wave energy fluxes triggered by intensified teleconnection patterns. Geophysical Research Letters, 44, 2416-2426. DOI: https://doi.org/10.1002/2016GL072488.

Mentaschi, L., Vousdoukas, M. I., Pekel, J.-F., Voukouvalas, E., and Feyen, L. (2018). Global long-term observations of coastal erosion and accretion. *Scientific Reports*, 8(1):12876.

Morim, J., Hemer, M. A., Cartwright, N., Strauss, D., Andutta, F. (2018). On the concordance of 21st century wind-wave climate projections. *Global and Planetary Change*, 167, 160-171.

Morim, J., Hemer, M. A., Wang, X., Cartwright, N., Trenham, C., Semedo, A., Young, I., Bricheno, L., Camus, P., Casas-Prat, M., Erikson, L., Mentaschi, L., Mori, N., Shimura, T., Timmermans, B., Aarnes, O., Breivik, Ø., Behrens, A., Dobrynin, M., Menendez, M., Staneva, J., Wehner, M., Wolf, J., Kamranzad, B., Webb, A., Stopa, J., Andutta, F. (2019). Robustness and uncertainties in global multivariate wind-wave climate projections. *Nature Climate Change*, 9, 711-718.

Nerem, R.S., Chambers, D.P., Choe, C., Mitchum, G. T. (2010). Estimating Mean Sea Level Change from the TOPEX and Jason Altimeter Missions. *Mar. Geod.*, *33*, 435–446. doi:10.1080/01490419.2010.491031.

Neumann, B., Vafeidis, A. T., Zimmermann, J., Nicholls, R. J. (2015). Future Coastal Population Growth and Exposure to Sea-Level Rise and Coastal Flooding - A Global Assessment. *PLoS One*, 10(3): e0118571. DOI: https://doi.org/10.1371/journal.pone.0118571.

Nunes, A. J., Cordeiro, M. F. N. (2013). Alteração da linha de costa entre a Figueira da Foz e S. Pedro de Moel após o prolongamento do molhe norte do Mondego. *Actas do VI Congresso Nacional de Geomorfologia*, Coimbra, pp 6-10.

Oliveira, F. S. B. F., Brito, F. A. (2015). Evolução da morfologia costeira a sul da embocadura do rio Mondego, de 1975 a 2011. VIII Congresso sobre Planeamento e Gestão das Zonas Costeiras dos Países de Expressão Portuguesa, Universidade de Aveiro, Aveiro, 15 p.

Peltier, W. R., Argus, D. F., Drummond, R. (2015). Space geodesy constrains ice age terminal deglaciation: The global ICE-6GC (VM5a) model. *Journal of Geophysical Research: Solid Earth*, 120, 450–487.

Pereira, C., Coelho, C. (2013). Mapas de Risco das Zonas Costeiras por Efeito da Acção Energética do Mar. *Revista da Gestão Costeira Integrada*, 13(1), 27-43.

Perez, J., Menendez, M., Camus, P., Mendez, F., Losada, I. (2015). Statistical multi-model climate projections of surface ocean waves in Europe. *Ocean Model.*, 96(Part 1), 161–170. DOI: 10.1016/j.ocemod.2015.06.001.

Perez, J., Menendez, M., Mendez, F., Losada I. (2014). Evaluating the performance of CMIP3 and CMIP5 global climate models over the north-east Atlantic region. *Clim. Dyn.*, 43(9-10), 2663–2680. DOI: 10.1007/s00382-014-2078-8.

Pinto, C. A. (2016). Coastal erosion and sediment management in Portugal. Proceedings of the CEDA Iberian Conference—Dredging for Sustainable Port Development, Lisbon, Portugal.

Pinto, C. A., Silveira, T. M., Taborda, R. (2015). Alimentação artificial das praias da Costa da Caparica: síntese dos resultados de monitorização (2007 a 2014). 3ª Conferencia sobre morfodinâmica estuarina e costeira. Universidade do Algarve, 14-15 May 2015. Faro.

Pinto, C. A., Silveira, T. M., Teixeira, S.B. (2020). Beach nourishment practice in mainland Portugal (1950–2017): Overview and retrospective. *Ocean Coast. Manag.*, 192, 105211.

Pinto, C. A., Taborda, R., Andrade, C. (2007). Evolução recente da linha de costa no troço Cova do Vapor – S. João da Costa da Caparica. 5as Jornadas Portuguesas de Engenharia Costeira e Portuária, Lisboa. PIANC. AIPCN. Lisboa, p. 13.

Pinto, C., Taborda, R., Andrade, C., Baptista, P., Silva, P., Alves; Mendes, D., Pais-Barbosa, J. (2022). Morphological Development and Behaviour of a Shoreface Nourishment in the Portuguese Western Coast. *Journal of Marine Science and Engineering*, 10, 2, 146. DOI: http://dx.doi.org/10.3390/jmse10020146.

Pinto, C. A., Teixeira, S.B. (2022). Evolution and behaviour of beach nourishments in Vale do Lobo (Algarve -Portugal). 6th Conference of Estuarine and Coastal Morphodynamics (MEC). LNEC. Lisbon. Pp. 23-24 (in Portuguese).

Ponte Lira, C., Nobre Silva, A., Taborda, R., Freire de Andrade, C. (2016). Coastline evolution of Portuguese low-lying sandy coast in the last 50 years: an integrated approach. *Earth Syst. Sci. Data*, 8, 265–278. DOI: https://doi.org/10.5194/essd-8-265-2016.

Poulter, B., Halpin, P.N. (2007). Raster modelling of coastal flooding from sea-level rise. Int. J. Geogr. Inf. Sci., 1–16. ISSN 1362-3087. doi:10.1080/13658810701371858.

Ranasinghe, R., Callaghan, D., Stive, M. J. F. (2012). Estimating coastal recession due to sea level rise: beyond the Bruun rule. Climatic Change, 110 (3–4), 561-574. DOI: 10.1007/s10584-011-0107-8.

Ranasinghe, R. (2016). Assessing climate change impacts on open sandy coasts: A review. *Earth-science reviews*, *160*, 320-332.

Ranasinghe, R. (2020). On the need for a new generation of coastal change models for the 21st century. Scientific Reports, 10, 1. DOI: https://doi.org/10.1038/s41598-020-58376-x.

Rascle, N., Ardhuin, F. (2013). A global wave parameter database for geophysical applications. Part 2: Model validation with improved source term parameterization. *Ocean Model.*, 70, 174–188. DOI: 10.1016/j.ocemod.2012.12.001.

Riahi, K., Rao, S., Krey, V., Cho, C., Chirkov, V., Fischer, G., Kindermann, G., Nakicenovic, N., Rafaj, P. (2011). RCP 8.5 – a scenario of comparatively high greenhouse gas emissions. *Climatic Change*, 109, 33-57, DOI: 10.1007/s10584-011-0149-y.

Rocha, C., Antunes, C., Catita, C. (2020). Coastal Vulnerability Assessment Due to Sea Level Rise: The Case Study of the Atlantic Coast of Mainland Portugal. Water., 12(2):360, DOI: org/10.3390/w12020360

Roelvink, J. A., Van Banning, G. K. F. M. in *Hydroinformatics*: Design and Development of DELFT3D and Application to Coastal Morphodynamics (eds Verwey, A., Minns, A.W., Babovic, V. and Maksimovic, C.) 451-456 (Balkema, Rotterdam, The Netherlands, 1994).

Roelvink, J.A, Reniers, A., van Dongeren, A., van Thiel de Vries, J., McCall, R., Lescinski, J. (2009). Modeling storm impacts on beaches, dunes and barrier islands. *Coastal Engineering*, 56, 1133-1152.

Roelvink, D. (2011). A guide to modeling coastal morphology 12.

Roelvink, J. A., Huisman, B., Elghandour, A., Ghonim, M., Reyns, J. (2020). Efficient Modeling of Complex Sandy Coastal Evolution at Monthly to Century Time Scales. Frontiers in Marine Science, 7, 535.

Roemmich, D., Gilson, J. (2009). The 2004–2008 mean and annual cycle of temperature, salinity, and steric height in the global ocean from the Argo Program. Prog. *Oceanogr.*, 82, 81–100. DOI: 10.1016/j.pocean.2009.03.004.

Semedo, A., Behrens, R., Sterl, A., Bengtsson, L., Günther, H. (2013). Projection of Global Wave Climate Change toward the End of the Twenty-First Century. *Journal of Climate*, 26, 8269-8288.

Semedo, A., Dobrynin, M., Lemos, G., Behrens, A., Staneva, J., de Vries, H., Sterl, A., Bidlot, J., Döscher, R., Murawski, J., Miranda, P. (2018b). CMIP5 Derived Single-Forcing, Single-Model and Single-Scenario Wind Wave Climate Simulations: Ensemble Configuration and Performance Evaluation. *Journal of Marine Science and Engineering*, 6, 90, 28pp.

Senechal, N., Coco, G., Bryan, K. R., & Holman, R. A. (2011). Wave run-up during extreme storm conditions. *Journal of Geophysical Research: Oceans*, 116(C7).

Serafin, A. K., Ruggiero, P., Stockdon, H. F. (2017). The relative contribution of waves, tides, and nontidal residuals to extreme total water levels on U.S. West Coast sandy beaches. *Geophys. Res. Lett.*, 44, 1839–1847.

Storlazzi, C., Gingerich, S. B., Dongeren, A., Cheriton, O., Swarzenski, P., Quataert, E., Voss, C., Field, D., Annamalai, H., Piniak, G., McCall, R. (2018). Most atolls will be uninhabitable by the mid-21st century because of sea-level rise exacerbating wave-driven flooding. *Science Advances*, 4(4). DOI: 10.1126/sciadv.aap9741.

Sweet, W.V., Kopp, R.E., Weaver, C.P., Obeysekera, J., Horton, R.M., Thieler, E.R., Zervas, C. (2017). Global and Regional Sea Level Rise Scenarios for the United States. In *NOAA Technical Report*; NOAA: Silver Spring, MD, USA, NOS CO-OPS 083.

Taborda, R., Ribeiro, M. (2019). Modeling shoreline evolution and headland sediment bypassing at platform beaches. *Proceedings of Coastal Sediments 2019*, 2746-2760. DOI: https://doi.org/10.1142/9789811204487_0235.

Taherdoost, H. (2017). Decision Making Using the Analytic Hierarchy Process (AHP); A Step by Step Approach. *International Journal of Economics and Management Systems*, 2, 244-246.

Tolman, H. L. (2002). User manual and system documentation of WAVEWATCH-III version 2.22. *Tech. report 222*, NOAA/NWS/NCEP/MMAB.

Veloso Gomes, F., Costa, J., Rodrigues, A., Taveira Pinto, F., Barbosa, J. P., Neves, L. (2009). Costa da Caparica artificial sand nourishment and coastal dynamics. *J. Coast. Res. Spec.*, 56, 678–682.

Veloso-Gomes, F., Taveira-Pinto, F., Neves, L. (2004). Esposende – Ofir stretch – Case study. Coastal Practice Network. Project part-funded by the European Union.

Vieira, R., Antunes, C., Taborda, R. (2012). Caracterização da sobreelevação meteorológica em Cascais nos últimos 50 anos. In Proceedings of 2as Jornadas de Engenharia Hidrográfica, Lisbon, Portugal, 21–22 June 2012; pp. 21–24. ISBN 978-989-705-035-0.

Vitousek, S., Vos, K., Splinter, K. D., Erikson, L., Barnard, P. L. (2023). A Model Integrating Satellite-Derived Shoreline Observations for Predicting Fine-Scale Shoreline Response to Waves and Sea-Level Rise Across Large Coastal Regions. Journal of Geophysical Research: Earth Surface, 128, 7, e2022JF006936. DOI: https://doi.org/10.1029/2022JF006936.

Vousdoukas, M. I., Voukouvalas, E., Annunziato, A., Giardino, A., Feyen, L. (2016a). Projections of extreme storm surge levels along Europe. *Clim. Dyn.*, 47(9), 3171– 3190. DOI: 10.1007/s00382-016-3019-5.

Vousdoukas, M. I., Mentaschi, L., Voukouvalas, E., Verlaan, M., Feyen, L. (2017). Extreme sea levels on the rise along Europe’s coasts. *Earth’s Future*, 5(3), 304-323.

Vousdoukas, M. I., Ranasinghe, R., Mentaschi, L., Plomaritis, T. A., Athanasiou, P., Luijendijk, A., Feyen, L. (2020). Sandy coastlines under threat of erosion. Nat. Clim. Chang. 10, 260–263. DOI: https://doi.org/10.1038/s41558-020-0697-0.

Wang, X. L., Feng, Y., Swail, V. R. (2014). Changes in global ocean wave heights as projected using multimodel CMIP5 simulations. *Geophysical Research Letters*, 41, 1026-1034.

Watson, C. S., White, N. J., Church, J. A., King, M. A., Burgette, R. J., and Legresy, B. (2015). Unabated global mean sea-level rise over the satellite altimeter era. *Nature Clim. Change*, 5 (6):565-568.

Webb, A., Shimura, T., Mori, N. (2018). A High-Resolution Future Wave Climate Projection for the Coastal Northwestern Atlantic. *The 65th Coastal Engineering Lectures*, 74(2).

WMO. (2011). Guide to Storm Surge Forecasting. *WMO-No. 1076*. 120pp.